Modelleren van geneesmiddelenverdeling en -transport
tijdens intraperitoneale chemotherapie

Modeling of Drug Delivery and Transport during Intraperitoneal Chemotherapy

Margo Steuperaert

UNIVERSITEIT
GENT

Supervisors:
Prof. Dr. Ir. Patrick Segers
Prof. Dr. Wim Ceelen
Prof. Dr. Ir. Charlotte Debbaut

Research lab:
Institute Biomedical Technology
Biofluid, Tissue and solid Mechanics for medical applications (bio-MMeda)
Ghent University
Corneel Heymanslaan 10 - blok B (entrance 36)
B-9000 Gent, Belgium

Members of the exam committee:

Chairman:

prof. Dr. Ir. Patrick De Baets	Faculty of Engineering and Architecture, UGent

Secretary:

Prof. Dr. Christian Vanhove	Faculty of Engineering and Architecture, UGent

Reading committee:

Prof. Dr. Christian Vanhove	Faculty of Engineering and Architecture, UGent
Prof. Dr. Katrien Remaut	Faculty of Pharmaceutics, UGent
Prof. Dr. Ir. Pascal Verdonck	Faculty of Engineering and Architecture, UGent
Prof. Dr. Ir. Geraldine Heynderickx	Faculty of Engineering and Architecture, UGent
Dr. Steven Sourbron	Department of Medical Physics, University of Leeds (UK)

TABLE OF CONTENTS

LIST OF FIGURES

LIST OF TABLES

ABBREVIATIONS AND SYMBOLS

The following list summarizes the most commonly used abbreviations and symbols in this thesis.

Abbreviations

2D	Two-dimensional
3D	Three-dimensional
ADC	Apparent Diffusion Coefficient
APD	Absolute Penetration Depth
AUC	Area Under the Concentration-time curve
CAF	Cancer Associated Fibroblast
CC	Completeness of Cytoreduction
CFD	Computational Fluid Dynamics
CRS	Cytoreductive Surgery
CT	Computed Tomography
DCE-MRI	Dynamic Contrast Enhanced Magnetic Resonanc Image
DDS	Drug Delivery System
DNA	Deoxyribonucleic Acid
DW-MRI	Diffusion Weighted Magnetic Resonanc Image
ECM	Extracellular Matrix
FA	Flip Angle
HIPEC	Hyperthermic Intraperitoneal Chemoperfusion
IC50	Half maximal Inhibitory Concentration
IFP	Interstitial Fluid Pressure
IFV	Interstitial Fluid Velocity
IP	Intraperitoneal
IPC	Intraperitoneal Chemotherapy
IV	Intravenous
LP50	Distance over which the pressure drops over 50%
MDCT	Multidetector Computed Tomography
MRI	Magnetic Resonanc Image

MW	Molecular Weight
PC	Peritoneal Carcinomatosis
PCI	Peritoneal Cancer Index
PD	Pharmacodynamics
PD%	Relative Penetration Depth percentage
PET	Positron Emission Tomography
PET/CT	Positron Emission Tomography Computated Tomography
PIPAC	Pressurized Intraperitoneal Aerosol Chemotherapy
PK	Pharmacokinetics
PM	Peritoneal Metastasis
RER	Rough Endoplasmatic Reticulum
ROI	Region Of Interest
TE	Echo Time
TR	Repetition Time
US	Ultrasound

Symbols

$\bar{\bar{\tau}}$	Stress tensor
β	First order elimination constant
$\frac{J_v}{V}$	Plasma filtration rate per unit volume
μ	Dynamic viscosity
∇	Divergence operator
∇^2	Laplacian operator
ϕ	Interstitial fluid volume fraction
Π_i	Interstitial osmotic pressure
Π_v	Vascular osmotic pressure
ρ	Density of the fluid
$\rho\vec{g}$	Gravitational force
σ	Osmotic reflection coefficient of vessels
$\vec{F}$	External body force
$\vec{v}$	Fluid velocity vector
c	Osmotic reflection coefficient for tracer
C_0	Boundary drug concentration
C_B	Concentration of drug in the systemic compartment
C_P	Concentration of drug in the peritoneal compartment
C_v	Concentration of drug in the vascular system
c_{AIF}	Concentration of the tracer in the plasma
C_{drug}	concentration of the drug present in the interstitial space
c_{GD}	Concentration of the tracer in the interstitial space
D	Diffusion coefficient

F_l	Lymphatic drainage term for interstitial fluid
F_v	Fluid gain from the blood
Hct	Hematocrit value
K	Conductivity of the tissue for interstitial fluid
k	Intrinsic permeability of the tissue
k_e	Elimination coefficient of drug from the systemic compartment
L	Length
L_e	Entrance length
L_i	Distance measured from the inlet of the catheter to the i$^{\text{th}}$ perforation
L_p	Hydraulic conductivity of the vasculature
p	Pressure
P_c	Permeability of the vessel wall
P_i	Interstitial fluid pressure
P_v	Vascular pressure
PA	Permeability-area product
Pe_v	Peclet number
Q	Flowrate
r	Radius
r_1	Relaxivity
r_i	radius of the i$^{\text{th}}$ perforation
Re	Reynolds number
S	Sink in drug concentration
S/V	Surface to volume ratio of vasculature
T	Temperature
t	Time
T_{10}	Native relaxation time
u	Interstitial fluid velocity
V_B	Distribution volume of the systemic compartment
V_P	Distribution volume of the peritoneal compartment

SAMENVATTING

INLEIDING

Kankers van organen in de peritoneale holte of van het peritoneum zelf geven vaak aanleiding tot een lokale verspreiding van tumoren in de vorm van peritoneale metastasen (PM). De prognose van patiënten met PM is pover en de levenskwaliteit is laag door complicaties zoals darmobstructie en ascites. Bovendien kunnen PM niet doeltreffend behandeld worden met intraveneuze chemotherapie (IV) door de beperkte bloedtoevoer naar de peritoneale oppervlakten en de slecht doorbloede tumorknobbels. Intraperitonale (IP) toediening van medicatie biedt een unieke behandelingsmogelijkheid voor patiënten met PM aangezien het peritoneum optreedt als barrière en de systemische blootstelling aan de medicatie inperkt. Ondanks een sterke rationale en veelbelovende klinische resultaten, wordt algemeen gebruik van de techniek momenteel belemmerd door de beperkte penetratiediepte van de geneesmiddelen in het tumorweefsel en de moeilijkheid om een adequate oppervlakteblootstelling van het gehele peritoneum te bekomen. Het is daarom van cruciaal belang om een beter inzicht te krijgen in de processen die ten grondslag liggen aan het transport van geneesmiddelen tijdens IP chemotherapie en het relatieve belang van de parameters die deze beïnvloeden.

In het eerste deel van dit manuscript wordt een achtergrondoverzicht gegeven van zowel peritoneale anatomie als pathofysiologie, gevolgd door een samenvatting van de stand van zaken van intraperitoneale chemotherapie. Het deel eindigt met een inleiding tot het medicijntransportproces tijdens intraperitoneale chemotherapie en de definitie van de onderzoeksdoelen van dit proefschrift. Het tweede deel richt zich op het oorspronkelijke onderzoek dat werd gedaan in het kader van dit proefschrift. In het eerste hoofdstuk wordt een nieuwe toedieningsmethode voor het maximaliseren van de peritoneale oppervlakte blootstelling tijdens interperitoneale chemotherapie (IPC) gepresenteerd. Hoofdstuk 2 richt zich

op de verschillende modellen voor IPC in de literatuur, terwijl we in hoofdstuk 3 ons eigen model presenteren voor het transport van geneesmiddelen tijdens IPC. In hoofdstuk 4 is het model aangepast om realistische geometrieën en ruimtelijk variërende vasculaire parameters te omvatten. Deel drie besluit dit proefschrift en suggereert enkele richtingen voor toekomstig onderzoek.

DEEL 1: INLEIDING, ACHTERGROND EN DOELSTELLINGEN VAN DIT PROEFSCHRIFT

Hoofdstuk 1: Anatomie en fysiologie van het peritoneum

In hoofdstuk één wordt de anatomie van het peritoneum zowel op macroscopisch als microscopisch niveau geïntroduceerd. Daarnaast worden de belangrijkste functies van het peritoneum besproken, zoals transmembraantransport, ontstekingsreactie en antigenpresentatie en de rol ervan bij weefselherstel. Het laatste deel van dit hoofdstuk beschrijft de peritoneale vloeistofstroom. Peritoneaal vocht heeft de neiging te stagneren in bepaalde gebieden in de peritoneale holte vanwege de complexe aard van de vloeistofstroom in combinatie met de specifieke peritoneale anatomie. Alle gebieden waar de vloeistof de neiging heeft om te stagneren zijn gewoonlijk de eerste plaatsen die betrokken zijn bij de peritoneale verspreiding van infecties en metastasen.

Hoofdstuk 2: Pathofysiologie van peritoneale metastasen

Patiënten met peritoneale carcinomatose lijden aan een verspreide groei van tumorknobbels in de peritoneale holte. De oorsprong van deze knobbeltjes kan gerelateerd zijn aan lokale peritoneale kankers of kan metastatisch zijn van een aantal verschillende intra- en extra-abdominale kankers. In dit hoofdstuk worden de meest voorkomende primaire en secundaire kankers die tot peritoneale carcinomatose leiden besproken. Een meer gedetailleerd overzicht van alle pathologieën die leiden tot peritoneale carcinomatose is opgenomen in bijlage 1. De vier verschillende types van verspreiding en tumorgroei worden besproken, met speciale aandacht voor het uitzaaien van tumorcellen via het peritoneale vocht. Verder worden de verschillende beeldvormingstechnieken besproken die worden gebruikt bij de diagnose, het beheer en de follow-up van patiënten met peritoneale carcinomatose. Zowel positron-emissie tomografie-computertomografie (PET-CT) als diffusie-gewogen magnetische resonantie beeldvorming (DW-MRI) kunnen PM weergeven met zeer goede

gevoeligheids- en specificiteitsresultaten en de keuze tussen beide technieken is vaak gebaseerd op expertise en voorkeur. Geen enkele techniek is op dit moment echter in staat om peritoneale metastasen met 100% zekerheid te diagnosticeren en / of te stadiëren en daarom blijft de noodzaak voor een laparoscopie of een kijkoperatie tot op heden bestaan.

Hoofdstuk 3: Intraperitoneale chemotherapie

De rationale achter intraperitoneale chemotherapie is dat bij toediening van cytotoxische geneesmiddelen direct in de peritoneale holte, het peritoneum als een barrière werkt en de geneesmiddelabsorptie in de systemische circulatie beperkt. Dit resulteert in hogere lokale concentraties van het geneesmiddel in het tumorweefsel terwijl systemische bijwerkingen worden geminimaliseerd. Sinds deze farmacokinetische voordelen van IPC aangetoond zijn, startten veel groepen klinische studies over deze techniek. Hoewel de lokale hoge geneesmiddelconcentraties experimenteel zijn aangetoond, wordt het algemeen gebruik van IPC beperkt door de beperkte penetratiediepte van de geneesmiddelen in het tumorweefsel. Momenteel is er een grote verscheidenheid aan IPC-procedures, wat de directe vergelijking tussen verschillende onderzoeken bemoeilijkt. Niet alleen de gebruikte medicijnen en doseringen verschillen, maar er zijn ook verschillen in chirurgische technieken, duur en timing van de behandeling. In het laatste deel van dit hoofdstuk worden de verschillen tussen IPC-protocollen besproken.

Hoofdstuk 4: Geneesmiddeltransport tijdens intraperitoneale chemotherapie

Geneesmiddeltransport tijdens intraperitoneale chemotherapie is een complex proces dat niet alleen bepaald wordt door medicijn- en therapie-gerelateerde parameters, maar ook door weefsel-parameters. Om beter te begrijpen hoe al deze parameters de penetratie van het medicijn tijdens IPC beïnvloeden beschrijft dit hoofdstuk de verschillende stappen die optreden in het geneesmiddeltransport proces tijdens de IPC. Een tweede deel van dit hoofdstuk concentreert zich op studies die bepaalde parameters van dit geneesmiddeltransport tijdens IPC wijzigden, en de effecten die deze wijzigingen hadden op de therapeutische resultaten.

Hoofdstuk 5: Uitdagingen voor intraperitoneale chemotherapie en onderzoeksdoelstellingen

Hoewel er een sterke rationale is voor intraperitoneale chemotherapie en klinische resultaten haar nut in talrijke gevallen heeft bewezen, zijn er een aantal problemen die het algemeen gebruik van de techniek beperken. Dit hoofdstuk belicht de twee belangrijkste beperkingen voor IPC: een onvoldoende oppervlakblootstelling en de beperkte penetratiediepte van het geneesmiddel in het weefsel. Ons eerste onderzoeksdoel is het ontwerp en de ontwikkeling van een nieuw kathetertype dat een adequate behandeling van het volledige peritoneale oppervlak mogelijk zal maken, terwijl de problemen met instillatie van grote hoeveelheden vloeistof worden vermeden, en langdurige continue infusie mogelijk wordt met behulp van een door de patiënt gedragen pomp. Het tweede onderzoeksdoel van dit werk richt zich op de ontwikkeling van een wiskundig model om de verdeling van geneesmiddelen tijdens intraperitoneale chemotherapie te bestuderen.

DEEL 2: MODELLERING VAN MEDICATIETRANSPORT TIJDENS INTRAPERITONEALE CHEMOTHERAPIE

Hoofdstuk 6: Een nieuw mechanisme voor toediening van medicatie voor intraperitoneale chemotherapie: ontwerp, ontwikkeling en testen.

Omdat PM moeilijk te behandelen zijn en significante en invaliderende symptomen kunnen veroorzaken, is er een toenemende interesse van clinici in de combinatie van cytoreductieve chirurgie met intraperitoneale (IP) geneesmiddeltoediening. Op dit moment wordt IP-chemotherapie ofwel in een open, laparoscopische of gesloten opstelling toegediend. De meeste op dit moment gebruikte methoden zijn niet compatibel met een langdurige of continue IP-geneesmiddeltoediening, hetgeen meer en meer wordt erkend als een belangrijke bepalende factor voor de werkzaamheid tegen kanker van het geneesmiddel. Bij behandelingen waarbij meerdere rondes IPC worden toegediend, is de operatieve plaatsing van een katheter met één filament (Tenckhoff-type) diep in het bekken de meest voorkomende techniek. Deze methode staat echter niet toe om het aangetaste peritoneale oppervlak op een homogene en effectieve manier te behandelen. In dit hoofdstuk presenteren en bespreken we een eenvoudige maar innovatieve multifilamentkatheter die een meer homogene en langdurige toediening van IPC mogelijk maakt. Het ontwerp

van de katheter is gebaseerd op praktische en theoretische overwegingen met gebruik van computationele vloeistofdynamica-modellering van de stroming door de katheterarmen. De ontwerpen werden vervaardigd door microdrilling of laserablatie van de perforaties en werden hydraulisch getest. Hoewel alle voorgestelde geometrieën goed presteerden in simulaties, presteerde geen van deze eerste prototypes goed tijdens de in vitro testen. De reden voor deze teleurstellende prestaties was terug te voeren op productieproblemen en onnauwkeurigheden.

Hoofdstuk 7: Modelleren van geneesmiddeltransport tijdens intraperitoneale chemotherapie: een literatuurstudie

Geneesmiddelpenetratie in vaste tumoren is een complex massatransportproces dat bepaald wordt door een velvoud aan parameters die niet alleen betrekking hebben tot de gebruikte cytotoxische geneesmiddelen, maar ook tot de tumorweefseleigenschappen en zelfs de therapeutische opzet. Mathematische modellering kan unieke inzichten bieden in de verschillende transportbarrières die optreden tijdens IP-chemotherapie, en biedt ook de mogelijkheid om verschillende protocollen of geneesmiddelen te testen zonder de noodzaak voor in vivo experimenten. In dit hoofdstuk wordt de stand van zaken van het modelleren van IPC gepresenteerd. Er wordt een onderscheid gemaakt tussen drie verschillende typen modellen op basis van de gebruikte schaal in het model: op schaal van het hele orgaan, waarbij het peritoneum als een enkel compartiment wordt beschouwd; op schaal van het weefsel, waarbij het weefsel van de tumor wordt beschouwd als een homogeen mengsel van cellen, interstitium en vasculatuur; en tot slot het cellulaire model, dat elke cel expliciet modelleert. Voor elk model hebben we besproken welke stappen in het transportproces zijn opgenomen, en waar welke veronderstellingen en aannames zijn gemaakt. Hoewel alle relevante transportstappen tijdens IP-chemotherapie reeds gemodelleerd zijn, is er tot op heden geen model dat in staat is om alle complexe processen die optreden tijdens IP-chemotherapie volledig te modelleren. De bestaande modellen zijn divers en zijn niet goed en niet slecht, maar hebben elk hun eigen voordelen en beperkingen.

Hoofdstuk 8: Wiskundige modellering van intraperitoneale chemotherapie: simulatie van de geneesmiddel verdeling in een tumorknobbel

Hoewel de intraperitoneale (IP) toediening van chemotherapie hogere intratumor-concentraties van het geneesmiddel mogelijk maakt in

vergelijking met intraveneuze toediening, is de penetratie van het geneesmiddel in het tumorweefsel nog steeds beperkt tot enkele millimeters. Het is dus noodzakelijk om de beperkende factoren van deze gelimiteerde penetratie beter te begrijpen om de doeltreffendheid van IP-chemotherapie te verbeteren. Door het ontwikkelen van een driedimensionaal numeriek stromingsmodel (computational fluid dynamics; CFD) voor geneesmiddeltransport in een tumorknobbel, onderzochten we de impact van een aantal belangrijke parameters op het geneesmiddeltransport en de penetratiediepte tijdens IP-chemotherapie. Het model omvatte het diffusief-convectief transport met de karakteristieke radiaal-naar-buiten gerichte stroming van interstitiële vloeistof ten gevolge van de hoge interstitiële vloeistofdruk in de vaste tumor, evenals andere kenmerken zoals vasculaire opname en cellulaire opname van het medicijn. Baseline-cases van het model werden voorgesteld voor twee verschillende groottes van drie verschillende geometrieën. Het model werd gebruikt om de invloed van vasculaire normalisatietherapie, diffusiviteit van verschillende geneesmiddelen, de aanwezigheid van een necrotische kern en weefselpermeabiliteit op de geneesmiddelpenetratie te bestuderen. De penetratiedieptes van geneesmiddelen gevonden in dit werk waren in goede overeenstemming met de gedefinieerde bereiken beschreven in experimentele studies. Over het algemeen vertoonden kleinere tumoren een betere penetratie dan grotere, wat kan worden toegeschreven aan de lagere interstitiële vloeistofdruk (IFP) in kleinere tumoren. Bovendien toonde het model grote verbeteringen in penetratiediepte wanneer de tumorknobbels vasculaire normalisatietherapie ondergingen. Het illustreerde eveneens het belang van welk medicijn gebruikt wordt voor de therapie. Het expliciet modelleren van de necrotische kern had een beperkt effect op de gesimuleerde penetratie. Gelijklopend hiermee bleef de penetratiediepte vrijwel constant wanneer de Darcy-permeabiliteit van het weefsel veranderde.

Hoofdstuk 9: Een 3D CFD-model van interstitiële vloeistofdruk en geneesmiddeldistributie in heterogene tumorknobbels tijdens intraperitoneale chemotherapie

In dit hoofdstuk werd het 3D CFD -model van het geneesmiddelentransport in de geïdealiseerde tumorknobbels tijdens IP-chemotherapie zoals beschreven in hoofdstuk 8 uitgebreid met realistische tumorgeometrieën en ruimtelijk variërende vasculaire eigenschappen. Om deze te implementeren, werd gebruik gemaakt van een muismodel met peritoneale

metastasen waaruit enerzijds de tumorgeometrieën konden gesegmenteerd worden en waarin anderzijds interstitiële vloeistofdrukken invasief gemeten konden worden ter validatie van het model. We modelleerden drie verschillende tumorknobbel-geometrieën van verschillende groottes en leidden ruimtelijk variërende microvasculatuur gerelateerde parameters van dynamic contrast enhanced magnetische resonantie afbeeldingen (DCE-MRI) af voor elk van de proefdieren. Met behulp van deze parameters werden drukvelden gesimuleerd in de tumoren en het transport van geneesmiddelen werd bestudeerd in elk van de drie tumorgeometrieën in de aanwezigheid van het overeenkomstige drukveld. We stelden vast dat de resulterende interstitiële drukprofielen in tumoren sterk afhankelijk waren van de onregelmatige geometrieën en aanwezigheid van verschillende zones. De tumorspecifieke cisplatine-penetratiedieptes varieerden van 0.32 mm tot 0.50 mm, wat goed overeenstemt met het experimenteel gedefinieerde bereik. We vonden dat de positieve correlatie tussen tumorgrootte en IFP niet langer aanwezig was in de aanwezigheid van zones met verschillende vasculaire eigenschappen, terwijl we wel een positieve relatie vonden tussen het percentage levensvatbaar tumorweefsel en de maximale IFP. Deze bevindingen benadrukken het belang van het opnemen van zowel de onregelmatige tumorgeometrieën als verschillende vasculaire zones in CFD-modellen van IPC.

DEEL 3: CONCLUSIES

De conclusies vatten kort de belangrijkste bevindingen van dit werk samen en werpen een kritische blik op de impact en de beperkingen van dit werk om een goed overzicht te krijgen van waar we nu zijn met dit onderzoek en wat de toekomst zou kunnen brengen.

SUMMARY

Cancers originating from organs in the peritoneal cavity or the peritoneum itself are prone to loco-regional spread in the form of peritoneal metastasis (PM). The prognosis of patients who develop PM is usually poor and quality of life is low due to complications, such as bowel obstructions and ascites. Furthermore, PM cannot be adequately treated by using intravenous (IV) chemotherapy due to the poor blood supply to the peritoneal surfaces and poorly vascularized tumor nodules. Intraperitoneal drug delivery offers a unique treatment opportunity for those patients with oncological malignancies confined to the peritoneal cavity, because of the peritoneum acting as a barrier and thereby limiting systemic drug exposure. Despite a strong rationale and promising clinical results, widespread use of the technique is currently hampered by the limited penetration depth of the drugs into the tumor tissue and the difficulty to obtain an adequate surface exposure of the entire peritoneum. It is therefore crucial to gain a better understanding of the processes that underlie the drug transport and the relative importance of the parameters influencing it.

In the first part of this manuscript, we will provide a background overview of both peritoneal anatomy and pathophysiology, followed by a summary of the state of the art of intraperitoneal chemotherapy. This part ends with an introduction into the drug transport process during intraperitoneal chemotherapy and the definition of the research goals of this dissertation. The second part focusses on the original research that was done in the context of this dissertation. In the first chapter a novel delivery method to maximize the peritoneal surface exposure during intraperitoneal chemotherapy (IPC) is presented. Chapter 2 focusses on the different mathematical and computational models for IPC while in chapter 3, we present our own model for the drug transport during IPC. In chapter 4, the model is adapted to include realistic tumor geometries and spatially varying vascular parameters. Part three concludes this dissertation and suggests some perspectives for future research.

PART 1: INTRODUCTION, BACKGROUND AND GOAL OF THIS DISSERTATION

Chapter 1: Anatomy and physiology of the peritoneum

In chapter one, the anatomy of the peritoneum is introduced on both the macroscopic and microscopic level. In addition, the main functions of the peritoneum are discussed, such as transmembrane transport, inflammation response and antigen presentation and its role in tissue repair. The final section of this chapter features the hallmarks of peritoneal fluid flow. The peritoneal fluid tends to stagnate at certain regions within the peritoneal cavity due to the complex nature of the fluid flow combined with the specific peritoneal anatomy. Any areas in which the fluid tends to stagnate are commonly the first sites to be involved in the peritoneal spread of infections and metastases.

Chapter 2: Pathophysiology of peritoneal metastases

Patients with peritoneal carcinomatosis suffer from a widespread growth of tumor nodules in the peritoneal cavity. The origin of these nodules can be related to either native, peritoneal cancers or can be metastatic from a number of different intra- and extra abdominal cancers. In this chapter, the most common primary and secondary cancers that lead to peritoneal carcinomatosis are discussed. A more detailed overview of all pathologies leading to peritoneal carcinomatosis can be found in Appendix 1. The four different types of dissemination and tumor growth are discussed, with a special attention to the seeding of tumor cells through the peritoneal fluid. Furthermore, the different imaging modalities used in the staging, management and follow-up of patients with peritoneal malignancies are discussed. Both positron-emission tomography-computed tomography (PET-CT) and diffusion-weighted magnetic resonance imaging (DW-MRI) are able to show PM with very good sensitivity and specificity results and the choice between both techniques is often based on expertise and preference. However, no technique is at this point able to diagnose and/or stage peritoneal metastasis with 100% certainty and the need for a laparoscopy or exploratory surgery remains at this point.

Chapter 3: Intraperitoneal chemotherapy

The rationale behind intraperitoneal chemotherapy is that upon administration of cytotoxic drugs directly into the peritoneal cavity, the peritoneum acts as a barrier and limits the drug absorption in the systemic

circulation. This results in higher local drug concentrations in the tumor tissue while minimizing the development of systemic side effects. Since the demonstration of these pharmacokinetic advantages obtained through during IPC, numerous groups started clinical trials using the technique, but even though the local high drug concentrations have been shown experimentally, the widespread use of IPC is limited by the insufficient penetration depth of the drugs into the tumor tissue. Currently, there is a huge variety in IPC procedures that are performed, complicating the direct comparison between different studies. Not only do the drugs used and dosages differ, but there are also differences in surgical techniques, duration and timing of the treatment. In the final part of this chapter, the differences between various IPC protocols are discussed.

Chapter 4: Drug transport during intraperitoneal chemotherapy

Drug transport during intraperitoneal chemotherapy is a complex process that is governed not only by drug- and therapy-related parameters, but also by tissue-related parameters. To better understand how these parameters influence the drug penetration during IPC, this chapter will provide an overview of the different steps that occur in the drug transport process during IPC. A second part of this chapter focusses on the studies that modified some of the governing parameters of drug transport during IPC and their effects on therapeutic outcomes.

Chapter 5: Current challenges for intraperitoneal chemotherapy and research goals

Although there is a strong rationale for intraperitoneal chemotherapy and clinical results have proven their merit on numerous occasions, there are a number of issues that limit the widespread use of the technique. This chapter will highlight the two main limitations for IPC: inadequate surface exposure and limited penetration depth of drug into the tissue. Our first research goal is the design and development of a novel catheter type that will allow adequate treatment of the complete peritoneal surface while avoiding the problems related to the instillation of large volumes of fluid, and permitting prolonged continuous infusion using a patient wearable pump. The second research goal of this work focusses on the development of a mathematical model to study drug distribution during intraperitoneal chemotherapy.

PART 2: MODELING DRUG TRANSPORT DURING INTRAPERITONEAL CHEMOTHERAPY

Chapter 6: A new drug delivery system for intraperitoneal chemotherapy: design, development and bench testing

Despite advances in systemic anticancer therapy, treatment of peritoneal metastases (PM) remains a considerable challenge. Since PM are difficult to treat and may cause significant and invalidating symptoms, there is increasing interest from clinicians in the combination of cytoreductive surgery with intraperitoneal (IP) drug delivery. Currently, IP chemotherapy is administered either in an open, laparoscopic or closed set-up. Most currently used methods do not allow prolonged or continuous IP drug instillation, which is increasingly recognized as a major determinant of the anticancer efficacy of the IP drug. Current state of the art of the treatments where multiple rounds of IPC are envisioned include the operative placement of a single-filament catheter (Tenckhoff Type) deep in the pelvis. This method however does not allow to treat the affected peritoneal surface in a homogenous and effective manner. In this chapter, we propose and discuss a simple yet innovative multi-filament catheter that allows for a more homogeneous and prolonged delivery of IPC. The design of the catheter was based on both theoretical considerations and computational fluid dynamics modeling of the flow through the catheter arms. The designs were manufactured by either microdrilling the perforations or laser ablation and underwent hydraulic testing. Even though all proposed geometries performed well in simulations, none of these first prototypes performed well during the in vitro testing. The reason for this underwhelming performance was traced back to manufacturing issues and inaccuracies.

Chapter 7: Modeling drug transport during intraperitoneal chemotherapy: a literature review

Drug penetration into solid tumors is a complex mass transport process that involves multiple parameters not only related to the used cytotoxic agents, but also to the tumor tissue properties and even the therapeutic set-up. Mathematical modeling can provide unique insights in the different transport barriers that occur during IP chemotherapy, as well as offer the possibility to test different protocols or drugs without the need for in vivo experiments. In this chapter, the state of the art of the modeling of IPC is presented. A distinction is made between three different types

of models based on the used scale in the model: the whole organ scale, which considers the peritoneum as a single compartment; the tissue scale, which considers the tissue of the tumor as a homogenous mixture of cells, interstitium and vasculature; and finally the cellular model, which models each cell explicitly. For each model, we discussed which steps of the transport process are included and where assumptions are made. Although all relevant transport steps during IP chemotherapy have been modeled, there is to date no model that is able to fully model all the complex processes that occur during IP chemotherapy. The existing models are diverse and each one is neither good nor bad but comes with its own set of advantages and limitations.

Chapter 8: Mathematical modeling of intraperitoneal drug delivery: simulation of drug distribution in a single tumor nodule

Although the intraperitoneal (IP) administration of chemotherapy allows for higher intratumor concentrations of the cytotoxic agent compared to intravenous administration, the drug penetration depths into the tissue are still limited to a few millimeters. It is thus necessary to better understand the limiting factors behind this poor penetration in order to improve IP chemotherapy delivery effectiveness. By developing a three-dimensional computational fluid dynamics (CFD) model for drug penetration in a tumor nodule, we investigated the impact of a number of key parameters on the drug transport and penetration depth during IP chemotherapy. The model included the diffusive-convective transport with the characteristic radially outward flow of interstitial fluid due to the high interstitial fluid pressure in the solid tumor as well as other typical features such as vascular uptake of the drug and cellular uptake. Baseline cases of the model were presented for two different sizes of three different geometries. The model was used to study the influence of vascular normalization therapy, drug diffusivity, the presence of a necrotic core and tissue permeability on the drug penetration. All penetration depths of drugs found in this work were in good agreement with the defined ranges described in experimental studies. Overall, smaller tumors showed better penetration than larger ones, which could be attributed to the lower interstitial fluid pressure (IFP) in smaller tumors. Furthermore, the model demonstrated large improvements in penetration depth by subjecting the tumor nodules to vascular normalization therapy and illustrated the importance of the drug that is used for therapy. Explicitly modeling the necrotic core had a limited effect on the simulated penetration. Similarly, the penetration depth remained virtually constant when the Darcy permeability of the tissue changed.

Chapter 9: A 3D CFD model of the interstitial fluid pressure and drug distribution in heterogeneous tumor nodules during intraperitoneal chemotherapy

In this chapter, we expanded the 3D Computational Fluid Dynamics (CFD) model of the drug mass transport in idealized tumor nodules during IP chemotherapy as described in chapter 8 to include realistic tumor geometries and spatially varying vascular properties. To do so, a mouse peritoneal metastases model was used from which tumor geometries could be obtained and interstitial fluid pressures could be measured invasively as a validation. We modeled three different tumor nodule geometries of different sizes and extracted spatially varying microvasculature related parameters from dynamic contrast enhanced magnetic resonance images (DCE-MRI) for each animal. Using these parameters, pressure fields were simulated in the tumors and drug transport was studied in all three tumor geometries in the presence of the corresponding pressure field. We found that the resulting interstitial pressure profiles within tumors were highly dependent on the irregular geometries and different zones. The tumor-specific cisplatin penetration depths ranged from 0.32 mm to 0.50 mm, which is in good agreement with the experimentally defined range. We found that the positive relationship between tumor size and IFP did not longer hold in the presence of zones with different vascular properties, while we did observe a positive relationship between the percentage of viable tumor tissue and the maximal IFP. These findings highlight the importance of incorporating both the irregular tumor geometries and different vascular zones in CFD models of IPC.

Part 3: conclusions

Here, we recapitulate the key findings and achievements of this work and offers some critical considerations of the limitations and impact of our research to get a sense of where we are now and what could be next.

INTRODUCTION AND PROBLEM STATEMENT

Cancers originating from organs in the peritoneal cavity or the peritoneum itself are prone to loco-regional spread in the form of peritoneal metastasis (PM). The prognosis of patients who develop PM is usually poor and quality of life is low due to complications, such as bowel obstructions and ascites. Furthermore, PM cannot be adequately treated by using intravenous chemotherapy due to the poor blood supply to the peritoneal surfaces and poorly vascularized tumor nodules. Intraperitoneal drug delivery offers a unique treatment opportunity for those patients with oncological malignancies confined to the peritoneal cavity, because of the peritoneum acting as a barrier and thereby limiting systemic drug exposure. Despite a strong rationale and promising clinical results, widespread use of intraperitoneal chemotherapy is currently hampered by the limited penetration depth of the drugs into the tumor tissue and the difficulty to obtain an adequate surface exposure of the entire peritoneum.

RESEARCH OBJECTIVE

The scope of the Biommeda research group is very broad with research ranging from the study of flow and transport processes in blood and biological fluids in the cardiovascular system and artificial organs to biomechanical aspects of the cardiovascular and the skeleto-muscular system and medical devices. The group has been located at the campus of the Ghent university hospital since 2007 and has made the most of this location by collaborating with numerous pharmacology, biomedical and medical groups. One of these collaborations was the FWO-project: "Integrated Dynamic Functional Imaging and Numerical Simulation of Mass Transport for the Assessment of Intraperitoneal Chemotherapy for Carcinomatosis" supervised and co-supervised by Patrick Segers, Wim Ceelen, Christian

Vanhove and Olivier De Wever. It is the context of this project and due to its funding that the research in this dissertation was done.

The research objective of this work is to use computational fluid dynamic modelling of intraperitoneal drug delivery to both propose a novel drug delivery mechanism and to gain insight in how different parameters potentially influence drug penetration depths, all with a view to improve outcomes of IPC.

STRUCTURE OF THIS DISSERTATION

This dissertation is divided in three parts:

- Introduction, background and goal of this dissertation

- Modeling drug transport during intraperitoneal chemotherapy

- Conclusion

In the first part of this manuscript, we provide a background overview of both peritoneal anatomy and physiology (chapter 1) and pathophysiology of peritoneal metastases (chapter 2). chapter 3 summarizes the rationale behind intraperitoneal chemotherapy and its current state of the art. The drug processes underlying mass transport during intraperitoneal chemotherapy and its determining parameters are introduced in chapter 4. At the end of this part, we focus the attention to the main limitations of intraperitoneal chemotherapy at this point in time and use these to define the research goals of this dissertation.

The second part focusses on the original research that was done in the context of this dissertation. In the first chapter a novel delivery method to maximize the peritoneal surface exposure during intraperitoneal chemotherapy (IPC) is presented. chapter 2 summarizes the literature on the different mathematical and computational models for IPC while in chapter 3, we present our own model for the drug transport during IPC. In chapter 4, the model is enhanced to include realistic tumor geometries and spatially varying vascular parameters.

Part three concludes this dissertation and suggests some perspectives for future research.

L<small>IST OF PUBLICATIONS</small>

First author peer-reviewed papers:

- Margo Steuperaert, Giuseppe Falvo D'Urso Labate, Charlotte Debbaut, Olivier De Wever, Christian Vanhove, Wim Ceelen and Patrick Segers, Mathematical Modeling of Intraperitoneal Drug Delivery: Simulation of Drug Distribution in a Single Tumor Nodule. DRUG DELIVERY, 2017, 24:491-501

- Margo Steuperaert, Charlotte Debbaut, Patrick Segers, Wim Ceelen, Modelling Drug Transport During Intraperitoneal Chemotherapy. PLEURA AND PERITONEUM, 2017, 2(2). p.73-83

- Margo Steuperaert, Charlotte Debbaut, Charlotte Carlier, Olivier De Wever, Benedicte Descamps, Christian Vanhove, Wim Ceelen and Patrick Segers, A 3D CFD model of the interstitial fluid pressure and drug distribution in heterogeneous tumor nodules during intraperitoneal chemotherapy, DRUG DELIVERY, 2019, VOL. 26, NO. 1, 404–415.

Co-author peer-reviewed paper:

- Charlotte Carlier, Ada Mathys, Emiel De Jaeghere, Margo Steuperaert, Olivier De Wever and Wim Ceelen, Tumour tissue transport after intraperitoneal anticancer drug delivery. INTERNATIONAL JOURNAL OF HYPERTHERMIA, 2017, 33(5), 534-542.

I

Introduction, background and goal of this dissertation

Understanding peritoneal anatomy -both macro and microscopically- and physiology, is key in understanding the origins and spread of peritoneal metastasis. In the first chapter we provide a general introduction to these concepts as well as a section devoted to the flow of intraperitoneal fluid. In the second chapter the pathophysiology of peritoneal metastasis (PM) is discussed with special attention to the origins, pathways of dissemination, prognosis and imaging techniques used. In a third introductory chapter, the rationale behind intraperitoneal chemotherapy will be explained and the state-of-the-art of IPC will be discussed. The drug transport process during IPC is the subject of chapter 4 and in chapter 5 the research goals of this dissertation will be proposed based on a brief summary of the current limitations and challenges of IPC.

ANATOMY AND PHYSIOLOGY OF THE PERITONEUM

1.1 MACROSCOPIC ANATOMY

The peritoneum is the largest serous membrane in the body with a total surface area of approximately 1.8 m^2 and consists of the parietal peritoneum, which forms the lining of the abdominal wall, and the visceral peritoneum, which covers the abdominal organs (figure 1.1a) [295]. In men, the peritoneal cavity is closed (figure 1.2a), but in women, it is discontinuous at the ostia of the oviducts, providing a communication between the peritoneal cavity and the lower pelvis, which is extraperitoneal (figure 1.2b). The parietal peritoneum, which is thought to account for around 20% of the total surface derives its blood supply from the vasculature of the abdominal wall [295]. It also shares the same nerve supply as the region of the abdominal wall it lines and is sensitive to pressure, temperature and laceration[147, 271] with pain originating from the visceral peritoneum being well-localized.

The visceral peritoneum on the other hand, accounts for the remaining 80% of total peritoneal surface and gets its vascular supply mainly from the superior mesenteric artery and drains in the portal vein [147]. It has the same nerve supply as the viscera it covers and pain originating from this region is poorly localized and only sensitive to stretch and
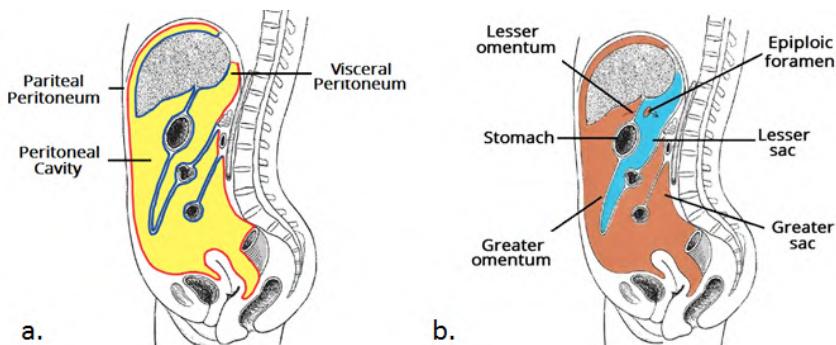
Figure 1.1: Sagittal section of the sub-diaphragmatic space. (A) Visceral peritoneum covering the intraperitoneal organs and parietal peritoneum lining the abdominal wall. (B). The greater (brown) and lesser sac (blue) are two cavities in the peritoneal space. Both spaces are connected by the epiploic formamen. Source URL: https://teachmeanatomy.info/abdomen/areas/peritoneum/

chemical irritation [271]. The space between the visceral and parietal peritoneum is the peritoneal cavity and it is comprised of a number of ligaments, the greater and lesser omentum (figure 1.1b), as well as a number of mesenteries and several peritoneal folds, pouches and recesses.

The omentum is a double layer of visceral peritoneum that contains fatty tissue, lymph nodes and blood vessels and extends from the stomach and proximal part of the duodenum to other abdominal organs (figure 1.1b). The greater omentum descends from the greater curvature
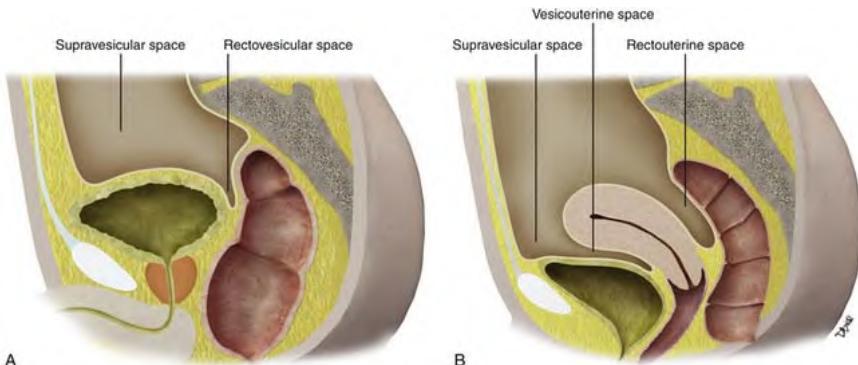
Figure 1.2: Sagittal views of the male (A) and female (B) pelvis demonstrate the peritoneal covering. In males, the greater peritoneal cavity is a closed continuous cavity. In females, it is in contact with the extraperitoneal pelvis through the fallopian tubes. Source URL: https://clinicalgate.com/peritoneal-cavity-and-gastrointestinal-tract/

of the stomach and proximal part of the duodenum, overlies the small intestine and folds back upwards to connect to the anterior surface of the transverse colon. The lesser omentum extends between the liver and the lesser curvature of the stomach. Historically, mesenteries were described as two folds of visceral peritoneum that connect a portion of the bowel to the retroperitoneum. Recent works however showed that the mesentery is in fact continuous, from duodenum to rectum and might be classified as a separate organ [47]. The mesentery consists of connective tissue, adipocytes, the intestinal vasculature, lymphatics and two layers of mesenteric peritoneum. It arises from the mesenteric root (location where the parietal peritoneal lining of the abdominal wall detaches) and suspends the intestines in the abdominal cavity [2]. Ligaments are double layers of visceral peritoneum that support organs in the peritoneal cavity. The latter can contain lymph nodes, vasculature and are usually named after the two structures it interconnects. (e.g. gastrocolic ligament connecting the stomach and the colon, splenocolic ligament connecting the spleen and the colon, . . .) [24, 147, 295].

1.2 MICROSCOPIC ANATOMY

Microscopically, both the visceral and parietal peritoneum consist of three distinctive layers: a single layer of mesothelial cells and a layer of submesothelial stroma, separated by a basal lamina (figure 1.3).

1.2.1 Mesothelial layer and basal lamina

The mesothelium consists of a single layer of predominantly flattened squamous and in lesser numbers cuboidal mesothelial cells (figure 1.4a and figure 1.4b). Both cell types differ in their intracellular structure with squamouslike mesothelial cells containing little mitochondria, a poorly developed Golgi apparatus and only a small amount of rough endoplasmatic reticulum (RER) and a round or oval nucleus [200, 218]. Cuboidal mesothelial cells on the other hand have a more prominent central nucleolus, abundant mitochondria and RER, a well-developed Golgi apparatus, as well as more pronounced microtubules and microfilaments [135, 196, 197]. The cuboidal mesothelial cells can be found in various areas of the peritoneal membrane including the peritoneum of the liver and spleen and the milky spots of the omentum [145, 291]. Milky spots are on a microscopic level characterized by stomata in the mesothelial cell layer and the presence of leukocytes (figure 1.4c). The stomata are cavities
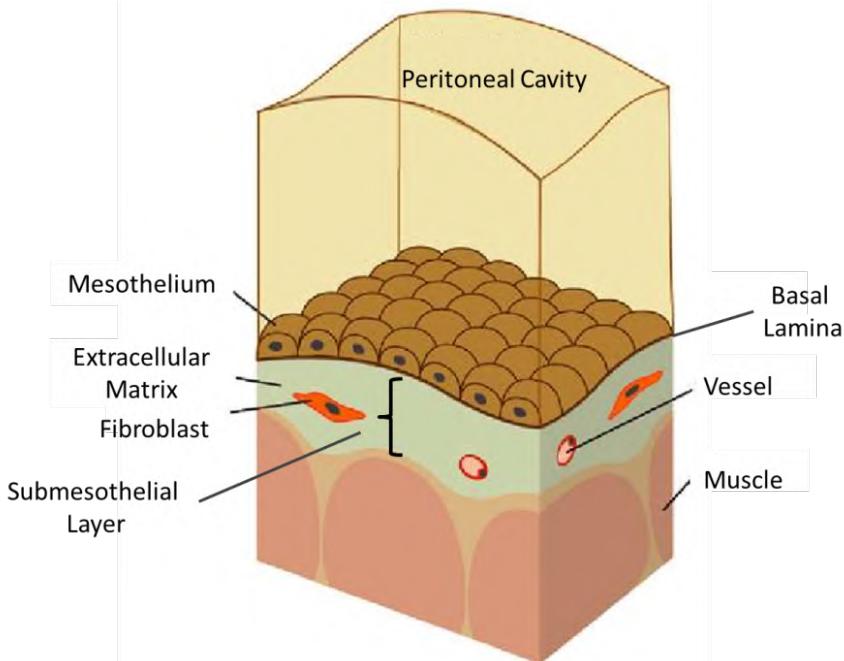
Figure 1.3: Microscopic anatomy of the peritoneum showing the three distinctive layers. Adapted from: http://dx.doi.org/10.5772/56598

at the junction of two or more mesothelial cells. They have a 3-12 μm diameter and provide a direct access to the underlying submesothelial lymphatic system allowing for the rapid removal of fluid, cells, bacteria and particles [136, 199, 200]. This is important in the context of this work as they provide a direct link between the peritoneal and abdominal cavities. Clinical findings indicate that peritoneal metastases are often found at the milky spot such as the greater omentum (but also at other regions with a large number of milky spots such as the mesenterium and pelvic floor). The preferential attachment of cancer cells to the exposed extracellular matrix (ECM) has been proposed as a possible explanation for this finding [136, 199, 200].

The basement membrane has a thickness smaller than 100 nm and its main function is to suppor the mesothelial layer and act as a selective barrier to macromolecules entering the submesothelial layer below [295].

1.2.2 Submesothelial layer

The submesothelial layer consists of an ECM made up of collagen fibers, glycoproteins, glycosaminoglycans and proteoglycans. In this layer blood
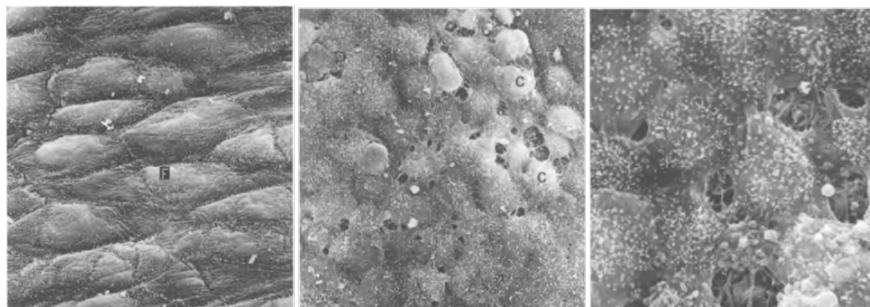
Figure 1.4: Scanning electron microscopy images of mesothelium of the human pelvic peritoneum. a. Squamous mesothelial cells b. Cuboidal mesothelial cells c. The lymphatic stomata appear as shallow pits and the fibers of the submesothelial connective tissue can be seen through these stomata. Adapted from: https://doi.org/10.1016/S0940-9602(97)80104-5.

vessels, lymphatics, and various cell types (fibroblasts, resident tissue macrophages, and mast cells) can be found as well as some immune cells (figure 1.5).

1.2.2.1 Microvasculature anatomy

The peritoneal microcirculation is located in the submesothelial stroma and comprises of arterioles, venules and capillaries. The parietal peritoneum gets its blood supply from the arteries of the abdominal wall and by parietal pelvic arteries, and drains into the inferior vena cava. The mesenteric, coeliac and visceral pelvic arteries supply blood to the visceral
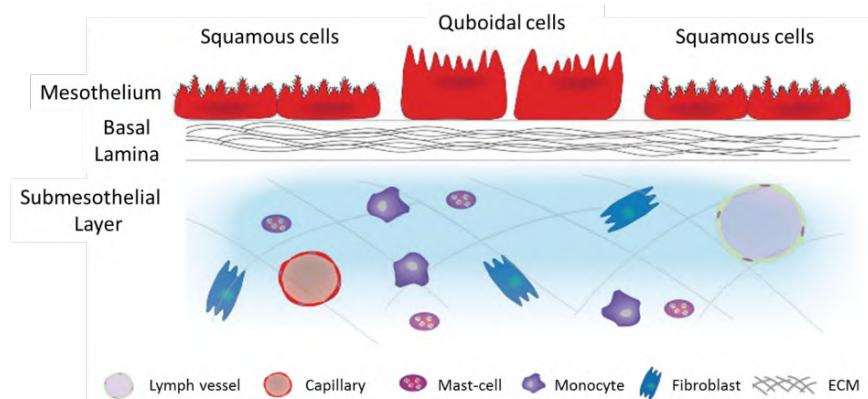
Figure 1.5: Microscopic anatomy of the peritoneum showing both types of mesothelial cells (squamous and quboidal) and the structure of the submesothelial layer. Adapted from: DOI: 10.3748/wjg.v22.i34.7692

peritoneum and the venous blood drains into the portal vein [295]. This is an important anatomical and physiological consideration as it means that drugs that are absorbed at the microcirculation of the visceral peritoneum, pass through the hepatic circulation before reaching the systemic circulation (first-pass). Exchange of solutes occurs at the capillary level and the solute and water transport capacity of the peritoneum depends on the capillary density and perfusion [147].

1.2.2.2 Lymphatic anatomy

The peritoneum has a well-defined lymphatic system in which intraperitoneal fluid is transported through the mesothelial lining of the peritoneum (i.e. the lymphatic stomata), into the celiac, superior mesenteric, and periportal lymph node groups before flowing into the thoracic duct by efferent visceral lymphatics [147]. Fluid in the abdominal cavity also drains via diaphragmatic lymphatic channels towards the caudal and anterior mediastinal lymph nodes [147].

1.3 PHYSIOLOGY OF THE PERITONEUM

Up to a few decades ago, the peritoneum was considered to be a passive membrane that supported the abdominal organs and facilitated intracoelomic movements with its lubricating function [295]. While the above is true, it has been determined since that peritoneal cells play a crucial role in regulation of the homeostasis of the abdominal cavity. Other functions of the peritoneum are transmembrane transport, inflammation response, antigen presentation and tissue repair [199, 207]. In addition to these functions, peritoneal cells have also been found to play an important role in the development of a number of peritoneal diseases such as endometriosis, mesothelioma and peritoneal carcinomatosis [295].

1.3.1 Transmembrane transport

The capacity of the peritoneum to transport solutes and fluids is a well-known property that is often exploited during peritoneal dialysis and which is the base principle of intraperitoneal chemotherapy [88]. The peritoneum itself does not pose a significant barrier to solute and water transfer but rather allows for passive transport of fluids and solutes along both hydrostatic and osmotic pressure gradients. In addition to this passive diffusion through intercellular junctions and stomata, active transport

through (micro)pinocytic vesicle formation has also been reported [200]. The endothelial lining the capillaries and venules of the peritoneum does prove to be a barrier for solute transport [88].

1.3.2 Inflammation response

The inflammatory response of the peritoneum is a multi-step response that leads to the recruitment of immune cells, enhanced vascular perfusion, accumulation of macrophages with subsequent attraction of more infiltrating immune cells and the release of pro- and anti-inflammatory mediators [295]. The macrophages that are present in the submesothelial stroma play a key role in the recognition of foreign material and recruit inflammatory leukocytes from the blood. The mesothelial cells secrete a number of inflammatory mediators in response to these recruited leukocytes. Peritoneal fibroblasts in the stroma and mesothelial cells participate actively in the peritoneal immune defense and are able to respond to physiological and pathological changes within their microenvironment [199, 200].

1.3.3 Antigen presentation

Antigen presentation and T-cell activation are the first steps in the generation of a specific immune response. Normally, antigen presentation is done by highly specialized cells that have major histocompatibility complex - II molecules that can recognize foreign material. Mesothelial cells have also been shown to have the ability to present antigens to T-cells and contribute to the T-cell activation. This suggest that mesothelial cells effectively contribute to antigen presentation to T-cells to generate a cell-mediated immune response to pathogens [295].

1.3.4 Tissue repair

Due to surgical trauma or pathologies (eg: peritonitis, endomitriosis), the peritoneum can become damaged. The mesothelial cells have a crucial role in mediating the tissue repair by releasing growth factors which initiate cell proliferation, differentiation and migration of mesothelial and submesothelial cells surrounding the lesion. Additionally, the mesothelial cells can produce, organize and regulate a variety of ECM molecules crucial for cell function and repair. [34, 42, 145, 199, 200]. The balance between fibrin deposition and its degradation is another crucial step in peritoneal healing that is influenced by mesothelial cells. When the

inactive plasminogen becomes plasmin, it is highly effective in the degradation of fibrin, and the conversion of plasminogen into plasmin is thus an important step in fibrinolysis. Mesothelial cells mediate this balance between fibrin deposition and breakdown by producing both plasminogen activators and plasminogen-activating inhibitor. When this balance is off, a reduced fibrin clearance will act as a scaffold for collagen secreting fibroblasts and capillary ingrowth which can result in adhesion formation. [295]

1.4   PERITONEAL FLUID FLOW

Although the peritoneal cavity is a true cavity, most works refer to it as a "potential space" as it only becomes apparent on imaging in pathological conditions when filled with abnormal fluid or gas. In normal, physiological conditions, there is approximately 50–100 ml of serosal fluid present in the peritoneal cavity [295]. This fluid is continually produced, circulated, and resorbed, and total production amounts to 1 l per 24 h.

The flow of this fluid is not uniform nor completely random but rather follows a predictable path that is partly due to gravity, diaphragmatic
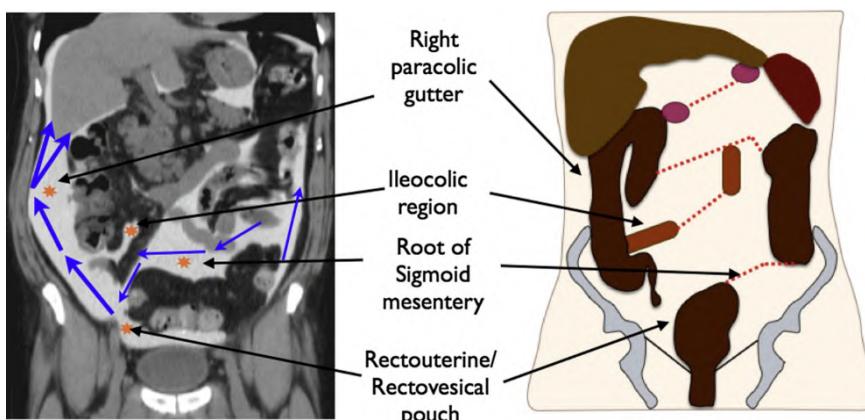
Figure 1.6: The peritoneal cavity. A subdivision into several anatomical spaces can be made using hallmark ligaments and mesenteries as borders. The flow of the intraperitoneal fluid is directed by the pressure gradients resulting from gravity, diaphragmatic movement, and peristalsis with the ligaments, omenta and mesenteries acting as watersheds for this flow. The intraperitoneal fluid flow in the peritoneum with the main directions of flow is indicated with blue arrows, the watersheds restricting this flow are red dotted lines and the regions of preferential fluid stasis are indicated by *. Source: Intraperitoneal Cancer Therapy: Principles and Practice: Part 1, chapter 3, page 27

movement, peristalsis and their resulting pressure gradients within the abdominal cavity. The fluid flow is further directed by the presence of the ligaments within the peritoneal cavity which act as watersheds [147]. The pressure below the diaphragm is subatmospheric, and during inspiration, pressure decreases even further. This creates an upward pressure gradient which encourages fluid to flow up the paracolic gutters even in an upright position [295]. As the right paracolic gutter is deeper and wider than the left one, the peritoneal fluid will predominantly flow on the right as it will take the path of least resistance. Through the paracolic gutter on the right, the fluid will flow to the right subhepatic space (Morison's pouch) and can enter the greater sac (bursa omentalis)through the epiploic foramen. Fluid also flows upwards to the right subphrenic space but flow between right and left subphrenic space is limited by the falciform ligament. On the left, the phrenocolic ligament limits the fluid flowing through the left paracolic gutter to the inframesocolic recess [136, 147, 295]. Due to this complex nature of the fluid flow, combined with the specific anatomy of the peritoneum, fluid tends to stagnate at certain regions within the peritoneal cavity. Any area at which the fluid tends to stagnate are commonly the first sites to be involved in the peritoneal spread of infections and metastases. These include the rectovesical/rectouterine pouch, the right lower quadrant at the termination of the small bowel mesentery, the root of the sigmoid mesentery, and the right paracolic gutter (figure 1.6) [295, 259]. This specific intraperitoneal fluid (IPF) flow pattern combined with the complex peritoneal anatomy hinders the adequate exposure of the peritoneal surfaces to the cytotoxic drugs during intraperitoneal drug delivery. Using a catheter consisting of a single (perforated) tube as source of the drugs is unlikely to reach all different peritoneal regions. For that reason, a part of this work (chapter 7) focuses on a new catheter design that allows for a better surface exposure of the peritoneum during IPC.

PATHOPHYSIOLOGY OF PERITONEAL METASTASES

2.1 ORIGIN OF PERITONEAL CARCINOMATOSIS

Patients with peritoneal carcinomatosis suffer from a widespread growth of tumor nodules in the peritoneal cavity. These nodules can either be native peritoneal cancers (primary peritoneal cancers) or can be metastatic from a number of different intra- and extra abdominal cancers (secondary peritoneal cancers). In this section we will briefly introduce both primary and secondary cancers that can lead to peritoneal carcinomatosis and some of their characteristics that are relevant in the context of this thesis. For the secondary peritoneal cancers, a first division is made based on whether the origin is intra-abdominal or not. In the case of extra-abdominal origins, the disease is not considered to be loco-regional and intraperitoneal chemotherapy (IPC) is not relevant to these cases. For the intra-abdominal origins, the metastases are often confined to the peritoneal cavity (loco-regional metastases) and IPC might offer survival benefit. In this chapter we limited the discussion of the cancers of intra-abdominal origins to the most prevalent or relavant ones, but a more complete overview can be found in Appendix 1.

2.1.1 Primary peritoneal cancers

A number of different primary peritoneal cancers exist. A subdivision can be made based on their origins, as follows (figure 2.1):

- Mesothelial – Epithelial origin; this group can be subdivided in:
    - Peritoneal malignant mesothelioma (PMM)
    - Benign Multicystic Peritoneal Mesothelioma (BMPM)
    - Well-differentiated papillary mesothelioma of the peritoneum (WDPMP)
    - Adenomatoid tumors
    - Primary peritoneal serous carcinoma (PPSC)
    - Primary peritoneal serous borderline tumor (PPSBT)
- Smooth muscle: Leiomyomatosis peritonalis disseminato
- Endothelial origin: Primary Peritoneal Angiosarcoma
- uncertain origin; This group can be subdivided in:
    - Desmoplastic small round cell tumors (DSRCT)
    - Solitary fibrous tumor (SFT)

Most of them are rare to very rare and when malignant, prognosis is usually grim.

2.1.1.1 *Peritoneal cancers with mesothelial –epithelial origin*

Malignant peritoneal mesothelioma

Malignant peritoneal mesothelioma is an aggressive tumor that originates in the peritoneum, and is like other malignant mesotheliomas often associated with exposure to asbestos fibers [30]. Early stage disease is usually asymptomatic, resulting in the majority of patients presenting with late-stage, difficult to resect disease [29]. Historically, treatment consisted of systemic chemotherapy but results were poor with survival after diagnosis usually not exceeding the one year mark [198]. More recently, several trials in which a combination of cytoreductive surgery (CRS) was combined with hyperthermic intraperitoneal chemoperfusion (HIPEC))
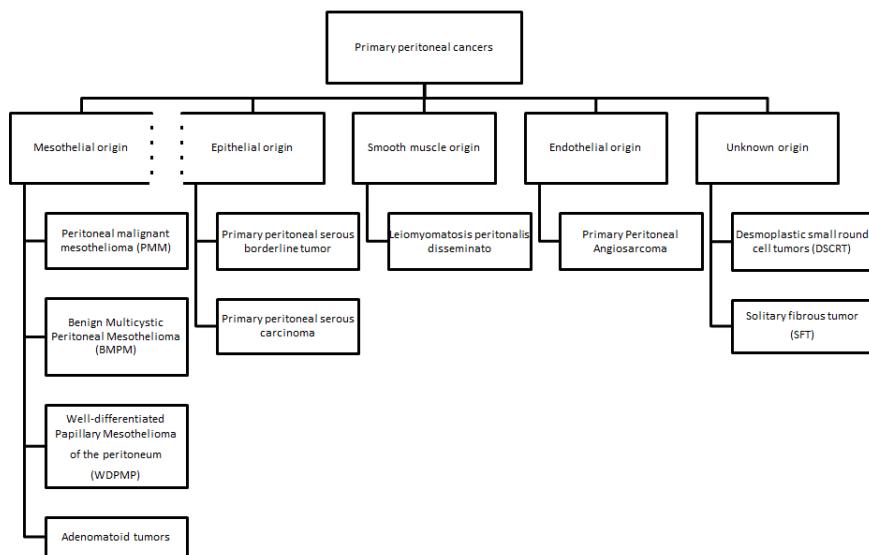
Figure 2.1: Overview of primary peritoneal cancers with subdivision based on their origins

or other IPC techniques, showed an improvement both of median survival ranges and 5-year survival rates [121]. Tumor histology, disease burden, and the ability to achieve adequate surgical cytoreduction are essential prognostic factors in MPM patients undergoing CRS-HIPEC.

Benign Multicystic Peritoneal Mesothelioma

With fewer than 200 reported cases in literature worldwide until 2017, benign multicystic peritoneal mesothelioma (BMPM) is considered a very rare native peritoneal cancer [207]. Mostly young women are affected, although some male cases have been reported [151]. Treatment usually includes an en bloc resection of the lesion to which HIPEC has been added to prevent recurrence . Although it is classified as a benign tumor, the recurrence rate is high and case reports exist of malignant transformations after repeated postoperative recurrences [151, 207].

Well-differentiated papillary mesothelioma of the peritoneum

Well-differentiated papillary mesothelioma of the peritoneum (WDPMP) is a rare subtype of epithelioid mesothelioma. It is predominantly seen in women and is usually benign although it occasionally manifests itself in a more aggressive form [18]. Different treatment strategies can be used based on the disease status [169]. If the tumor is completely resectable, resection itself seems to be sufficient. When the tumor load is high or cannot be fully resected or when the disease is accompanied by symptoms, chemotherapy should be considered. Traditionally, intravenous chemotherapy has been administered in such cases, but reports of intraperitoneal chemotherapy being administered exist [127].

Adenomatoid tumors

Adenomatoid mesothelioma of the peritoneum (AMP) is a rare benign tumor with a mean age of onset in the fourth decade [175]. Only a minority of patients have symptoms and treatment usually consists of open abdominal surgical resection of the lesion. AMP may present local recurrence, but it is thought to have no real potential for malignant transformation [117].

Primary peritoneal serous carcinoma

Primary peritoneal serous carcinoma (PPSC) is a malignancy arising from the peritoneal epithelium, with a poor prognosis. Postmenopausal women are most likely to be affected, and most patients are diagnosed at an advanced stage of the disease [323]. Optimal treatment of PPSC consists of surgical resection and chemotherapy, with recent publications favoring intraperitoneal chemotherapy [11]. Epithelial ovarian carcinomas and PPSC both arise from tissues that share the same embryological origin and are therefore thought to be identical with respect to treatment and histology.

Primary peritoneal serous borderline tumor

Primary peritoneal serous borderline tumors (PPSBT) are a rare epithelial neoplasm, distinguishable from primary peritoneal serous carcinoma

(PPSC) because tumor cells do not invade the underlying tissue and affected patients have a good prognosis. Treatment usually consists of surgical debulking of the nodules and due to its low malignant potential, chemotherapy is usually not indicated [101].

2.1.1.2 *Primary peritoneal cancer from smooth muscle origin: Leiomyomatosis peritonalis disseminate*

Leiomyomatosis peritonealis disseminata (LPD) is a benign cancer presenting with a large quantity of smooth muscle nodules on the peritoneum. Most cases are described in women of reproductive age, where it is associated with high estrogen levels, but cases in men and postmenopausal women have been described as well [227]. LPD is usually benign and treatment consist of surgical resection, but in rare cases malignant transformation may occur and more aggressive treatment is appropriate [37, 19].

2.1.1.3 *Primary peritoneal cancer of endothelial origin: Peritoneal angiosarcoma*

Angiosarcomas are malignant endothelial vascular neoplasms that can arise from vasculature at a number of different sites. Peritoneal angiosarcomas are usually very aggressive, resulting in almost 100% mortality [176]. The treatment consists of radical surgery with complete resection and – if possible - adjuvant radiotherapy for the local disease or systemic chemotherapy. Because early stage disease is often asymptomatic, it is often diagnosed when spreading has already widely occurred [43]. A recent study described two cases of pediatric peritoneal ovarian angiosarcoma for which treatment involved cytoreductive surgery and HIPEC with promising results [295].

2.1.1.4 *Primary peritoneal cancer of unknown origin*

Desmoplastic small round cell tumors

Desmoplastic small round cell tumor (DSRCT) is a rare soft tissue sarcoma, that mainly affects adolescents and young adults with a strong male predominance (4:1) [328]. Most patients present with metastatic disease at the time of diagnosis and median survival ranges from 17 to 25 months. The diagnosis of DSRCT is histologically confirmed when biopsies show

small round blue cells in nests separated by an abundant desmoplastic stroma [328]. The usual treatment includes surgical debulking in combination with high-dose, multiagent chemotherapy. Hyperthermic intraperitoneal chemotherapy and adjuvant radiotherapy have been studied with resulting improvements on survival, but neither has proven to be curative [128, 118].

Solitary fibrous tumor (SFT)

Solitary fibrous tumors (SFT) are slow-growing cancers of fibroblastic or myofibroblastic origin. They are often asymptomatic and occur most frequently in middle-aged adults, with equal distribution among men and women [20]. Surgical resection of the tumor is usually performed and the 5-year survival is very high when performed successfully [27]. Some cases in which malignant transformation occurs have been described [154].

2.1.2 Secondary peritoneal cancers

2.1.2.1 *Gastric cancer*

Gastric cancer is known for its aggressive nature and is one of the main causes of death from cancer worldwide. Adenocarcinoma is the most
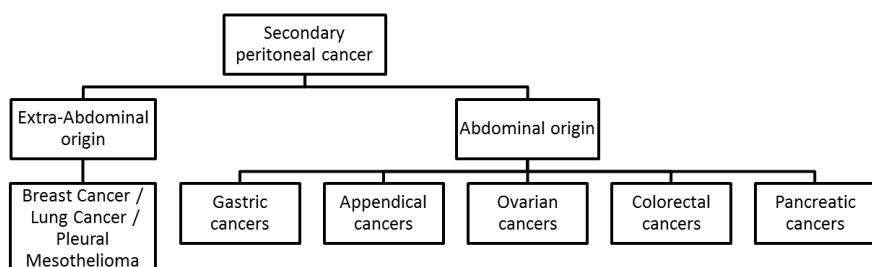
Figure 2.2: Overview of secondary peritoneal cancers that give rise to peritoneal metastases

prevalent gastric cancer with reported incidences of 90 to 95%, while remaining gastric cancer cases include lymphomas, gastrointestinal stromal tumors (GIST) and carcinoid tumors [236]. Peritoneum and liver are among the most common metastatic sites and when present, prognosis is usually grim. Intraperitoneal chemotherapy has been used to prevent peritoneal recurrence after a curative gastrectomy in high risk patients and has been proven to improve both overall survival and disease free survival. For selected patients presenting with a low number of PM, where complete cytoreduction is possible, hyperthermic, intraperitoneal chemotherapy (HIPEC) can be considered a valuable therapy [26].

Adenocarcinoma is a malignant epithelial tumor that develops from the cells of the innermost lining of the stomach. It is commonly subdivided in intestinal and diffuse-type [67]. Diffuse-type cancers diffusely infiltrate the stroma of the stomach and often exhibit deep infiltration of the stomach wall while intestinal-type cancers grow in expanding, rather than infiltrative patterns . The latter are associated with a better prognosis than diffuse-type gastric cancers [67].

Gastric carcinomas are often asymptomatic when superficial and resectable, and the majority of patients diagnosed with gastric adenocarcinoma therefore present with unresectable locally advanced or metastatic disease [goetze]. Intraperitoneal chemotherapy has been studied in the management of gastric cancer and a recent meta-analysis showed that interperitoneal chemotherapy was associated with an increased 1-year, 2-year, and 3-year survival rate, but had little to no effect on the incidence of 5-year survival rate [142, 143].

2.1.2.2 Appendical origin

Cancers of the appendix are rare and early disease is often asymptomatic. Hence, most of them are found during appendectomies performed for appendicitis. The primary appendical cancers can be subdivided in colonic-type adenocarcinoma of the appendix, mucinous appendical neoplasms, and neuroendocrine carcinoma. The management of primary appendix cancer depends on the histologic subtype and extent of disease. Because they are quite rare, therapy is mainly based on retrospective insights and small trials.

Colonic-type adenocarcinoma of the appendix

Colonic-type adenocarcinoma of the appendix is most prevalent in the 5th and 6th decade, and has a slight male sex predominance. Diagnosis is often made following appendectomy for appendicitis, or when a palpable abdominal mass is present. Colonic-type adenocarcinoma is known to perforate and distend into adjacent structures although this is less likely than in mucinous adenocarcinomas. The peritoneum is the most common site for metastases, and for selected patients for whom complete cytoreduction can be achieved, intraperitoneal chemotherapy has been used [149].

Mucinous appendiceal neoplasms (MAN)

Mucinous appendical neoplasms (MAN) can be subdivided in low-grade appendical mucinous neoplasm, high-grade appendical mucinous neoplasm, mucinous adenocarcinoma and poorly differentiated mucinous adenocarcinoma [15]. This distinction is crucial in determining prognosis and treatment: high-grade MAN exhibits a more aggressive clinical course than low-grade MAN. Both types of cancer are known to rupture, leading to pseudomyxoma peritonei (PMP). PMP is characterized by poorly-circumscribed gelatinous masses filled with malignant mucin-secreting cells. Both types of MAN are unlikely to spread extraperitonealy and are as such good candidates for cytoreductive surgery and intraperitoneal chemotherapy. Additionally, even in patients presenting with a high peritoneal carcinomatosis index, complete or near-complete cytoreduction can be obtained. These factors have made cytoreductive surgery in combination with heated intraperitoneal chemotherapy the standard of treatment for patients with PMP with excellent survival rates.

2.1.2.3 *Ovarian cancer*

Ovarian cancer constitutes the fifth most frequent cause of cancer death in women in the Western world, accounts for an estimated 239,000 new cases and 152,000 deaths worldwide annually [230]. Malignant ovarian tumors are classified in different groups: epithelial, stromal and germ cell tumors, but rare exceptions fall outside these groups [1].

Epithelial tumors

Epithelial tumors, also called ovarian carcinomas (OCs), are the most common group, accounting for 90% of ovarian cancer diagnoses [45]. This group is further subdivided in low-grade serous carcinoma (LGSC, less than 5% of cases), high-grade serous carcinoma (HGSC, around 70% of cases), mucinous carcinoma (MC, 3% of cases), endometrioid carcinoma (EC, around 10% of cases) and clear cell carcinoma (CCC, around 10% of cases) [225]. Different groups are characterized by differences in risk factors, molecular genetic abnormalities, natural history, and response to chemotherapy [98]. Since early disease tends to be asymptomatic and no effective screening programs exist, more than 75% of the patients are diagnosed at an advanced stage (FIGO stage III or IV) [69]. At these advanced stages, patients already show extensive tumoral dissemination on the peritoneal surfaces, known as peritoneal carcinomatosis (PC) or peritoneal metastasis (PM) [72]. Historically, standard treatment consisted of a combination of cytoreductive surgery and systemic chemotherapy. Intravenous chemotherapy however does not effectively penetrate into peritoneal tumor nodules, and in recent years locoregional treatment in the form of intraperitoneal chemotherapy treatment has been investigated with promising results [50]. Due to these promising results, intraperitoneal chemotherapy, in combination with cytoreductive surgery, has become a generally accepted protocol in most advanced high grade epithelial ovarian cancers [236].

2.1.2.4 *Colorectal origin*

Colorectal carcinoma (CRC) is not a homogenous disease, but can be classified into different subtypes, which are characterised by specific molecular and morphological alterations. Subdivions include adenocarcinoma, mucinous adenocarcinoma, signet-ring cell carcinoma, small cell carcinoma, squamous cell carcinoma, adenosquamous carcinoma, medullary carcinoma and undifferentiated carcinoma. Incidence of CRC is high and in the western world it accounts for approximately 10% of all cancer-related mortality [160].

Peritoneal metastases (PM) are common in colorectal cancer, with up to 10% of patients presenting synchronously with the primary tumor, and up to 25% developing PM at a later stage [184]. A recent review found that 3.4 to 6.3% of patients with non-metastatic colorectal cancer develop peritoneal metastases after curative surgery [129]. Risk factors to develop PM include [276]:

- Visible evidence of peritoneal metastases

- Ovarian cysts showing adenocarcinoma suggested to be of gastrointestinal origin

- Perforated cancer or positive margins of excision

- Positive cytology either before or after cancer resection

- Adjacent organ involvement of cancer-induced fistula

- T3 mucinous cancer

- T4 cancer or positive 'imprint cytology' of the primary cancer

- Cancer mass ruptured with the excision

- Obstructed cancer

In the risk group mentioned above, intraoperative HIPEC is being investigated as a way to minimize the occurrence of PM. Another treatment strategy is the so called second-look surgery, which aims at the early detection of PM and can be combined with HIPEC when indicated.

In addition to the preventive role of HIPEC in the development of PM in colorectal cancer patients, intraperitoneal chemotherapy can also be used with a curative, therapeutic of palliative aim. Taking into account the high morbidity and mortality of the combination of cytoreductive surgery combined with intraperitoneal chemotherapy, patients should be selected based on their general fitness, peritoneal cancer index (PCI), prior surgical score, histopathology of the primary tumor, etc. In highly selected cases, the combination of CRS + HIPEC has led to improved median survival [276].

2.1.2.5 *Pancreatic origin*

Pancreatic cancer is one of the deadliest cancers with a 5 year survival rate below 5% [315]. A distinction between endocrine and exocrine can be made with the latter being far more common than the former. Most exocrine tumors of the pancreas have an epithelial origin, with other origins such as mesenchymal (leiomyosarcomas, malignant gastrointestinal stromal tumours, solitary fibrous tumours) and lymphatic (lymphoma) being very rare. The most common type of epithelial neoplasm of the pancreas arises from the ductal epithelial cells of the exocrine pancreas

and have the ductal adenocarcinoma histological subtype (PDAC). Other subtypes according to the WHO histological classification include: solid-pseudopapillary neoplasms, pancreatoblastomas, acinar cell carcinomas, papillary mucinous neoplasms, mucinous cystic neoplasms and serous cystic neoplasms.

PDAC is an aggressive disease associated with a poor clinical prognosis, little effective therapeutic options, and a lack of early detection methods. Complete surgical removal of the tumor remains the only chance for cure, however 80-90% of patients have disease that is surgically incurable at the time of clinical presentation [244]. Because of the often late detection and the chemoresistance of these tumors, the five-year survival rate is only around 5–7% and one-year survival is achieved in less than 20% of cases [288]. Even when a complete resection has been performed, the rate of reccurence is high and the most common sites of recurrence are the liver, the peritoneal surfaces and the pancreatic bed [309]. Recently, in a preliminary study, cytoreductive surgery in combination with intraperitoneal chemotherapy was found to be beneficial in highly selected patients with pancreatic cancer with peritoneal metastasis [289].

2.1.2.6 *Extra abdominal origins*

Other, extraperitoneal cancers such as pleural mesothelioma and breast and lung cancers are also known to metastasise to the peritoneal cavity. In these cases, the spread of the metastasis is however not considered to be loco-regional and the use of intraperitoneal chemotherapy is more controversial.

2.2 METHODS OF DISSEMINATION AND TUMOR GROWTH

Peritoneal metastases disseminates throughout the peritoneum in four ways [119, 120]. A first method is the direct invasion from primary tumors to noncontiguous organs occurs along the peritoneal reflections (ligaments, mesentery and omentum). Secondly, seeding of cancer cells through the peritoneal fluid is an important pathway of peritoneal dissemination. Spontaneous detachment of tumor cells from a primary tumor is favored by the high interstitial pressure, the osmotic pressure, and downregulation of cell–cell adhesion molecules caused by epithelial to mesenchymal transition. Free cancer cells (or cancer cell aggregates)

float in the intraperitoneal cavity and follow the typical fluid flow of the intraperitoneal fluid. As a first step, cells suspended in this fluid attach to the mesothelial lining of the peritoneum but in order for metastases to grow and proliferate, they must gain access to the submesothelial connective tissue. Several possible pathways have been described for the destruction of the mesothelial layer and basal membrane and invasion process [61].

As the metastases continue to grow, passive diffusion of oxygen is no longer sufficient for the tumor cells at the center of the nodules, and they become hypoxic as a result. These hypoxic tumor cells will produce angiogenic factors which in turn lead to the formation of new vessels that will supply oxygen to the tumor nodule [61].

This pathway is also very relevant in the context of abdominal surgery. Not only is it likely that there is an increased number of cancer cells present due to the handling of the tumor, but the surgical wound also causes inflammation, which has been described in recent years as one of the hallmarks of cancer.

A third method of dissemination is lymphatic extension, cancer cells gain access to the subperitoneal lymphatic system through the lymphatic stomata. Unlike other dissemination processes, no proper invasion of the peritoneal mesothelial and subperitoneal tissue layer is required. Lymphatic metastases play a minor role in the intraperitoneal dissemination of metastatic carcinoma [119, 120].

Embolic hematogenous spread is the fourth dissemination method. Hematogenous peritoneal metastases can originate from both intra-abdominal and extra-abdominal primary tumors, but most commonly originate from melanoma, breast, and lung cancer. The disseminated tumor cells are transported by the mesenteric arteries and deposited on the antimesenteric border of the bowel in the smallest branches, where they grow into mural nodules [119, 120].

2.3 THE ROLE OF IMAGING IN THE MANAGEMENT OF PERITONEAL METASTASES

Imaging techniques are a crucial component in the management of peritoneal metastases. A correct and accurate detection of all PM is important not only for detection and staging of the oncological pathology, but also for treatment planning. Tumor debulking surgeries are performed only if

complete cytoreduction is thought to be feasible. An a priori knowledge of the extent and anatomical location of peritoneal metastases will determine the feasibility of cytoreductive surgery and predicts the surgical outcome. Post-surgical and follow-up scans can assess the surgery and treatment outcome and for patients in remission, long-term follow-up scans will determine their remission [107, 165]. Although having reliable imaging data is crucial in all these stages, obtaining these images remains a challenge as complex peritoneal anatomy and the often very small size of tumor nodules, complicate the reliable detection of all tumor nodules in PM. In this section we will discuss the most commonly used imaging techniques with their respective advantages and limitations as well as some emerging techniques.

2.3.1 Ultrasound imaging

Ultrasound imaging has a very limited role in the management of PM [217]. An abdominopelvic ultrasound is likely to be one of the first diagnostic tests in patients presenting with abdominal pain or when a clinical suspicion of peritoneal carcinomatosis exists [107]. Superficial peritoneal metastases have a high chance of being detected using ultrasound imaging, but Ye et al. found that due to the overlay of fat layers and intestinal gas, the same could not be said for the nodules on the deeper lying peritoneal regions [320]. With the development and introduction of higher frequency probes, it was found that deeper lying tumor nodules could also be detected using ultrasound (even those of very limited size, figure 2.3) but results depend of the experience of the operator and obtaining reliable results for obese or post-operative patients is difficult [113]. Due to these limitations and the emergence of more accurate and reliable techniques, US is not commonly used to confirm and stage PM. It is however often, the modality of choice to perform needle guided biopsies to achieve histological diagnoses [125]. The main advantages and limitations of US and all other relevant imaging techniques for peritoneal carcinomatosis are summarized in table 2.1 [165].

2.3.2 Multidetector computed tomography imaging

Multidetector computed tomography (MDCT) systems are equipped with multiple parallel detector arrays and utilize a synchronously rotating tube and detector array. Their advantages include their good spatial resolution, robustness and relatively short scan times. Historically it has been established as the imaging modality of choice in the management
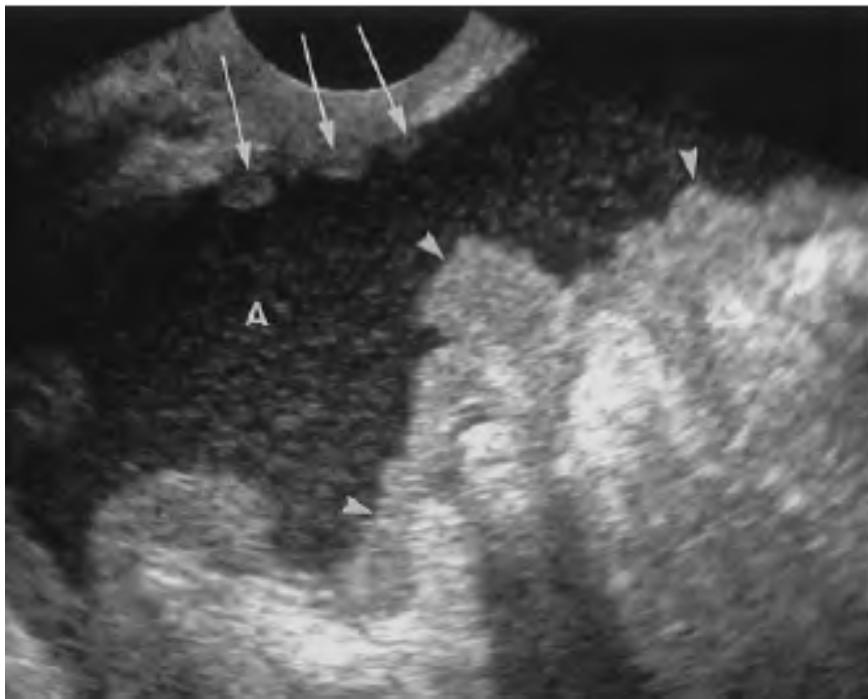
Figure 2.3: Example of ultrasound imaging of peritoneal metastases: Tiny peritoneal implants in a 53-year-old woman with papillary serous ovarian cancer. Transverse transvaginal US image of the right adnexa shows particulate ascites (A), a "rind" of hypoechoic seeding on the serosal surfaces of small bowel loops (arrowheads), and tiny parietal peritoneal implants in the near field (arrows), which measure 2 mm in maximum diameter. Source: DOI: 10.1148/rg.233025712

of peritoneal metastases, although recently, DW-MRI and PET/CT have been investigated as alternatives [158, 190, 217, 222, 228, 243].

2.3.3 MRI imaging techniques

The use of MRI in the management of peritoneal metastasis has increased over the last decades due to the development of better protocols and a higher accessibility to the technique [77]. MRI alone does not hold a diagnostic advantage over other imaging techniques, but diffusion-weighted magnetic resonance imaging (DW-MRI) has shown to improve diagnostic accuracy.

Table 2.1: Overview of different imaging modalities with their respective advantages and disadvantages

Modality	Advantages	Disadvantages
US	Good spatial resolution in superficial tissue High specificity No radiation exposure	Operator dependency Restricted viewing window Low sensitivity for deeper lying lesions in the absence of ascites
CT	General availability High spatial resolution Short examination times Little movement artifacts	Limited sensitivity for small lesions Limited sensitivity in the area of the mesentery and small intestine Radiation exposure
MRI	Higher soft tissue contrast Higher or comparable accuracy than CT Diffusion weighting possible to combine function and morphology No radiation exposure	Longer scan times Prone to respiratory artifacts Limited sensitivity for small lesions Relatively high costs
PET-CT	Combination of function and morphology Higher sensitivity than single methods Detection of extraperitoneal metastases	Limited availability High costs Limited sensitivity for small lesions Radiation exposure

2.3.3.1 *Diffusion-weighed magnetic resonance imaging (DW-MRI)*

DW-MRI uses the Brownian diffusion of water to quantify different tissues. Extracellular water molecules are less restricted than intracellular ones, and differences in the rate of water diffusion at a location is dependent on the cellular environment and thus tissue type. Different tissues of the human body have a characteristic cellular architecture and proportions of intra and extracellular compartments, hence they have characteristic diffusion properties. In high grade malignancies the intracellular proportion is increased due to the uncontrolled division of cells and corresponding high cell density, and as a result the diffusion becomes relatively more restricted [93, 107, 165, 242].

Apparent diffusion coefficient (ADC) images provide a quantitative measure of the magnitude of the diffusion in tissues by eliminating T2 effects from the DW-MRI. To obtain these maps, multiple DW-MRI images with different amounts of DW weighing are taken, the rate of diffusion is estimated from the change in intensity at each pixel.

Recent studies have shown that DW-MRI may be the imaging modality of choice for small peritoneal metastasis as well as anatomically difficult to image sites, but no clear consensus exists on whether DW-MRI or PET-CT should be the golden standard. A notable advantage of the DW-MRI includes the absence of radiation while disadvantages include long scan times and susceptibility to artefacts [107, 165, 158, 217].
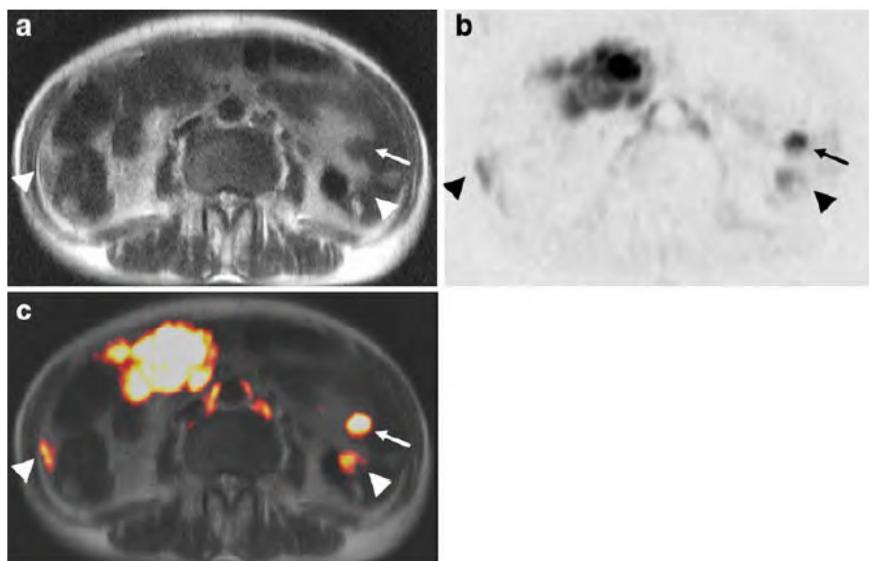
Figure 2.4: Example of the use of DW-MRI for imaging peritoneal metastases: 71-year-old woman with peritoneal dissemination caused by ovarian sereous adenocarcinoma. a. HASTE image(TR/TE: 1,000/93). b. DW image (TR/TE: 9,500/73; b value, 1,000 s/mm^2). c. DW and HASTE fusion image. DW image wich clearly demonstrates a relatively large omental mass and relatively small mesenteric mass (arrows). The small masses in the bilateral paracolic gutters show moderately abnormal signal intensity on DW image but are more apparent on the fusion image (arrowheads). Source: DOI 10.1007/s00330-007-0732-9

2.3.3.2 *Dynamic contrast enhanced magnetic resonance imaging (DCE-MRI)*

Like DW-MRI, DCE-MRI is an MRI technique that not only provides anatomical but also functional information. DCE-MRI tracks the concentration of an injected contrast agent over time. By coupling these concentration versus time curves to a physiological model of contrast transport, estimates for vascular permeability, volume fraction of extracellular space, etc. can be calculated. Although DCE-MRI has been described in the context of peritoneal metastasis, the technique does not add a diagnostic advantage at this point. Due to the nature of DCE-MRI imaging, spatial resolution of DCE-MRI is too small to detect small lesions as there is an important trade-off between spatial and temporal resolution.

2.3.4 PET and PET/CT scans

Positron-emission tomography (PET) is a nuclear medicine functional imaging technique widely used in clinical oncology for diagnosis, sta-

ging, and monitoring treatment of cancers. The technique is based on the detection of pairs of gamma rays emitted indirectly by an injected positron-emitting radiotracer. The most common radiotracer is fluorine-18 (F-18) fluorodeoxyglucose (FDG) and this tracer is a glucose analog that is taken up by glucose-using cells and phosphorylated by hexokinase (whose mitochondrial form is greatly elevated in rapidly growing malignant tumors) and concentrations of tracer imaged will therefore be representable for tissue metabolic activity. Peritoneal tumor nodules will appear as nodular soft tissue masses, with increased activity.

Disadvantage of this technique include its low spatial resolution of 0.4-0.6 cm when compared to the smaller intraperitoneal tumor nodules and its unsuitability for tumors with low proliferation rates such as mucinous appendicael neoplasms. Additionally, there should be sufficient malignant cells present to change the glucose metabolism in order for detection to occur. The result of the previous disadvantages is that small nodules are not always detected. Also, the tracer is not specific to malignant processes, but will also reflect increased uptake due to other processes such as the physiological increased glucose turnover in the bowel or inflammation. Other disadvantages of PET scans are the associated radiation exposure and higher cost. Combinations of PET and CT imaging are interesting
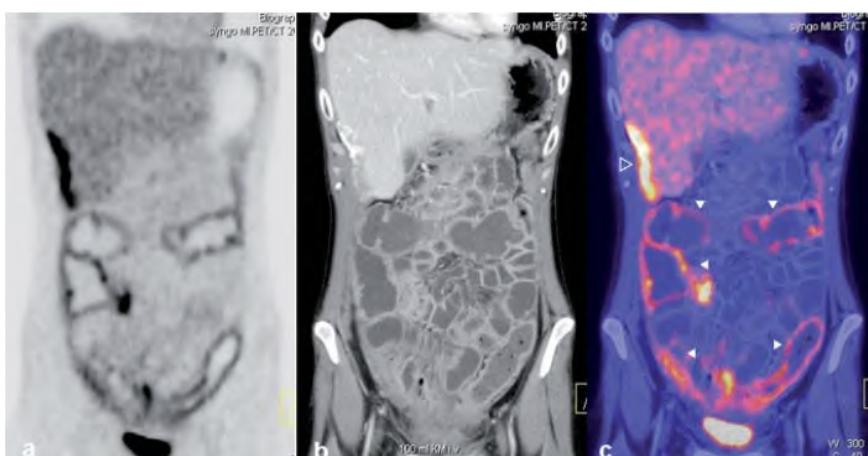
Figure 2.5: Example of the use of PET-CT for imaging peritoneal metastases a. PET scan b. Contrast enhanced CD scan c. Fused PET-CT scan of the same patient presenting with peritoneal metastases secondary to ovarian cancer. Diffuse tracer uptake along the entire colon (white arrowheads) with correlative wall thickening on CT indicative of advanced intestinal infiltration. The open arrowhead indicates partially calcified, metabolically enhanced peritoneal metastases on the liver capsule. Source URL: http://dx.doi.org/10.1055/s-0031-1281979

due to their whole-body coverage and co-registration of anatomical and functional imaging, which allows them to detect metastatic disease not located in the peritoneal cavity [222, 217, 243, 107, 165, 158].

2.3.5   Conclusion

Imaging of peritoneal malignancy is key in the staging, management and follow-up of patients with secondary peritoneal malignancies. The size and complexity of the peritoneal anatomy, especially when compared to the small tumor nodules, present a challenge and the shared characteristic between other peritoneal malignancies further complicates the imaging as well as the presence of ascites fluid in the abdomen. Several imaging techniques are able to show PM with very good sensitivity and specificity results and choice between different techniques is often based on expertise and preference. No technique is however at this point able to diagnose and/or stage peritoneal metastasis with 100% certitude and the need for a laparoscopy or exploratory surgery remains at this point [191, 247, 286]. The main limitations of the imaging techniques today are the detection of small (sub-resolution) lesions, the level of infiltration of the tumor in the underlying tissues and the difficulty to predict the peritoneal cancer index (PCI) in the small bowel regions and mesentery.

INTRAPERITONEAL CHEMOTHERAPY

3.1 INTRODUCTION

Intraperitoneal chemotherapy (IPC) is a generic term used for all treatments in which anticancer drugs are administered directly into the abdominal cavity. This technique is different from intravenous chemotherapy, during which the drug is introduced in the bloodstream and transported by the cardiovascular system throughout the entire body. To understand the difference between both techniques, a distinction should be made between local and system effects of anticancer drugs. The local effect is the effect of the chemotherapy at the site of the malignancy. This can be the original tumor or –as will most often be the case for intraperitoneal chemotherapy- the location of the metastasis. The systemic effect on the other hand, is the effect the drug will have throughout the entire body. The aim of intraperitoneal chemotherapy is to expose tumor nodules in the peritoneal cavity to a high dose of cytotoxic drugs while reducing the undesired systemic toxic effects. Although a systemic cytotoxic effect could theoretically benefit patients suffering from distant metastasis, many of the primary cancers discussed in chapter 3 present with a loco-regional spread in which metastases will remain confined to the abdominal cavity. In such cases, increasing the systemic effect is not a target as it would only add systemic toxicity without additional therapeutic benefit.

The first described use of local drug therapy was in the context of the management of ascites. The experiment, dating from 1744, called for Bristol water and Claret (wine) to be mixed and administered in the peritoneal cavity [308]. Throughout the years, several experiments were conducted with intraperitoneal therapy, but it wasn't until 'mid-seventies, that the technique had its first big breakthrough [62-64]. This chapter will highlight the pharmacokinetic rationale of IPC and its current state of the art.

3.2 PHARMAKODYNAMIC RATIONALE OF INTRAPERITONEAL CHEMOTHERAPY

3.2.1 Two-compartment model

With the revived interest in intraperitoneal chemotherapy, came a better understanding of the rationale of the therapeutic advantage [62-64]. The idea that was put forward was that upon administration of cytotoxic drugs directly into the peritoneal cavity, the peritoneum would act as a barrier and limit the drug absorption in the systemic circulation. This would result in higher local drug concentrations in the tumor tissue while minimizing the development of systemic side effects [106, 148, 187, 297].

The basis of this model is a two-compartment pharmacokinetic model, in which the compartments are the vascular, whole body compartment and the peritoneal compartment. This model assumes each of both compartments to be a well-mixed, homogeneous compartment with fixed distribution volume (V_B and V_P respectively). Exchange between the compartments is characterized by a permeability-area (PA) product of the peritoneum and clearance from the systemic compartment is a first order elimination process. Using this model, the drug concentration in both compartments over time can be derived:

$$V_B \cdot \frac{dC_B}{dt} = PA * (C_p - C_B) - k_e \cdot C_p \qquad (3.1)$$

$$V_p \cdot \frac{dC_p}{dt} = PA \cdot (C_p - C_B) \qquad (3.2)$$

With V_B and V_P the distribution volume of the systemic and peritoneal compartment respectively [m^3]; C_B and C_P the concentration of drug in

Figure 3.1: Two-compartment model of IPC. The systemic (body) compartment is characterized by a drug distribution volume (V_B) and the systemic concentration (C_B) and drugs are cleared from this systemic compartment at a rate defined by the elimination constant (k_e). The peritoneal compartment is characterized by a peritoneal distribution volume (V_P) and drug concentration (C_P). Mass transport of the drug occurs over the peritoneal barrier, characterized by a permeability-area (PA) product.

the systemic and peritoneal compartment respectively [mol/m^3]; k_e the elimination coefficient of drug from the systemic compartment [m^3/s] and PA the permeability-area product of the peritoneum [m^3/s]. When solved simultaneously for the concentration this gives:

$$C_B = PA \cdot \frac{e^{-\alpha t} - e^{-\beta t}}{V_B(\beta - \alpha)} \tag{3.3}$$

$$C_P = \frac{e^{-\alpha t}}{\beta - \alpha}\left(\frac{PA + k}{V_B} - \alpha\right) - \frac{e^{-\beta t}}{\beta - \alpha}\left(\frac{PA + k}{V_B} - \beta\right) \tag{3.4}$$

Where α and β can be calculated from:

$$\alpha + \beta = \frac{PA}{V_P} + \frac{PA}{V_B} + \frac{k}{V_B} \tag{3.5}$$

And:

$$\alpha \cdot \beta = \frac{PA \cdot k}{V_P \cdot V_B} \tag{3.6}$$

The therapeutic advantage of intraperitoneal drug delivery can be expressed as the ratio of the area under the concentration-time curve (AUC) in the peritoneal compartment divided by the AUC in the systemic compartment. In the case of a fixed peritoneal concentration, this ratio can be expressed as [166]:

$$\frac{C_P}{C_B} = \frac{1+k}{PA} \tag{3.7}$$

From this equation, it is clear that the therapeutic advantage is proportional to the systemic drug clearance and inversely proportional to the permeability area product of the peritoneum. When k greatly exceeds PA, a larger therapeutic advantage is to be expected as the local, peritoneal concentration will be much higher than systemic concentrations.

Since the first definition of this model, it has been established that it is not the peritoneal mesothelial layer nor the submesothelial stroma that pose a physical barrier to the drug transport. The rate-limiting step of drug uptake into the systemic circulations is the uptake through the endothelial cells of the microvasculature present in the submesothelial layer [57, 91, 267, 298]. In addition to this two-compartment model, other, more complex, compartment models have been proposed by other groups [270]. A more extensive discussion of these models is given in chapter 7 of this work.

It is important to note that even though the term 'therapeutic advantage' is used in this section, it might be more suited to use the term "therapeutic opportunity". The concentration of drug in the peritoneal cavity C_P might be the concentration to which free floating or outer layer tumor cells are exposed, but this is not true for the deeper laying tumor cells. Due to their nature, compartmental models do not take into account the distribution of drug within a single compartment but consider it to be well-mixed and homogeneous. In order to capture the true distribution of drug in the peritoneal compartment, a distributed model is needed that uses different assumptions [87]. For more details on the existing literature on both compartmental and distributed models, we refer to chapter 7 of this work.

3.2.2 First pass effect

The two compartment model discussed in section 3.2.1 is a simplification of the reality, with the whole body lumped in the systemic, whole body

compartment. This implies that the liver is lumped together in the whole body compartment. The visceral peritoneum, accounting for approximately 80% of the total peritoneal surface, drains into the portal vein. Drugs that are absorbed at the microcirculation of the visceral peritoneum therefore pass through the hepatic circulation before reaching the systemic circulation (figure 3.2) [187]. When a drug is chosen that is metabolized during the first pass through the liver into nontoxic metabolites, systemic toxicity can be minimized, even for high peritoneal concentrations.

3.2.3 Hallmarks of the ideal drug for intraperitoneal chemotherapy

Even though the pharmacokinetic two-compartment model is a simplification of the actual drug transport during intraperitoneal chemotherapy, it provides valuable insight in what properties are desirable in a candidate drug for IPC. Some necessary/desired characteristics are given below:

- The drug has a proven activity against the cancer type of origin

- There should be a positive correlation between the drug concentration and its cytotoxicity

- The pharmacokinetic advantage should be as high as possible. The drug should be slow to exit the peritoneal compartment and rapidly cleared from the systemic circulation

- The drug should not cause direct toxicity to the peritoneum
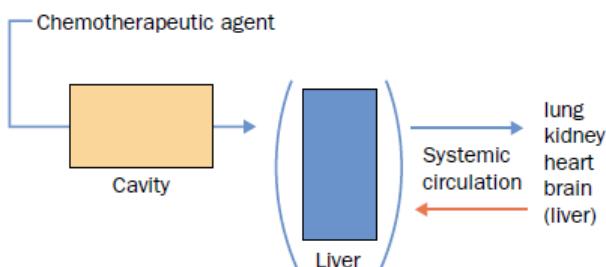
Figure 3.2: Schematic representation of the first-pass effect in the liver that occurs during intraperitoneal chemotherapy. The microvasculature of the visceral peritoneum (80% of total peritoneal surface) drains in the portal vein. In the liver, cytotoxic drugs that have entered the peritoneal microcirculation can be metabolized, which lowers the systemic drug concentration. Reprinted with permission from [187]

- A fast hepatic metabolism to a non-toxic metabolite (first-pass effect)

Some additional requirements include:

- The administration duration of IPC ranges from 30–120 minutes. Given this limited timeframe and the importance of the duration of exposure for cancer cell kill, non-cell-cycle specific drugs are preferable

- As IPC is often performed in a perioperative context with an open abdomen, safety concerns can also influence the suitability of a drug. Drugs that are volatile between 20 to 43°C should be avoided.

- If the drug is to be used in hyperthermic conditions, there should be a thermal enhancement of cytotoxicity

3.3 State of the art of IPC

3.3.1 Introduction

Since the demonstration of the pharmacokinetic advantages obtained through during IPC, numerous groups started clinical trials using the technique [49, 85, 94, 131, 263, 279, 280, 303, 331]. Even though the local high drug concentrations have been shown experimentally, the widespread use of IPC is limited by the penetration depth of the drugs into the tumor tissue [89]. Reports show penetration depths ranging from a few cell layers to a couple of mm at best. Given this very limited penetration depth [180, 213, 296], in current practice, IPC with the aim to cure is only performed when a complete or near complete resection of all visible tumor is possible.

Currently, there is a huge variety in IPC procedures that are performed. Not only do the used drugs and dosages differ, but there are also differences in surgical technique, duration and timing of the treatment. These protocol differences often complicate the direct comparison of different studies. In this chapter, we will discuss the base characteristics of intraperitoneal chemotherapy and give a brief overview of the differences in treatment protocols.

3.3.2 Therapeutic goal of IPC

A first difference between different intraperitoneal chemotherapy regimens is based on what the aim of the intraperitoneal chemotherapy is. A distinction can be made between a therapy with a curative, life-prolonging or palliative goal. The term curative therapy is straightforward, the therapy aims for a cure of the patient and its impact can be assessed by the disease free survival of the patient after >5 years of observation. Often, however, the therapy is thought to be life-prolonging, meaning that it will offer a survival benefit, but not be curative. In palliative therapy the intent of the surgical intervention is not focused on treating the cancer, but on relieving the patients' symptoms. It is possible that patients receiving palliative treatment have a survival advantage, but in this case this is not the main goal.

Historically, the morbidity and mortality rates of IPC regimens limited the use of the technique to the curative therapies. More recently, with increasing experience with the technique, especially at high volume hypertermic intraperitoneal chemotherapy (HIPEC) centers, it was found that IPC morbidity and mortality equaled that of other major abdominal surgeries [92]. As the expertise grew, a growing interest amongst IPC surgeons to use the technique as life-prolonging or palliative therapy could be noted. Especially in the presence of malignant ascites, IPC has been used to improve quality of life without a curative aim. In the cases where the aim is palliative, laparoscopic IPC has been suggested as a less invasive method for IPC [58, 167, 257, 303].

3.3.3 Patient selection for IPC

Due to the associated morbidity and mortality of cytoreductive surgery combined with intraperitoneal chemotherapy, selecting patients who are most likely to benefit from treatment protocols is crucial. A number of clinical assessments of peritoneal metastases are commonly used to determine whether a patient is a good candidate [9, 148, 234, 251]:

- The histopathology to assess the invasive character of the malignancy

- The preoperative scans of the abdomen and pelvis

- The peritoneal cancer index (PCI)

- Prior surgical score (if relevant)

- The completeness of cytoreduction (CC) score

The assessment of the aggressiveness of a malignancy is a key element in the treatment plan. Pre-operative scans are necessary to exclude systemic metastasis outside the abdominal cavity, which are not likely to be responsive to IPC. For a number of different malignancies, certain radiological features are good predictors of the likelihood that complete cytoreduction will be obtained. The peritoneal cancer index takes into account the peritoneal implant size and distribution of nodules on the peritoneal surface [99]. Although estimates of the PCI can be obtained from CT images, the most accurate results are obtained by direct visual inspection during laparoscopic surgery (figure 3.3). The lesion size score relates to the largest tumor nodule (excluding the site of the primary) found in a certain region and ranges from 0 for no visible tumor to 3 for tumor nodules exceeding 5 cm or when a confluence of tumor nodules is observed between any abdominal or pelvic structures. These individual lesion size scores are then summated over the 13 regions that can be found in figure 3.3 to obtain the final PCI. Numerous studies have shown the predictive value of PCI on outcomes [53, 74, 100, 102], although there are also some exceptions that apply (e.g. for non-invasive cancers with a high PCI , complete cytoreduction might still be feasible [187]). Most centers will apply cut-off values of the PCI to determine whether a patient is a candidate for cytoreductive surgery and IPC [102].

Patients who already underwent prior attempts at cytoreduction to a certain extent prior to the definitive cytoreduction combined with IPC generally have a lower survival rate [219]. During surgery, the tissue planes that are opened are favorable sites for cancer cell adherence. Once the tumor is imbedded in the scars, it becomes more difficult or even impossible to remove by peritonectomy or to eradicate by intraperitoneal chemotherapy.

The final clinical assessment that should be considered is the completeness of the cytoreduction that is achieved. It has been shown to be a major prognostic indicator in both noninvasive and invasive peritoneal surface malignancy. The completeness of cytoreduction (CC) is scored from 0 to 3. A CC score of 0 indicates that no visible tumor is left following the cytoreduction. When tumor nodules persisting after cytoreduction are less than 2.5 mm, a CC score of 1 is given. A CC score of 2 indicates tumor nodules ranging between 2.5 mm and 2.5 cm in diameter and for

Peritoneal Cancer Index
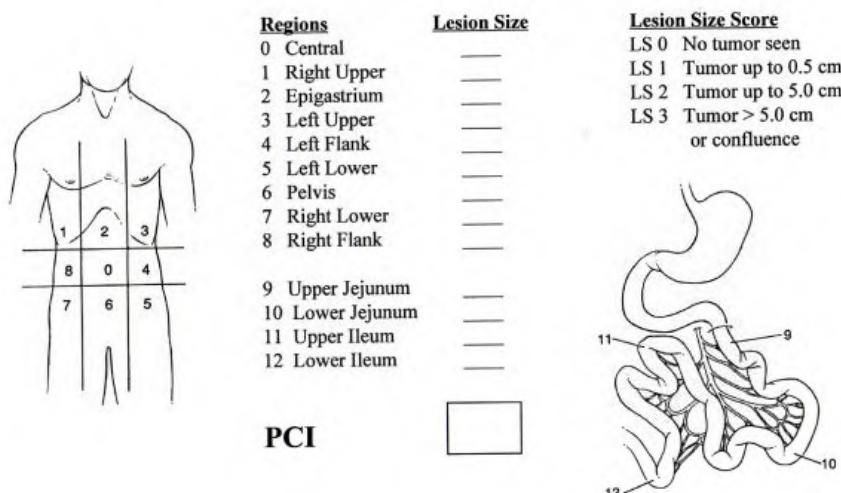
Figure 3.3: Illustration of the peritoneal cancer index (PCI) scoring system. The abdomen is divided in 13 regions, and a value of 0 to 3 is assigned to each region , depending on the presence and extent of lesions in this region. The sum of the 13 values is the PCI of the patient. Figure reprinted with permission from [99]

any tumors larger than 2.5 cm a CC will equal 3. Although only CC = 0 equals complete cytoreduction, tumor nodules smaller than 2.5 mm are thought to be responsive to IPC due to their limited size.

Ideally, all 5 of the clinical assessments should be taken into account when the fitness of a patient to undergo cytoreductive surgery combined with intraperitoneal chemotherapy is considered.

3.3.4 Open, laparoscopic and closed intraperitoneal chemotherapy

IPC can be performed in an open, laparoscopic or closed setup (figure 3.4). In the former setup, the cytotoxic agent is administered directly into the cavity that is created by the suspended abdominal wall and allowed to circulate using in- and outflow catheters and peristaltic pumps. Advantages of this approach include the limited risk for spillage and a good homogeneity in drug distribution and temperature within the solutions as semi-manual stirring is feasible in this setup. Disadvantages include the occupational hazards for the surgical staff and the significant expertise needed to perform this technique [106].

A closed IPC setup on the other hand is performed through a water-tight closure of the abdominal wall after insertion of in- and outflow catheters. In order to obtain a more homogeneous distribution within the peritoneal cavity, the operation table can be tilted into different positions or the patient's abdomen can be manipulated. Although this technique eliminates most of the risks for the staff and is less cumbersome in general, there are concerns that the drug distribution is less homogeneous than in the open set-up, resulting in possible toxicity for the healthy surrounding tissues [5]. In some other cases, IPC has been administered laparoscopically, thereby limiting the need for open abdominal surgery. Indications for this technique usually included either a palliative setting or very limited PM [80].

3.3.5 Timing of intraperitoneal chemotherapy

Based on the timing of the treatment, a distinction can be made between early postoperative (perioperative) intraperitoneal chemotherapy, intraoperative intraperitoneal chemotherapy, and protracted postoperative intraperitoneal chemotherapy [55, 56]. Studies have shown to favor intraperitoneal chemotherapy as early as possible after surgery [168]. Not only does this technique not require the implantation of a catheter with its related infection risks [4, 186], but it is also thought to minimize the free tumor cell implantation in an effective way [143]. Furthermore, it is compatible with an open abdominal technique, which allows for the stirring of the fluid and an optimal surface exposure. Despite the disadvantages connected to protracted postoperative intraperitoneal chemotherapy, it does offer the possibility for repeated therapy.

Figure 3.4: Three different approaches to intraperitoneal chemotherapy. A. open, IPC technique, B. closed IPC technique and C. laparoscopic IPC technique Source: a: doi: 10.3978/j.issn.2078-6891.2015.105, b.DOI:10.5152/UCD.2015.2990, c. url: https://www.umms.org : Cytoreductive Surgery and HIPEC - FAQs

3.3.6 Drugs used in intraperitoneal chemotherapy protocols

Depending on the origin of the cancer, the stage of the disease and the treatment history of the patient, different cytotoxic drugs are available for IPC. In this section we will discuss the commonly used drugs with special attention to the characteristics discussed in section 1.3.2.2 concerning the desirable features of a drug used for IPC [55, 56, 281, 297]. Table 3.1 provides an overview of the discussed drugs and their main features.

3.3.6.1 5-Fluorouracil

5-Fluorouracil has shown clinical activity for a wide variety of tumors and is used in a number of gastrointestinal cancer chemotherapy regimens and has a high area under the curve ratio [148]. Its method of action is however cell-cycle-specific, which is not desirable in intraperitoneal chemotherapy due to the relative short duration of the therapy. Some of the 5-FU metabolites however do have a direct cytotoxic effect and 5-FU has also been shown to be thermosensitive [55]. The use of 5-fluorouracil as a single component for IPC is usually limited to postoperative intraperitoneal chemotherapy, but it is added to numerous combination therapies. In the context of repeated postoperative intraperitoneal chemotherapy, a treatment protocol spread over 5 treatment days with 23 hours of dwelling and a dose of $650 \, mg/m^2$ is common. Penetration depths of 5-Fluorouracil of 0.2 mm are reported in literature after IPC [279].

3.3.6.2 Carboplatin

Carboplatin is a higher molecular weight platinum compound than cisplatin, mainly used for IP use in PM from ovarian origin. Its main advantage is its decreased renal toxicity when compared to cisplatin, allowing for higher doses to be used (350–800 mg/m²) [5, 281, 297]. Additionally, there is a reduced chance of neuropathy associated with carboplatin, which makes it more suited to be used in combination with other neurotoxic drugs, such as the taxanes. The area under the curve ratio of carboplatin is low, with reported values ranging from 1.9–5.3 and the drug thus enters the systemic compartment in high concentrations following intraperitoneal administration (due to the very limited metabolism of the platinum compounds in the liver) [281, 297]. Carboplatin has been shown to be thermosensitive but it is often used in normothermic intraperitoneal chemotherapy protocols for advanced ovarian cancer.

Table 3.1: Main characteristics of drugs commonly administered in intraperitoneal chemotherapy.

Drug	MW (Da)	IP dose (mg/m^2)	AUC ratio	Penetration depth	Thermal enhancement	Cell-cycle specific
Alkylating agents						
Mitomycin C	334.3	35	10-23.5	3 mm	yes	yes
Melphalan	305.2	50-70	17-63	NA	yes	yes
Platinum compounds						
Cisplatin	300.1	90-250	13-21	1-3 mm	yes	no
Carboplatin	371.3	350-800	1.9-5.3	0.5 mm	yes	no
Oxaliplatin	397.3	200-460	3.5-16	1-2 mm	yes	no
Antimicrotubule agents						
Paclitaxel	853.9	20-175	1000	0.5 mm	?	yes
Docetaxel	861.9	40-159	207	NA	yes	yes
Topoisomerase interacting agents						
Topotecan	457.9	NA		NA	?	yes
Irinotecan	677.2	NA		NA	±	yes
Mitoxantrone	517.4	28	15.2	5-6 cell layers	±	yes
Doxorubicine	543.5	60-75	162	4-6 cell layers	yes	yes
Antimetabolites						
5-Fluorouracil	103.1	650	117-1400	0.2 mm	±	yes
Gemcitabine	300	120-1000	847	NA	+	yes

3.3.6.3 Cisplatin

Both normothermic and hyperthermic IP applications of cisplatin have been used in the treatment of ovarian cancer, gastric cancer, desmoplastic small round cell tumor, and peritoneal mesothelioma [55, 58]. The penetration depth of cisplatin into tumor nodules was studied by several groups. Los et al. for the first time described intratumoral distribution of cisplatin after IP administration and suggested that the advantage over IP versus IV administration was maximal in the first 1.5 mm [180].

3.3.6.4 Docetaxel

Docetaxel belongs to the family of taxanes and has a very large pharmacokinetic advantage after intraperitoneal delivery with an area under the curve ratio of 207. The taxanes show a therapeutic action against a broad range of tumors and local toxicity in the abdomen of taxanes is usually the dose limiting factor. Taxanes are not thought to be thermosensitive and their working principle is cell cycle specific [278, 293].

3.3.6.5 Doxorubicin

One of the earliest drugs researched for intraperitoneal chemotherapy was doxorubicin due to its activity against a broad range of malignancies. It has

a very high area under the curve ratio of intraperitoneal to intravenous concentration times of 162, due to its metabolisation as a single pass through the liver. Doxorubicin is often mixed with other chemotherapy agents (usually cisplatin) and has shown thermosensitive behavior. Doses of 40–159 mg/m² have been described but due to the severe side-effects associated with the higher doses, doses are generally on the lower end of this spectrum [281, 297].

3.3.6.6 Gemcitabine

Gemcitabine is the prodrug for the cell-cycle specific active agent, gemcitabine triphosphate. In the context of intraperitoneal chemotherapy, gemcitabine has been investigated as both a perioperative and post-operative therapy for pancreatic cancer and ovarian carcinoma. The area under the curve ratio was estimated to be around 847 and the administered doses range from 120–1000 mg/m^2 [278, 293].

3.3.6.7 Melphalan

Melphalan is a cytotoxic drug that shows a very large thermosensitive effect and is active against a wide range of malignancies. Its area under the curve ratio is 17-63 and a typical dose ranges from 50–70 mg/m^2. It is used as a salvage drug for previously failed therapies or in chemoresistant tumors [281, 297].

3.3.6.8 Mitomycin C

Mitomycin C has shown to obtain good cytotoxicity in ovarian, appendiceal, gastric, and colorectal peritoneal carcinomatosis patients. The area under the curve ratio is 23.5 and commonly used doses are in the range of 15–35 mg/m$_2$. It is one of the drugs most used in intraperitoneal chemotherapy, although the shorter infusion times needed for the platinum derivative drugs might shift the preference towards platinum derivatives [281, 297].

3.3.6.9 Oxaliplatin

Oxaliplatin is a platinum complex with proven cytotoxicity in colon and appendiceal metastasis. It is thermosensitive, but has a rather low area under the curve ratio (3.5 – 16). This low AUC ratio is however compensated

by the rapid absorption of the drug into the tissue. The instability of oxaliplatin in chloride-containing solutions necessitates a dextrose-based carrier, which in its turn may lead to serious electrolyte disturbances and hyperglycemia during the treatment [281, 297].

3.3.6.10 *Paclitaxel*

Paclitaxel has a high AUC ratio of 1000 and is used in a neoadjuvant intraperitoneal and systemic chemotherapy setting as well as intraoperatively and postoperatively. Novel formulations of taxanes such as Abraxane, aiming at an increased bioavailability are under investigation. Just like Docetaxel, Paclitaxel shows a therapeutic action against a broad range of tumors and local toxicity in the abdomen of taxanes is usually the dose limiting factor. Paclitaxel is not thought to be thermosensitive and the working method is cell cycle specific [281, 297].

3.3.6.11 *Other drugs*

In addition to the most commonly used drug listed above, some other agents have been used in clinical trials or earlier treatment protocols. These drugs include: mitoxantrone, etoposide, floxuridine, irinotecan and pemetrexed [281].

3.3.7 Hyper- versus normothermic IPC

Another difference between IPC protocols is the temperature of the drug solution. The delivery can be performed normothermic (T=37-38°C) or hyperthermic (T=40-41°C). Several authors have studied chemotherapy concentrations in tumor tissue after hyperthermic IP delivery and different results have been obtained for different drugs [51, 166].

The positive effect of hyperthermia can be attributed to a number of factors [55, 56, 66, 126]:

- The diffusion coefficient is proportional to the temperature and inversely proportional to the viscosity of the medium according to the Einstein equation, which predicts increased drug diffusion with increasing temperature.

- The hydraulic conductivity of the interstitium is also higher with increasing temperature as the matrix permeability increases and fluid viscosity reduces at higher temperature.

- Heat (40° < T < 45°) has a selective direct cytotoxic effect for malignant cells while there is minimal toxicity for normal tissue.

- Contrary to vasodilation in the healthy tissues, the microcirculation in most malignant tumors exhibits a decrease in blood flow or even complete vascular stasis in response to hyperthermia. In addition, the combination of the inhibition of oxidative metabolism in tumor cells subjected to hyperthermic conditions and unaffected anaerobic glycolysis, leads to accumulation of lactic acid and lower pH in the microenvironment of the malignant cell. This causes an increase in the activity of the lysosomes (which are increased in under hyperthermic conditions) which in its turn causes accelerated cell death of the more fragile malignant cells [70, 251].

- The combination of heat and antineoplastic drugs often results in increased cytotoxicity although this is not confirmed for all drugs [166].

- Inhibition of repair mechanisms.

Even though a lot of advantages of hyperthermia have been described, the actual therapeutic benefit remains a subject of discussion. In an open, circulating set-up, temperature control is quite easy to achieve but in a closed or laparoscopic IPC set-up, inadequate circulation of heated fluids may cause acute and late systemic side-effects.

3.3.8 Duration and repetition

A wide variation in the duration (ranging from 30 to 120 minutes) of IPC protocols are reported in literature. A longer exposure time will enhance the cytotoxic effects of the cytotoxic drugs but should be carefully weighed against systemic exposure and its accompanying toxicity. Regimens using mitomycin C generally have infusion times ranging from 90 to 120 minutes, whereas regimens using platinum based compounds are shorter with infusion times of around 60 minutes for cisplatin, and 30 to 60 minutes for oxaliplatin [106].

Certain laparoscopic IPC protocols include the repeated infusion of drugs in the abdominal cavity by means of a catheter that was implanted during a prior surgery. In such cases, the carrier fluid containing the drugs is not always evacuated from the intraperitoneal space but in some cases left to infuse for a prolonged period of time (up to 24h) until both drug

and carrier fluid are absorbed. It is clear that in these protocols, both the amount of infused carrier fluid and the dose of drug should be adjusted accordingly.

3.3.9 Alternative delivery methods of intraperitoneal chemotherapy

To overcome the two main limitations of intraperitoneal chemotherapy (limited surface exposure and penetration depth [89]), research into alternative delivery methods for intraperitoneal chemotherapy is being conducted. Other limitations of IPC are the invasiveness of the procedure and the limited possibilities for repeated IPC. In this section we will discuss two different approaches that attempt to circumvent these limitations: delivery by means of pressurized aerosols and delayed release of drugs using drug delivery systems.

3.3.9.1 *Aerosol*

During pressurized intraperitoneal aerosol chemotherapy (PIPAC), chemotherapy compounds are delivered in the form of a pressurized aerosol into the abdomen (figure 3.5). Advantages of this technique include its limited invasiveness, as the procedure is performed laparoscopically as well as an enhanced penetration depth that is being reported [257, 258, 287]. As the technique is performed laparoscopically, it becomes feasible to perform repeated PIPAC sessions, further opening the possibility of palliative and therapeutic applications of the technique.

3.3.9.2 *Drug delivery systems*

To increase this exposure time of tumor cell to the advantageous higher peritoneal drug concentrations, a number of different drug delivery systems (DDS) are currently under investigation [36, 59]. Micelles, microspheres or hydrogels often act as carrier to obtain a controlled, prolonged release of the drugs in these devices. In addition to the advantage of prolonged exposure, the implantation or injection of drug delivery systems does not require the same level of technical set-up as conventional IPC and it less time-consuming. An overview of drug delivery systems under investigation for intraperitoneal drug delivery can be found in chapter 4 section 4.3.1.3.
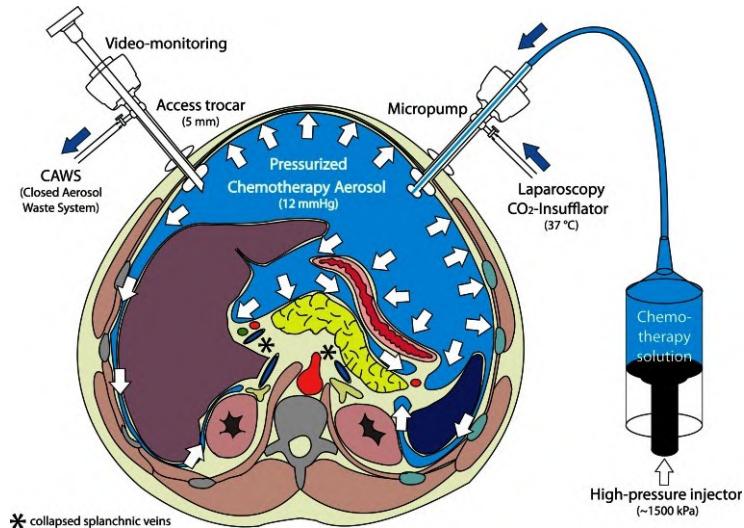
Figure 3.5: Pressurized intraperitoneal aerosol chemotherapy (PIPAC) set-up. The chemotherapy solution is nebulized with a micropump into the tightly closed abdominal cavity, and maintained for 30 min. The toxic aerosol is then exhausted through a closed system and released into the external environment. Source: DOI: 10.1245/s10434-013-3213-1

4

DRUG TRANSPORT DURING INTRAPERITONEAL CHEMOTHERAPY

4.1 INTRODUCTION

Drug transport during intraperitoneal chemotherapy (IPC) is a complex process that is governed not only by drug- and therapy-related parameters, but also by parameters related to the tumor tissue. To better understand how these parameters influence the drug penetration during IPC, this section will provide an overview of the different steps that occur in the drug transport process during IPC.

From a theoretical point of view, any parameter that has an influence on the drug transport is a possible target to improve the therapeutic outcome. The distinction between a good target and a less interesting one however, is based on how sensitive the outcome is to this parameter. Traditionally, this is done by either in silico, in vitro or in vivo models (or more often a combination of all three) and/or clinical trials. A second part of this chapter will focus on some of these studies that modified some of these governing parameters and what their outcome was on therapeutic outcome.

4.2   BASIC MECHANISMS OF TISSUE DRUG TRANSPORT

In chapter three of this work, the current state of the art of intraperitoneal chemotherapy was summarized and although a lot of differences exist between different protocols with respect to drugs used, dosage, volume of instillation fluid, technique, etc.. , almost all protocols will have the same underlying transport mechanisms.

Once suspended in the carrier fluid the cytotoxic drug is administered in the peritoneal cavity and has to be absorbed into the peritoneal tumor tissue. It has been shown that the peritoneal mesothelial lining does not constitute an explicit barrier for drug uptake [57, 91]. The administered dose and diffusion coefficient of the drug in the carrier fluid will determine the amount of drug that is initially available for transport. Cytotoxic agents do not remain stable over prolonged periods of time in the peritoneal cavity and their decay rate is an important factor that will influence the absorption. The remaining concentration of drug in the carrier fluid at each point in time will also determine the concentration gradient and therefore the magnitude of the inward diffusive flux. The carrier solution on the other hand will also have an influence on drug absorption: the amount of carrier fluid in the peritoneal cavity will determine how high the hydrostatic pressure is and will provide a driving force for the convectional transport across the peritoneum. Recently there has been an interest in the use of aerosols and an elevated intra-abdominal pressure as a means of increasing the contribution of convective transport to the drug transport [258]. Furthermore, other properties of the carrier fluid such as osmolality might also influence this first step in the transport process [79, 140, 156]. Finally, temperature is also likely to have an influence as a higher temperature influences the diffusion coefficient through the Einstein-Stokes equation [73].

Once entered in the tumor tissue, the drug will penetrate into the tumor by means of diffusive-convective transport.

- The diffusive transport will be dependent on the diffusivity constant of the drug in the extracellular fluid and the aforementioned used concentration of the drug.

- The convective transport on the other hand depends on both the tissue permeability and the fluid velocity. Tissue permeability is a parameter that describes the resistance that a porous medium (like human tissue) exerts on a fluid. The extracellular matrix (ECM) of

solid tumors is composed of two main constituents: fibrous proteins (e.g., collagen, elastin) and polysaccharides (e.g., hyaluronan, glycosaminoglycan) [41]. Tumor tissue is characterized by an increased deposition of collagen I [226] and as a result, tumor stroma is characterized by increased stiffness when compared to normal tissue [317]. A difference in ECM composition and the higher cell density that is associated with tumors can lead to a difference in tissue permeability and therefore a different resistance to convective drug flow. The fluid velocity will be radially outward due to the high interstitial fluid pressure at the center of the tumor [121].

This elevated IFP of solid tumors is caused by a number of contributing factors, including the leaky and irregularly shaped microvasculature, the lack of a functional lymphatic system, a denser extracellular matrix, an increased number of cancer associated fibroblasts (CAF's) and a larger cell density [138]. Peak IFP values of up to 60 mmHg have been measured and the higher this IFP is, the larger the pressure gradient and thus the convective drug outwash will be.

Due to its significant impact on drug delivery, IFP and its underlying causes have been the subject of numerous studies [5, 139, 284, 312] and several different targets for lowering tumor IFP have been explored. The importance of high IFP has been further established by its role as prognostic factor in several different solid tumors with high IFP correlating with poor prognosis. Despite its significance, the measurement of IFP is not part of clinical routine and when performed, IFP measurement techniques are usually invasive.

- Furthermore, not all drug molecules entering the interstitial space of the tumor remain available for transport as a fraction will bind (reversibly or irreversibly) to the proteins in the ECM.

As the therapy progresses, part of the drug entering the tumor tissue interstitium will be absorbed by the tumor vasculature and thereby add to the systemic effect of the therapy. The amount of drug that will cross the vascular wall will depend on drug related parameters such as the osmotic reflection coefficient and the diffusion coefficient and on tissue dependent parameters such as the surface to volume ratio of the vasculature, the vascular density, the permeability of the vessel wall for the drug, the oncotic pressure in both tissue and vasculature, the IFP and pressure in the vasculature, and the plasma concentration of the drug [16]. Uptake by the vascular component is a reversible process and therefore drug molecules can again enter the interstitial space from the blood pool.

From the interstitial space, the drug can then be taken up by cancer cells by both active and passive processes. Depending on the drug used, different mechanisms will be responsible for cellular uptake. The amount of drug that will be incorporated in the cells will depend on the cell-dependent factors such as cell density and drug-dependent parameters including molecule size, charge and molecular weight, but also on other therapy related factors such as temperature, local drug concentration and duration of exposure [38].
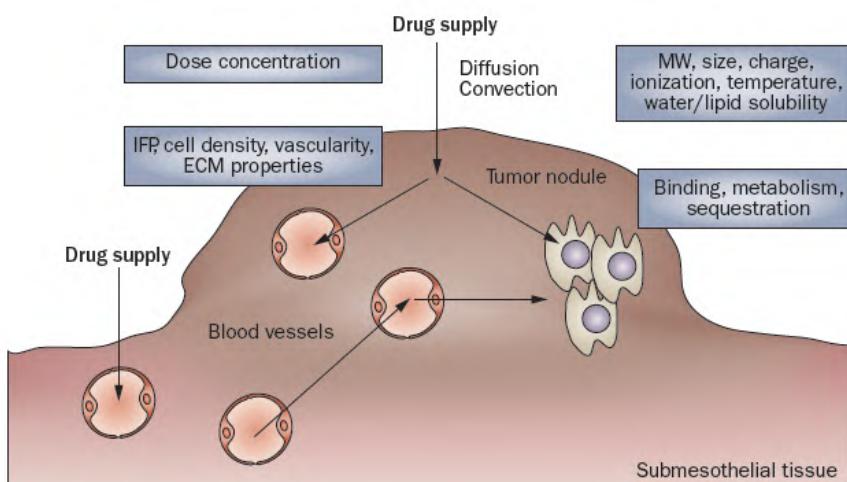
Figure 4.1: Schematic representation of drug transport during intraperitoneal chemotherapy. Drug transport during IPC is a complex process that is governed by drug- tissue- and therapy-related parameters. Figure reprinted with permission from [38]

4.3 STRATEGIES TO IMPROVE INTERSTITIAL DRUG TRANSPORT

A thorough understanding of the transport mechanisms during IPC allows for the identification of interesting targets to be influenced in order to improve therapeutic outcome. Several physical and pharmacological interventions have been attempted in order to improve drug transport and tissue penetration.

In analogy to the subdivision of the parameters influencing drug transport, the possible interventions can be subdivided into different groups: drug, tumor tissue and therapy- related parameters. Several cytotoxic agents in a range of different doses are currently approved and used for IPC (chapter 3, section 2) and therefore drug related parameters such as

substituting one cytotoxic agent for another or increasing the drug dose, will not be considered in this section. A third group of co-therapies will however be described.

4.3.1 Therapy related parameters

4.3.1.1 Pressure

Solid tumors are characterized by an elevated interstitial fluid pressure (IFP) in their center, which decreases sharply at the tumor periphery, resulting in a net outward convective flow of interstitial fluid [121]. The IFP can range from 4 to 100 mmHg, which is very high compared to the hydrostatic pressure exerted by the IP fluid column (average of 7.4–14.8 mmHg) [166]. Increasing the intra-abdominal pressure could reduce the net outward convective flow (or in extreme cases even reverse it) and thereby improve convection-driven drug transport. Several studies in animal studies showed that increasing the IP pressure resulted in a drug penetration in tumor tissue and improved survival while being well tolerated by the animals [79, 81, 137]. A novel method to increase the intra-abdominal pressure during intraperitoneal chemotherapy using pressurized aerosols has been studied recently with promising results [25, 257, 258, 287].

4.3.1.2 Temperature

The use of hyperthermia has been well described in the context of intraperitoneal chemotherapy [82, 116, 178, 246, 324] and different results have been obtained for different drugs. The positive effect of hyperthermia can be attributed to a number of factors:

- The diffusion coefficient is proportional to the temperature and inversely proportional to the viscosity of the medium according to the Einstein equation, which predicts increased drug diffusion with increasing temperature. item The hydraulic conductivity of the interstitium is also higher with increasing temperature as the matrix permeability increases and fluid viscosity reduces at higher temperature.

- Heat ($40° < T < 45°$) has a selective direct cytotoxic effect for malignant cells while there is minimal toxicity for normal tissue
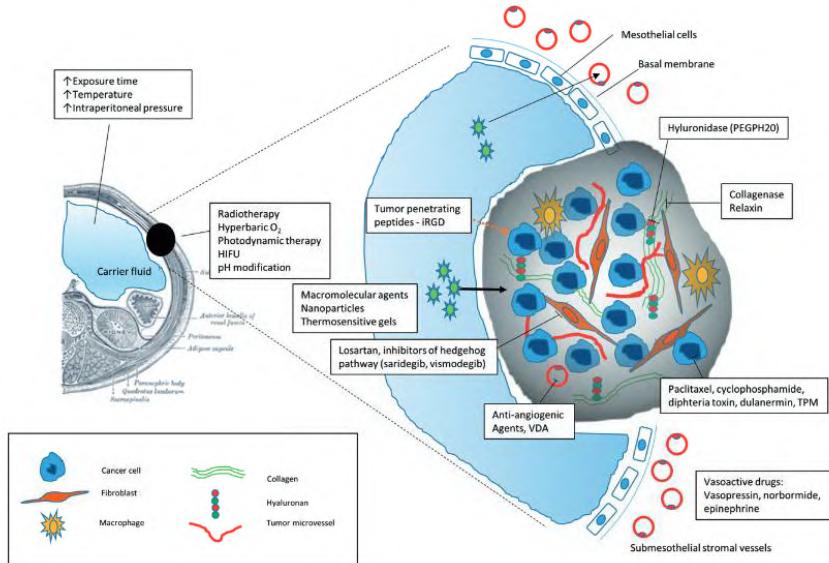
Figure 4.2: Schematic representation of the different parameters that have been targeted to improve drug penetration during intraperitoneal chemotherapy (IPC) – figure reprinted with permission from [36]

- Contrary to vasodilation in the healthy tissues, microcirculation in most malignant tumors exhibits a decrease in blood flow or even complete vascular stasis in response to hyperthermia. In addition, the combination of the inhibition of oxidative metabolism in tumor cells subjected to hyperthermic conditions and unaffected anaerobic glycolysis, leads to accumulation of lactic acid and lower pH in the microenvironment of the malignant cell. This causes an increase in the activity of the lysosomes (which are increased in under hyperthermic conditions) which in its turn causes accelerated cell death of the more fragile malignant cells.

- The combination of heat and antineoplastic drugs often results in increased cytotoxicity although this is not confirmed for all drugs

- Inhibition of repair mechanisms

Although hyperthermia is part of clinical practice in a number of different treatment centers, literature does not unanimously confirm these theoretical benefits. A possible reason for is that as temperature increases, vasodilation occurs which increases blood flow and peritoneal drug clearance. For a more detailed review of the contradicting literature on hyperthermia, Lagast et al. [166] can be consulted.

4.3.1.3 Exposure time

Exposure time of the cancer cells to the cytotoxic agent is a critical parameter for cancer cell kill. To increase this exposure time, a number of studies have been performed using prolonged drug delivery systems (DDS). The experiments made use of either nanoparticles, micelles, microspheres or hydrogels as carriers for the drugs in order to improve their exposure time. Other works proposed such a DDS be implanted to prevent peritoneal spread after resective surgery of primary gastrointestinal tumors or application of DDS in the treatment of malignant ascites [36, 59]. The implantation of DDS does not require the same level of technical set-up as conventional IPC and it less time-consuming. Most of these studies with DDS were done using animal models and found that either tumor volume decreased or median survival increased without added systemic toxicity. These studies are however very heterogeneous with respect to the choice of drug, dose and carrier, which complicates the comparison of different studies [36, 59].

Table 4.1: Advantages and disadvantages of drug delivery systems used for IPC. Adapted from [59].

Drug delivery system	Advantages	Disadvantages
Microspheres	Prolonged rentention time	Limited tumor penetration Risk of peritoneal ashesions
Nanoparticles	Small size passive targeting Avoiding MDR Lower incidence of peritoneal adhesions	Rapid clearance out of the abdominal cavity
Liposomes	Similar to nanoparticles Active targetting by varying parameters	Similar to nanoparticles
Micelles	Prolonged retention time	Increasing the systemic toxicity
Injectable systems	Prolonged retention time Localized and sustained drug delivery Lower systemic toxicity Prevention against peritoneal adhesion	Viscosity issues
Implantable systems	Similar to injectable systems	Invasive Surgical expertise

4.3.1.4 Carrier solution

In addition to prolonging exposure by means of DDS, changes to the carrier fluid in which the drug is dissolved or suspended might also increase exposure time. An ideal carrier solution for IP chemotherapy should expose all cancerous surfaces or residual tumor cells to high levels of cytotoxic agents for as long as possible and ensure a uniform distribution of the drug in the abdominal cavity [162, 196, 283].

Current IP chemotherapy protocols often administrate drug using isotonic electrolyte solutions (e.g., 5% glucose and 0.9% sodium chloride) which are rapidly absorbed due to their low molecular weight. The use of hypotonic solutions was ruled out as bleeding and thrombocytopenia occurred, while no pharmacokinetic advantages were observed. With the use of hypertonic solutions, prolonged retention times of fluid in the abdominal cavity was observed, but their main disadvantage is the dilution of the intraperitoneal drug due to fluid shift to the peritoneal cavity. Both 4% icodextrin, a colloid osmotic agent of the α-1,4 linked glucose polymer, and 6% hydroxyethyl starch (hetastarch), an isoosmolar solution have been proven to prolong retention of intraperitoneal chemotherapy [162, 196, 283].

4.3.2 Tissue related parameters

4.3.2.1 Stromal components

Tumor stroma consists of adipose tissue, smooth muscle and epithelial cells, but also includes pericytes, endothelial cells, leukocytes and cancer-associated fibroblasts. The increased deposition of collagen I in tumor stroma increases the stiffness of tumor tissue compared to normal tissue [310]. Although targeting the tumor stroma alone is unlikely to eliminate an entire tumor, IPC improvement techniques could include strategies to target and constrain the tumor stroma as a pretreatment. Not only does the tumor stroma pose a physical barrier to drug transport in the deeper tumor tissue layers (as reflected by the tissue permeability), but the tumor tissue is also known to promote tumorigenesis. A number of different stromal components have been targeted, both in mouse models as well as in clinical trials with promising results [36].

4.3.2.2 Tumor cell density

Pre-treatment with certain agents may reduce the cellular density of solid tumors, lower the IFP and enhance the subsequent IPC. One of the agents of interest is paclitaxel as it has shown both in human and animal models to reduce the microvascular pressure (MVP) and the IFP [197, 283]. It also increased the diameter of tumor vessels without a change in tumor vascular density, thus suggesting that taxanes increase the blood flow, blood volume, and vascular surface area for exchange of small therapeutic agents in tumors. Other pre-treatments used to decrease the tumor cell density before treatment include: cyclophosphamide, diphtheria toxin, etc... [97, 135].

4.3.2.3 Targeting the vascular system

The leaky, irregular microvasculature is one of the main contributing factors to the high IFP in solid tumors [121]. Pre-treatment of tumors with the angiogenesis-inhibiting agents (AIAs) like Bevacizumab and Pazopanib, have been described in the context of intraperitoneal chemotherapy [36]. In a mouse model, it was found that pre-treatment with either bevacizumab or pazopanib not only lowered IFP but also enhanced oxaliplatin penetration after IPC. Vaso-active agents which prevent outward transport of the drug by vasoconstriction of the tumor capillary bed and thereby improving tissue drug retention have been the subject of recent studies. Studied agents include norbormide, epinephrine and vasopressin and initial animal studied showed promising results, prompting a number of phase 1 clinical trials [36, 166].

4.3.3 Additional interventions

4.3.3.1 Ultrasound

Although it has not yet been tested in combination with IP chemotherapy, high-intensity focused ultrasound (HIFU) has been shown to increase the outcome of systemic chemotherapy for gastric cancer with abdominal lymph node metastasis [172, 306]. A similar approach could be tested for peritoneal metastases and peritoneal chemotherapy.

4.3.3.2 Radiotherapy

Some patients with peritoneal metastasis have received additional radiation therapy (RT) and while this improved overall survival compared to historic controls, it came at a cost of severe toxicities [54, 210, 332]. In another study concerning IP drug delivery and radiotherapy, various irradiation doses did not enhance the penetration of doxorubicin after pressurized aerosol delivery (PIPAC) in an ex vivo model on porcine peritoneal samples. Other findings from in vivo animal models were that fractionated RT was able to lower IFP and improve tissue oxygenation in a human tumor xenograft and a two- to four-fold increase in tumor uptake of doxorubicin after RT in a mouse xenograft model [150].

4.3.3.3 Phototherapy

Photodynamic therapy (PDT) may lower the IFP by impairment of the tumor microcirculation. Several works have shown in animal models that

low-dose PDT not only decreased IFP, but also enhanced tumor tissue distribution of doxorubicin in treated animals [36, 170, 220]. In the context of IP cancers, the use of PDT can only be considered when a CRS is planned. The photosensitizer should be administered a sufficient amount of time before the CRS and once the debulking is performed, the (laser) light delivery should be initiated.

4.3.3.4 Oxygen therapy

Hyperbaric oxygen (HBO) treatment have been used extensively for conditions involving hypoxia and ischemia, by enhancing the amount of dissolved oxygen in the plasma and thereby increasing O_2 delivery to the tissue. Solid tumors often contain hypoxic areas due to the abnormal tumor vasculature and the degree or presence of hypoxic zones plays an important role as a negative prognostics and predictive factor. Several recent work have shown that HBO treatment increases the uptake of cytotoxic agents, among which the work in which peritoneal delivered [3H]-5FU was administered [36, 195].

CURRENT CHALLENGES FOR INTRAPERITONEAL CHEMOTHERAPY AND RESEARCH GOALS

Although there is a strong rationale for intraperitoneal chemotherapy (IPC) and clinical results have proven its merit on numerous occasions [38], there are a number of issues that limit the widespread use of the technique [63]. This chapter will highlight the two main limitations for IPC and research goals for this dissertation will be formulated in this context.

5.1   LIMITATION 1: SURFACE EXPOSURE

5.1.1   Description of limitation

The first limitation of current IPC regimens is that due to complex anatomy of the peritoneum and the additional presence of disturbances such as adhesions and tumor nodule clusters of the diseased peritoneum, it is very difficult to obtain a good surface exposure of the entire peritoneal membrane during intraperitoneal chemotherapy [63, 89, 237]. To obtain a sufficient distribution of the solution throughout the entire abdominal cavity, IPC is often performed immediately after the cytoreductive surgery

(CRS) when the abdomen is still open so that stirring or other manipulation techniques can be used. This open technique, although efficient has several disadvantages [278, 277]:

- Cytoreductive surgery by itself is already a demanding procedure with a high associated morbidity and mortality [5]. The addition of IPC only adds to the length of the procedure and might add to the morbidity and mortality

- The open abdominal method increases the exposure of operating room personnel to chemotherapy. The staff member who will manually manipulate the chemotherapy during the perfusion has an additional risk for contact exposure. Furthermore, the additional safety measures during the procedure are cumbersome and further contribute to the cost of the surgery [105, 108, 311].

- The method using an open abdominal cavity does not allow for prolonged or continuous IP drug instillation, which is increasingly recognized as a major determinant of the anticancer efficacy of IP drug [253].

Alternatively, IP drugs can also be delivered in a closed set-up after the placement of a Tenkhof type catheter, the tip of which is positioned in the pelvic space. Chemotherapy is then diluted in a carrier fluid which is either drained by a set of outflow catheters (when performed intra-operatively) or not aspirated at all but allowed to resorb from the peritoneal cavity (when performed post-operatively) [79, 223, 277, 297]. This method has several disadvantages:

- The pelvic position of the catheter does not allow to treat the affected peritoneal surface in a homogenous and effective manner. Specifically, many patients have tumor deposits in the upper abdomen and diaphragmatic surfaces, which are unlikely to be adequately treated

- In the case of hyperthermic IPC, the inhomogeneous distribution of the solution can lead to local temperature spikes above the tolerable region which in its turn will add to the morbidity of the procedure. [277]

- The instillation of large volumes of fluid, when the carrier solution is not drained, frequently causes significant pain and distress

- The currently used intra-operative method does not allow to provide prolonged or continuous IP drug instillation, which is increasingly recognized as a major determinant of the anticancer efficacy of IP drug. [253]

5.1.2 Research Objective 1

In order to overcome these limitations, a first research goal will be the design and development of a novel catheter type that will allow adequate treatment of the complete peritoneal surface while avoiding the above mentioned problems related to the instillation of large volumes of fluid, and permits prolonged continuous infusion using a patient wearable pump. In order to meet this research goal, a number of questions should be answered.

- What design features should an ideal catheter have for this application?

- Can we theoretically design a catheter that meets these design requirements?

- Can we manufacture a prototype of the theoretically designed catheter?

- Does the prototype perform as predicted and does it meet the design requirements?

The first chapter of the second part of this dissertation will describe the conceptual design, theoretical considerations, prototype development and computational simulations, manufacturing and in-vitro testing of the prototype of a novel catheter design.

5.2 LIMITATION 2: PENETRATION DEPTH OF DRUGS

5.2.1 Description of limitation

A second major limitation of intraperitoneal chemotherapy is the very limited penetration depth of the cytotoxic drugs into the tumor tissue [63]. Due to this limited penetration, IPC is generally only performed after complete cytoreduction or when minimal residual disease (< 2.5

mm) is present after cytoreduction. Understanding the physical transport mechanisms occurring during IPC that will determine the final penetration depth of drugs in the tumor and surrounding tissue layers is crucial and allows for the identification of therapeutic targets that can be altered to improve the therapeutic outcome. A summary of the additions and alterations to the IPC standard of care that have been investigated was discussed in chapter 4.

5.2.2 Research Objective 2

Although the identification of possible targets can usually be done by theoretical considerations, subsequent steps to confirm the hypothesis generally require extensive in vitro or in vivo studies, which are not only labor and time consuming but also expensive. In this context, the use of a mathematical model proposes a fast and relatively low cost technique to gain more insight in the influence of single parameters on drug penetration depth. The second research goal of this work focusses around the development of a mathematical model to study drug distribution during intraperitoneal chemotherapy. To meet this research goal, a number of questions will be answered:

- What is the current state of the art of modelling drug transport during intraperitoneal chemotherapy? What are the differences between the existing models and what do we aim to add to this state of the art?

- Can we formulate a model for IP drug transport that includes hallmarks such as the outward convective IF flow, vascular uptake and in a number of idealized geometries? Does the model perform well when compared to available literature data and how sensitive is it to changes in the governing parameters such as drug diffusivity, permeability, vascular permeability etc?

- Can we expand the developed model to include realistic geometries and vascular properties obtained from imaging and does this add value to the model? Are the trends of the idealized model still true for the expanded model?

- Is this expanded model able to correctly predict the IFP and drug penetration?

To answer the first question, the second chapter of part 2 (chapter 7) will provide a summary of the state of the art in the modelling of intraperitoneal chemotherapy.

A mathematical model of IPC is proposed in the third chapter and the solution for the model is presented in 6 idealized baseline tumor geometries of different size and shape. Using these baseline results, the relative influence of different parameters on the penetration is studied and general trends are derived from these results.

In the nineth chapter, the model from chapter 8 will be expanded to include realistic geometries and vascular permeability data derived from dynamic contrast-enhanced magnetic resonance imaging (DCE-MRI) data in a mouse model. The findings of the IPC model will be compared to those in chapter 8 to assess the added value of incorporating subject specific geometries and vascular data. Additionally, invasively measured pressure data will be compared to calculated pressure profiles for each tumor to test the performance of the IFP prediction of the model. A final part will summarize the main findings of this dissertation and refer back to the research goals and questions formulated in this section and propose some future directions.

II

Modeling intraperitoneal drug delivery and transport

6

A NEW DRUG DELIVERY SYSTEM FOR INTRAPERITONEAL CHEMOTHERAPY: DESIGN, DEVELOPMENT AND BENCH TESTING

Despite advances in systemic anticancer therapy, treatment of peritoneal metastases (PM) remains a considerable challenge. Since PM are difficult to treat and may cause significant and invalidating symptoms, there is increasing interest from clinicians in the combination of cytoreductive surgery with intraperitoneal (IP) drug delivery. Currently, IP chemotherapy is administered by a single-filament catheter (Tenckhoff Type) that is put in place operatively deep in the pelvis (figure 6.1). This method however, has a number of inherent restrictions. First, positioning a single catheter in the abdominal cavity does not allow to treat the affected peritoneal surface in a homogenous and effective manner. Specifically, many patients have tumors in the upper abdomen and diaphragmatic surfaces, which are unlikely to be adequately treated using this method. Furthermore, the administration of large volumes of fluid which is usually the case during IPC frequently causes significant pain and distress to the patients. The currently used method also does not allow to provide prolonged or continuous IP drug instillation, which is increasingly recognized as a major determinant of the anticancer efficacy of the IP drug.
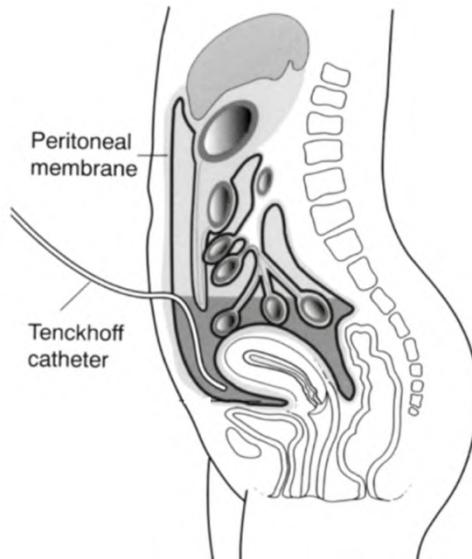
Figure 6.1: Placement of intraperitoneal catheter in the pelvis. Source:
https://www.ouh.nhs.uk/patient-guide/leaflets/files/48046Prenal.pdf

In this chapter, we propose and discuss a simple yet innovative multi-
filament catheter that allows for a more homogeneous and prolonged
delivery op IPC.

6.1 INTRODUCTION

Currently, there is no standard IPC protocol that is used to treat PM. In
section 3.3, the state of the art of IPC was discussed with special atten-
tion to the differences between available protocols. One of the main
challenges for intraperitoneal chemotherapy (IPC) is the poor surface
exposure of the peritoneal surface during intraperitoneal chemotherapy
[127] and for this reason, IPC is often performed using an open abdomen
technique, so that the drugs can be manually stirred. The downsides of
this technique include the occupational hazards for the surgical staff, the
significant expertise needed to perform this technique and the inability
to perform repeat cycles of IPC. In closed IPC techniques on the other
hand, in- and outflow catheters are placed in the abdominal cavity, after
which a water-tight closure of the abdominal wall is performed. The
drug distribution is thought to be less homogeneous than in the open
abdomen set-up, resulting in possible toxicity for the healthy surround-
ing tissues, whilst temperature control is also more challenging than in

closed IPC techniques. Additionally, repeat cycles of IPC are not possible in most open techniques, as the catheters are usually removed after the IPC cycle and the abdomen is properly closed. With recent interest in metronomic chemotherapy [137], closed IPC set-ups have been used outside the operative context, which can then be used for repeated, prolonged exposures. The complete drug delivery setup in this case consists of an infusion pump, a gripper needle, an implantable port catheter and a single perforated catheter (figure 6.2). As in other closed IPC techniques, the non-homogeneous distribution of the instilled fluid in the peritoneal cavity is one of the main disadvantages of this technique. In this chapter, a new, closed IPC set-up will be proposed that aims to improve the drug distribution in the peritoneal cavity.
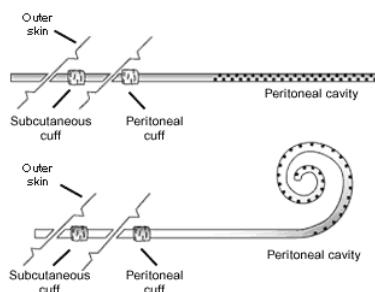
Figure 6.2: Single perforated catheter for intraperitoneal dialysis or drug delivery.

6.2 DESIGN OF THE CATHETER PROTOTYPE

The set-up proposed in this chapter, aims to replace the single perforated outflow catheter, with a non-perforated inflow catheter that attaches to a connector piece, which in turn connects to seven perforated outflow catheters with end pieces (figure 6.3). Only these three elements make up the new prototype, with other elements being commercially available and equal to the current single catheter set-up/ The infusion pump is also added to the set-up to deliver the flow of drug and carrier fluid as opposed to the classic set-up which relies on gravitational infusion of the drug. To connect the single (now non-perforated) inflow catheter from the implantable port catheter to the seven outflow catheters a custom connector piece was developed and 3D-printed (in a biocompatible material). The connector piece consists of a body with a small eyelet (for attachment with a stitch), a single inflow support and seven smaller outflow supports, evenly spaced around the body, to which the catheter arms can be attached, each with a length of one cm. The inner dimensions

of both the in- and outflow supports match the inner diameter of the
in- and outflow catheters respectively. The wall thickness of the in- and
outflow supports was chosen (t = 1 mm) based on a trade-off between the
ease of assembly and the need to provide a good support and connection
the connector piece. The attachment of the small eyelet to the body of
the connector piece allows for a stable anchoring of the piece within the
abdominal cavity. The connector pieces were assessed in a qualitative
way to ensure that no obstruction was present. When differences in the
outflow patterns between the different catheter arms were noted for the
first time, the arms were rotated along the connector piece to exclude
issues with the connector pieces as the cause for these in homogeneities.
The end pieces are 3D-printed, tapered cylinders with a radius ranging
from 100 to 120% of the inner radius of the outflow catheters. At the end
of each end piece, an eyelet was placed to anchor the catheter arm within
the abdominal cavity. The design of the perforated catheter arms was the
main focus of this work and will be discussed in more detail in the next
section.

1. Infusion Pump
2. Gripper Needle
3. Port-a-Cath
4. Non-Perforated Transport Catheter
5. Connector Piece
6. Perforated Outflow Catheters
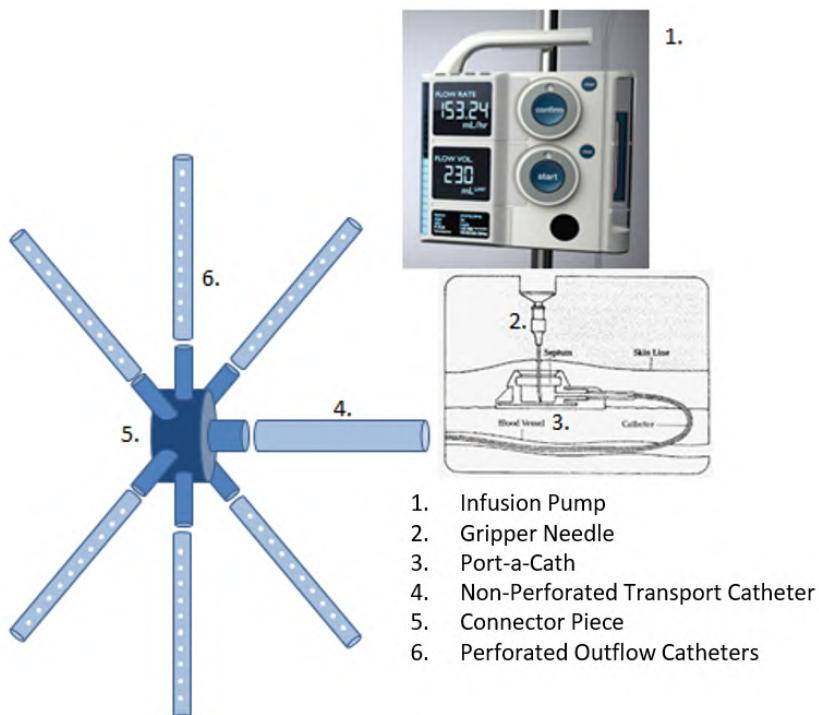
Figure 6.3: Full set-up for intraperitoneal drug delivery

The main design idea of this novel drug delivery system is that mul-
tiple, thinner catheters will be used to administer the cytotoxic solution,

with each of these thinner catheters having multiple perforations along its full length, resulting in a more homogeneous drug delivery in the abdominal cavity. Although the design is simple in idea, in order for it to perform well, a well-considered choice should be made in number and size of perforations and their spacing. In this section we will describe the theoretical considerations that were made to obtain an idea of the optimal distribution and size of the perforations to generate an equal distribution of the chemotherapy solution along the catheter length. Using these theoretical considerations, 3D models of different catheter designs were then created and the steady solution for a continuous infusion was calculated in ANSYS FLUENT. The outflow at each perforation was used to assess the performance of each catheter design. Based on both theoretical and computational results, a number of different designs for the perforated catheters were chosen to be prototyped and undergo in vitro testing.

6.2.1 Theoretical catheter design

The number, size and spacing of the perforations along the catheter length are considered to be variable in this work; all proposed designs shared all other basic geometrical features as listed in table 6.1. In order to find an optimal distribution and diameter for the perforations, pressure drops over each perforation were calculated according to Poiseuille's law. Poiseuille's law relates the pressure drop and flow of an incompressible, Newtonian fluid in steady laminar flow flowing through a long cylindrical pipe of constant cross section:

$$\Delta p = \frac{8\mu L Q}{\Pi R^4} \tag{6.1}$$

With p the pressure in Pa, L the length of the tube in m, R the radius of the tube in m, Q the flowrate in m^3/s and μ the dynamic viscosity in $Pa \cdot s$. The resistance to flow for each perforation is calculated as the sum of the resistance in both the longitudinal (z; along the tube) and radial (r; through the perforation) direction (figure 6.4). By making sure the total resistance at each perforation is similar, the desired uniform outflow pattern along the catheter can be approximated.

For a theoretical case with n perforations, the resistances for each perforation can be written as:

$$Perforation1: R_z^{(1)} + R_r^{(1)} = \frac{8\mu}{\pi}\left(\frac{L}{R^4} + \frac{l}{r_1^4}\right) \tag{6.2}$$
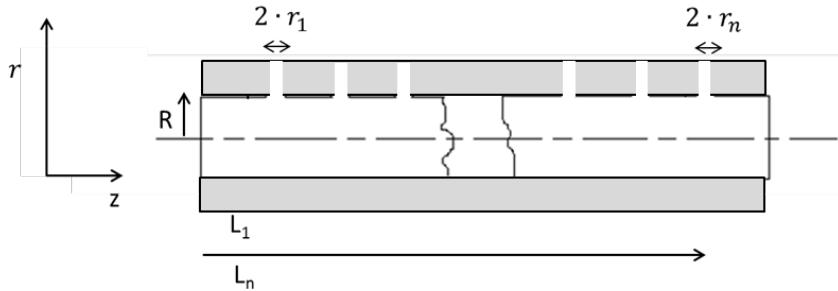
Figure 6.4: Section of a catheter arm along its long (z) axis with the parameters used in this chapter. Note that only the fluid zone is modeled in this work (shown in white on the figure) and the catheter wall is not explicitly modeled. Instead of explicitly modeling the catheter solid zone, all boundaries except in and outflow surfaces were described using a wall boundary condition, meaning that no transport is possible over these surfaces. R is the inner radius of the catheter, r_i is the radius of the ith perforation, l is the wall thickness of the catheter, L_i is the distance measured from the inlet of the catheter to the ith perforation.

Table 6.1: Shared geometrical features for all possible catheter designs

Design Feature	Value [mm]
Length	300
Inner diameter	1
Outer diameter	1.8

$$Perforation 2: R_z^{(2)} + R_r^{(2)} = \frac{8\mu}{\pi}\left(\frac{\beta_1 L}{R^4} + \frac{l}{\alpha_1 r_1^4}\right) \tag{6.3}$$

$$Perforation n: R_z^{(n)} + R_r^{(n)} = \frac{8\mu}{\pi}\left(\frac{\beta_{n-1} L}{R^4} + \frac{l}{\alpha_{n-1} r_1^4}\right) \tag{6.4}$$

Where α and β are α=f(z) and β=f(z,N$_p$). The α values (α_1, α_2, ..., α_{n-1}) relate the radius of each of the perforations back to the first one; the β values (β_1, β_2,..., β_{n-1}) are corrective factors for the spacing between the perforations. A graphical representation of the parameters is given in figure 6.4. The design problem for these catheter arms is now reduced to finding a suitable set of $\alpha(z)$ and $\beta(z, N_p)$ that will lead to the desired homogenous outflow. This can be accomplished by requiring the total resistance for each of the different perforations to be equal:

$$R_z^{(1)} + R_r^{(1)} = R_z^{(2)} + R_r^{(2)} = \cdots = R_z^{(n-1)} + R_r^{(n-1)} \tag{6.5}$$

Which in turn leads to:

$$R_z^{(1)} + R_r^{(1)} - \left(R_z^{(2)} + R_r^{(2)}\right) = \cdots = R_z^{(n-1)} + R_r^{(n-1)} - \left(R_z^{(n)} + R_r^{(n)}\right) = 0 \tag{6.6}$$

Because the hydraulic resistance is more sensitive to the radius of the perforation and to a far lesser extent to the distances between the perforations of the catheter it was decided to fix the distance between the perforations, reducing $\beta_1, \beta_2, \ldots, \beta_{n-1}$ to $2,3, \ldots, N$ respectively. The next design choice that was made was to fix the number of perforations to nine, resulting in a distance of 30 mm between two perforations.

For a catheter with nine perforations, the problem is then to solve eight independent equations, each one in a unique variable (respectively $\alpha_1, \alpha_2, \ldots, \alpha_8$).

For the first and the second perforations, we have:

$$\frac{8\mu}{\pi}\left(\frac{L}{R^4} + \frac{l}{r_1^4} - \frac{2L}{R^4} - \frac{l}{\alpha_1 r_1^4}\right) = 0 \tag{6.7}$$

From which α can be calculated as:

$$\frac{1}{\alpha} = 1 - \frac{L}{l}\left(\frac{r_1}{R}\right)^4 \tag{6.8}$$

In an analogous way, the following general formula is derived:

$$\frac{1}{\alpha_n} = \frac{1}{\alpha_{n-1}} - \frac{L}{l}\left(\frac{r_1}{R}\right)^4 \tag{6.9}$$

As can be seen from the equation above, an initial value for the radius of the first perforation is needed to find a distribution of the perforations. table 6.2 shows an example of a possible catheter design with corresponding alpha values and perforation diameters in the case where the radius of the first penetration $r_1 = 0.075 \ mm$.

Table 6.2: Catheter design example with corresponding alpha values

Diameters [mm]	A
0.15	-
0.15	1
0.155	1.039
0.162	1.08
0.17	1.131
0.177	1.18
0.186	1.237
0.195	1.3
0.2	1.37

6.2.2 Computational validation of proposed designs

Based on the theoretical considerations described in the previous section and on a number of practical considerations (i.e. the possibility to only manufacture perforations with a 'rounded' number as diameter, the minimal diameter for perforations along a catheter arm to avoid flow obstructions due to biofilm generation, ...), several different designs were selected to be validated by computational fluid dynamics (CFD) modeling. The proposed designs are listed in table 6.3.

Table 6.3: Proposed designs for which CFD modeling was performed

Geometry	Number of perforations	Spacing between perforations [mm]	Diameters used	Occurrence
Geometry 1	9	30	1	0.30 mm (9x)
Geometry 2	9	30	1	0.20 mm (9x)
Geometry 3	9	30	1	0.15 mm (9x)
Geometry 4	9	30	1	0.10 mm (9x)
Geometry 5	9	30	3	0.30 mm (3x) / 0.40 mm (3x) / 0.45 mm (3x)
Geometry 6	9	30	5	0.20 mm (1x) / 0.227 mm (1x) / 0.262 mm (1x) 0.312 mm (1x) / 0.5 mm (3x)
Geometry 7	9	30	8	0.15 mm (2x) / 0.155 mm (1x) / 0.162 mm (1x) 0.17 mm (1x) / 0.177 mm (1x) / 0.186 mm (1x) 0.195 mm (1x) / 0.20 mm (1x)
Geometry 8	9	30	2	0.15 mm (5x) / 0.20 mm (4x)

The different geometries were created and meshed in ANSYS Workbench. All meshes used tetrahedral elements and were refined around the locations of the perforations. The boundary condition imposed at the inlet of the catheter was based on the typical flow rate of infusion pump. The pump can deliver a flow rate anywhere between 0.1 ml/h and 1200 ml/h. The simulations were performed with a volumetric flow

rate at the inlet of 10 ml/h, which results in a velocity inlet of 0.000504 m/s when assuming a flat velocity profile and a Reynolds number ranging from 0.146 to 0.728. These Reynolds numbers are very small, indicating the strong laminar behavior of the flow in the catheter. To make sure that a fully-developed velocity profile was present at the inlet, the length of the catheter was increased, according to the formula L_e=0.035 Re where Re is the Reynolds number and L_e is an entrance length needed for the build-up to the parabolic profile. A summary of the used boundary conditions can be found in table 6.4.

The numerical simulations performed for this study were carried out using FLUENT (Ansys) in which fluid flow problems are solved by calculating the Navier–Stokes equations using a finite volume method. In cases such as these (steady, incompressible flow with no heat transfer) only the conservation equations for mass and momentum are solved. The continuity equation for an incompressible fluid is given by:

$$\nabla \cdot \vec{v} = 0 \qquad (6.10)$$

in which $\vec{v}$ is the velocity vector. The conservation of momentum is given by:

$$\frac{\partial}{\partial t}(\rho \vec{v}) + \nabla \cdot (\rho \vec{v} \vec{v}) = -\nabla p + \nabla \cdot (\bar{\bar{\tau}}) + \rho \vec{g} + \vec{F} \qquad (6.11)$$

in which ρ is the density of the fluid, $\vec{v}$ the fluid velocity vector, p the static pressure, $\rho \vec{g}$ the gravitational force, $\bar{\bar{\tau}}$ the stress tensor and $\vec{F}$ the external body force.

The governing equations were solved using the segregated solver (SIMPLE) with a semi-implicit method for pressure-linked equations. Second-order upwind accuracy was used both for pressure and momentum. Convergence was said to be reached when the residuals of continuity and velocity had at least dropped by 4 orders of magnitude. A mesh sensitivity analysis was carried out to assure independence of the solution to the used mesh.

Upon comparison of the obtained outflow distributions for the 4 geometries with a single perforation diameter (geometries 1-4 in table 6.3), it can be seen that the outflow profiles are more uniform with decreasing perforation diameter. For geometry 1, the difference between the outflow

Table 6.4: Summary of the boundary conditions used for all the geometries

Location	Specifications
Inlet	Type: velocity inlet Velocity =5.04e^{-4} m/s
Outlet	Type: pressure outlet Pressure = 0 Pa
Perforations	On outlet surface: Type: pressure outlet Pressure = 0 Pa On lumen: Type = wall
Lumen	Type = wall
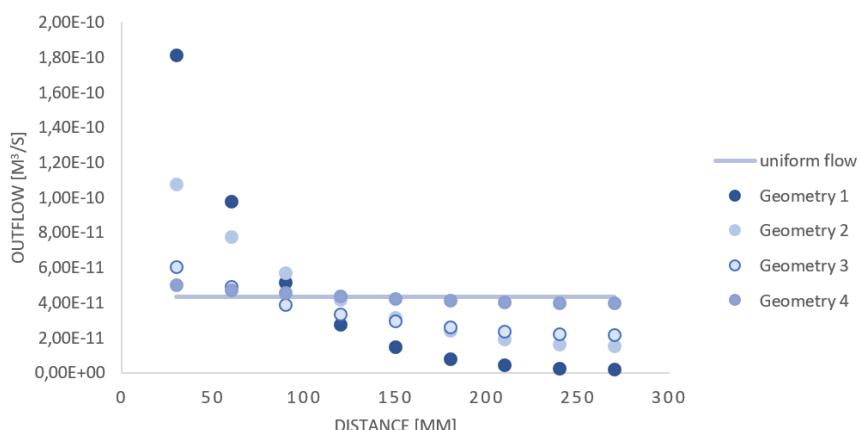
Figure 6.5: Outflow at all perforations in function of distance to inlet for the 4 first geometries decribed in table 6.3 with uniform perforations.

at the first and last perforation exceeds two orders of magnitude while for geometry 4 it is almost zero.

From these results (figure 6.5), it can be concluded that using a single perforation diameter is feasible, provided that the used diameter is very small. The smaller the perforation however, the bigger the chance of it becoming obstructed by biofilm. To avoid the use of very small perforation sizes while avoiding an uneven flow profile, different perforation diameters were used along the length of the catheter. The smallest diameters were used close to the inlet whereas the larger ones were used closer to the outlet according to what was found in the previous section.
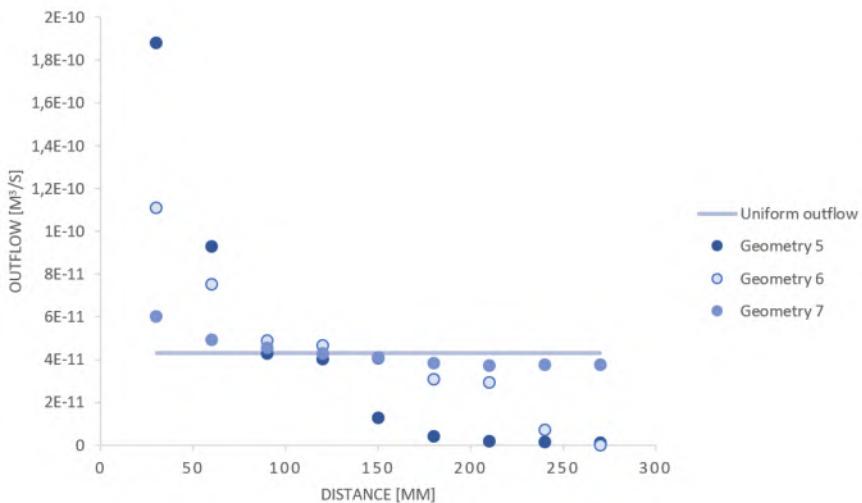
Figure 6.6: Graphical representation of the outflow in function of distance to inlet for the three last geometries in table 6.3 with different perforation diameters along the length of the catheter.

From figure 6.6, it can be noted that using different diameters improves the uniformity of the outflow through the perforations. Upon comparison of geometry 2 to geometry 6 (which both share an initial perforation diameter of 0.20 mm), an improvement in flow homogeneity in the 5 middle perforations can be noted, resulting in a profile that is almost uniform from the third to the seventh perforation. Similar improvements can be noticed when comparing geometry 3 to geometry 7.

Based on these simulated flow distributions a number of different catheter designs were created as prototypes both to validate the numerical model and to provide an in vitro test setup for the catheter (catheters 1-5 and 8 from table 6.3).

6.3   IN VITRO TESTING OF THE PROTOTYPES

6.3.1   In vitro test: single catheter

Prototypes of single perforated catheter arms were manufactured accord-
ing to the specifications in table 6.3. Once the prototypes were made, tests
were performed by connecting these catheter arms to an infusion pump
(flow rate of 10 ml/h; duration of 1 hour) and measuring the outflows
through each perforation. Distilled water was used at room temperature
for all experiments. The experimental results where then compared to the
results of the CFD simulations.
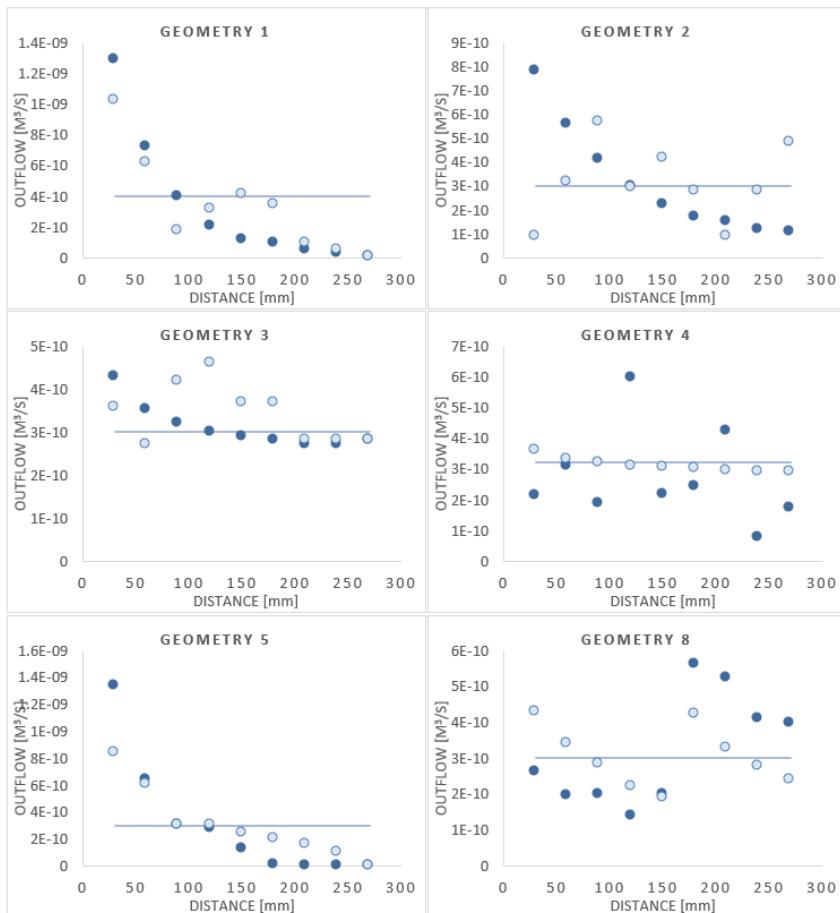
Figure 6.7: Comparison between experimental and simulated flow profiles

By looking at figure 6.7, it is clear that the experimental and CFD
results are not in full agreement. Not only do the numerical values of

the outflow differ between both results, but not even the general trends present in the CFD results are present in the experimental data. Through additional repeatability experiments and microscopic inspection, it was found that manufacturing issues with the microdrilling of the perforations where at the bases of these discrepancies (section 6.3.3) and microdrilling was ultimately abandoned as a result.

6.3.2 In vitro test: full set-up

In addition to the single catheter tests, two complete, branched catheters were assembled and underwent hydraulic testing. Each test spanned 3 full days during which demineralized water was infused at a rate of 500 ml/day. The full set-up further consisted of an infusion pump with attached fluid reservoir, the connector piece, the 7 perforated catheter suspended on a Styrofoam base, the end piece for each of the 7 arms and 9 collector tubes per catheter arm (one for each perforation) (figure 6.8).

1) Power plug of infusion pump
2) CADD-Solis VIP ambulant infusion pump set to 500 ml/day for 3 consecutive days
3) Fluid reservoir
4) Perforated catheter arm
5) Outflow collection
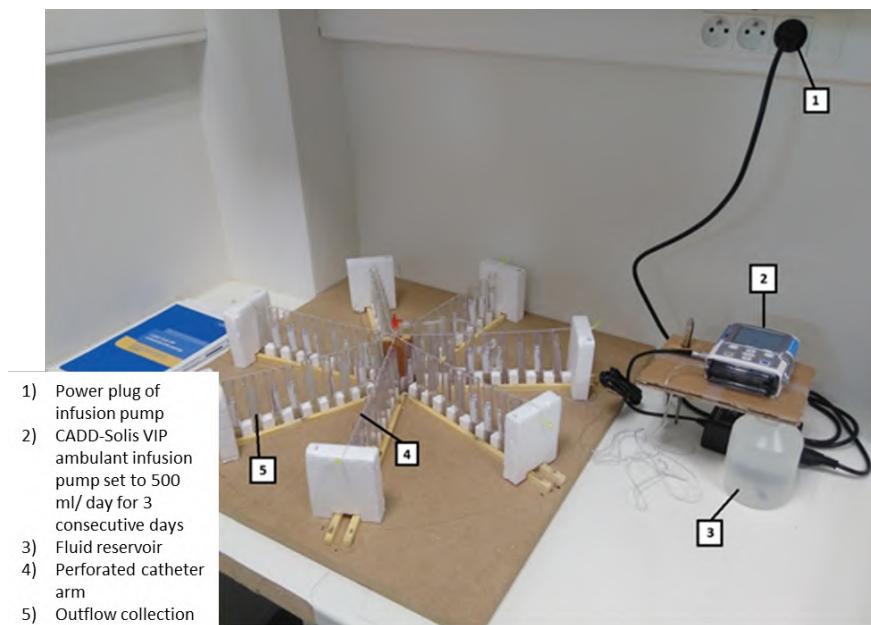
Figure 6.8: Experimental set-up of the full catheter

For the first catheter, flow rates through the 7 different arms varied from 127 to 361 ml (figure 6.9) and flow rates through single perforations varied from 0 to 185 ml. In total, 26 of the 63 perforations (±40%) of the branched catheter showed no outflow over the three days. Results for the second catheter were even less homogeneous with flow rates through the

different arms ranging from 18 to 741 ml. From these results, it was clear that the fluid distribution of the prototypes is nowhere near to homogeneous.
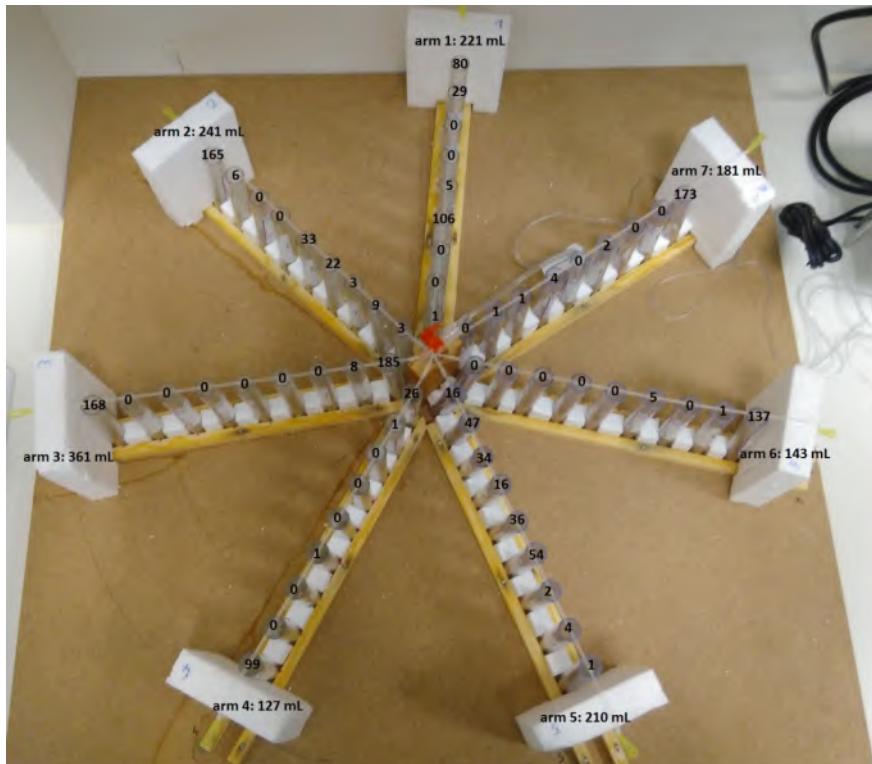
Figure 6.9: Outflow for each perforation after three days of infusion at 500 ml/day

6.3.3 Manufacturing methods and issues

The results of the previous sections show persistent differences between experimental results and CFD simulations. To test our hypothesis that manufacturing issues were at the base of these discrepancies, several reproducibility experiments were performed. Three theoretically identical designs with 9 perforations with a 0.30 mm diameter were tested and outflow patterns for the 3 experiments were compared. The same experiment was repeated for a catheter design with 9 perforations of 0.10 mm diameter. All the catheters were manually drilled by the same operator from the same batch of tubing and using the same drillbits. The tests were performed using the same equipment and same settings at a pump flow rate of 10 ml/h for one hour.
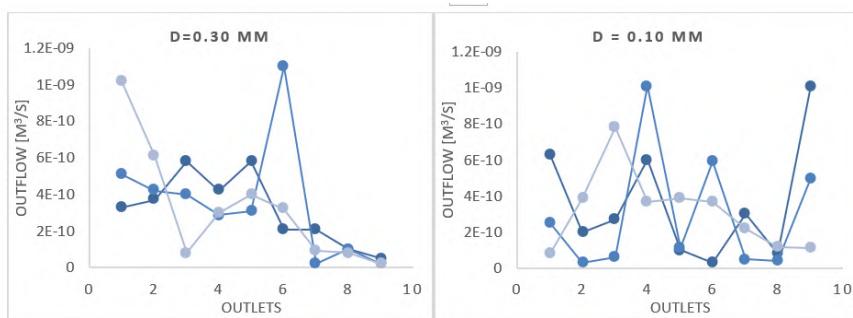
Figure 6.10: Flow profiles for three manufactured catheters with identical design specifications

Figure 6.10 shows that there are large differences in the outflow patterns of catheters that should theoretically give almost identical results. As all other testing and manufacturing conditions were kept equal for all cases, these results strongly suggest that geometrical differences in the perforations, due to manual manufacturing had a strong influence on the catheters performance.

For these first sets of prototypes, all perforations were manually drilled using small microdrillbits according to the proposed designs specifics proposed in table 6.3. Further microscopic investigation of the drilled perforations revealed a number of manufacturing issues such as burr formation (figure 6.11), non-round perforations, incomplete perforations, and perforations inconsistent in size. It should be noted that these issues were not only present on the smallest perforations (0.1 -0.15 mm) but also on the larger perforations (0.3-0.35 mm). Due to these issues and the fragility of the small microdrillbits, our initial manufacturing process was abandoned and other manufacturing options were explored.

In a second set of prototypes, the perforations were made using a laser with a spot size of 30 micron. The beam shape consisted of several of these spots and the circular perforation is created after the edge of the perforation is ablated in a number of subsequent layers and the middle (waste) piece falls through. The process of creating the perforations using a laser beam was more cumbersome as both the energy and the number of pulses had to be calibrated to the used tubing material and thickness. Both the energy level used and the amount of pulses were a trade-off between obtaining a cylindrical perforation with neat, circular edges devoid of any debris on the one hand and maintaining the integrity of the opposite catheter wall. Although initial microscopic images of the perforations showed neat albeit slightly tapered perforations, hydraulic
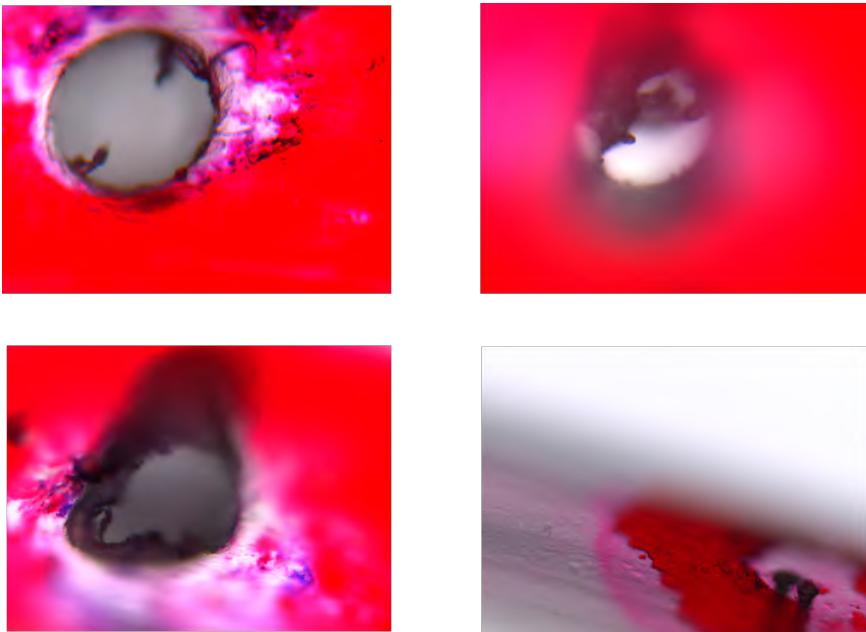
Figure 6.11: Microscopic images of the microdrilled perforations showing the presence of burrs and uneven perforations

testing again revealed inhomogeneous flow profiles that could be traced back to manufacturing issues.

6.3.4   Numerical simulations of measured prototype

As mentioned in section 6.3, the experimental results consistently differed from the obtained numerical results. To exclude numerical errors in our model as a possible explanation for the discrepancies, the actual perforation diameters (both on the inner and outer wall) of a catheter that was designed to have 9 perforations with a 0.30 mm diameter, were measured using microscopy. Based on these measurements, the actual catheter geometry was created in FLUENT, with the perforations being modeled as tapered cylinders. Upon simulation of the flow through the actual geometry, a very good agreement could be found between the model and the in vitro set-up figure 6.12).

These results seemed to confirm our hypothesis that manufacturing issues where at the base of the discrepancy between simulated and experimental results.
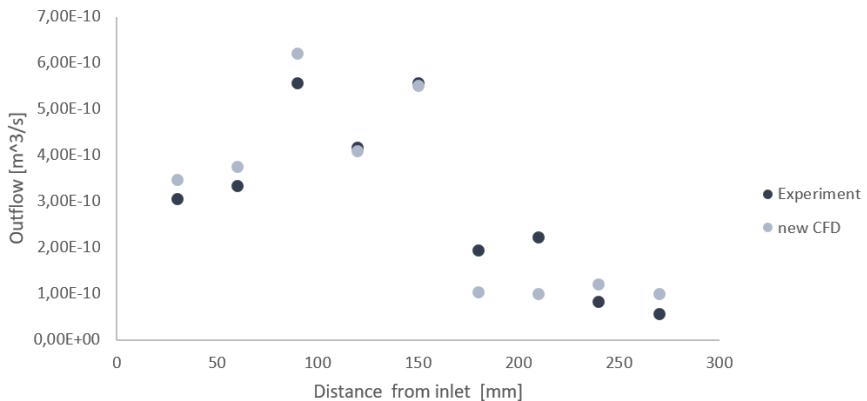
Figure 6.12: Model validation using experimentally measured geometry

6.4 FUTURE DIRECTIONS

In this chapter we presented a novel approach for IPC that shows potential to overcome one of the main limitations of current IPC practice: the limited surface exposure of the peritoneal surfaces. Through both computational and theoretical modeling, we were able to propose a number of valid catheter designs which were then manufactured using two different techniques. Even though all proposed geometries performed well in simulations, none of the first prototypes performed well during hydraulic testing. The reason for this underwhelming performance was traced back to manufacturing issues and inaccuracies and as a result, the first manufacturing approach (microdrilling) was abandoned in favor of laser ablation. Despite solving some of the manufacturing issues (i.e. presence of debris, double perforations, non-spherical perforations, ..), laser ablated catheters did not outperform the previous catheters. As the measurement of the final perforations obtained through laser ablation revealed, a minimal standard deviation of 30 micron is to be expected on the perforations size as well as a tapering factor of approximately 50%. Given these tolerances on the perforation size and shape, none of the proposed catheter geometries remain feasible. Future work should therefore focus on the search for a novel manufacturing method that is able to produce perforations with reproducible results and acceptable tolerances. The final material selected for this catheter should be flexible enough to be easily positioned in the abdominal cavity, be compatible with the manufacturing technique and should not interfere with the flow of the drug molecules (such as binding, polarity, ...). Until now, the validation of the connector piece was only done in a quantitative way. Future work

should also include hydraulic testing of the 3D-printed connector pieces and microscopic measurements of its final inner diameters to assess the influence of the manufacturing tolerances on the flow pattern.

MODELLING DRUG TRANSPORT DURING INTRAPERITONEAL CHEMOTHERAPY

This chapter is based on "Modelling Drug Transport During Intraperitoneal Chemotherapy", as published in Pleura and peritoneum, 2(2). p.73-83 [270].

7.1 INTRODUCTION

In 1978, Dedrick et al [64] hypothesized that the peritoneum-plasma barrier, which was previously considered to be an obstacle for drug transport, might rather offer a unique treatment opportunity for patients with oncological malignancies confined to the peritoneal cavity. The idea was put forward that when cytotoxic drugs are administered directly into the peritoneal cavity, the peritoneum would limit the drug absorption in the systemic circulation. This would result in higher local drug concentrations in the tumor tissue while minimizing the development of systemic side effects, an idea that has been proven to be true by different groups since then [115, 194].

The higher drug concentrations that are locally obtained in the tumor tissue are important because of the steep dose-response relationship for

cytotoxic agents on the one hand and because it can prevent the development of resistance of the tumor against the used chemotherapeutic agent. Additionally, some peritoneal metastasis are nearly avascular and are consequently not treatable by intravenous chemotherapy as there is simply no vascular drug source present within the tumor [38]. The direct contact between the cytotoxic drug and the tumor tissue does allow for these poorly vascularized tumors to be exposed to the chemotherapeutic agent. Additional to these high local tumor tissue concentrations, there is uptake of the drug by the vascular component of the tumor tissue which results in a systemic drug effect. This systemic effect is of the same order of magnitude as the one obtained during intravenous (IV) chemotherapy, meaning that for the same systemic toxicity, the local tissue concentration obtained by intraperitoneal chemotherapy can exceed the tissue concentrations that would be obtained by conventional chemotherapy [194].

Even though the rationale behind intraperitoneal chemotherapy (IPC) has been well established, it has not yet become standard of care mainly due to the limited penetration depth of the cytotoxic agent into the tumor tissue [202, 296, 192, 178, 7, 239]. Drug transport during IPC is a complex process that is governed by a multitude of parameters which can be separated in three distinctive categories: tissue-related parameters, drug-related parameters and therapy-related parameters (table 7.1). In the next paragraph an overview of the different steps that occur in the transport process during IPC will be given and all relevant parameters will be briefly discussed.

Mathematical modelling of drug delivery started in the 1960's [159, 235] and has since then become an important tool for the cancer researcher due to its relative ease and its low cost. Furthermore, modelling of drug transport allows for the variation of single parameters over large ranges of values, which makes it especially suited to study the relative influence of parameters on therapeutic outcome without the need for expensive experiments. In this review, we will focus on the work that has been done on mathematical and computational modelling of intraperitoneally administered anti-cancer drugs acting on tumor tissues. In this work, we chose to subdivide the existing models based on the used scale of the model. A distinction will be made between three different scales: the whole organ scale, which considers the peritoneum as a single compartment; the tissue scale, which considers the tissue of the tumor as a homogenous mixture of cells, interstitium and vasculature; and finally the cellular model, which models each cell explicitly.

It is important to note, that even though mathematical and computational models are designed to mimic and predict natural behaviour, they remain a simplification of the reality and knowing which simplifications or assumptions are made is a crucial factor to consider when conclusions are drawn from the obtained results.

7.2   DRUG TRANSPORT STEPS DURING INTRAPERITONEAL CHEMOTHERAPY

In this section, we summarize the path along which the intraperitoneally administrated drug will travel, the mechanisms behind this and discuss the barriers it might encounter on its path (figure 7.1).
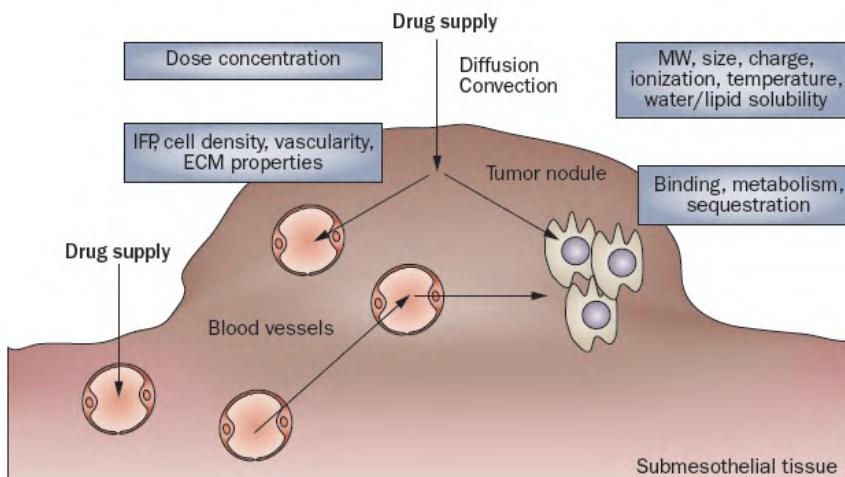
Figure 7.1: Schematic representation of the drug transport process during intraperitoneal chemotherapy and some of its determining factors. IFP:Interstitial fluid pressure; ECM:Extracellular matrix; MW: molecular weight. Reprinted with permission from [37]

Once administered in the peritoneal cavity, the cytotoxic drug has to be absorbed into the peritoneal tumor tissue. It has been shown that the peritoneal mesothelial lining does not constitute an explicit barrier for drug uptake [91, 301]. The administered dose and diffusion coefficient of the drug will determine the amount of drug that is initially available for transport. Cytotoxic agents do not remain stable over prolonged periods of time in the peritoneal cavity and their decay rate is an important factor that will influence the absorption. The remaining concentration of drug

in the carrier fluid at each time point will also determine the concentration gradient and therefore the magnitude of the inward diffusive flux. The chosen carrier solution on the other hand will also have an influence on drug absorption: the amount of carrier fluid in the peritoneal cavity will determine how high the hydrostatic pressure is and will provide a driving force for the convectional transport across the peritoneum. Recently there has been an interest in the use of aerosols and an elevated intra-abdominal pressure as a means of increasing the contribution of convective transport to the drug transport [258]. Furthermore, other properties of the carrier fluid such as osmolarity might also influence this first step in the transport process [140, 156, 79]. Finally, temperature is also likely to have an influence as a higher temperature influences the diffusion coefficient through the Einstein-Stokes equation [73].

Once entered in the tumor tissue, the drug will penetrate deeper into the tumor by means of diffusive-convective transport. The diffusive transport will be dependent on the diffusivity constant of the drug in the extracellular fluid and the aforementioned used concentration of the drug. The convective transport on the other hand depends on both the tissue permeability and the fluid velocity. Tissue permeability is a parameter that describes the resistance that a porous medium (like human tissue) exerts on a fluid. The extracellular matrix (ECM) of solid tumors is composed of two main constituents: fibrous proteins (e.g., collagen, elastin) and polysaccharides (e.g., hyaluronan, glycosaminoglycan) [41]. Tumor tissue is characterized by an increased deposition of collagen I [226] and as a result, tumor stroma is characterized by increased stiffness when compared to normal tissue [317]. A difference in ECM composition and the higher cell density that is associated with tumors can lead to a difference in tissue permeability and therefore a different resistance to convective drug flow. The fluid velocity will be radially outward due to the high interstitial fluid pressure at the centre of the tumor [121]. This characteristic elevated IFP is caused by a number of contributing factors, including the leaky and irregularly shaped microvasculature, the lack of a functional lymphatic system, a denser extracellular matrix, an increased number of cancer associated fibroblasts (CAF's) and a larger cell density [138]. The higher this IFP is, the larger the drug outwash will be. Furthermore, not all drug molecules entering the interstitial space of the tumor remain available for transport as a fraction will bind (reversibly or irreversibly) to the proteins in the ECM.

As the therapy progresses, part of the drug entering the tumor tissue interstitium will be absorbed by the tumor vasculature and thereby add to the systemic effect of the therapy. The amount of drug that will cross the

vascular wall will depend on drug related parameters such as the osmotic reflection coefficient and the diffusion coefficient and on tissue dependent parameters such as the surface to volume ratio of the vasculature, the vascular density, the permeability of the vessel wall for the drug, the oncotic pressure in both tissue and vasculature, the IFP and pressure in the vasculature, and the plasma concentration of the drug. Uptake by the vascular component is a reversible process and therefor drug molecules can again enter the interstitial space from the blood pool.

From the interstitial space, the drug can then be taken up by cancer cells by both active and passive processes. Depending on the drug used, different mechanisms will be responsible for cellular uptake. The amount of drug that will be incorporated in the cells will depend on the cell-dependant factors such as cell density and drug-dependant parameters including size, charge and molecular weight, but also on other therapy related factors such as temperature, local drug concentration and duration. Table 7.1 summarizes the parameters that are involved in the drug transport during intraperitoneal chemotherapy that are mentioned above.

Table 7.1: Summary of the parameters that are involved in the drug transport during intraperitoneal chemotherapy. The parameters are subdivided in three main categories: therapy related, drug related and tumor tissue related

Parameters involved in drug transport during intraperitoneal chemotherapy		
Therapy related	Drug related	Tumor Tissue related
Dose	Molecular weight	Permeability
Temperature	Ionic Charge	Vascularity
Carrier fluid	Membrane binding	Interstitial fluid pressure (IFP)
Volume of carrier fluid	Solubility	Cell density
Intra-abdominal pressure	Diffusivity	Extracellular Matrix composition
Vaso-active agents		
Surfactant use		
Duration		

7.3 WHOLE BODY LEVEL: COMPARTMENTAL MODELS

As mentioned in the introduction, the rationale and theoretical basics of intraperitoneal drug therapy were first described by Dedrick et al [64]. In order to do so, a compartmental model consisting of two compartments was used. The first compartment consists of the entirety of all body water (contained intra- and extravascular, and intra- and extra cellular) and

communicates with the second compartment, being the fluid in the intraperitoneal cavity. As the clearance for the peritoneal compartment, the product of the peritoneal permeability and the peritoneal surface area was used. Using this model and peritoneal permeability values estimated from literature, the authors predicted a difference of 1-3 logs between the drug concentrations in the two compartments, with the higher concentration predicted in the peritoneal compartment.

A different compartmental model considered the concentrations in and the exchange between extracellular and intracellular cisplatin in order to predict the dependence of cancer cell survival on the time course of extracellular drug exposure [76]. The model was created to test the validity of extracellular area under the curve (AUC) as a predictor of cytotoxicity, as experimental studies on this subject had shown conflicting results [182, 78]. The exchange between the compartments is considered to be reversible. Once it has entered the cells, the drug can either leave the cell again or bind to DNA. The DNA-bound cisplatin can then be released again during DNA repair but it will no longer be available for binding at that point [240]. The authors propose two different models for cell survival based on the calculated drug concentrations, and compare these with four others that were available in literature [212, 171, 255, 96] by fitting all models to three datasets available in literature [171; 293-161]. It was found that the proposed models relating cell survival to the peak concentration of DNA-bound intracellular platinum provided the best fit for cisplatin cytotoxicity in three different cancer cell lines for a wide range of exposure times. The models were fitted to in-vitro datasets and several transport parameters are therefore not included in this model (i.e the vascular uptake, the uptake of the drug from the peritoneal cavity). It does however offer the opportunity to be incorporated in models that do include these transport steps and to serve as a bridge to the scale gap and offer an extra step in predicting therapeutic outcome.

In 2005, a three compartment model developed by Miyagi et al. [194] compared the resulting AUC's obtained by intravenous and intraperitoneal carboplatin administration. The three described compartments were the peritoneal cavity, the serum, and the peripheral tissue compartment. The model contained five a priori unknown transfer coefficients: 4 intercompartmental clearances and a plasma elimination factor. In order to estimate all parameters, a group of 22 patients received randomized treatment (11 IV/11IP) plasma and peritoneal drug concentrations were used to estimate all parameters on a patient to patient basis. Using these estimated parameters in the described three-compartment model to predict both the intraperitoneal AUC and plasma AUC yielded a good agreement

between the calculated and experimental values. This work demonstrates an interesting technique to predict platinum AUC in the different compartments based on the total dose delivered, regardless of the administration route. The omission of the tumor as a separate compartment makes it however difficult to gain insight in therapeutic outcome and the dataset that was used to estimate the pharmacokinetic parameters was rather limited, resulting in high standard deviations for certain parameters.

To study the influence of co-administration of anti-angiogenic therapies on the drug penetration in tumors after intraperitoneal chemotherapy a physiologically based multi-compartment model was described by Shah et al. [248]. Although the model presented in this work is a compartmental model, it does allow for the visualisation of concentration profiles as the tumor is not modelled as a single compartment, but rather as five concentric spheres. Each of these 5 tumor layers communicates with both adjacent tumor layers and the vascular compartment except the innermost, which only communicates with the second layer and the vascular compartment and the outermost layer, which communicates with the layer below, the vascular component and the peritoneal space. The model predicted that when tumor blood flow was reduced by antiangiogenic drugs (to 50, 75, and 90%, of the baseline value of 0.06 ml/min/g) an increase in tumor drug concentration after intraperitoneal chemotherapy would be found.

Colin et al. studied the influence of the dosing of intraperitoneally administrated paclitaxel in a pharmacokinetics / pharmacodynamics (PK/PD) model [48]. Key findings of the models include the observation that the AUC of the drug in the tumor compartment reaches a maximum at a particular paclitaxel concentration and increasing the concentration beyond this point will not increase the AUC in the tumor anymore. Given the fact that the AUC in the plasma compartment does not exhibit this saturation behaviour, the model can then be used to estimate, for each therapy duration, an optimal paclitaxel dose for which the AUC in the tumour compartment over the AUC in the plasma compartment ratio is as high as possible. Although these compartmental parameter models (figure 7.2) can accurately predict peritoneal, plasma, intracellular and extracellular drug concentrations based on the pharmacological data present in literature, there are certain inherent features of all compartmental models that limit their relevance.

The first limitation is the assumption that each compartment is a homogeneous well-mixed entity. It is therefore impossible to obtain concentration gradients within a certain compartment (e.g. tumor tissue)

using a lumped parameter model. Furthermore, as the name suggests, these lumped parameters do not reflect a single physiological process but are rather representing the lumped effect of several processes and it might therefore be difficult to gain more insight into the exact physiological processes that underlie the result.
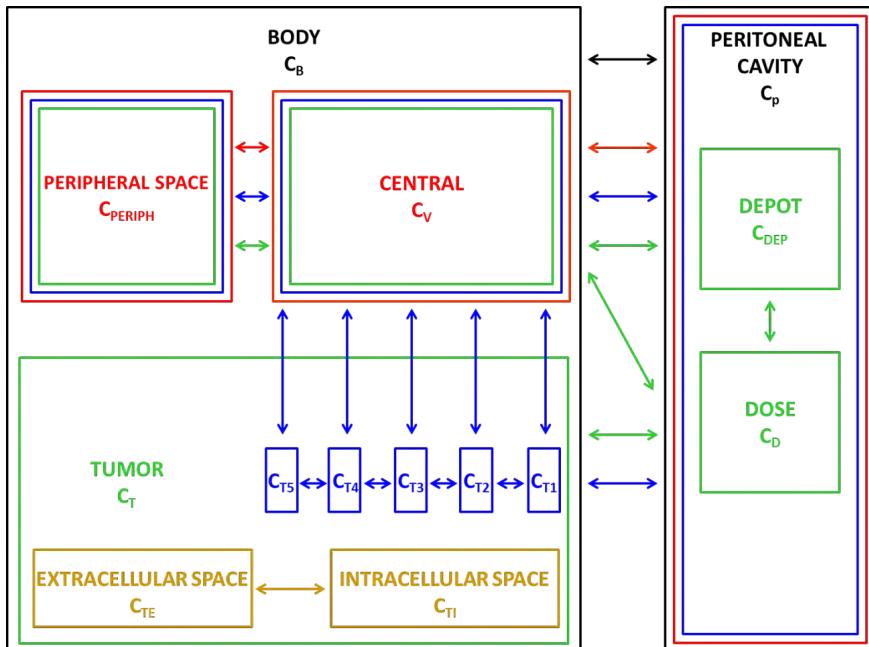
Figure 7.2: Schematic representation of the five different compartmental models highlighting their mutual relationships. The model by Dedrick et al [64] is shown in black, the one of El-Kareh et al [76] in yellow, the one of Myjagi et al [194] in red, the one by Colin et al [48] in green and the one by Shah et al [248] in blue.

7.4 TISSUE LEVEL: DISTRIBUTED MODELS

Due to the need for a better understanding of the actual transport process within the tissue and the possibility of calculating concentration gradients and profiles (figure 7.3), a first distributed model for peritoneal drug transport was described by Flessner et al [90].

In this model, the tissue space is considered to be distributed. A mass balance equation for the drug, taking into account the diffusion and convection in the tissue surrounding the peritoneal cavity as well as the exchange with a vascular component is solved in the distributed peritoneal tissue compartment. Simulations were performed using drug
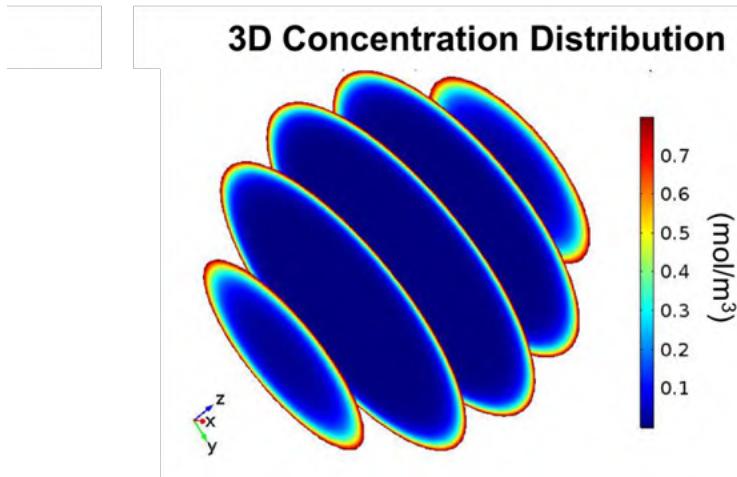
Figure 7.3: Spatially varying cisplatin concentration after intraperitoneal chemotherapy in a spherical tumor nodule. Reprinted from [269].

properties of sucrose. One of the assumptions made in this early work was that the rate of convection in tissue can be approximated by an average value. In a follow-up paper the group validated the model using autoradiographic images and an agreement was found between measured and simulated pressure profiles [87]. A clear overview of the differences between a lumped parameter compartmental model and a distributed model of IPC was published in 1985 by Dedrick et al. [87]. Further advances using this model were done by Statchowska-Pietka et al [41] and Flessner et al [42] in order to include pressure gradients.

Similarly, further research on the lumped parameter model by El-Kareh et al [75] included the simulation of the effect of hyperthermia on the drug penetration distance. As opposed to their previous work however, the peritoneal surface was considered separately and an equation was formulated that described the (one-dimensional) transport of drugs into the peritoneal tissue. Factors included in this equation were the inward diffusive drug transport from the peritoneal cavity and the clearance between extracellular and intracellular compartment. To account for the effect of hyperthermia, two different approaches are pursued. The first one involves the use of extracorporeal heat sources, resulting in a uniform tissue temperature and the second one involves the administration of heated drugs. In the latter case, the temperature gradient along the tissue is described by the bioheat equation, which describes the temperature distribution in the living tissues based on the provided boundary conditions [39]. The effect of the temperature on the vascular component is

included by changing the surface to volume ratio of the vasculature as well as the perfusion parameter. Furthermore, based on the experimental observation that cellular uptake of cisplatin increases for increasing temperatures [72, 163], the clearance from the interstitial towards the intracellular component was increased. A similar choice to increase the rate of DNA binding was made based on the experimental observation that the same concentration of cisplatin causes a higher cytotoxic effect at higher temperatures [163, 124]. A notable result of the model was that the elevated intracellular platinum levels up to a depth of 3-5 mm [296] were due to penetration of heat, causing increased cell uptake of drug. Limitations of the model included the omission of the high interstitial fluid pressure (IFP) and resulting radially outward convective flow, the ECM drug binding and the effect of increased temperature on the diffusion coefficient.

In 2014, a spatiokinetic model for interperitoneal administration of paclitaxel was described by Au et al [10]. In a single spherical tumor nodule model (r = 2 mm) which consists of three separate layers, the cellular level of the tumor tissue was averaged and modelled as a homogeneous, isotropic porous medium. Similarly, vasculature was not explicitly taken into account, but the vascular component of the tissue was considered to represent a homogeneous source and sink term for both paclitaxel and interstitial fluid. These assumptions reduced the momentum conservation equation to Darcy's law and allowed for the incorporation of a source term of interstitial fluid in the mass conservation equation to represent the build-up of the high IFP. This mass source term was modelled after the Starling law, an approach first described in the context of IFP build-up by Baxter and Jain [16]. Three different equations for drug transport were written for each of the considered species: the transport of drug in the vascular component, transport of the unbound drug and the transport of the drug immobilized on the cells. Data used to describe the relation between bound and unbound drug was based on previous experimental studies of the same group [181, 294]. The drug concentration boundary conditions imposed at the edge of the tumor and in the vascular component were also based on prior experiments by this group. This model is, to the best of our knowledge, the first model for IP tumor that incorporates spatially varying parameters by assigning three different zones. Parameters that were assumed to be spatially varying were the volume fractions of the different components (interstitium, vasculature and cellular), the drug diffusivity, the surface to volume ratio of the vascular component, and the tissue permeability. The model was validated using the data of a mouse model with IP tumors (n=4) and the experimental results were in good

agreement with the simulated results with a 1% deviation for the total drug AUC and 23% deviations for individual data points [10].

Based on the groundwork done by Baxter and Jain on the drug transport in solid tumors [16], our group created a parametric single tumor nodule model to study the influence of several different parameters on the penetration depth of various drugs (cisplatin, paclitaxel) [269]. Six different geometries were created to mimic the wide variety in shape and size existing among peritoneal tumor nodules ($r_{min} = 1mm$, $r_{max} = 4mm$). In each of these geometries, equations of mass and momentum conservation were solved as well as a drug transport equation in which vascular re-uptake (both by diffusion and convection) and cell uptake were included in addition to the diffusion and convection terms. Interestingly, the model showed that the presence of a necrotic core and permeability of the tumor tissue had very little effect on the penetration depth of the drug. Smaller tumors showed better penetration than larger ones, which could be attributed to the lower IFP in smaller tumors. Furthermore, the model demonstrated significant improvements in penetration depth by subjecting the tumor nodules to vascular normalization therapy, and illustrated the importance of the drug that is used for therapy. Overall, a shape effect could also be noted in the non-symmetrical geometries, highlighting the importance of using 3D geometries. The obtained penetration depths were compared to values in literature and a close agreement was found (simulated penetration depth range of 0.36 to 0.49 mm; experimentally defined range of 0.41-0.56 [7]). Similar agreements were found when vascular normalization therapy was applied in our model and the resulting penetration depths were then compared to the recent experimental data in which IP tumors were pre-treated with several different VEGF(R) inhibitors to normalize the microvasculature before subjecting them to IP chemotherapy [111] (simulated penetration depth range 1.6 to 2.1 mm; experimentally defined 1.68 mm).

7.5 CELLULAR MODELS

To study the tumor penetration of cisplatin and pertuzumab when delivered by two alternative routes (IV/IP) in disseminated ovarian cancer a cellular Potts model (CPM) was used by Winner et al [314]. In this type of model a lattice-based computational modelling method is used to simulate the collective behaviour of cellular structures [22, 46]. Each lattice site represents a single cell and during each timestep transport equations
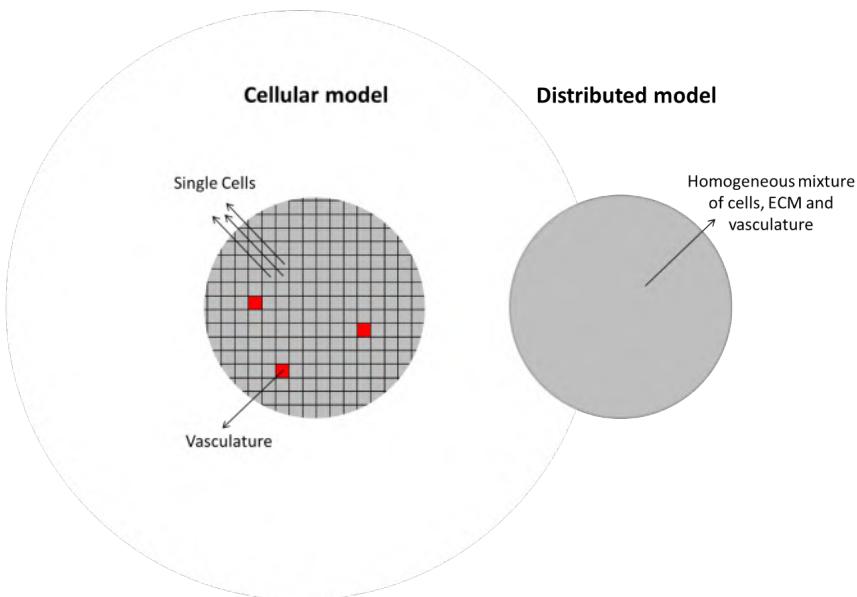
Figure 7.4: Schematic representation of the lattice used in the described cellular
Potts model. Each computational cell represents either a single cell or a vascular
component. This method differs from distributed models (righthandside) where
all cells in the computational domain represent a homogeneous mixture of cells,
extracellular matrix and vasculature.

for IL-8, Growth Factor 2, VEGF and oxygen were solved for each cell
(figure 7.4).

According to their local chemical concentrations, each cell will then
update their current state after which the cell lattice is then updated
assuming chemical concentrations stay constant. The CPM model for
ovarian cancer (OvTM) was first proposed by the same group to study
ovarian cancer cell attachment, chemotaxis, growth, and vascularization
[266] and was then extended to include a transport equation for the used
drug. The drug concentration in both the vasculature and the peritoneal
fluid at each timepoint were estimated from data in which simultaneous
measurements of the drug concentration in plasma and ascites were
performed after administration by either route [266].

In addition to avascular tumors, small vascular tumors with vascular
densities ranging between 2 and 10% were also studied. This range of used
vascular densities was based on the analysis of 9 ovarian cancer patient
samples. Using this model, the authors found that the intraperitoneal

infusion route is the superior route for drug delivery for both investigated drugs (cisplatin and pertuzumab) and both investigated tumor types (avascular tumors and small vascular tumors). The vascular density did influence the accumulation of drug in the tumor and a sink effect could be noted due to the presence of the vessels. These sinks caused drug accumulation patterns that were noticeably less spatially homogeneous. This is, to the best of our knowledge, the only spatial model currently available in the context of intraperitoneal drug therapy that explicitly models the tumor vasculature instead of a distributed source. Limitations include the omission of the effect of the convective bulk interstitial fluid flow on drug concentrations and the use of fixed concentration profiles obtained from literature in both the IP and IV compartment during both delivery routes. Also, the very high spatial and temporal resolution of the model results in simulation durations in the range of 6 to 9 days for a single simulation.

7.6 CONCLUSIONS AND FUTURE DIRECTIONS

In this review, we discussed various models that were created to study the drug transport that occurs during intraperitoneal chemotherapy. Although all relevant transport steps during IP chemotherapy have been modelled, there is to date no model that is able to fully model all the complex processes that are occurring during IP chemotherapy such as the uptake of the drug from the carrier fluid, the diffusive-convective transport of the drug in the interstitium, the cell binding and uptake of the drug, the vascular uptake and systemic effect of the drug, etc.. The existing models are diverse and each one is neither good nor bad but comes with its own set of advantages and limitations.

The models were categorized based on the length scale over which the drug concentration was averaged. Traditionally, the most abundant models in this context where the compartmental models. These models have the advantage that they are easy to fit to experimental data, and can accurately predict the concentrations of the drug in multiple organs. They, however, cannot describe gradients within different compartments nor can their parameters be directly related to the underlying transport processing.

The distributed models considered tissue to be a continuous mixture of several cell types. The advantage of this technique is that resulting drug profiles can easily be visualised and the processing of larger tumors can

still be done in a reasonable timeframe. It is however not possible to gain information from these models on the single cell level.

In cell-level models, modelling single cell uptake of nutrients and drugs becomes possible. These models are a good fit to describe the naturally very heterogeneous nature of cancerous tissues. The main limitation of these models is that the high spatial resolution comes at a high computational cost. Furthermore, due to the high spatial resolution, the temporal resolution also has to be sufficiently high, thereby further adding to the computational cost.

In numerous works the drug transport is said to be diffusion driven, and often the radially outward convective flow is neglected in these models. Given the strong influence of the high IFP on the drug penetration both in IV and IP chemotherapy models [269, 316], models incorporating this convective interstitial fluid (IF) flow might be more suited to determine which transport processes are limiting in different cases. In the context of IV chemotherapy, there have been some reports of the use of spatially varying parameters that were determined on a pixel to pixel basis from imaging data [152, 302]. The incorporation of accurate IFP profiles might offer a significant advantage over using an idealised pressure profile. Au et al [10] created three different tumor zones in their model to account for the spatial variations of certain parameters within the tumor tissue.

For IV and intratumor drug delivery, several distributed models have been described based on patient datasets [101, 8, 174, 294]. To date, no such patient-specific models have been described in the context of IP chemotherapy. Given the size and shape effect of the tumor on drug penetration that our group found, the accuracy of the model might benefit of the use of realistic geometries. Furthermore, none of the distributed models accounted for the vasculature in an explicit way. Vessels have been shown to act as local sinks for drug molecules [291] and drug distribution in the tumor is expected to be more heterogeneous than predicted by these distributed models. The CPM described by [314] does model the vascular component explicitly and their findings illustrate the occurrence of a more heterogeneous drug distribution.

Most investigated models limited the studied timeframe to a period in which it is safe to say that no tissue growth or remodelling will occur. This assumption allows for all tissue related parameters to remain constant during the procedure duration. Exception here is the work by Winner et al in which growth and tissue remodelling are explicitly present in the model on a single cell level [314]. Additionally, the work by Colin et al. [48] does

estimate the changes in tumor volume based on a PDPD link suggested by [2]. Given the recent interest in metronomic chemotherapy in the context of IP chemotherapy [320], extending models to include growth and cell survival might become more frequent.

A main limitation of mathematical models in the context of cancer is that validation of the model can be quite difficult. Two different types of validation are necessary: the single parameter validation and the full model validation. The behaviour of each of the different presented models in this work, is governed by a number of parameters. Reliable values for these parameters might not be available in literature and experimental determination of these single parameters is needed. These single parameters can be notoriously difficult to quantify due to the interference with other parameters. The full model also has to be validated, this can be done in vitro, in animal models and using clinical data. It is important to note however that due to the high number of parameters in most models, and the often limited sample sizes in validation studies, care should always be taken not to over-fit the model to a certain dataset.

In summary, mathematical modelling has shown some promising insights in the transport processes of drugs during IP chemotherapy and could identify new strategies to improve penetration deeper into the tumor tissue. The amount of work done in this field is however still quite limited. Far more work has been done in the modelling of IV chemotherapy and extensive reviews about mathematical modelling of drug penetration in tumor tissue and multiscale cancer modelling have recently been published [65, 153].

MATHEMATICAL MODELING OF INTRAPERITONEAL DRUG DELIVERY: SIMULATION OF DRUG DISTRIBUTION IN A SINGLE TUMOR NODULE

This chapter is based on "Mathematical modeling of intraperitoneal drug delivery: simulation of drug distribution in a single tumor nodule", as published in Drug delivery, Drug Delivery, 24:1, 491-501 [269].

8.1 INTRODUCTION

Patients with peritoneal carcinomatosis suffer from a widespread metastatic growth of tumor nodules in the peritoneal cavity. This disease often originates from ovarian or colon carcinoma, and prognosis and expected quality of life is usually poor with a 5-year survival rate of less than 40% for advanced stage ovarian cancer and 12.5% for colorectal cancer [32, 84]. Conventional intravenous (IV) chemotherapy does not offer a substantial improvement in the prognosis of the patients, while being very demanding on the patients due to its side-effects. The intraperitoneal (IP) administration of chemotherapy is an alternative treatment, that allows for higher intratumor concentrations of the cytotoxic agent compared to

intravenous administration, while maintaining the same plasma concentrations [194]. When the chemotherapeutic agent is administered IP, the tumor nodule surfaces are in direct contact with the drug solution. In contrast, in IV delivery the drug is first transported convectively through the bloodstream, after which it extravasates through of the microcirculation and finally penetrates the tumor tissue via diffusion and convective transport. Although IP chemotherapy is a promising technique, its actual clinical application is still limited due to the poor drug penetration (typically no more than a few millimeters) in the tumor tissue [180, 7, 239].

Drug penetration into solid tumors is a complex process that involves multiple of parameters not only related to the used cytotoxic agent (e.g. diffusivity, etc.), but also to the tumor tissue properties (e.g. permeability, etc.) and even the therapeutic set-up (e.g. concentration, etc.). Like many solid tumors, the peritoneal tumor nodules often exhibit a high interstitial fluid pressure (IFP). This high IFP is caused by a number of contributing factors, including the leaky and irregularly shaped microvasculature, the lack of a functional lymphatic system, a denser extracellular matrix, an increased number of cancer associated fibroblasts (CAF's) and a larger cell density [121]. The net effect of all these factors is a radially outward pressure gradient and convective flux in the interstitium, as fluid flows towards the outer layers of the tumor [138]. The latter effectively obstructs the diffusive penetration of the drug from the outer edge to the center of the tumor during IP chemotherapy. Due to the imbalance between supply and demand of oxygen and nutrients in the rapidly growing tumor, the majority of the tumor nodules have a necrotic core in which no viable cells or functional vascular system are located and, hence, no blood flow or cellular drug uptake is present. Additionally, not all of the drug that penetrates the tumor tissue will enter the cancer cells, as a part of the drug will be resorbed by the tumor microvasculature and convectively transported throughout the systemic circulation, or can be lost due to binding to the extracellular matrix. These processes further limit the amount of free drug that is available for deeper tissue penetration.

Drug tissue penetration is influenced by multiple parameters; the use of computational fluid dynamics (CFD) modeling has the benefit of being able to change single parameters and study their relative influence on the therapeutic outcome of the treatment without influencing other parameters. Changing some of the essential parameters over a well-defined region of interest allows for a better understanding of their impact on treatment outcome and thus allows for the optimization of drug transport during IP chemotherapy.

Previously, a number of modeling studies focused on the classical IV delivery of drugs and parameters of importance were vascular supply, drug release and activation, drug diffusive transport, drug advective transport and drug decay, deactivation and cellular uptake [153]. Recently, CFD has been used to study a combination of these models whereby the implemented equations are usually based on the groundwork done by Baxter and Jain [16]. Substantial CFD modeling efforts have been done mainly in the area of brain tumors with a special focus on the comparison of different drug release systems [145, 304, 305, 285, 174, 8] and the incorporation of transient flow due to edema [290]. A two-dimensional model, in which the delivery of doxorubicin to a hepatoma segmented of a patient CT-scan was simulated, included the extracellular binding and DNA binding of the drug [104]. More parametric CFD models on solid tumors in general have been developed to study the influence of tumor size [261], shape [260] and the effect of different therapeutic options such as vascular normalization therapy [214] or thermosensitive drug delivery [326].

Simulation of drug delivery via the IP route requires a model that is similar to the description of the drug transport equations of IV delivery, but requires unique source terms in the transport equations and different boundary conditions in the model formulation. Previous models in the area of peritoneal transport include pharmacokinetic (PK) compartmental models describing the transport processes occurring during peritoneal dialysis [88, 265] and peritoneal chemotherapy [88, 248]. Additionally, a theoretical model describing the IP transport of cisplatin was created [76] but no convective transport was taken into account. Similarly, a model comparing the IP and IV delivery of drugs was published [314], which also does not take into account the outward convective transport due to high IFP. A recent computational model described the transport of paclitaxel at three scales (i.e. tumor, IP cavity, whole organism) in a two-dimensional pie-shaped tumor segment during IP chemotherapy [10].

We present a fully three-dimensional model to study drug transport in an isolated intraperitoneal tumor nodule during IP chemotherapy. The model includes convective, diffusive and reactive drug transport in different tumor geometries and sizes and allows for testing the influence of changing therapy-related parameters (e.g. different types of drugs, tissue permeability...) on the tissue penetration.

8.2   MATERIALS AND METHODS

8.2.1   Model geometry

The tumor nodules in peritoneal carcinomatosis have a large variety in shape and size. Therefore, three different geometries will be considered in this study.

The first geometry consists of a spherical tumor nodule with a radius $r = 10$ mm, labeled as LS (figure 8.1a). The tumor is composed of two zones: a necrotic tumor zone ($0 < r \leq 5$ mm), where neither living cells nor functional vascular or lymphatic system is present, and a viable tumor zone ($5 < r \leq 10$ mm), where living cells and a functional vasculature are present, but a functional lymphatic system is also lacking.

The second geometry, labeled as LE, has an ellipsoidal volume with the half length of the long axis (LA) (r_l) and short axis (SA) (r_s) equaling 20 mm and 10 mm, respectively. The necrotic zone is defined by 50% of the axis length of the viable tumor (i.e. $0 < r_{ln} \leq 10$ mm and $0 < r_{sn} \leq 5$ mm for the longer and smaller axis, respectively) (figure 8.1b).

As a third geometry, the elliptic shape is cropped along the shorter axis, resulting in a more realistic tumor nodule geometry (LT) for a peritoneal metastasis. The length of the LA (r_l) is kept at 20 mm, but the length in the perpendicular direction is reduced to 10 mm. The necrotic core in this case has a similar shape with the length of the longer axis (r_l) being 8.7 mm and the length in the perpendicular direction being 4.53 mm (figure 8.1c).

As clinical evidence suggests that patients with carcinomatosis of ovarian origin do not benefit from IP therapy if the nodules exceed a 10 mm diameter [13], the same three geometries were also scaled down by a factor 5 (obtaining the geometries SS, SE and ST respectively) to correlate the results with clinical data. All geometric properties are summarized in figure 8.1d-f.

8.2.2   Governing equations

In this section, the equations describing the transport of the drug in the tumor tissue are presented based on seminal work by Baxter and Jain [16].
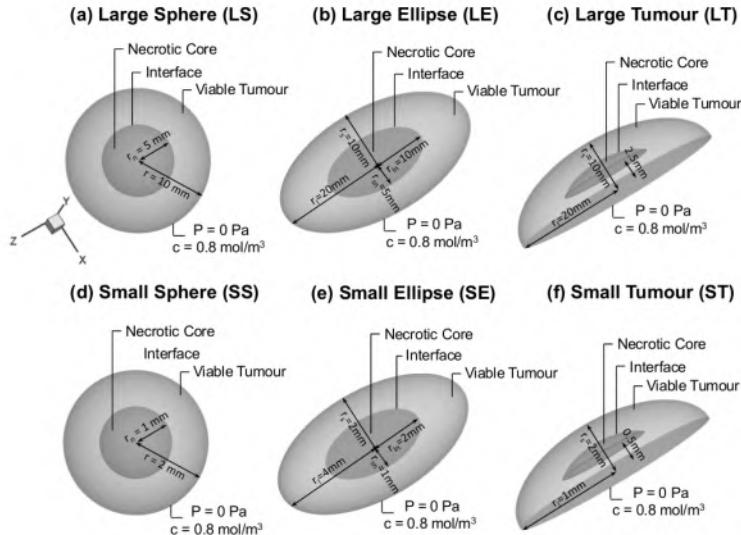
Figure 8.1: Visualization of the six used geometries in our model. a, d Geometries of spherical tumour shape comprising two different zones: a necrotic centre of radius rn (darker grey area) and the viable tumour zone. A concentration and pressure boundary condition are applied at the outer edge of the tumour. b, e Geometries of an ellipsoid tumour shape. c, f Geometries of the peritoneal tumour shape

8.2.2.1 Interstitial fluid pressure distribution

In a rigid porous medium like the interstitium, the momentum equation can be reduced to Darcy's Law [23]:

$$u = -K\nabla P_i \tag{8.1}$$

Where u represents the interstitial fluid velocity (in m/s); K the conductivity of the tissue for interstitial fluid ($m^2/Pa\cdot s$) and P_i the interstitial fluid pressure (Pa). K is often defined in function of the dynamic viscosity of the fluid μ ($Pa\cdot s$) and the intrinsic permeability of the tissue k (m^2):

$$K = \frac{k}{\mu} \tag{8.2}$$

The steady-state continuity equation for the incompressible interstitial fluid flow in normal tissue is given by [23]:

$$\nabla u = F_v - F_l \tag{8.3}$$

where ∇ represents the divergence operator; F_l a lymphatic drainage term for interstitial fluid (s^{-1}) and F_v the fluid gain from the blood (s^{-1}). Since there is a known lack of functional lymphatics in solid tumors, $F_l=0$. The constitutive relation for F_v is based on Starling's hypothesis [16]:

$$F_v = \begin{cases} 0 & \text{if } r \leq r_n. \\ \frac{L_p S}{V}\left(P_v - P_i - \sigma(\Pi_v - \Pi_i)\right) & \text{if } r > r_n. \end{cases} \tag{8.4}$$

with L_p the hydraulic conductivity of the vasculature ($m/Pa \cdot s$), S/V the surface to volume ratio of the vasculature (m^{-1}), P_v the vascular pressure (Pa), P_i the interstitial fluid pressure (Pa), σ the non-dimensional osmotic reflection coefficient, Π_v the vascular osmotic pressure (Pa) and Π_i the interstitial osmotic pressure (Pa). In this relation, a difference is made between the necrotic core ($r \leq r_n$ with r_n the radius of the necrotic core), where no functional vasculature is present, and the viable tumor zone ($r > r_n$) (figure 8.1)

8.2.2.2 Species transport

Mass conservation of the drug is given by [23]:

$$\frac{dC_{drug}}{dt} = D\nabla^2 D_{drug} - \nabla\left(uC_{drug}\right) - S \tag{8.5}$$

with C_{drug} the time-dependent concentration of the drug present in the interstitium (mol/m^3), D the diffusion coefficient (m^2/s), ∇^2 the laplacian operator, ∇ the divergence operator and S the sink in drug concentration (mol/m^3). The sink term S is in this work composed of 2 different terms:

$$S = S_{bl} + S_{cell} \tag{8.6}$$

where S_{bl} represents the sink in the drug concentration related to the vascular uptake (mol/m^3) and S_{cell} the sink in drug concentration due to cellular uptake (mol/m^3). The closure term for the loss due to the

cellular uptake of the drug is described by a first order elimination, an approach commonly used in literature with β being a first order elimination constant ($1/s$):

$$S_{cell} = \beta \cdot C_{drug} \tag{8.7}$$

The closure term of the resorption by the vascular system finally is given by the following equation [16]:

$$S_{bl} = F_v(1-\sigma)C_v + \frac{P_cS}{V}(C_v - C_i)\frac{Pe_v}{e^{Pe_v} - 1} \tag{8.8}$$

with σ the reflection coefficient of vessels for the drug, C_v the concentration of drug in the vascular system (mol/m^3), P_c the permeability of the vessel wall for the drug (m/s), and Pe_v the Peclet number that expresses the ratio of the mass transport contributions by convection to that by diffusion across the microvascular walls given by:

$$Pe_v = \frac{F_v(1-\sigma)}{\left(\frac{P_cS}{V}\right)} \tag{8.9}$$

Given that the tumor volume is low compared to the total body volume and the therapeutic time window is relatively small (typically 30 min - 1 hour), the assumption is made that the vascular drug concentration remains negligible throughout the entire procedure. Given this assumption, equation (8.4)b reduces to:

$$S_{bl} = -\frac{P_cS}{V}C_i\left(\frac{Pe_v}{e^{Pe_v} - 1}\right) \tag{8.10}$$

8.2.3 Baseline model

Because the time needed for tissue remodeling to occur is substantially larger than the therapeutic time scale, the outer boundary conditions for both the necrotic core and the tumor nodule are assumed to be constant throughout the simulation. At the interface between the two tumor zones (necrotic and viable zone), an interface boundary condition is imposed, implying continuity of all properties. On the edge of the tumor nodule, where the cytotoxic solution is in direct contact with the tumor tissue, a

fixed drug concentration is maintained (i.e. 0.8 mol/m^3) and the outlet pressure is set to 0 Pa. This zero outlet pressure boundary condition is a simplifications as, in reality, this pressure is likely to range anywhere between 0 to 20 Pa based on an abdominal surface area ranging between 1 m^2 and 2 m^2, and an instillation fluid volume of 2l [205]. This approximation was justified in this work by our observation that due to the high values of IFP in the nodules, small changes in this outlet pressure did not have a large influence on the results. All transport parameters are also being considered constant throughout the simulation and are summarized in table 8.1.

8.2.4   Parameter study

The baseline model presented in the previous section was then used to study drug diffusivity, the influence of vascular normalization therapy, the presence of a necrotic core and tissue permeability on the drug penetration.

Currently, a number of different drugs are used for IP chemotherapy. The influence of drug diffusivity on the penetration depth was studied to study whether a higher diffusivity resulted in an increase in penetration depth. For all baseline cases, drug related parameters were taken from cisplatin (table 8.1).

We then compared results of these cisplatin baseline cases to cases where the drug diffusivity of paclitaxel was used. A summary of the values used for the different drugs can be found in table 8.2; all values that are not reported in this table remain equal to those used in the baseline cases.

Certain vascular normalization therapies have been shown to normalize the architecture and permeability of the microvasculature, resulting in a lower IFP and better drug distribution [95]. Recently, works by Shah et al. [248] and Gremonprez et al. [111] showed similar improvement in drug penetration after vascular normalization therapy for IP chemotherapy. We attempted to mimic vascular normalization to test whether our model would be able to reproduce the results from these works. In the first step, all vascular related properties (L_p ; $\frac{S}{V}$; σ) were interpolated halfway between typical tumor tissue and normal tissue values. In the second step, full normalization of all vascular related parameters was simulated (table 8.2) [16]. Results of these two cases will then be compared to their respective baseline values.

The presence of necrotic regions in solid tumors is well documented but the exact size and location of the necrotic core is not always known. In

Table 8.1: Parameters used for baseline simulations

Parameter	Unit	Value	Reference
r	m	0.01	-
r_n	m	0.005	-
ρ	kg/m^3	1000	[290]
L_p	m/$Pa \cdot s$	2.10 x 10^{-11}	[16]
K	m^2/$Pa \cdot s$	3.10 x 10^{-14}	[16]
μ	$Pa \cdot s$	1.10 x 10^{-3}	[290]
k	m^2	3.10 x 10^{-17}	[16]
$\frac{S}{V}$	m^{-1}	2.00 x 10^4	[16]
P_v	Pa	2.08 x 10^3	[16]
Π_b	Pa	2.67 x 10^3	[16]
Π_i	Pa	2.00 x 10^3	[16]
σ		0.82	[16]
MW	g/mol	300	[248]
D	m^2/s	2.50 x 10^{-10}	[248]
β	1/s	7.32 x 10^{-4}	[248]
σ		8.17 x 10^{-5}	-
P_c	cm/s	1.43 x 10^{-4}	[248]

Table 8.2: Parameter values used to study the influence of several transport related parameters. All parameters that are not listed in this table, are kept at their baseline value (table 8.1) for each simulation

Vascular Normalization Simulations				
	S/V [m^{-1}]	L_p [m/$Pa \cdot s$]	σ [-]	ref
Baseline Values	2.00 x 10^4	2.10 x 10^{-11}	0.820	[16]
50% Vascular Normalization	1.35 x 10^4	1.19 x 10^{-11}	0.865	[-]
100% Vascular Normalization	7.00 x 10^3	2.70 x 10^{-12}	0.910	[16]
Drug Diffusion Simulations				
	Diffusion Coefficient [m^2/s]	ref	IC50 [mol/m^3]	ref
Cisplatin	2.50 x 10^{-10}	Shah, 2009	6.20 x 10^{-3}	[60]
Paclitaxel	0.77 x 10^{-10}	Winner, 2016	1.40 x 10^{-6}	[256]
Permeability Simulations				
			Intrinsic Permeability [m^2]	ref
Normal tissue			6.4 x 10^{-18}	[16]
Commonly used value			3.1 x 10^{-17}	[16]
Lower limit of the range			6.4 x 10^{-17}	[-]

order to estimate the impact of this uncertainty on our model, we omitted
the necrotic core that was implemented in the baseline case by setting
the conditions in this region equal to those of viable tumor tissue, and
compared the resulting pressure profiles and penetration depths.

Due to the differences in ECM, cell density and the presence of CAFs,
the tumor tissue permeability is likely to be significantly different from
the healthy surrounding tissue permeability. As tissue permeability is
notoriously difficult to quantify, no reliable values are currently present in
literature, and most models use an arbitrary tenfold of the healthy tissue
value [16]. The influence of this assumption on the penetration depth of
the drug was investigated by varying the permeability and comparing the
penetration depth to the baseline cases. A summary of the permeability
range used can be found in table 8.2.

8.2.5 Numerical methods

All geometries were created and meshed in COMSOL multiphysics (COM-
SOL, Inc., Burlington, USA). All equations mentioned in the methods
section were also implemented in COMSOL. A segregated approach was
used for solving the continuity, momentum transport and mass trans-
port equations. All cases were run both in steady state and as a transient
model. Due to the length of the IP therapy procedure (typically ranging
from 30 min to 1 hour), a time resolution of 30 seconds was chosen when
transient simulations were performed. As a convergence criterion, a drop
of 4 orders of magnitude in the residuals was chosen.

8.2.6 Analyzed variables

For all simulations, pressure and concentration profiles were analyzed
along either the x-axis (spherical geometries) or along both x- and z- axis
(ellipsoid and tumor geometries) (figure 8.2 c and figure 8.2 d). We will
characterize the pressure profile by the maximal IFP (IFP_{max}) and the
steepness of the profile (figure 8.2 e). Steepness is characterized by the
LP50 value, which we define as the distance starting from the tumor center
over which the pressure drops to 50% of its maximal value. The steeper
the pressure profile, the higher the LP50 value will be.

From the concentration profiles along the axis, the penetration depth
is determined. Penetration depth is represented in this work by two
different metrics. On the one hand, absolute penetration depths (APD) are
reported, defined as the maximal depth along the axis of interest where the

drug concentration exceeds the corresponding half maximal inhibitory concentration IC50 value of the drug (figure 8.2f). The second metric is the relative penetration depth percentage (PD%), representing the percentage of the radius where concentration values exceed the corresponding IC50 value of the drug used.

During IP chemotherapy, the diffusive and convective drug transport happens in different directions: the diffusive transport is directed inwards into the tumor, whereas the convective transport is directed outwards out of the tumor. The penetration depth of the drug will be determined by the relative influence of both contributions. In the study of transport phenomena, the Péclet number (Pe) is a dimensionless number that expresses the ratio of the mass transport contributions by convection to that by diffusion of the drug into the tumor tissue. In the context of mass transport, it is defined as:

$$Pe = \frac{L \cdot u}{D} \tag{8.11}$$

with L the characteristic length of the system [m], u the maximal velocity magnitude [m/s] and D the diffusion coefficient of the drug [m^2/s].

8.3 RESULTS

8.3.1 Baseline Cases

As illustrated in figure 8.2, the simulations allow us to determine 3-dimensional pressure and concentration distributions in all geometries.

The maximal interstitial fluid pressure reached in the model was 1533.88 Pa (11.5 $mmHg$), and this value was reached in all three large geometries. The shape of the pressure profiles, however, differed between these three cases with the least steep profile being the one for the SA of the ST geometry (LP50 = 0.89) (figure 8.3c) and most steep for the LA of the LE geometry (LP50 = 0.99) (figure 8.3b). Overall, the steeper the pressure profile, the higher the maximal interstitial fluid velocity, and therefore the higher the radial outward convective flow will be.

APD ranged from 0.36 mm (SA-LT) to 0.49 mm (LA-ST) with the corresponding PD% ranging from 1.81% to 21.29% (Appendix 2). Furthermore, the IFP was found to be consistently lower and penetration depths higher
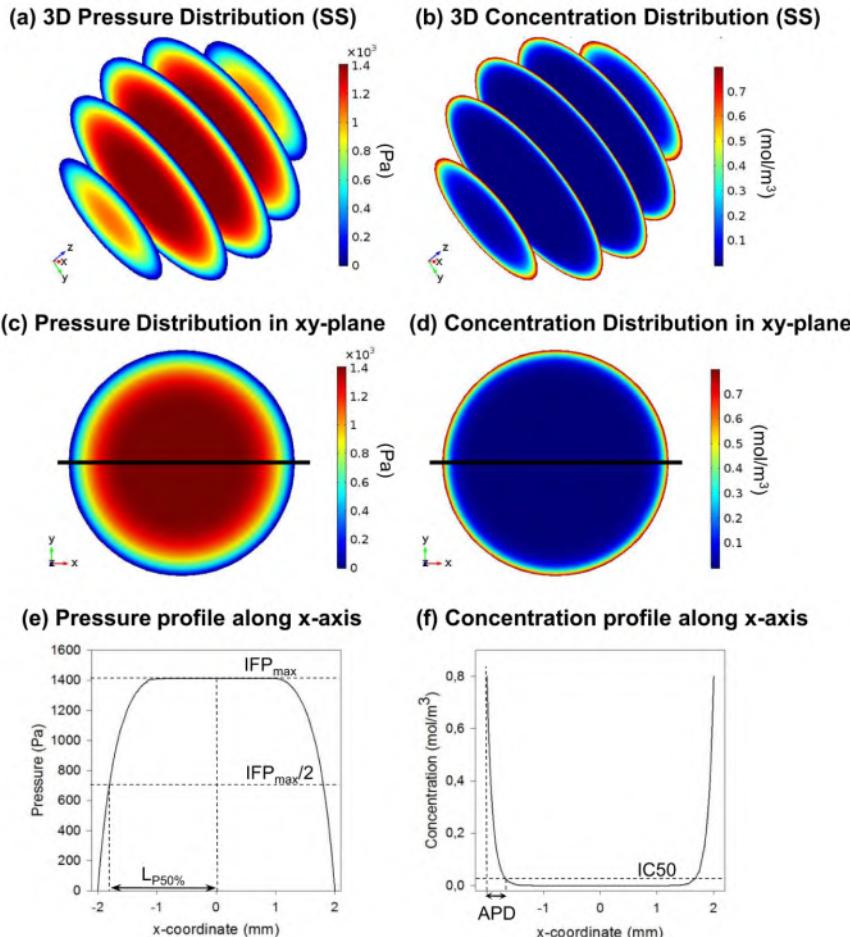
Figure 8.2: Summary of model output and analysed variables. a, b three-dimensional pressure and concentration distributions in the small spherical geometry (SS). c, d two-dimensional pressure and concentration distributions in the xy-plane of the SS geometry. The x-axis is plotted on the figures in black. e, f one-dimensional pressure and concentration profiles along the x-axis in the SS geometry. All analysed variables as discussed in section 3.6 are presented on the figure.

in all smaller sized geometries (figure 8.3). In the elliptical and tumor geometries, a shape effect could be noted, resulting in different APDs and PD%s along the short and long axis.
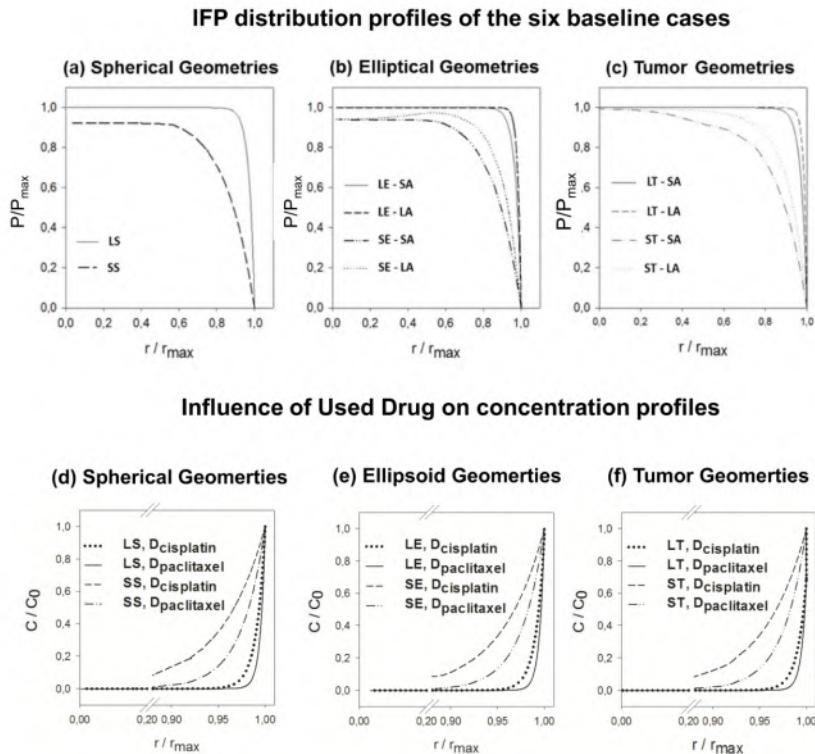
Figure 8.3: a-c Interstitial fluid pressure (IFP) distribution profiles of the six baseline cases. Both length along the axis and IFP are normalized; the former with respect to the maximal length along the axis, the latter with respect to the overall maximal pressure (IFPmax = 1533.88 Pa). d-f show a comparison between the resulting concentration profiles after IP chemotherapy in which cisplatin or paclitaxel is used. Concentrations are normalised with respect to the boundary concentration ($C_0 = 0.8\ mol/m^3$).

8.3.2 Drug type

When comparing the pressure profiles characteristics, it is clear that the IFPmax and LP50 do not change in any of the cases (Appendix 2). Concentrations of cisplatin are consistently higher in all geometries, at all points (figure 8.3 d,e,f). However, due to the large difference in IC50 values between different drugs (table 8.2), the APD and PD% are higher for paclitaxel when compared to cisplatin (Appendix 2). APD ranged from 0.54

mm (SA-LE) to 0.75 mm (SA-ST) for paclitaxel versus 0.36 mm (LA-LE) to 0.49 mm (SA-ST) for cisplatin. In general, smaller geometries showed a larger improvement in penetration depth (Appendix 2). As changes in the diffusion coefficient only influence the diffusive transport of the drug, all pressure profiles were equal to the ones found in the corresponding baseline cases.

8.3.3 Vascular Normalization

The effect of vascular normalization therapy during IP chemotherapy on the IFPmax, LP50, APD en PD% was simulated in two steps (50% vascular normalization and 100% vascular normalization) (table 8.2). We found that vascular normalization lowered the IFP in all cases and decreased the steepness of all pressure profiles. The lowest IFPmax was reached in the case of the small spherical geometry (IFPmax = 259.4 Pa) and the lowest LP50 was obtained along the short axis of the small tumor geometry (LP50 = 0.70) (Appendix 2).

Results of the 100% vascular normalization simulation in the small tumor showed a penetration depth exceeding half of the tumor radius (PD% = 51.64, absolute penetration = 1.0 mm) along the short axis (figure 8.4c). In general, vascular normalization showed a non-linear, positive effect on the penetration depth in all cases (Appendix 2). APDs ranged from 0.45 mm to 0.58 mm for 50% vascular normalization and between 0.65 mm and 1.03 mm for 100% vascular normalization. Relative improvements with respect to the respective baseline PD% ranged from 0.39% (LA-LE) to 7.34% (SA-SE) for the 50% normalization and between 0.69% (LA-LT) to 29.35% (SA-ST) for 100% vascular normalization.

8.3.4 Necrotic core

Omitting the necrotic core from the computation and thus describing the tumor as a single homogeneous zone increased the IFP_{max} in all three smaller geometry cases. In the larger geometries a further increase was not possible and therefore IFPmax remained the same. The maximal interstitial fluid velocities (IFV_{max}) were however lower in most cases without necrotic core when compared to the baseline cases, with the exception of the small ellipse and tumor geometry. Overall, the effect on the penetration depth was limited with differences in PD% never exceeding 3.56% (SA-SE) (Appendix 2).

Influence of Vascular Normalization on concentration profiles
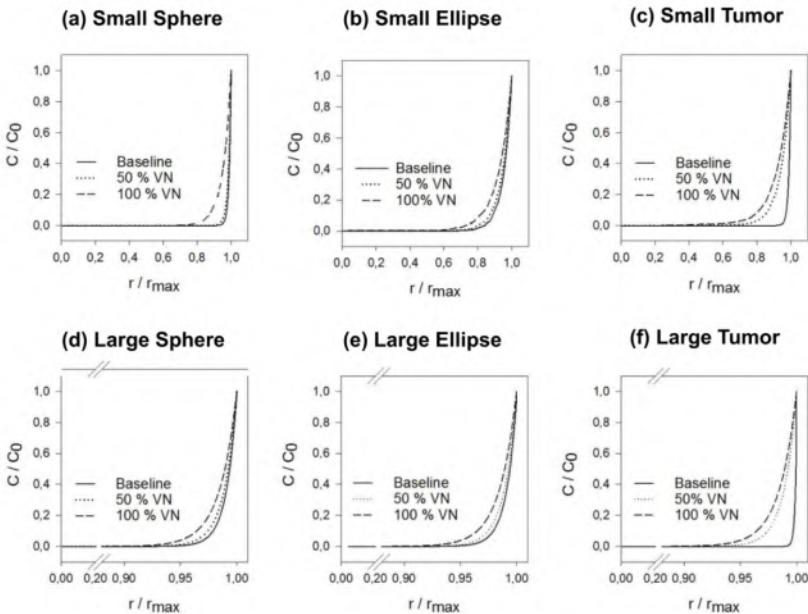
Figure 8.4: Normalized concentration profiles in which both length along the axis and concentration are normalized; the former with respect to the maximal length along the axis, the latter with respect to the boundary concentration ($C_0 = 0.8 \, \text{mol/m}^3$). a-f show the resulting concentration profiles after vascular normalization therapy for all geometries.

8.3.5 Permeability

Tissue permeability marginally influences penetration depth. Overall lower permeabilities lead to lower IFV_{max} and higher IFP_{max}, however no measurable differences larger than 0.19% could be noted in relative penetration depth (Appendix 2).

8.4 DISCUSSION AND CONCLUSION

In this study, a 3D CFD model of a peritoneal tumor nodule was developed to study the mass transport of drugs during IP chemotherapy. The model is, to our knowledge, the first fully 3D parametrical model that studies the influence of different parameters on the penetration depth of drugs during IP chemotherapy. Baseline cases of the model are presented for 2

different sizes of 3 different geometries. The model was used to study the influence of vascular normalization therapy, drug diffusivity, the presence of a necrotic core and tissue permeability on the drug penetration.

When comparing our results of the baseline cases with those obtained in previous studies, it was found that APD in all baseline cases ranged from 0.36 to 0.49 mm, which is in good agreement with the experimentally defined range of 0.41-0.56 mm where carboplatin (another platinum based drug of roughly the same size) was used [7]. One of the main findings of the baseline cases was the profound effect of the tumor size on the drug penetration depth. When averaged over all baseline cases, the smaller tumors were shown to have higher PD% (PD%average = 17.83% for tumors with a diameter/characteristic length of 2-4 mm) than the larger ones (PD%average = 3.24% for tumors with a diameter/characteristic length of 10-20 mm). These findings are consistent with the results obtained by Bakarat et al. [13] and Ansaloni et al. [7], stating that tumor nodules with a radius larger than 10 mm and 2.5 mm, respectively, do not benefit from IP chemotherapy. Hence, there seems to be a critical size of tumor nodules that are responsive to IP treatment, showing the importance of removing nodules of larger sizes before the onset of IP chemotherapy. In this work, we focused on vascular tumors. If no vasculature is present, the IFP will not build-up in the tumor tissue, thereby eliminating the large outward convective flow that limits the inward diffusion of the drug. Additionally, no drug will be resorbed through the tumor vasculature and subsequently lost for further transport. Given these two differences, the outward flow and blood sink terms are cancelled in equation (8.5) and the model would predict full penetration of the drug regardless of the tumor size, given sufficient time.

During IP chemotherapy, the diffusive and convective drug transport occurs in different directions: the diffusive transport is directed inwards into the tumor, whereas the convective transport is directed outwards out of the tumor. The Péclet number gives an idea of the relative influence of these two opposing modes of transport. In all baseline cases, Péclet numbers are larger than one (1.09 - 22) and therefore convective transport will be dominant above diffusive transport. The convective transport is governed by the pressure differences inside the tumor and this work showed that smaller tumors had consistently lower IFP_{max} ($IFP_{max,av}$ = 1477.1 Pa) than larger ones ($IFP_{max,av}$ = 1533.9 Pa) (figure 8.3). In agreement, Ferretti et al. [86] measured higher IFP's for tumor nodules of larger sizes (typically a diameter in the range of 10 – 20 mm) grown from the same cell lines. We can therefore account the lower penetration depths

in the larger geometries (Pe = 1.09 – 10.52) to the increase in the outward convective flow when compared to the smaller geometries (Pe = 6.7 - 22).

The demonstrated shape effect on the penetration depth (figure 8.4 a,b,c) illustrates the added value of using fully three-dimensional models. Spherical tumors had uniform radial penetration, whereas elliptical tumors had different penetration depths along different axes (i.e. deeper percental penetration along the SA; e.g. Large Ellipsis: PD%=3.77 (SA) - PD%=1.96 (LA)). The tumor with its flat side, mimicking the contact area with the peritoneum, had an even more pronounced shape effect (e.g. Large Tumor: PD%=3.82 (SA) - PD%=1.81(LA)) (Appendix 2).

We also compared CFD results for the penetration depth of two commonly used drugs in IP treatment, i.e. cisplatin and paclitaxel. In the model, the difference between the two drugs is primarily reflected in a different diffusion coefficient, which is much higher for cisplatin. As such, when using the same drug dose/boundary conditions, concentrations were consistently higher for cisplatin in all geometries at all times (figure 8.4 d,e,f). The drug's IC50 values, however, are substantially different (i.e. the IC50 value of cisplatin is a factor 4500 larger than the IC50 of paclitaxel; see also section 8.2.2). As the penetration depth as defined in this work uses the IC50 value as the cut-off between zones with and without significant drug penetration, this large difference in IC50 values translates into a higher APD and PD% for paclitaxel when compared to cisplatin (Appendix 2). APD for paclitaxel ranged from 0.54 mm (LA-SA) to 0.75 mm (ST-SA) and APD for cisplatin ranged from 0.36 mm (SA-LT) to 0.49 mm (LA-ST). Nonetheless, it should be noted that in these simulations, the same boundary concentration of 0.8 mol/m^3 was used for both drugs, which is a value that is equivalent to a used dose of 120 mg/m^2 cisplatin, but does not correspond with the clinical practice for paclitaxel. Therefore, an additional case was set-up in a spherical geometry with a 10 mm radius and a paclitaxel boundary concentration of 0.14 mol/m^3, which corresponds with a clinical dose of 60 mg/m^2 [146]. The APD of paclitaxel was 0.64 mm in this case which is, when compared to the penetration depth of cisplatin used at the clinical dose (APD = 0.40 mm), still an improvement.

Note that the IC50 values are taken from in-vitro analysis and protein-binding in an in-vivo setting might influence these values [325]. Therefore, we found that when considering different drugs to use for IP chemotherapy, not only transport parameters, but also biological parameters like IC50 values and protein binding should be taken into account.

When applying different degrees of vascular normalization to our model, we found significant improvements in drug penetration with APD ranging from 0.45 to 0.70 mm in the larger tumors and from 0.52 to 1.03 mm in the smaller tumors when compared to the baseline range of 0.36 to 0.49 mm. The relationship between high IFP in solid tumors and the abnormal microvasculature has been well documented in literature [121]. The tumor blood vessel's leakiness and irregular shape lead to the excessive ultrafiltration of interstitial fluid, which is one of the contributing factors of high IFP. We then compared our in-silico data with the recent experimental data, in which IP tumors were pre-treated with several different VEGF(R) inhibitors to normalize the microvasculature before subjecting them to IP chemotherapy [111]. Tumor size was 124.85 mm^3 on average, which would be equivalent to a spherical tumor with a 5 mm radius and pre-treating the tumors with certain VEGF(R) inhibitors decreased the IFP. An increased platinum concentration, measured by laser ablation inductively coupled mass spectrometry (LA-ICP-MS), was detected in the peritoneal border area (up to 1.68 mm) of the pre-treated tumors with lower IFP. When a detection limit similar to the one of LA-ICP-MS is applied to the concentration profile obtained after 50% and 100% vascular normalization in a 10 mm radius sphere, we found APD's of 1.6 mm and 2.1 mm respectively, which is in good agreement with experimental data [111].

Interestingly, explicit modeling of a central necrotic core in the tumor had little influence on the penetration depth (i.e. maximal APD difference was 0.05 mm (SE-LA)). These results are important, as the existence of a necrotic core is a well described property of solid tumors, but little is known about the shape, size and even the number of necrotic regions. Our work shows that the inaccuracy in the model due to the uncertainty about the necrotic core will be relatively small (max. 3.56 PD%). It is likely that - due to the different drug sources in IV and IP therapy (the vascular network and the outer edge of the tumor, respectively) - these results are unique for the case of IP drug delivery, and cannot be extrapolated towards IV chemotherapy.

The variation of the intrinsic tissue permeability over an order of magnitude did not affect penetration depth significantly (rel PD% < 0.19%). We calculated the Pe number for each simulated case in order to determine a possible cause for this effect. We found an increase in IFP$_{max}$ and a decrease in IFV$_{max}$ when permeabilities were lower. Overall, Péclet numbers ranged from 0.6 to 348.7. Pe values below 1 were noted in some cases, indicating that the diffusive transport is likely to become the dominant transport phenomenon in very low permeability cases. All these findings

however, did not translate to quantifiable differences in APD, suggesting that the model might be fairly robust towards changes in permeability.

Although it might not replace in-vivo experiments, this parametrical CFD model for IP chemotherapy is a powerful tool that allows us to gain insight in how much influence certain parameters have on the penetration depth of the drug. It is to our knowledge the first parametrical CFD model in the context of IP chemotherapy that allows for the prediction of drug penetration depths. Furthermore, the model could be used to reproduce a number of literature validated trends (e.g. effect of tumor size on penetration depth; effect of vascular normalization therapy) and the calculated penetration depths proved a good match to the ones found in literature.

A number of assumptions were made when developing the numerical models. For example, in this work drug concentration at the outer edge of the tumor is fixed during the entire simulation due to unavailability of suitable experimental data. We aim to sample IP fluid during the IP chemotherapy in follow-up validation experiments in order to implement a more accurate inlet concentration boundary condition. Due to the large redistribution volume and substantial first pass effect of most drugs used in IPC, the assumption was made that the vascular concentration of the drug C_v equals zero at all times. In future work, the vascular reabsorption could be included as well for more accurate results. Moreover, the entire model treats the vasculature as a distributed source without taking into account the, sometimes large, spatial heterogeneities within tumors. Implementing more realistic boundary conditions for the concentration at the outer edge of the tumor and allowing for the spatial variation of vascular properties, would further improve the model. Another limitation of the model is the lack of sink terms implemented that represent the effect of other physiological phenomena such as ECM binding and plasma protein binding.

Future work will include the validation of the model in an animal model of peritoneal carcinomatosis. Given the importance of tumor size and the noted shape effect, MRI images of the tumor nodules will be used to segment the actual tumor geometries.

In conclusion, a parametrical 3D CFD model was developed for the drug mass transport in a single tumor nodule during IP chemotherapy. Tumors of smaller sizes respond better to treatment when compared to larger ones. Vascular normalization therapy lowered the IFP and steepness of pressure profiles, thereby increasing drug penetration depths. When

selecting a drug for IP therapy, not only transport properties should be taken into account, but also biological properties (e.g. IC50-value), as these may have an influence on the therapeutic outcome. Furthermore, both modeling of the necrotic core and the intrinsic tissue permeability had a limited effect on the predicted penetration depth.

A 3D CFD-MODEL OF THE INTERSTITIAL FLUID PRESSURE AND DRUG DISTRIBUTION IN HETEROGENEOUS TUMOR NODULES DURING INTRAPERITONEAL CHEMOTHERAPY

This chapter is based on "A 3D CFD model of the interstitial fluid pressure and drug distribution in heterogeneous tumor nodules during intraperitoneal chemotherapy", as published in Drug delivery, [268].

9.1   INTRODUCTION

Cancers originating from organs in the peritoneal cavity are prone to locoregional spread in the form of peritoneal metastasis (PM). The prognosis of patients who develop PM is usually poor and quality of life is low due to complications, such as bowel obstructions and ascites. Furthermore, PM cannot be adequately treated by using intravenous (IV) chemotherapy due to the poor blood supply to the peritoneal surfaces and poorly vascularized tumor nodules [109]. In 1978, Dedrick et al. [64] hypothesized that

the peritoneum-plasma barrier offers a unique treatment opportunity
for patients with oncological malignancies confined to the peritoneal
cavity, introducing intraperitoneal drug delivery as a therapeutic strategy.
Despite a strong rationale and promising clinical results [194], widespread
use of the technique is currently hampered by the limited penetration
depth of the drugs into the tumor tissue [178, 239, 7]. It is therefore crucial
to gain a better understanding of the processes that underlie the drug
transport and the relative importance of the parameters influencing it.

Intraperitoneal drug delivery encompasses a complex transport
process that depends on a large number of different parameters.
The final drug distribution in the tumor tissue is influenced by
therapy-related factors such as dose, temperature, (volume of) carrier
fluid, intra-abdominal pressure, the potential use of vaso-active agents
or surfactant and duration. It is also heavily dependent on factors
related to the drug itself like molecular weight, ionic charge, membrane
binding, solubility, diffusivity and the on properties of the tumor tissue
(e.g. permeability, vascularity, interstitial fluid pressure (IFP), cell
density, extracellular matrix (ECM) composition, ...) [270]. Due to its
relatively low cost and versatility, mathematical modeling has become
an important research tool to better understand and optimize drug
delivery. Most existing models of chemotherapeutic drug delivery,
however, have been created for systemic drug delivery [153], while only a
limited number of models focuses on intraperitoneal chemotherapy [270].
Historically, intraperitoneal drug transport has often been described
using a compartmental model [76, 248, 48], in which drug concentrations
are typically averaged over the entire tumor. More recent works also take
into account spatial variations in drug concentrations on a tissue level
[90, 265, 88, 75, 10, 269] and even on the single-cell level [314].

The use of DCE-MRI to gain information about physiological tissue
characteristics has been previously applied to the field of oncology. Pishko
et al. [224] created spatially-varying porosity and vascular permeability
maps from two-compartment analysis of DCE-MRI data using a rescaled
AIF from literature. They incorporated these maps in a 3D computational
fluid dynamics (CFD) porous media model to predict interstitial fluid
pressure and velocities (IFP and IFV respectively) as well as tracer trans-
port in mice sarcomas. Using the same mathematical model, DCE-MRI
dataset and post-processing techniques, Magdoom et al. [185] used a
voxelized modeling methodology to eliminate the time-intensive tumor
segmentation step. Zhao et al. [329] similarly used DCE-MRI to generate
normalized spatial variation maps of vascular permeability to calculate

IFV, IFP, and tracer transport within a solid murine tumor. The tracer concentration in the plasma was assumed to be proportional to the relative change in signal intensity and AIF functions were taken from literature. The effect of heterogeneous microvessel density extracted from DCE-MRI on drug concentrations in the extra- and intra-cellular space was studies by Zhan et al. [327]. Using a 2D liver tumor geometry, the tracer concentration in the plasma was assumed to be proportional to the relative change in signal intensity. Bhandari et al. [22] used DCE-MRI data and patient-specific AIFs to determine kinetic perfusion parameters in human brain tumors and predict IFP, IFV and tracer transport.

Previously, we developed a 3D computational fluid dynamics (CFD) model that accounts for the diffusive, convective and reactive drug transport during intraperitoneal chemotherapy [269]. We demonstrated the important influence of both tumor nodule geometry and interstitial fluid pressure (IFP) on the penetration depth of cytotoxic drugs in idealized geometries. In this paper, we extend our previous work and present a workflow to implement both realistic geometries and IFP profiles in our existing 3D CFD model. The input for the computational model was obtained from experiments in a murine cancer model. The IFP data was obtained both by direct measurements using a pressure tip catheter and estimated from dynamic contrast enhanced magnetic resonance images (DCE-MRI). The modeled geometries were all mouse-specific based on anatomical MRI images.

9.2 MATERIAL AND METHODS

A mouse PM model was used from which tumor geometries could be obtained and IFP could be measured invasively. As described in more detail below, we performed an imaging protocol to monitor tumor growth and to estimate tumor IFP values from DCE-MRI parameters. Pressure and concentration distributions were then calculated using the estimated, spatially varying transport parameters obtained based on the DCE-MRI images. Figure 39 shows a schematic illustration of the workflow.

All animal experiments were approved by the local Ethics Committee on Animal Experiments of the Faculty of Medicine, Ghent University, and were performed according to Belgian and European legislation on animal welfare (Directive 2010/63/EU). Animals were group housed and kept under environmentally controlled conditions (12h light/dark cycles, 20 – 23 °C, 40 – 60% relative humidity) with food and water ad libitum.

9.2.1 Cell line

Human ovarian cancer cells (SKOV3-Luc-IP1) [60] were cultured in Dulbecco's Modified Eagle's Medium (Life technologies/ThermoFisher, Ghent, Belgium) and supplemented with 2% penicillin/streptomycin + 0.005% fungizone (Bristol-Myers-Squib B.V., Utrecht, The Netherlands) and 10% fetal calf serum (Sigma-Aldrich, Diegem, Belgium).
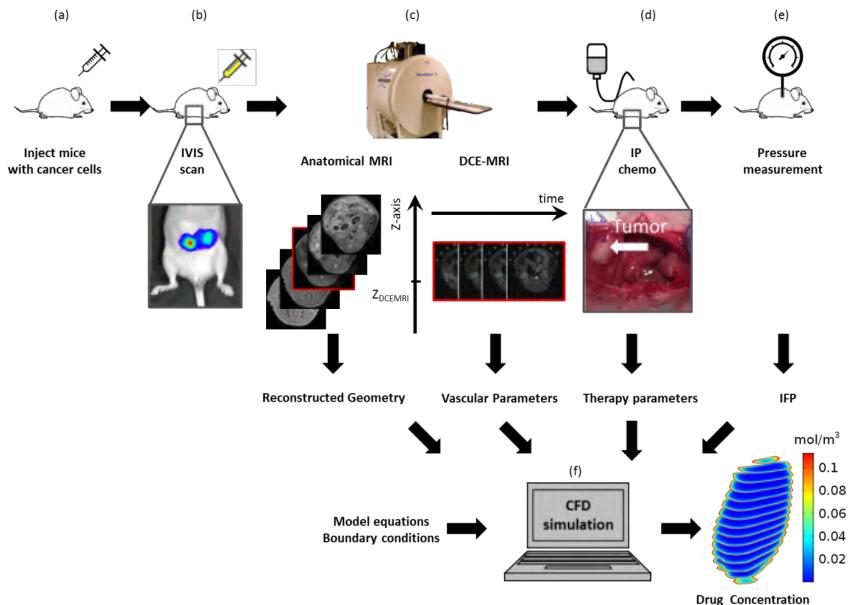
Figure 9.1: Schematic illustration of the workflow described in this work. a: Subperitoneal injection of SKOV3-Luc-IP1 cells suspended in Matrigel in female athymic, nude-foxn1nu mice by a growth phase. b. in vivo in situ (IVIS) scan was done 14 days post-injection to assess tumor growth. c. Scanning protocol as described in the section MRI protocol consisting of an anatomical scan to segment the tumor geometries, a FLASH sequence to obtain native relaxation times of the tissues and a DCE-MRI from which vascular parameters of the tumor tissues were derived. The anatomical MRI slice with a red circumference has the same applicate as the DCE-MRI plane. d. Mice positive for tumor growth underwent 30 minutes of intraperitoneal chemotherapy (IPC) with cisplatin. The therapy parameters (dose, duration) that were used in the experiment were used in the model setup as boundary conditions. e. Immediately after IPC, the IFP was measured using a pressure tip catheter. The resulting pressures were used to validate the simulated tumor pressures in a later stage. f. The equations for both the IFP build-up using the vascular parameters derived from the DCE-MRI data and the drug mass transport were implemented in COMSOL and solved using the same initial and boundary conditions as the experimental setup. The resulting pressure and drug distributions are reported in the results section.

9.2.2 Mouse model

Eight week old, female athymic, nude-foxn1nu mice (21 g average body weight, ENVIGO, NM horst, the Netherlands) were monitored for general health during one week before the start of the study. After conditioning, 12 mice underwent a midline laparotomy under general anesthesia with Sevoflurane (Baxter, Deerfield, USA) after which they were bilaterally injected via the subperitoneal route with 5.0×105 SKOV3- Luc-IP1 cells suspended in 50 µl of Matrigel® (Life Sciences, Antwerp, Belgium) to facilitate the growth of peritoneal tumor nodules (figure 9.1a). All mice were given subcutaneous pain relief (Ketoprofen, 150µl) immediately after the procedure. Their weight and general wellbeing were monitored during recovery.

To assess the success rate of tumor induction and monitor tumor growth, a bioluminescence scan (IVIS Lumina II, Perkin Elmer) was acquired 14 days post-injection (Figure 39b). Each animal was injected intraperitonealy with Luciferine (D-Luciferin, PerkinElmer, Waltham, USA) using a dose of 150 mg/kg body weight. During the first scan, a calibration series was performed to assess the time after injection at which the signal was maximal. For subsequent scans, the same waiting period was maintained.

9.2.3 MRI protocol

MRI scanning (figure 9.1c) was performed using a 7 T MR system (PharmaScan 70/16, Bruker, Ettlingen, Germany) with a mouse body volume coil. During the scanning protocol, all mice were anesthetized with isoflurane (5% induction, 1.5% maintenance, 0.3 L/min) and their body temperature was maintained using a heating blanket. An anatomical scan was obtained using a T1-weighted sequence (RARE) with the following settings: repetition time (TR) 1455 ms, echo time (TE) 9.0184 ms, flip angle (FA) 180°, in-plane resolution 120 µm, slice thickness 600 µm, and an acquisition of 30 contiguous transverse slices. Using this anatomical scan, a single slice was chosen in which both tumor nodules were visible. Native relaxation times were calculated in this slice from a FLASH sequence with four different TR values, i.e. 100 ms, 502 ms, 1184 ms and 5000 ms. Other scanning parameters were: TE 100 ms, FA 180°, in-plane resolution 268 µm. The DCE-MRI series was acquired for the chosen slice using a FLASH sequence with TR 12 ms, TE 3.4 ms, FA 25°, in-plane resolution 268 µm, 550 repetitions, and temporal resolution 1.344 s, resulting in a total acquisition time of 12 min 19 s. After 60

seconds of baseline signal measurements, a bolus of 0.2 $\frac{mmol}{kg}$ Gd-DOTA
(Dotarem^{TM}, Guerbet, Paris, France) was injected through a tail vein
catheter. Animals that did not show tumor growth were excluded from
the rest of this study.

9.2.4 Intraperitoneal chemotherapy

Three weeks after tumor inoculation, all mice positive for tumor growth
were put under general anesthesia and underwent 30 minutes of intraperi-
toneal chemotherapy (IPC) (figure 9.1d) with cisplatin (Hospira Benelux
BVBA, Antwerp, Belgium). The administered cisplatin dose was calculated
as 1/100th of the clinically used dose relative to the body surface area
(BSA) resulting in used values of 0.7 mg cisplatin/mouse (concentration in
solution of 113 µmol/l). The cisplatin solution circulated in a circuit con-
sisting of an inlet and outlet probe fitted with temperature sensors (TM
9604; Ellab A/S, Hilleroed, Denmark), a connecting tubing that passed
through a 520 U process pump (Watson-Marlow NV, Zwijnaarde, Belgium)
and a M3 LAUDA heat exchanger (LAUDA-Brinkmann, New Jersey, USA)
[24]. All procedures were performed on a heating pad and the chemo-
therapeutic solution temperature was kept at 37–38°C (normothermic
conditions).

9.2.5 Interstitial fluid pressure measurement

Immediately after IPC, the chemotherapeutic solution was drained from
the abdominal cavity, after which the peritoneal surfaces were pat dried.
A SPR-320 pressure tip catheter connected to a PCU-2000 pressure control
unit and PowerLab 35 Series data acquisition system (Millar, Houston,
USA) was manually inserted in the center of each tumor and held there
until a stable pressure output signal was measured [111].

9.2.6 Data processing, fitting and interpolation

During DCE-MRI scanning, a series of MRI scans is acquired in rapid suc-
cession following the intravenous injection of the paramagnetic contrast
agent. The underlying principal of the technique relies on the fact that as
the contrast agent disperses through the tissue, it changes the MR signal
intensity of the tissue depending on its local concentration.

Following Zhu et al [330], T2∗ relaxation was neglected to compute
the contrast profiles due to the use of short TR's and TE's (rendering

the attenuation of signal due to the terms related to T2* contribution ($e^{-TE/T2*}$) negligible for low contrast concentrations). We thus applied equation (9.1) for the contrast concentration c:

$$c = \frac{1}{r_1 TR} \log \left[E_{10} \frac{1 + \cos(\alpha)(RIE(E_{10} - 1) - 1)}{RIE(E_{10} - 1) + E_{10}(1 - \cos(\alpha))} \right] \quad (9.1)$$

with

$$E_{10} = \exp \left(-\frac{TR}{T_{10}} \right) \quad (9.2)$$

The relative intensity enhancement (RIE) was calculated as $RIE = \frac{(S-S_0)}{S_0}$ with S_0 the baseline signal calculated from 60 seconds of measurement prior to contrast injection, S the signal at that timepoint and r_1 is the relaxivity of Dotarem (3,5 mM-1s-1 [132]) in the interstitial fluid, T_{10} the native relaxation time calculated from the four images with different TR, and α is the flip angle. Equation (9.1) is solved for each pixel of the tumorous region of interest (ROI) and for each timepoint after contrast injection. By tracking the concentration values of each pixel in function of time, $c(t)$ profiles can be calculated.

In addition to calculating the concentration profiles of the contrast agent from the equations above, we can describe the transient concentration of the Gd-DOTA (c_{GD}) tracer in the region of interest by a two-compartment model [329], with the two compartments being the interstitial space and the blood plasma:

$$\phi \cdot \frac{dc_{GD}}{dt} = P \frac{S}{V}(C_{AIF} - C_{GD}) + \frac{J_v}{V}(1 - \sigma)C_{AIF} \quad (9.3)$$

in which c_{GD} and c_{AIF} are the concentration of the tracer in the interstitial space and the plasma, respectively. c_{AIF} is also known as the arterial input function (AIF). ϕ is the interstitial fluid volume fraction ($\phi = 0.3$), P is the permeability coefficient of the vasculature for the tracer, S/V is the surface to volume ratio of the vasculature, σ the osmotic reflection coefficient for the tracer ($\sigma = 0.6$), and $\frac{J_v}{V}$ the plasma filtration rate per unit volume. In order to obtain a good estimate for the parameters $P\frac{S}{V}$ and $\frac{J_v}{V}$, it is crucial to provide an AIF that is as accurate as possible. To extract a mouse-specific AIF from the DCE-MRI dataset, a high temporal resolution is needed throughout the series. This in turn limits the spatial

resolution that can be achieved in the DCE-MRI plane. To obtain the AIF, equation (9.1) was again used to calculate the contrast concentration on candidate AIF pixels that were identified on the anatomical image. The contrast concentration calculated in these pixels represents the blood concentration of contrast (c_b) so to obtain the plasma concentration of contrast (c_{AIF}), an additional scaling had to be performed, taking into account the hematocrit value (Hct) of the mouse (equation (9.4)) [292].

$$C_{AIF} = \frac{c_b}{1 - Hct} \tag{9.4}$$

The resulting plasma concentration curve was then filtered and fitted to a bi-exponential curve that was further used in its analytical form as the AIF. Using the corresponding mouse-specific AIF for each tumor ROI, the solution to this first order differential equation (c_{GD}, equation (9.3)) can be fitted on a voxel to voxel basis to the contrast profiles that were calculated from the DCE-MRI (equation (9.1)) series to obtain estimates for $P\frac{S}{V}$ and $\frac{J_v}{V}$.

To implement spatially varying vascular parameters in our model we used an approach previously described by Zhao et al. [329] in which the J_v/V values are rescaled to the product of the vascular hydraulic conductivity and surface-to-volume ratio of the microvasculature $L_p\, S/V$. In order to do so, all J_v/V values were first normalized with respect to the average value $\left(\frac{J_v}{V}\right)_{mean}$ of all fitted pixels in the ROI and then scaled by multiplying the normalized values with the product of the baseline values typically used for hydraulic conductivity and vascular surface to volume ratio in literature [269] ($L_{p,0} = 2.1 \cdot 10^{-11}\, m/(Pa \cdot s); \left(\frac{S}{V}\right)_0 = 2.00 \cdot 10^4\, m^{-1}$) (equation (9.5)).

$$\left(\frac{L_p S}{V}\right)_{i,j} = Lp,0 \cdot \left(\frac{S}{V}\right)_0 \cdot \frac{\left(\frac{J_v}{V}\right)_{i,j}}{\left(\frac{J_v}{V}\right)_{avg}} \tag{9.5}$$

The extrapolated $\frac{L_p S}{V}$ values were then used as input for the Starling term in our model for IF flow (see further).

The need for a high temporal resolution (to extract the AIF from the data) and the available MRI hardware, limited us to a 2-dimensional DCE-MRI series. To provide 3D spatially varying parameters, extrapolation of the available data was needed. Upon inspection of the estimated resulting parameter maps, two distinctively different regions could be detected in

each tumor. In tumors 1 and 2, there were interior zones with pixels that could not be fit by equation (9.3), whereas the surrounding tissue was fit well by the same equation. In tumor 3 on the other hand, the majority of interior pixels was well fit but two zones for which the $\frac{L_P S}{V}$ parameter yielded very different results, could be distinguished. These different regions were then related back to the anatomical scans (T1 weighed scans) and traced in each slice of the anatomical scan of the tumor geometry thereby effectively segmenting a second 3D zone within the original tumor. The mean $\frac{L_P S}{V}$ value averaged over all fitted pixels in the sub-ROI was then assigned to each of the different regions. Implications of this extrapolation will be discussed in the discussion section.

9.2.7 Computational model

For this work, three different tumors were selected based on their respective sizes. The tumor geometries were segmented using Mimics (Materialise, Leuven, Belgium) and the resulting geometries were smoothed and meshed in 3-matic (Materialise, Leuven, Belgium) before they were imported as stl-files in COMSOL multiphysics (COMSOL, Inc., Burlington, USA). A similar procedure was followed to obtain the boundary of any additional internal zones that were present in the tumors. Volume meshes where created in COMSOL multiphysics using the same element size for each geometry ($1.7 \cdot 10^{-4} mm^3$) based on the mesh independence study of the model, resulting in the mesh sizes listed in table 9.1. The equations for both the IFP build-up and the mass transport that were implemented in COMSOL were previously described by our group [269] and summarized below. In a rigid porous medium like the tumor interstitium, the momentum equation can be reduced to Darcy's Law [23]:

$$u = -k\nabla P_i \tag{9.6}$$

where u represents the interstitial fluid velocity vector (in m/s); K the conductivity of the tissue for interstitial fluid ($3.1 \cdot 10^{-14} m^2/Pa \cdot s$ [16]), P_i the interstitial fluid pressure (Pa) and ∇ the gradient operator.

The steady-state continuity equation for the incompressible interstitial fluid flow in normal tissue is given by [23]:

$$\nabla \cdot u = F_v - F_l \tag{9.7}$$

were ∇ represents the divergence operator; F_v the fluid gain from
the blood (s^{-1}) and F_l a lymphatic drainage term for interstitial fluid
(s^{-1}). Since there is a known lack of functional lymphatics in solid tumors,
$F_l = 0$. The constitutive relation for F_v is based on Starling's hypothesis
[16] (equation (9.8)):

$$F_v = \frac{L_p S}{V}\left(P_v - P_i - c(\pi_v - \pi_i)\right)$$ (9.8)

with L_p the hydraulic conductivity of the vasculature $(m/Pa \cdot s)$, $\frac{S}{V}$
the surface to volume ratio of the vasculature (m^{-1}), P_v the vascular pres-
sure (Pa), P_i the interstitial fluid pressure (Pa), c the non-dimensional
osmotic reflection coefficient, Π_v the vascular osmotic pressure (Pa) and
Π_i the interstitial osmotic pressure (Pa). IFP profiles were calculated by
solving the steady state form of the momentum and continuity equations.
When more than one zone was present in the tumor, the source and sink
terms (i.e. Starling source) were adapted in each zone to include the cor-
responding estimated $L_p S/V$ value as discussed in the data processing
section.

Mass conservation of the drug is given by equation (9.9) [23]:

$$\frac{\partial C_{drug}}{\partial t} = D\nabla^2 C_{drug} - \nabla \cdot \left(u C_{drug}\right) - S$$ (9.9)

with C_{drug} the time-dependent concentration of the drug present
in the interstitium (mol/m^3), D the diffusion coefficient (m^2/s), ∇^2 the
Laplacian operator, ∇ the divergence operator and S the sink in drug
concentration (mol/m^3). This sink term includes losses due to cellular
uptake and resorption by the vascular system [269]. To calculate the IF
flow, the pressure at the outer edge of the tumor is kept constant at 0
Pa and at the interface between two different tumor zones, an interface
boundary condition is imposed, implying continuity of all properties. On
the edge of the tumor nodule, where the IPC drug is in direct contact
with tumor tissue, a fixed drug concentration is maintained (i.e. 0.113
mol/m^3). Initial values for pressure and concentration in the domain
were set to 0 Pa and 0 mol/m^3, respectively. Values for all model parame-
ters mentioned above were taken from our previously published model of
the drug distribution in a single tumor nodule during IP chemotherapy
[269].

A segregated approach was used for solving the continuity equation, momentum transport and mass conversation of the drug. All three tumor cases were run as transient models with a time resolution of 30 s. As a convergence criterion, a drop of 4 orders of magnitude in the residuals was chosen.

9.2.8   Reported parameters

By solving the drug transport equation (equation (9.9)) using the pressure and velocity field calculated in the previous section, drug concentrations could be determined in the tumor geometries.

For all simulations, pressure and concentration profiles were analyzed along 2 or 3 perpendicular axes in the xy-plane with the same applicate as the one of the DCE-MRI plane. All lengths reported are distances that are normalized with respect to the corresponding length of the axis. The pressure profile along a certain axis is characterized by the maximal pressure (P_{max}) along this axis and the steepness of the pressure profile in that direction. In this work, steepness is characterized by the LP50 value, which we define as the distance starting from the tumor edge after which the pressure reaches 50% of its maximal value. The steeper the pressure profile, the lower the LP50 value will be.

From the concentration profiles along the axes, the penetration depth is determined. Both absolute penetration depths (APD) and relative penetration depth percentages (PD%) are reported. The APD is defined as the maximal depth along the axis of interest where the drug concentration exceeds the corresponding half maximal inhibitory concentration value of the drug (IC50). The PD% represents the percentage of the length of the axis where concentration values exceed the corresponding IC50 value of the drug used. The inclusion of different zones with varying vascular properties results in non-symmetric profiles along the axes. To highlight this phenomenon, values for the penetration depths are reported with respect to both sides of the axis (L = smallest abscissa; R = largest abscissa).

9.3   RESULTS

9.3.1   Geometry and segmentation

The three selected tumors significantly differed in size with reconstructed tumor volumes ranging from 45 mm^3 to 288 mm^3. Tumor 1 was the

largest with a volume of 288 mm^3. The interior zones that can be seen
on figure 9.2 can be related to the zones with varying vascular properties
that were segmented and ranged in volume from 8 mm^3 for tumor 3 to 69
mm^3 for tumor 1. The number of pixels in the tumor ROI of the DCE-MRI
images varied from 181 to 329. A summary of the geometric properties of
the different tumors is presented in table 9.1.
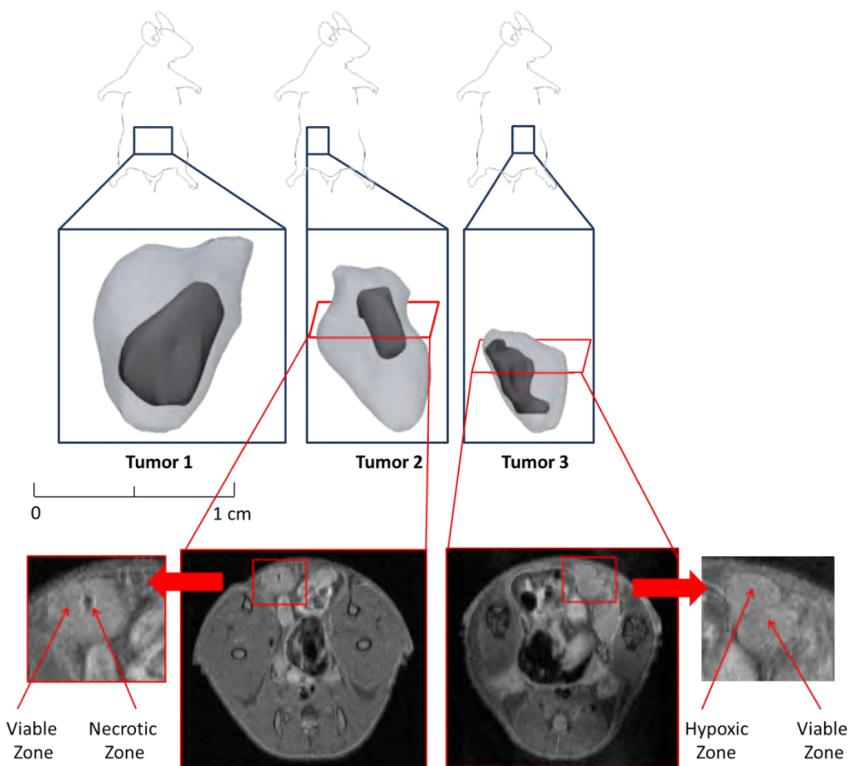
Figure 9.2: Visualization of the three segmented tumor geometries and their
different zones on a common scale. The tumors have reconstructed volume
values of 288; 121 and 45 mm^3, respectively.

9.3.2 Data Processing

For each of the 3 chosen animals, a suitable AIF could be fitted from
the concentration data. Using the animal-specific AIF, the parametric
solution for equation (9.3) was calculated and subsequently fitted to all
pixels within the ROI (ROI tumor 1: figure 9.3b, ROI tumor 2: figure 9.3h).
Upon fitting the pixels of the tumor ROI, we found that certain pixels were
not adequately fitted ($R^2 < 0.85$) (red pixels on figure 9.3c and figure 9.3i).
The contrast concentration c(t) increased fastest in the viable tissue areas

Table 9.1: Geometrical properties of the three segmented geometries.

Geometrical properties			
	Tumor 1	Tumor 2	Tumor 3
Tumor location	Right	Left	Right
Tumor Size	8 x 11 mm	6 x 8 mm	4 x 6 mm
Reconstructed tumor volume	288 mm^3	121 mm^3	45 mm^3
Reconstructed interior volume	69 mm^3	9 mm^3	8 mm^3
Mesh size (number of volume elements)	1693526	715057	421569
# pixels in DCE-MRI ROI	329	270	181

as a result of rapid Gd-DOTA uptake in this well-perfused region, followed by rapid washout (figure 9.3e and figure 9.3k). In hypoxic areas, however, there is typically a reduced vascularization which is reflected in a delayed Gd-DOTA signal build-up as well as a delayed and prolonged wash-out of signal (figure 9.3l). In necrotic regions of the tumor, there is no vascularity thought to be present and no washout of the contrast agent could be seen in the signal [330] (figure 9.3f).

Unlike pixels in the hypoxic and viable tissue areas, pixels in necrotic areas were not adequately fitted by equation (9.3). For the pixels that were adequately fitted, $\frac{J_v}{V}$ parameter maps were created and scaled to $\frac{L_p S}{V}$ maps (figure 9.3 d and figure 9.3 j). Upon inspection of the resulting $\frac{L_p S}{V}$ maps different zones within the tumor nodules could be identified (hypoxic/necrotic/viable tissue). The $\frac{L_p S}{V}$-values were then averaged over the different zones and the final values ranged from 0 in the necrotic areas to $3.946 \cdot 10^{-7} (Pa \cdot s)^{-1}$ in the outer zone of tumor 3.

9.3.3 Pressure measurement

The measured pressures in the three tumors were 15.5 mmHg (2067 Pa), 21.3 mmHg (2890 Pa) and 19 mmHg (2533 Pa) for tumor 1, 2 and 3 respectively. In table 9.2, the converted pressure values in Pa are summarized.

9.3.4 Pressure simulation

The model can calculate IFP pressures and concentration distributions in all geometries. The maximal IFP (table 9.2) reached in our simulations
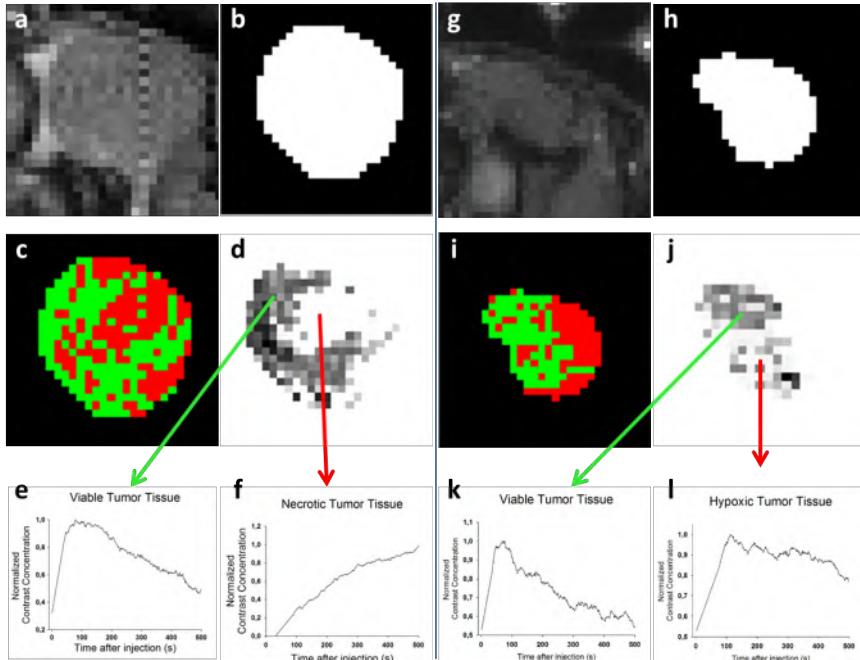
Figure 9.3: a. Baseline DCE-MRI image of the tumor 1 ROI. b. Mask created of
tumor 1 ROI based on the baseline image. c. Visualization of the pixels within
the tumor 1 ROI that were adequately fit ($R^2 > 0.85$) in green and the ones that
could not be fit in red d. $\frac{L_p}{V}$ map of the tumor 1 e. Representative c(t) profile
for the pixels in the darker, viable tissue zone of figure 9.3 d. f. Example of a c(t)
profile for the pixels in the white, necrotic tissue zone of figure 9.3d. Tumor 2 is
not included in the figures, but Representative c(t) profiles are similar to the ones
obtained in tumor 1 with both a viable and necrotic tumor tissue zone, albeit of
different size and shape. g. Baseline image of the tumor 3 ROI h. Mask created
of tumor 3 ROI based on the baseline image i. Visualization of the pixels within
the tumor 3 ROI that were adequately fit ($R^2 > 0.85$) in green and the ones that
could not be fit in red. j. LpS/V map of the tumor 3 with two distinctive zones
that can be noted. k. Representative c(t) profile for the pixels in the viable tissue
zone of figure 9.3j l. Example of a c(t) profile for the pixels in hypoxic tissue zone
of image figure 9.3j.

Table 9.2: Summary of pressure and penetration depth results.

Pressure and concentration results							
		Tumor 1		Tumor 2		Tumor 3	
	SA1	SA2	LA	SA	LA	SA	LA
Pmeas(Pa)		2067		2890		2533	
Pmax (Pa)	1385	1429	1411	1523	1525	1428	1468
LP50 (mm)	L: 0.0437	L: 0.0407	L: 0.0290	L: 0.0565	L: 0.0365	L: 0.0819	L: 0.0727
	R: 0.0428	R: 0.0351	R: 0.0401	R: 0.0519	R: 0.0378	R: 0.0708	R: 0.0603
APD (mm)	L: 0.361	L: 0.320	L: 0.412	L: 0.370	L: 0.422	L: 0.371	L: 0.495
	R: 0.331	R: 0.327	R: 0.404	R: 0.328	R: 0.281	R: 0.394	R: 0.463
PD% (%)	L: 5.63%	L: 5.50%	L: 5.33%	L: 7.96%	L: 4.96%	L: 10.3%	L: 7.92%
	R: 5.16%	R: 5.68%	R: 5.23%	R: 6.85%	R: 3.30%	R: 10.9%	R: 7.41%
Pvol% (%)		28.04%		28.04%		43.42%	

was 1525 Pa (11.44 mmHg), obtained in tumor 2. The shape of the pressure profiles (figure 9.4) differed strongly between the different tumor geometries and even along the longer and shorter axes in the same tumor geometry. It is interesting to note that the pressure profile along the short axis 1 of tumor 1 has a local minimum. Another pressure related parameter that showed a directional variability was the LP50 with a peak value of 0.819 mm for the left side of the long axis of tumor 3 and a minimum of 0.0290 for the left side of the long axis of tumor 1.

9.3.5 Drug distribution

Drug penetration was analyzed along the same axes mentioned above and all concentrations were normalized with respect to the initial concentration c = 113 µmol/l. Absolute penetration depths ranged from 0.281 mm to 0.495 mm and were highest along the long axis of tumor 3 and lowest along the long axis of tumor 2. Relative penetration percentage ranged from 3.30% to 10.9% and was highest along the short axis of tumor 3 and lowest along the long axis of tumor 2. The volume fraction of penetrated tumor tissue ranged from 28.04% to 43.42% and was highest for tumor 3 and lowest for tumor 1. A summary of the penetration depths can be found in table 9.2 and a visualization of the drug concentration profiles can be found in figure 9.5.

9.4 DISCUSSION

In this work, we expanded our previously developed three-dimensional CFD model for IPC in tumor nodules [269] to include realistic geometries
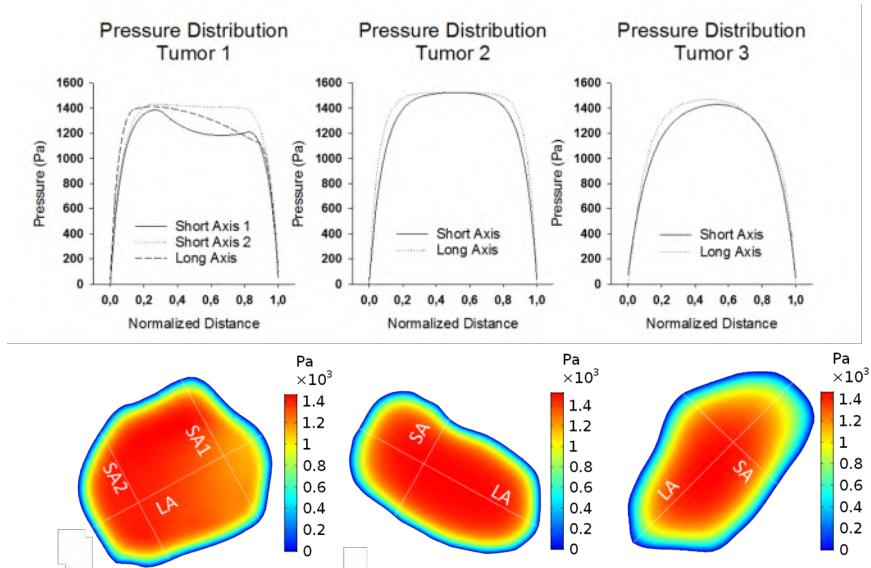
Figure 9.4: Pressure distributions in the different tumor geometries along the short and long axes (SA and LA respectively) presented at the bottom; tumor projections are not to scale. Pressures are noted in Pa and the distances are normalized with respect to the total respective length of the axis.
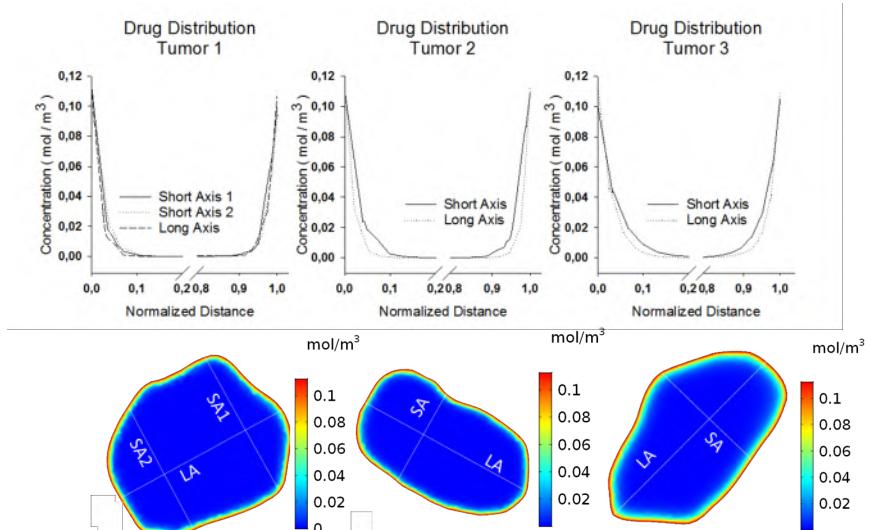
Figure 9.5: Drug distribution in the different tumor geometries along the axes as shown in the bottom; tumor projections are not to scale. Concentrations are noted in mol/m³ and the distances are normalized with respect to the total respective length of the axis.

and pressure profiles. We modeled three different tumor nodule geometries of different sizes ($288\,\text{mm}^3$, $121\,\text{mm}^3$, $45\,\text{mm}^3$) and extracted spatially varying microvasculature related parameters from DCE-MRI images. Using these parameters, pressure fields were simulated in the tumors and drug transport was studied in all three tumor geometries in the presence of the corresponding pressure field.

In any work relying on DCE-MRI data, a trade-off has to be made between spatial and temporal resolution [14]. We opted for a small temporal resolution to extract an animal-specific AIF. Due to this high temporal resolution and the available MRI hardware, we were limited to a single slice and had to extrapolate the vascular properties estimated from this slice to three-dimensional data. Other works in which mice tumors were studied have used AIF functions from literature to allow for a lower temporal resolution [224, 185, 329]. The extrapolation of data from 2D to 3D inevitably leads to inaccuracies in the determination of the interior tumor zones that were determined. In the future, a more realistic estimation of vascular parameters in the tumors could be obtained using multiple slices throughout the tumor during the DCE-MRI and applying the data processing workflow for each slice. Recently, Bhandari et al. [21] used a 3D DCE-MRI sequence combined with a high temporal resolution in the study of human brain tumors with good results. It is, however, impossible to compensate for physiological and hardware differences by extrapolating scan parameters from one setup to another. We found that, upon fitting the DCE-MRI data to equation (9.1), not all pixels could be adequately fit. In some cases, this was due to poor signal quality (too much noise) in these pixels and for a second subset of pixels, located at the edge of the ROI, this was because of overestimations in the initial ROI segmentation, most likely caused by partial volume effects [12]. Studying the contrast concentration profiles in the border areas of the initial ROI's could in the future allow for a better distinction between tumor and surrounding tissue and a more refined ROI.

A final group of pixels that could not be fit by equation (9.3) were pixels that exhibited the typical signal shape of necrotic zones. Both tumor 1 and tumor 2 were found to have necrotic cores, with the pixels in the dark regions on figure 9.3 exhibiting the typical relation between time and signal intensity for necrotic zones as was also found in [44]. The necrotic zone in tumor 1 (largest tumor), however, was estimated to be a factor 8 larger than the one in tumor 2.

In tumor 3, two different zones could also be distinguished (figure 9.3), but neither of them was necrotic. Pixels from the interior zone of tumor 3

displayed a relation between time and signal intensity that was more close to that of a hypoxic zone with a slower contrast uptake and a prolonged wash-out compared to perfused tumor tissue. Contrast concentration curves of pixels belonging to the outer shell of each of the three tumors followed the typical relation for viable, well-perfused tumor tissue with a sharp peak in contrast concentration and a rapid wash-out due to the abundance of leaky, tortuous microvasculature in this area.

The measured pressures varied between 2066 Pa and 2839 Pa with the largest value observed in tumor 2 and the smallest value in tumor 1. Overall, the lower the LP50, the steeper the pressure profile and the higher the maximal interstitial fluid velocity, and therefore the higher the radial outward convective flow will be. Calculated pressures showed a similar trend but were lower with values varying from 1384 Pa to 1525 Pa (largest value for tumor 2, smallest value in tumor 1). Tumor 2, which had the largest percentage of viable, well-perfused tumor tissue, presented with the highest IFP. It is important to note that in the CFD model only IFP is simulated by means of the Starling term. However, the invasively measured pressure yields the total pressure, i.e. the sum of the IFP and solid state (SS) pressure [28] with the SS pressure transmitted by the solid and elastic elements of the extracellular matrix and cells, as opposed to fluids (IFP). The difference between the measured and predicted IFP pressure may be a measure for the SS matrix pressure that exists in solid tumors [273]. Nonetheless, validation of this assumption is mandatory but not trivial, as most invasive pressure measurements will correspond to the total stress rather than one of its components. Deformation tests performed by Nia et al. [203] estimated the solid stress in solid tumors of colorectal and pancreatic origins to be in the range of 90 to 1000 Pa. Given this order of magnitude of the SS pressure as an indication, the SS pressure may explain the difference between the simulated IFP and the measured total pressure. Assuming that indeed the SS stress can be calculated as the experimentally measured total stress minus the calculated IFP, the SS pressures in the three tumor geometries equals 682 Pa for tumor 1, 1367 Pa for tumor 2 and 1105 Pa for tumor 3. Due to the differences in extracellular matrix (ECM), cell density and the presence of cancer associated fibroblasts (CAFs), the tumor tissue permeability is likely to be significantly different from the healthy surrounding tissue permeability. While we previously found that the IFP remained virtually constant when the Darcy permeability of the tissue changed, these changes are very likely to impact the SS pressure. To obtain a tumor-specific estimate of the SS pressure to add to the calculated IFP, an extra step could be added to the workflow in future work where – using a similar workflow as described

by Helmlinge et al. and Stylianopoulos et al. [274, 123] – the tumor deformation after cutting is used to determine the SS pressure.

The invasively measured total pressures in the tumors were within the range of previously measured pressures in tumors of similar size, location and origin (11 mmHg to 40 mmHg with a median of 22 mmHg [111] which equals a range of 1497 to 5333 Pa with a median of 2933 Pa).

In our previous work [269], we established a positive relationship between tumor size and maximal IFP. In this work, we found that this relationship does not longer hold in the presence of zones with different vascular properties, while we did observe a positive relationship between the percentage of viable tumor tissue and the maximal IFP. This is of particular interest as a recent work by Bhandari et al. [21] found no relation between tumor size and IFP. The different IFP values found for different tumor volumes in this work are thought to be due to the maximal IFP being reached in the geometries being lower than the maximal possible IFP. When this maximal pressure value is reached, the net volume flux out of the vasculature is zero and exceeding this pressure value would most likely result in the local collapse of the microvasculature. This maximal IFP value can be found by equaling the filtration rate of plasma fluid per unit volume ($\frac{J_v}{V}$) across the vessel wall as described by Starling's law to zero.

$$\frac{J_v}{V} = \frac{L_p S}{V}\left(P_v - P_i - c(\pi_v - \pi_i)\right) \tag{9.10}$$

This results in the following maximal IFP: $P_{i,MAX} = P_v - c(\pi_v - \pi_i)$ in which P_v is the vascular pressure, c the osmotic reflection coefficient and π_v and π_i the oncotic pressures in blood and interstitium, respectively. Using the parameters used in this work, this maximal interstitital pressure value equals $\pm$ 1530 Pa. The pressure obtained in the tumors described in the work of Bhandari et al., is close to the maximal interstitial pressure. Therefore, it is not expected that IFP will be different between different tumors geometries in the work of Bhandari et al. We also noted that the presence of the 3D necrotic zones resulted in heterogeneous IFP profiles in the tumors. These findings are of specific interest as previous works using symmetrical, idealized tumor and necrotic core geometries, found little to no influence of the necrotic core on the IFP profile [16]. A similar finding was done by Pishko et al. [224], where skewed IFP values were reported based on IFP calculations using 3D spatially varying tissue parameters.

The absolute penetration depths calculated in this work ranged from 0.32 mm to 0.50 mm. When comparing these results with those obtained in previous studies, they were found to be in good agreement with the experimentally defined range of 0.41 – 0.56 mm where carboplatin (another platinum-based drug of roughly the same size) was used [7]. The observed concentration profiles were highly dependent on both the probing location and direction. We calculated the volume percentage of each tumor where the local drug concentration after 30 minutes of IPC exceeded the IC50 value of cisplatin [60] and found a range of 28.04% to 43.42%, with the highest percentage occurring in tumor 3 and the lowest in tumor 2. In our previous work, we explored the relative importance of several different parameters that influenced the drug transport during IPC. One of the largest improvements in penetration depth was obtained by subjecting the tumor nodules to vascular normalization (VN) therapy with the APD doubling in certain cases. The results in this work indicate that penetration depths in certain tumors (i.e. tumor 3) could reach up to 47% when doubled and might be very good candidates for VN therapy.

As in all numerical models, some assumptions were made to make the model implementable. The model may incorporate different zones with different vascular parameters, but the reality is more complex. Using a higher spatial resolution and multiple slices (instead of 1 slice) to obtain DCE-MRI data throughout the tumor should allow for a more realistic distribution of vascular parameters in the tumors, possibly on a voxel per voxel basis. The estimates for $\frac{L_p S}{V}$ could be further refined by coupling model equations to the compartmental model that would yield a direct estimation of $\frac{L_p S}{V}$ values from the tracer signal instead of the proportionality to $\frac{J_v}{V}$ approximation [329]. In this work, we assumed that the variation of contrast tracer at early post-infusion times was from the vascular component to the interstitial space (extracellular space) only and vascular resorption was neglected. Future work could include the addition of a sink term in equation (9.3) to include vascular resorption. The model could be further refined by the addition of sink terms that represent the effect of other physiological phenomena, such as drug binding to the ECM and plasma protein binding. Additionally, a number of refinements could be made to the boundary conditions of the model, such as the inclusion of time dependent boundary concentrations to take into account the changing concentration of drug in the carrier fluid and non-zero boundary pressures to take into account the hydrostatic pressure head of the fluid in the abdomen. An additional sensitivity study using this model may include changing the drug concentration boundary concentration over a biologically relevant range to quantify possible penetration depth enhancements by using higher concentrations.

The results presented in this work are based on data obtained from three tumors in a mouse model. Applying the same workflow, with the possible inclusion of some of the adaptations mentioned above, to a larger group of animals would allow for the determination of a population-based average of the AIF and could also shed more light on the extent of tissue heterogeneity within different tumor geometries of the same origin. Applying the same protocol to human subjects should be feasible but there are a few aspects to take into consideration. Although DCE-MRI sequences for human tumor imaging exist, the location of the PM makes them susceptible to motion artifacts due to both respiration and peristaltic movement which could interfere with data quality. Additionally, the non-invasive pressure estimation presented in this work only estimated IFP pressures and does not account for SS pressures. To obtain an accurate, non-invasive estimation of total tumor pressure, the SS should be estimated non-invasively as well.

In conclusion, we expanded our previously developed 3D CFD model of the drug mass transport in a single tumor nodule during IP chemotherapy to include realistic tumor geometries and spatially varying vascular properties. DCE-MRI studies made it possible to distinguish between tumorous tissues with different vascular properties as well as the healthy surrounding tissues and necrotic zones. We found that tumor size no longer correlated to the maximal IFP when regions with different vascular properties were included. Using realistic geometries of both tumor nodules and necrotic cores had a big impact on the resulting penetration depth in this work, unlike the previous model in which the inclusion or absence of a necrotic core did not seem to influence the penetration depth significantly. We found that the resulting pressure profiles within tumors were highly dependent on the irregular geometries and different zones, indicating a strong need to include both aspects in the model. The total pressure was found to be higher for higher percentages of viable tumor tissue volume ratios. The presence of a significant solid state pressure in the tumor nodules may explain the difference between calculated IFP pressures and measured total pressures.

III

Conclusions and future perspectives

This chapter recapitulates the most important conclusions of this manuscript and offers some critical considerations of the limitations and impact of our research. We refer back to the research goals as defined in part I, chapter 5 to get a sense of the extent to which we achieved these goals and end this chapter by identifying directions for future work.

KEY FINDINGS

In this dissertation we studied (i) a novel approach to obtain a better surface exposure of the peritoneum to cytotoxic drugs and (ii) the determinants that influence the penetration depth of drugs in tumor nodules on the peritoneum. The connecting factors of both chapters were both the ultimate goal (i.e improving intraperitoneal chemotherapy) and the means by which we attempted to obtain this goal (i.e use of computational fluid dynamics). In the first chapter of part 2, a novel approach for IPC that shows potential to overcome one of the main limitations of current IPC practice: the limited surface exposure of the peritoneal surfaces, was presented. In chapter 8 of part II, we presented our own model for the drug transport during IPC, which, in chapter 9, was enhanced to include realistic tumor geometries and spatially varying vascular parameters.

It is obvious that in order for intraperitoneal chemotherapy to be efficient, the drug solution should reach all affected areas of the peritoneum in a sufficient manner. The presence of bulky tumor nodules and possible adhesions due to prior surgery modify the already complex peritoneal anatomy in such a way that homogeneous distribution of the drug carrier solution using a single inflow catheter is not feasible. Using a combination of theoretical considerations and computational fluid dynamic modeling, a number of different catheter designs consisting of multiple inflow arms were proposed. The proposed designs were manufactured from silicone tubing using a microdrilling technique to fabricate the perforations along the catheter arms. Hydraulic testing results where underwhelming with none of the manufactured prototypes resulting in desirable outflow patterns. The manufacturing issues leading to the non-homogeneous outflow included burr formations, non-round perforations, incomplete perforations, and perforations inconsistent in size. Due to these issues, the microdrilling technique was abandoned in favor of the laser ablation of the perforations. Despite solving several of the manufacturing issues (burr formation, incomplete perforations), others persisted with the non-round, tapered perforation shape and the inconsistency in size being the most notable ones. Hydraulic testing using the full catheter set-up with laser ablated perforations resulted in very heterogeneous flow due to these manufacturing inaccuracies in the different catheter arms, with the flow in the most perfused arm being a factor 40 larger than the flow in the least perfused arm.

Mathematical modelling can provide unique insights in the different transport barriers that occur during IP chemotherapy, as well as offer the

possibility to test different protocols or drugs without the need for in vitro or in vivo experiments. The current state of the art of the modelling of drug transport during intraperitoneal chemotherapy was summarized in chapter 7. We classified the existing models in three different categories based on the used scale in the model: the whole organ scale, which considers the peritoneum as a single compartment; the tissue scale, which considers the tissue of the tumor as a homogenous mixture of cells, interstitium and vasculature; and finally the cellular model, which models each cell explicitly. We found the existing models in literature to be diverse and each one coming with its own set of advantages and limitations. Multiple models did not take the high interstitial fluid pressure into account and neither of them used spatially varying tissue parameters. The inclusion of these aspects in our computational fluid dynamics model is one of the key features of this work.

In chapter 8, we presented a full three-dimensional model to study drug transport in an isolated intraperitoneal tumor nodule during IP chemotherapy. The model included convective, diffusive and reactive drug transport in different tumor geometries and sizes and we applied it to study the influence of changes in some of the therapy-related parameters (e.g. different types of drugs, tissue permeability...) on the tissue penetration. We found that the model reproduced a number of literature validated trends (e.g. effect of tumor size on penetration depth; effect of vascular normalization therapy) and the calculated penetration depths proved a good match to the ones found in literature. Tumor size and shape were important determinants of drug penetration depth as well as the extent and permeability of the microvasculature that was present in the tumor tissue. The explicit inclusion of the necrotic core in the model and changes in the intrinsic tissue permeability on the other hand had a limited effect on the predicted penetration depth.

Because of the noted dependence of drug penetration on both tumor size and shape and vascular properties, we expanded the previously developed three-dimensional CFD model to include realistic geometries and pressure profiles (part II, chapter 9) with data obtained from animal experiments. Even though the tumor nodules were often small and their location on the peritoneal surface made them prone to motion artifacts related to both breathing and peristaltic movement, segmentation of the nodules was feasible without any problem. More realistic pressure distributions were obtained by estimating vascular parameters from DCE-MRI datasets and subsequently using these as a spatially varying input in the Starling term of the mass balance equation for the interstitial fluid flow. In the presence of the realistic pressure distributions, penetration depth

of drugs was found to be far more inhomogeneous than in the previous model, thereby highlighting the importance of taking this factor into account. Interestingly, tumor size no longer correlated with the maximal IFP obtained in the tumor when regions with different vascular properties were included. Also, the presence of a necrotic core did seem to influence the IFP in these cases (as opposed to the model in chapter 8) with the percentage of viable to necrotic tissue correlating to the maximal IFP. The measured pressures in the tumor nodules were higher than the simulated pressures in each geometry. The presence of a significant solid state pressure in the tumor nodules may explain this difference between calculated IFP pressures and measured total pressures.

CONTRIBUTION AND IMPACT

In this work, computational fluid dynamic modeling was used for two very different applications that were linked by their shared goal: attempt to improve the current state of the art of intraperitoneal chemotherapy. The developed models can have a clinical impact in a several ways which will be discussed in this section.

Catheter design

Any design process is bound to be complicated by unexpected issues and findings along the way. And although no working prototype of the new catheter could be presented at this stage, there is merit to be found in the workflow of the design and benchmarking process of it. Theoretical design allowed for the creation of a number of idealized geometries that could lead to favorable outflow profiles. The impact of adapting these idealized geometries to a 'makeable' design could be assessed in a time and cost-efficient manner using computational fluid dynamics for a number of different geometries. When in vivo results proved to be different from the expected results and manufacturing issues were hypothesized to be at the base of this, the model was used to "reverse engineer" the manufactured catheter geometry and the results proved that these manufacturing issues were indeed at the base of these discrepancies. Should the road to clinical implementation of the catheter after solving the manufacturing issues lead to more setbacks that require adjustments to the catheter arm design, CFD modeling can be used as a quick, reliable tool to choose between different designs.

Therapeutic target identification

Penetration depths of cytotoxic drugs after intraperitoneal administration of chemotherapy are currently not sufficient to ensure the elimination or prevention of recurrence of peritoneal metastases. The transport processes occurring during IPC depend on numerous parameters and theoretically, any parameter that has an influence on the mass transport during chemotherapy is a possible target to modify and potentially improve the drug penetration depth. The distinction between a good target parameter and a less interesting one, is based on how sensitive the penetration depth is to this parameter. Traditional methods to evaluate the impact of changes in one of the governing parameters are in silico, in vitro or in vivo experiments or more often a combination of all three. Computational fluid dynamics models like the one presented in chapter three are able to predict changes in penetration depth in a time and cost-effective manner when certain parameters are varied. In chapter three, we found that penetration depth was far more dependent on the amount of vascular normalization therapy that was applied than to the intrinsic tissue permeability. By performing parameter sweeps over larger ranges for the governing parameters, we identified vascular normalization therapy and drug diffusivity as interesting therapeutic targets.

Protocol selection for IPC

In chapter 8, an attempt was made to provide an oversight of the differences between different IPC regimens and looking at this overview provides a sense of just how different treatment protocols are. Some differences are straightforward such as the choice of used drug, which relates to the effectiveness of the selected drug against the tumor of origin. Other choices such as the amount of carrier fluid, therapy duration, etc are more debatable and will often depend on hypothesis, expertise of the treating team and practical considerations. IPC duration for example should ideally be long enough so that the maximal potential penetration depth can be obtained and tumor cells are exposed to the drug concentrations over the longest possible period of time. It is however important to keep track of the total operation time, especially when a time consuming debulking operation has already been performed. The ideal IPC duration should be a compromise between both aforementioned factors and modeling the penetration depth of drugs for different IPC durations using a CFD model can help surgeons decide on this matter. The concentration of the drug in the carrier fluid should ideally be as high as possible, to maximize the concentration gradient and therefore diffusive drug transport

into the tumor tissue. A higher concentration is however a risk for on the patient, with chances for both local toxicities at the outermost surfaces and systemic burden thought to increase with higher concentrations. Simulations in which the concentrations are varied over a useful and safe range could help determine the optimal concentration to be maintained during IPC. It is possible that lower concentrations lead to approximately the same penetration depth of drug, due to the dominance of the convective transport over the diffusive one in tumors with high IFP. Other, similar examples to the previous two can be thought off, highlighting the potential of the model as a tool to aid the surgeons in the determination of optimal IPC protocol parameters.

LIMITATIONS AND FUTURE PERSPECTIVES

Catheter protoyping and manufacturing issues

Even though all proposed designs performed well in simulations, none of these first prototypes performed well during hydraulic testing. The reason for this underwhelming performance was traced back to manufacturing issues and inaccuracies and as a result, the first manufacturing approach (microdrilling) was abandoned in favor of laser ablation. Despite solving some of the manufacturing issues the laser ablated catheters did not outperform the previous catheters and at the conclusion of this dissertation, the feasibility of using laser ablation as a manufacturing technique for the catheter arms is not obvious. Searching for alternative manufacturing methods that are able to produce perforations with reproducible results and acceptable tolerances should be the subject of future research.

The connector pieces that were designed and used in the full catheter set-up were visually inspected and underwent some preliminary, qualitative hydraulic testing. More extensive, quantitative testing and microscopic inspections of the pieces were not performed because the issues with the perforated catheter arms were more significant. All manufacturing techniques are prone to small variations in physical dimensions and the variations in diameters of the outflow support pieces of the 3D-printed connector piece are likely to also have an influence of the homogeneity of the outflow pattern of the full catheter. Future work should therefore include proper, quantitative testing of these connector pieces to assess the impact of these variations.

Even when manufacturing issues are solved, there is still a long way ahead before clinical implementation. The minimal diameter of the per-

forations was limited to prevent occlusion of these perforations due to biological processes such as biofilm formation. The motivation behind this cut-off value is however arbitrary in this work and in vivo testing of the prototypes should clarify whether this value is substantiated.

Model assumptions and parameterization

In this work, we used a CFD and species transport model to study the distribution of drugs in tumor tissue after intraperitoneal chemotherapy. The tumor tissue is considered to be a homogeneous mixture of cells, extracellular matrix and microvasculature. Therefore, a distributed porous medium model was used with the Navier-Stokes equations describing the momentum transport reducing to the Darcy law. During IPC, it is assumed that the drugs enter from the intraperitoneal cavity through the extracellular, extravascular space and are either diffusively-convectively transported or are lost for further transport by cellular uptake or vascular uptake. In this work, both cellular and vascular uptake were considered to be one directional and are modeled as a sink term in the species transport equation. The convective transport of the drug in the extracellular space was strongly influenced by the elevated interstitial fluid pressure, which was modeled using the Starling term with permeabilities estimated using DCE-MRI data as spatially varying input. The presence of a necrotic core where no uptake (neither vascular nor cellular) of the drug was present was taken into consideration with only a limited effect on the results. The influence of different drugs was studied by changing drug diffusivity. Extracellular drug binding and plasma protein binding were not taken into account. To validate the computational model, an orthotopic mouse model was used starting from an ovarian cancer cell line from which the tumor geometries (volumes ranging from 45 to 288 mm^3) were segmented. Pressure measurements were made using a pressure tip catheter (pressure ranging from 2067 to 2890 Pa).

Given the strong influence of the IFP on the results, future work should focus on the accurate determination of this IFP in a non-invasive way. The mouse model used in this work was limited in spatial resolution due to the small tumor sizes and was prone to motion artifacts. As a human derived cell line was used in an immune compromised mouse, the micro-environment of the tumor is likely to be significantly different from that of an actual ovarian tumor. Switching to a rat model starting from a native cancer cell line, might facilitate the determination of an accurate, representative, non-invasive pressure measurement. Once such a protocol has been established, a shift in focus could be made to study

smaller tumors as they are the ones that are clinically of most interest. Also, these smaller nodules are interesting due to the expected conflicting contribution of both inward diffusive and radially outward convection (without the tumor pressure being elevated to such high pressures that the convective transport is entirely dominant).

Any model that mimics the behavior of tissue is bound to be limited in accuracy by the assumptions that have to be made in order to reduce the complexity of the human body to a more manageable level. We made an initiative to model the reactive transport of the drug in the tumor tissue, with sink terms representing the vascular re-uptake and cellular uptake of the drug, but the actual transport includes numerous other steps. We did not implement for example the sink terms representing the effect of other physiological phenomena such as extracellular matrix binding and plasma protein binding. Literature values quantifying these processes that would allow for straightforward implementation in the model were not available for these phenomena and the choice was made to omit them from the equations for now. Future work should include the determination and validation of these phenomena in a quantitative way if possible. Additionally, intraperitoneal chemotherapy is often performed using heated chemotherapy (HIPEC). In this work, the effect of hyperthermia was not taken into account because the method of action of hyperthermia is not related to a single model parameter and some of the effects described above might have opposite effects on the overall penetration depth. Validation of these separate effects with experimental data in order to include correct parameters was beyond the scope of this work but is therapeutically very relevant. In the future, hyperthermia can be included by changing the diffusivity of the used drug, the LD50, the viscosity for all fluids, the hydraulic permeability and the cellular uptake etc. With the inclusion of each additional phenomenon, the model becomes more complex and more difficult to solve. Adequate validation of single parameters on the one hand, and of total model performance on the other hand at each step along the way is imperative to obtain reliable results. At this point, validation of the drug penetration depths was done by comparing the simulated results to available literature data with a good agreement being found between both ranges. Future research should include the direct measurement of the penetration depths after intraperitoneal chemotherapy to provide a one-on-one validation of the total model.

Due to hardware limitations and data quality, we found that it was not possible to estimate vascular permeability maps on a voxel-to-voxel basis from the obtained DCE-MRI dataset and had to rely on averaging

and extrapolation of data in order to fill in the blanks. The extrapolation of data from 2D to 3D, and the averaging over groups of pixels with similar values, inevitably led to inaccuracies in the determination of the vascular permeabilities that were determined. In the future, a more realistic estimation of vascular parameters in the tumors could be obtained using multiple slices throughout the tumor during the DCE-MRI and applying the data processing workflow for each slice.

The (im)possibility for personalized medicine

Living tissue, and especially tumor tissue is not a uniform entity that can be quantified by single parameter values for quantities such as microvascular density, permeability, cell concentration, extracellular matrix compositions, etc. Values for such parameters are expected to range between different patients on the one hand and within a certain tissue on the other hand. In this work, we found that some general trends from the first model were not replicated in the subject-specific models. Tumor tissues are notoriously heterogeneous and using patient-specific geometries and tissue parameters, which is often the next step in improving personalized treatment efficacy, is not straightforward in the case of peritoneal metastases. The implementation of patient-specific tumor geometries is challenging to say the least with tumor nodules not only being small and distributed over a large surface area, but the amount of tumor nodules is often so high that segmentation of all nodules would be far too labor intensive. The model developed in this work should therefore not be considered as a first step towards a personalized medicine approach for IPC, but more as a tool to derive optimal treatment protocol parameters and derive general trends. To derive these general trends, an alternative approach taking into account the natural variations in human tissue parameters could consist of the segmentation of a diverse set of tumor geometries and using experimental determined ranges for relevant tissue parameters to perform Monte Carlo style simulations and attempt to derive general trends that include these tissue variations. From these general trends, it might be possible to determine subgroups of tumor nodules that are more likely to be adequately targeted by IPC or even alter treatment protocol parameters depending on the features of the found nodules. A patient with a large number of small nodules, might for example benefit more from a different protocol than a patient with fewer, larger tumor nodules. Deriving this sort of trends might be an interesting path for this research to continue and find its way into clinical application.

Measuring tumor pressure: what's in a name?

Like many other solid tumors, the peritoneal tumor nodules often exhibit a high interstitial fluid pressure. This high IFP is caused by a number of contributing factors, including the leaky and irregularly shaped microvasculature, the lack of a functional lymphatic system, a denser extracellular matrix, an increased number of cancer associated fibroblasts (CAF's) and a larger cell density. The model as implemented in this work, takes the altered microvasculature into account as well as the lack of the functional lymphatic systems. Total tumor pressure, is like any other tissue pressure composed of an interstitial fluid pressure and a solid-state pressure.

After the experiments, the conclusion in hindsight was that total pressures were measured instead of true IFP and upon subsequent review of the literature, it was often difficult in other works to distinguish whether only true IFP was measured, or total pressure. In other works, where the effect of techniques to lower tumor pressure are studied, this distinction might not be as relevant, but when it comes to validation of the IFP pressures in our model, which describes only the fluid phase of the tissue, it clearly is. The discrepancies between measured total pressures and simulated pressure might therefore be explained by the solid state pressure and experimental determination of this solid state pressure after the DCE-MRI protocol and subsequent invasive pressure measurement should ideally allow for this hypothesis to be accepted.

To the best of our knowledge, easy, accurate and non-invasive measurement of tumor IFP is not feasible at this point. Studies attempting to influence the IFP (and thereby therapy outcome) therefore rely mostly on invasive pressure measurement or other parameters that are a measure for IFP. Given that spread of cancer cells in the peritoneal fluid is one of the main dissemination routes for peritoneal metastases, invasive pressure measurement techniques, which effectively puncture the tumor capsule, are not feasible in the clinical context of peritoneal metastases. The influence of IFP on penetration depth was very pronounced however, indicating that vascular normalization therapy and other techniques aimed at lowering the IFP are interesting targets to improve the penetration depth of drugs. Further research should therefore focus further into developing accurate, non-invasive methods for measuring IFP in the context of peritoneal metastases.

Due to its limited invasiveness and promising reported enhancement in penetration depth, IPC delivery in the form of a pressurized aerosol (PIPAC) is increasingly being studied as an alternative IP delivery method.

Similarly to the work done in this dissertation, computational fluid dynamic modeling of PIPAC, might also offer some an insights in the governing parameters of drug transport during PIPAC and add to the determination of optimal treatment parameters.

APPENDIX 1: ABDOMINAL CANCERS

In this appendix, a more elaborate overview of different types of abdominal cancers than the one provided in Chapter 2 can be found.

GASTRIC CANCER

Gastric cancer is known for its aggressive nature and is one of the main causes of death from cancer worldwide. Adenocarcinoma is the most prevalent gastric cancer with reported incidences of 90 to 95%, while remaining gastric cancer cases include lymphomas, gastrointestinal stromal tumors (GIST) and carcinoid tumors [236]. Peritoneum and liver are among the most common metastatic sites and when present, prognosis is usually grim. Intraperitoneal chemotherapy has been used to prevent peritoneal recurrence after a curative gastrectomy in high risk patients and has been proven to improve both overall survival and disease free survival. For selected patients presenting with a low number of PM, where complete cytoreduction is possible, hyperthermic, intraperitoneal chemotherapy (HIPEC) can be considered a valuable therapy [26].

Adenocarcinoma

Adenocarcinoma is a malignant epithelial tumor that develops from the cells of the innermost lining of the stomach. It is commonly subdivided in intestinal and diffuse-type [67]. Diffuse-type cancers diffusely infiltrate the stroma of the stomach and often exhibit deep infiltration of the stomach wall while intestinal-type cancers grow in expanding, rather than infiltrative patterns . The latter are associated with a better prognosis than diffuse-type gastric cancers [67].

Gastric carcinomas are often asymptomatic when superficial and resectable, and the majority of patients diagnosed with gastric adenocarcinoma therefore present with unresectable locally advanced or metastatic disease [103]. Intraperitoneal chemotherapy has been studied in

the management of gastric cancer and a recent meta-analysis showed that interperitoneal chemotherapy was associated with an increased 1-year, 2-year, and 3-year survival rate, but had little to no effect on the incidence of 5-year survival rate [142].

Lymphoma

Primary gastric lymphomas are rare, accounting to approximately 5% of primary gastric cancers. A distinction can be made between low-grade and high-grade tumors, and treatment options will depend on the histologic subtype and stage of the disease. Antibiotic therapy, systemic chemotherapy and radiotherapy are often used in the management of gastric lymphomas, in contrast to surgery, which is avoided if possible [144].

Gastrointestinal stromal tumor (GIST)

Gastrointestinal stromal tumor (GIST) originate from the interstitial cells of Cajal which are present in the wall of the stomach. The tumors are considered to be potentially malignant. The standard treatment of a GIST without metastasis is surgical resection, but recurrence rates of up to 50% are reported even with complete resection [3]. Recurrent GIST or GIST with metastasis are usually treated by tyrosine kinase inhibitors but cases in which cytoreduction in combination with intraperitoneal chemotherapy have been used have been described [31].

Carcinoid tumor/ Gastro-enteropancreatic (GEP) neuroendocrine tumor (NET)

Gastric carcinoid tumors are rare endocrine-related tumors that develop within the gastric mucosa and are subdivided in three types: type 1, type 2, type 3 [307]. These cancers are mostly found by coincidence during endoscopy and can consist of a single lesion or multiple lesions of varying size. Type 1 gastric carcinoids usually consist of multiple small lesions, are slow growing and distant metastases are rare. Prognosis is usually good with a 5-year survival exceeding 95%. Type 2 gastric carcinoids also presents with multiple small lesions and are slow growing, but have an increased incidence of distant metastasis which is reflected in a lower 5-year survival (70% to 90%). Type 3 gastric carcinoids are generally solitary lesions and are often large. The biological behavior is more aggressive than type 1 and 2 with frequent metastases to regional nodes and liver and the 5-year survival is lower than 35% [307].

Other cancers

Other primary cancers of the stomach include squamous cell carcinoma, small cell carcinoma and leiomyosarcoma, but the incidence of each of these cancers is very rare [177].

Cancers of the appendix are rare and early disease is often asymptomatic. Hence, most of them are found during appendectomies performed for appendicitis. The primary appendical cancers can be subdivided in colonic-type adenocarcinoma of the appendix, mucinous appendical neoplasms, and neuroendocrine carcinoma. The management of primary appendix cancer depends on the histologic subtype and extent of disease. Because they are quite rare, therapy is mainly based on retrospective insights and small trials.

Colonic-type adenocarcinoma of the appendix

Colonic-type adenocarcinoma of the appendix is most prevalent in the 5th and 6th decade, and has a slight male sex predominance. Diagnosis is often made following appendectomy for appendicitis, or when a palpable abdominal mass is present. Colonic-type adenocarcinoma is known to perforate and distend into adjacent structures although this is less likely than in mucinous adenocarcinomas. The peritoneum is the most common site for metastases, and for selected patients for whom complete cytoreduction can be achieved, intraperitoneal chemotherapy has been used [149].

Mucinous appendiceal neoplasms (MAN)

Mucinous appendical neoplasms (MAN) can be subdivided in low-grade appendical mucinous neoplasm, high-grade appendical mucinous neoplasm, mucinous adenocarcinoma and poorly differentiated mucinous adenocarcinoma [15]. This distinction is crucial in determining prognosis and treatment: high-grade MAN exhibits a more aggressive clinical course than low-grade MAN. Both types of cancer are known to rupture, leading to pseudomyxoma peritonei (PMP). PMP is characterized by poorly-circumscribed gelatinous masses filled with malignant mucin-secreting cells. Both types of MAN are unlikely to spread extraperitonealy and

are as such good candidates for cytoreductive surgery and intraperitoneal chemotherapy. Additionally, even in patients presenting with a high peritoneal carcinomatosis index, complete or near-complete cytoreduction can be obtained. These factors have made cytoreductive surgery in combination with heated intraperitoneal chemotherapy the standard of treatment for patients with PMP with excellent survival rates.

Goblet cell adenocarcinoma (GCA)

Goblet cell adenocarcinoma (GCA), is a rare malignant cancer of the appendix accounting for approximately 14% to 19% of primary appendix cancers [238]. GCAs are typically diagnosed after appendectomy, and when detected early, controversy exist on whether additional right-hemicolectomy is indicated. The peritoneum is the most common site of metastases and in GCA patients with peritoneal involvement, various combinations of debulking surgery, systemic chemotherapy, and cytoreductive surgery with hyperthermic intraperitoneal chemotherapy (CRS+HIPEC) have been used. [188]

Neuroendocrine carcinoma

Primary appendical neuroendocrine carcinoma (ANC), is considered a subtype of midgut neuroendocrine carcinoma, and has better survival rates (>95%) compared to all other tumor types located in the appendix, even when peritoneal metastases are present [112].

OVARIAN CANCER

Ovarian cancer constitutes the fifth most frequent cause of cancer death in women in the Western world, accounts for an estimated 239,000 new cases and 152,000 deaths worldwide annually [230]. Malignant ovarian tumors are classified in different groups : epithelial, stromal and germ cell tumors, but rare exceptions fall outside these groups [1].

Epithelial tumors

Epithelial tumors, also called ovarian carcinomas (OCs), are the most common group, accounting for 90% of ovarian cancer diagnosis [45]. This group is further subdivided in low-grade serous carcinoma (LGSC, less

than 5% of cases), high-grade serous carcinoma (HGSC, around 70% of cases), mucinous carcinoma (MC, 3% of cases), endometrioid carcinoma (EC, around 10% of cases) and clear cell carcinoma (CCC, around 10% of cases) [225]. Different groups are characterized by differences in risk factors, molecular genetic abnormalities, natural history, and response to chemotherapy [98]. Since early disease tends to be asymptomatic and no effective screening programs exist, more than 75% of the patients are diagnosed at an advanced stage (FIGO stage III or IV) [69]. At these advanced stages, patients already show extensive tumoral dissemination on the peritoneal surfaces, known as peritoneal carcinomatosis (PC) or peritoneal metastasis (PM) [83]. Historically, standard treatment consisted of a combination of cytoreductive surgery and systemic chemotherapy. Intravenous chemotherapy however does not effectively penetrate into peritoneal tumor nodules, and in recent years locoregional treatment in the form of intraperitoneal chemotherapy treatment has been investigated with promising results [50]. Due to these promising results, intraperitoneal chemotherapy, in combination with cytoreductive surgery, has become a generally accepted protocol in most advanced high grade epithelial ovarian cancers [236].

Ovarian sex cord-stromal tumors

Ovarian sex cord-stromal tumors represent approximately 7% of all ovarian tumors and include a heterogeneous group of neoplasms that arise from the primitive sex cords or stromal cells [130, 245]. Although younger patients are most affected, cases with affected women of all ages have been described [114]. Presentation as a low-grade disease (stage I) is most common and usually the clinical course is non-aggressive with surgical resection alone leading to favorable prognosis [249]. In cases with recurrent or primary advanced disease, systemic chemotherapy has been used as well as intraperitoneal chemotherapy more recently [141, 68].

Ovarian germ cell tumors (OGCT)

Ovarian germ cell tumors derive from primordial germ cells of the ovary and can be either benign or malignant with the latter only accounting for only a small fraction of all OGCTs [204]. Platinum based chemotherapy is usually effective with reported survival rates of 90% in women with early stage OGCTs and up to 80% for more advanced disease [252]. Loco-regional spread to the peritoneum is rare but when present, prognosis is usually poor [322]. Recent studies showed that a combination of

cytoreductive surgery and hyperthermic intraperitoneal chemotherapy has promising and potentially curative results in cases with peritoneal metastasis [322, 118].

Epithelial tumors

Adenoma

Colorectal adenomas are benign tumors of the colon and the rectum. They are typical precursor lesions for colorectal adenocarcinoma. The size of the adenoma is one of the most important predictors for their malignant potential. Based on their size they can be subdivided in diminutive (1 to 5 mm in diameter), small (6 to 9 mm), and large (≤10 mm) adenomas. Studies have shown that adenomas are found in as much as 50% of asymptomatic persons who undergo screening by means of colonoscopy; 3.4 to 7.6% of these adenomas are advanced and 0.2 to 0.6% are cancerous [272].

Colorectal Carcinoma (CRC)

CRC is not a homogenous disease, but can be classified into different subtypes, which are characterised by specific molecular and morphological alterations. Subdivions include adenocarcinoma, mucinous adenocarcinoma, signet-ring cell carcinoma, small cell carcinoma, squamous cell carcinoma, adenosquamous carcinoma, medullary carcinoma and undifferentiated carcinoma. Incidence of CRC is high and in the western world it accounts for approximately 10% of all cancer-related mortality. [160]

Peritoneal metastases (PM) are common in colorectal cancer, with up to 10% of patients presenting synchronously with the primary tumor, and up to 25% developing PM at a later stage [184]. A recent review found that 3.4 to 6.3% of patients with non-metastatic colorectal cancer develop peritoneal metastases after curative surgery [129]. Risk factors to develop PM include [276]:

- Visible evidence of peritoneal metastases

- Ovarian cysts showing adenocarcinoma suggested to be of gastrointestinal origin

- Perforated cancer

- Positive margins of excision

- Positive cytology either before or after cancer resection

- Adjacent organ involvement of cancer-induced fistula

- T3 mucinous cancer

- T4 cancer or positive 'imprint cytology' of the primary cancer

- Cancer mass ruptured with the excision

- Obstructed cancer

In the risk group mentioned above, intraoperative HIPEC is being investigated as a way to minimize the occurrence of PM. Another treatment strategy is the so called second-look surgery, which aims at the early detection of PM and can be combined with HIPEC when indicated.

In addition to the preventive role of HIPIC in the development of PM in colorectal cancer patients, intraperitoneal chemotherapy can also be used with a curative, therapeutic of palliative aim. Taking into account the high morbidity and mortality of the combination of cytoreductive surgery combined with intraperitoneal chemotherapy, patients should be selected based on their general fitness, PCI, prior surgical score, histopathology of the primary tumor, etc. In highly selected cases, the combination of CRS + HIPEC has led to improved median survival [276].

Carcinoid tumors

Carcinoid tumors are the most common neuroendocrine tumor in the gastrointestinal system [173]. Although rectal carcinoids often behave in a relatively indolent manner, they are malignant and can metastasize. Estimated 5-year survival rates range from 88 to 100 for stage I, and from 0 to 38% for cases where distant metastases were present [189]. Chemotherapy and radiation therapy are used in the management of metastatic carcinoid tumors, but only resection is thought to be curative [319].

Colonic carcinoids are even rarer than their rectal counterparts and differ in clinical presentation, morphology and prognosis [206]. The lesions are usually large and aggressive and 50 to 60% of patients have metastases to the liver, lymph nodes, mesentery, or peritoneum. Prognosis is poorer than rectal carcinoids with a reported 5-year survival of approximately 50% [111].

Non-epithelial tumors

Non-epithelial tumors of colorectal origin include lipomas, leiomyomas, gastrointestinal stromal tumors, leiomyosarcomas, angiosarcomas, melanomas and lymphomas but each of these is very rare.

PANCREATIC ORIGIN

Pancreatic cancer is one of the deadliest cancers with a 5 year survival rate below 5% [315]. A distinction between endocrine and exocrine can be made with the latter being far more common than the former.

Endocrine tumors of the pancreas (PNET)

Pancreatic neuroendocrine tumors (PNETs) are rare pancreatic neoplasms that are generally indolent, but do have malignant potential [232]. Different types include insulinomas, gastrinomas, VIPomas, and glucagonomas. Due to this often indolent nature, a wait-and-see approach was common historically, but more recently more aggressive approaches are more common [71]. This aggressive approach consists of surgery, locoregional therapy, systemic therapy, and complication control [315]. The most common metastasis of PNET are the liver, although peritoneal metastases have also been described [300].

Exocrine tumors of the pancreas

Most exocrine tumors of the pancreas have an epithelial origin, with other origins such as mesenchymal (leiomyosarcomas, malignant gastrointestinal stromal tumours, solitary fibrous tumours) and lymphatic (lymphoma) being very rare. The most common type of epithelial neoplasm of the pancreas arises from the ductal epithelial cells of the exocrine pancreas and have the ductal adenocarcinoma histological subtype (PDAC). Other subtypes according to the WHO histological classification include: solid-pseudopapillary neoplasms, pancreatoblastomas, acinar cell carcinomas, papillary mucinous neoplasms, mucinous cystic neoplasms and serous cystic neoplasms.

Ductal carcinoma of the pancreas (PDAC)

PDAC is an aggressive disease associated with a poor clinical prognosis, weakly effective therapeutic options, and a lack of early detection methods. Complete surgical removal of the tumor remains the only chance for cure, however 80-90% of patients have disease that is surgically incurable at the time of clinical presentation [244]. Because of the often late detection and the chemoresistance of these tumors, the five-year survival rate is only around 5–7% and one-year survival is achieved in less than 20% of cases [289]. Even when a complete resection has been performed, the rate of reccurence is high and the most common sites of recurrence are the liver, the peritoneal surfaces and the pancreatic bed [309]. Recently, in a preliminary study, cytoreductive surgery in combination with intraperitoneal chemotherapy was found to be beneficial in highly selected patients with pancreatic cancer with peritoneal metastasis [288].

Serous cystic neoplasms (SCN)

SCNs of the pancreas are usually benign, but do have malignant potential, albeit a very small one. Due to this low malignant potential, most SCNs are observed without resection. In malignant cases, resection leads to excellent survival results and chemotherapy is not indicated [133, 299].

Mucinous cystic neoplasms (MCN)

MCN are rare neoplasms that occur almost exclusively in the pancreatic body and - tail of middle-aged women; they are usually solitary and their size ranges between 5 and 35 cm. The malignant potential of MCN is thought to be higher than for SCN with reported incidences of invasive carcinoma in MCN varying from 6% to 36% [201]. Surgical excision is indicated for all MCNs which is supplemented with Gemcitabine (GEM) chemotherapy in more advanced cases [250]. Even in malignant cases, 5-year disease-specific survival rates are much higher than for adenocarcinoma, with some studies reporting up to 57% 5-year disease-specific survival [52].

Intraductal papillary-mucinous neoplasms (IPMN)

Intraductal papillary mucinous neoplasms (IPMNs) of the pancreas are neoplasms that are characterized by ductal dilation, intraductal papillary

growth, and thick mucus secretion. Resection is recommended for most IPMN. The 5-year survival of patients after surgical resection for noninvasive IPMN is reported to be at 77-100%, while for those with invasive carcinoma, it is significantly lower at 27-60% [183]. Gemcitabine-based chemotherapy has been used as an adjuvant therapy, but literature does not agree on its effectiveness [35, 211].

Acinar cell carcinoma

Even though the pancreas is composed primarily of acinar cells, acinar cell carcinomas comprise only 1-2% of exocrine pancreatic neoplasms [209]. Most acinar neoplasms of the pancreas are solid and malignant, but the long-term survival for patients is somewhat better than the long-term survival of patients with pancreatic adenocarcinoma. Resection is recommended when deemed feasible as it is the only available treatment that can prove curative [40]. Both chemo- and radiotherapy are used in the neoadjuvant or adjuvant setting but no standardized approach to the treatment exists [321].

Pancreatoblastoma (PB)

Pancreatoblastoma (PB) is a rare malignant neoplasm of the pancreas that occurs mostly in the pediatric patients but rare cases in adults exist [208]. PB is an aggressive and malignant tumor with high rates of local invasion and recurrence. Adult patients with PB have a worse prognosis compared to pediatric patients [333]. Due to its rarity, no standardized guidelines exist for the treatment of PB. Surgery is usually indicated but the role of chemo- and radiotherapy remains unclear [241].

Solid-pseudopapillary neoplasm (SPN)

Solid pseudopapillary neoplasms (SPN) are extremely rare epithelial tumors with low malignant potential [318]. Surgical resection is performed even in cases of local invasion and metastases. For the metastases, surgical debulking should be performed, in contrast to other pancreatic malignancies. The overall five-year survival rate of patients with SPN is about 95% [216].

APPENDIX 2 – CHARACTERISTICS OF ALL SIMULATIONS IN PART II CHAPTER 8

Maximal interstitial fluid pressures (IFP_{max}) and distances necessary for the pressure to drop to 50% of its maximal value (LP50) are stated to characterize the pressure profile, absolute penetration depth (APD) and penetration depth percentages (PD%) are given to characterize the concentration profile. The stated differences in PD% are always with respect to the corresponding baseline case. A summary of all used geometries and their corresponding abbreviation can be found in figure 8.1. a Characteristics of the six baseline cases. b Characteristics of the vascular normalization (VN) simulations. c Characteristics of the drug diffusivity simulations. d Characteristics of the simulations with and without necrotic core (NC). e Characteristics of simulations with varying intrinsic permeability (k).

Characteristics of all simulations in part II chapter 8

Geometry	Characteristic	IFP_{max} [Pa]	LP50 [mm]	APD [mm]	PD% [-]	Difference in PD%
Baseline cases						
LS	Baseline Case	1533.9	0.98	0.40	4.04	-
SS	Baseline Case	1413.3	0.89	0.42	20.82	-
LE	Baseline Case	1533.9	0.98(SA)/0.99(LA)	0.38(SA)/0.39(LA)	3.77(SA)/1.96(LA)	-
SE	Baseline Case	1495.4	0.90(SA)/0.93(LA)	0.38(SA)/0.47(LA)	21.39(SA)/11.64(LA)	-
LT	Baseline Case	1533.9	0.98(SA)/0.99(LA)	0.38(SA)/0.36(LA)	3.82(SA)/1.81(LA)	-
ST	Baseline Case	1522.5	0.89(SA)/0.95(LA)	0.45(SA)/0.49(LA)	21.29(SA)/12.31(LA)	-
Effect of vascular normalization						
LS	50%VN	1503.8	0.97	0.49	4.85	0.81
LS	100%VN	1379.3	0.91	0.70	6.99	2.95
SS	50%VN	1078.4	0.87	0.53	26.71	5.89
SS	100%VN	259.4	0.84	0.78	38.76	17.95
LE	50%VN	1503.9	0.97/0.98	0.45/0.47	4.52(SA)/2.35(LA)	+0.75(SA)/+0.39(LA)
LE	100%VN	1446.7	0.91/0.94	0.65/0.68	6.53(SA)/3.39(LA)	+2.76(SA)/+1.43(LA)
SE	50%VN	1266.4	0.87/0.90	0.53/0.57	26.43 (SA)/14.20(LA)	+5.04(SA)/+2.56(LA)
SE	100%VN	370.6	0.84/0.84	0.72/0.89	35.82(SA)/22.33(LA)	+14.43(SA)/10.69(LA)
LT	50%VN	1503.9	0.97/0.98	0.46/0.50	4.58(SA)/2.50(LA)	+0.76(SA)/+0.69(LA)
LT	100%VN	1466.4	0.90/0.94	0.66/0.65	6.60(SA)/3.28(LA)	+2.78(SA)/+1.47(LA)
ST	50%VN	1389.8	0.83/0.88	0.52/0.58	25.82(SA)/14.42(LA)	+3.53(SA)/+2.10(LA)
ST	100%VN	531.1	0.70/0.77	1.03/0.74	51.64(SA)/18.50(LA)	+29.35(SA)/+6.4(LA)
Effect of drug diffusivity						
LS	Paclitaxel	1533.9	0.98	0.64	6.38	2.33
SS	Paclitaxel	1413.3	0.89	0.68	33.85	13.03
LE	Paclitaxel	1533.9	0.98(SA)/0.99(LA)	0.54/0.56	5.44(SA)/2.82(LA)	+1.67 (SA)/+0.86 (LA)
SE	Paclitaxel	1495.4	0.90(SA)/0.93(LA)	0.67/0.70	33.25(SA)/17.48(LA)	+11.86(SA)/+5.85(LA)
LT	Paclitaxel	1533.9	0.98(SA)/0.99(LA)	0.66/0.60	6.60(SA)/3.00(LA)	+2.79(SA)/+1.19(LA)
ST	Paclitaxel	1522.5	0.89(SA)/0.95(LA)	0.75/0.74	37.50(SA)/18.49(LA)	+15.21(SA)/+6.17(LA)
Effect of necrotic core						
LS	no NC	1533.9	0.98	0.41	4.13	0.09
SS	no NC	1519.5	0.89	0.44	21.89	1.08
LE	no NC	1533.9	0.98(SA)/0.99(LA)	0.42/0.41	4.15(SA)/2.05(LA)	+0.38(SA)/+0.09 (LA)
SE	no NC	1526.3	0.91(SA)/0.93(LA)	0.36/0.42	17.83(SA)/10.58(LA)	-3.56(SA)/-1.06(LA)
LT	no NC	1533.9	0.98(SA)/0.99(LA)	0.40/0.37	4.01(SA)/1.83(LA)	+0.20(SA)/ 0.02 (LA)
ST	no NC	1526.5	0.90(SA)/0.94(LA)	0.44/0.48	22.12(SA)/11.84(LA)	-0.17(SA)/-0.48 (LA)
Effect of intrinsic permeability						
LS	$k = 6.4 \cdot 10^{-17}$	1533.9	0.98	0.40	4.04	0
LS	$k = 3.1 \cdot 10^{-17}$	1533.9	0.98	0.40	4.04	-
LS	$k = 6.4 \cdot 10^{-18}$	1533.9		0.40	3.69	-0.35
SS	$k = 6.4 \cdot 10^{-17}$	1206.4	0.89	0.42	20.82	0
SS	$k = 3.1 \cdot 10^{-17}$	1413.3	0.89	0.42	20.82	-
SS	$k = 6.4 \cdot 10^{-18}$	1532.2	0.89	0.42	20.82	0
LE	$k = 6.4 \cdot 10^{-17}$	1533.9	0.97(SA)/0.98(LA)	0.39(SA)/0.41(LA)	3.91(SA)/2.07(LA)	+0.14(SA)/+0.11(LA)
LE	$k = 3.1 \cdot 10^{-17}$	1533.9	0.98(SA)/ 0.99(LA)	0.38(SA)/0.39(LA)	3.77(SA)/1.96(LA)	-
LE	$k = 6.4 \cdot 10^{-18}$	1533.9	0.98(SA)/0.99(LA)	0.38(SA)/0.38(LA)	3.77(SA)/1.89(LA)	0(SA)/-0.07(LA)
SE	$k = 6.4 \cdot 10^{-17}$	1256.4	0.88(SA)/0.91(LA)	0.43(SA)/0.47(LA)	21.39(SA)/11.65(LA)	0(SA)/+0.01(LA)
SE	$k = 3.1 \cdot 10^{-17}$	1495.4	0.90(SA)/0.93(LA)	0.38(SA)/0.47(LA)	21.39(SA)/11.64(LA)	-
SE	$k = 6.4 \cdot 10^{-18}$	1533.9	0.90(SA)/0.93(LA)	0.38(SA)/0.47(LA)	21.39(SA)/11.64(LA)	0(SA)/0(LA)
LT	$k = 6.4 \cdot 10^{-17}$	1533.9	0.97(SA)/0.98(LA)	0.38(SA)/0.38(LA)	3.82(SA)/1.90(LA)	0(SA)/+0.09(LA)
LT	$k = 3.1 \cdot 10^{-17}$	1533.9	0.98(SA)/0.99(LA)	0.38(SA)/0.36(LA)	3.82(SA)/1.81(LA)	-
LT	$k = 6.4 \cdot 10^{-18}$	1533.9	0.99(SA)/0.99(LA)	0.37(SA)/0	3.70(SA)/1.81(LA)	-0.12(SA)/0(LA)
ST	$k = 6.4 \cdot 10^{-17}$	1346.0	0.89(SA)/0.92(LA)	0.45(SA)/0.50(LA)	22.29(SA)/12.50(LA)	0(SA)/+0.19
ST	$k = 3.1 \cdot 10^{-17}$	1522.5	0.89(SA)/0.95(LA)	0.45(SA)/0.49(LA)	22.29(SA)/12.31(LA)	-
ST	$k = 6.4 \cdot 10^{-18}$	1522.5	0.85(SA)/0.90(LA)	0.45(SA)/0.49(LA)	22.29(SA)/12.30(LA)	0(SA)/-0.01(LA)

BIBLIOGRAPHY

[1] Abell, M. R. (1966). The nature and classification of ovarian neo-plasms. Can Med Assoc J, 94(21), 1102-1124.

[2] Ait-Oudhia S, Straubinger R, Mager D. Systems pharmacological analysis of paclitaxel-mediated tumor priming that enhances nanocarrier deposition and efficacy. J Pharmacol Exp Ther. 2013; 344:103–12.

[3] Akahoshi, K., & Oya, M. (2010). Gastrointestinal stromal tumor of the stomach: How to manage? World J Gastrointest Endosc, 2(8), 271-277.

[4] Almadrones, L., & Yerys, C. (1990). Problems associated with the administration of intraperitoneal therapy using the Port-A-Cath system. Oncol Nurs Forum, 17(1), 75-80.

[5] Al-Olama M, Wallgren A, Andersson B, Gatzinsky K, Hultborn R, et al. (2011) The peptide AF-16 decreases high interstitial fluid pressure in solid tumors. Acta Oncol 50: 1098–1104.

[6] Al-Quteimat, O. M., & Al-Badaineh, M. A. (2014). Intraperitoneal chemotherapy: rationale, applications, and limitations. J Oncol Pharm Pract, 20(5), 369-380.

[7] Ansaloni L, Coccolini F, Morosi L, Ballerini A, Ceresoli M, Grosso G, et al.. Pharmacokinetics of concomitant cisplatin and paclitaxel administered by hyperthermic intraperitoneal chemotherapy to patients with peritoneal carcinomatosis from epithelial ovarian cancer. British Journal of Cancer. 2015;112(2):306-312. doi:10.1038/bjc.2014.602.

[8] Arifin D, Yiu K, Lee T, Wang C. Chemotherapeutic drug trans-port to brain tumor. J Control Release. 2009; 137:203-10. doi:10.1016/j.jconrel.2009.04.013

[9] Ashvin, R., & Nikhilesh, J. (2016). Preoperative Preparation and Patient Selection for Cytoreductive Surgery and HIPEC. Indian Journal of Surgical Oncology, 7(2), 208-214

[10] Au J, Guo P, Gao Y, Lu Z, Wientjes M, Tsai M, Wientjes M. Multiscale Tumour Spatiokinetic Model for Intraperitoneal Therapy. The AAPS Journal 2014; 16(3):424–439. http://doi.org/10.1208/s12248-014-9574-y

[11] Bakrin, N., Gilly, F. N., Baratti, D., Bereder, J. M., Quenet, F., Lorimier, G., . . . Association Francaise de, C. (2013). Primary peritoneal serous carcinoma treated by cytoreductive surgery combined with hyperthermic intraperitoneal chemotherapy. A multi-institutional study of 36 patients. Eur J Surg Oncol, 39(7), 742-747.

[12] Ballester, M., Zisserman, A., Brady, M. (2002). Estimation of the partial volume effect in MRI. Medical image analysis, 6 4, 389-405

[13] Barakat R, Sabbatini P, Bhaskaran D, Revzin M, Smith A, Venkatraman E, Aghajanian C, Hensley M, Soignet S, Brown C, Soslow R, Markman M, Hoskins W, Spriggs D. Intraperitoneal chemotherapy for ovarian carcinoma: results of long-term follow-up. J Clin Oncol. 2002; 20(3):694-698. doi:-

[14] Barnes, S. L., Whisenant, J. G., Loveless, M. E., & Yankeelov, T. E. (2012). Practical dynamic contrast enhanced MRI in small animal models of cancer: data acquisition, data analysis, and interpretation. Pharmaceutics, 4(3), 442-78.

[15] Bartlett, D. J., Thacker, P. G., Jr., Grotz, T. E., Graham, R. P., Fletcher, J. G., VanBuren, W. M., . . . Sheedy, S. P. (2019). Mucinous appendiceal neoplasms: classification, imaging, and HIPEC. Abdom Radiol (NY), 44(5), 1686-1702.

[16] Baxter L, Jain R. Transport of fluid and macromolecules in tumors. I. Role of interstitial pressure and convection. Microvasc Research. 1989; 37:77-104. doi:10.1016/0026-2862(89)90074-5

[17] Baxter, L. T. , and Jain, R. K. , 1990, "Transport of Fluid and Macromolecules in Tumors II. Role of Heterogeneous Perfusion and Lymphatics," Microvasc. Res., 40(2), pp. 246–263.

[18] Bazine, A., Fetohi, M., Namad, T., Benzekri, A., Zainoun, B., Tanz, R., & Ichou, M. (2017). A Case of Well-Differentiated Papillary Mesothelioma of the Male Peritoneum: Successful Treatment by Systemic Chemotherapy. Cureus, 9(3), e1104.

[19] Bekkers, R. L., Willemsen, W. N., Schijf, C. P., Massuger, L. F., Bulten, J., & Merkus, J. M. (1999). Leiomyomatosis peritonealis disseminata: does malignant transformation occur? A literature review. Gynecol Oncol, 75(1), 158-163.

[20] Benabdejlil, Y., Kouach, J., Babahabib, A., Elhassani, M. E., Rharassi, I., Boudhas, A., . . . Dehayni, M. (2014). Intraperitoneal solitary fibrous tumor. Case Rep Obstet Gynecol, 2014, 906510.

[21] Bhandari A, Bansal A, Jain R, Singh A, Sinha N. Effect of Tumor Volume on Drug Delivery in Heterogeneous Vasculature of Human Brain Tumors. ASME. ASME J of Medical Diagnostics. 2019;2(2):021004-021004-10. doi:10.1115/1.4042195.

[22] Bhandari, A. , Bansal, A. , Singh, A. , and Sinha, N. , 2017, "Perfusion Kinetics in Human Brain Tumor With DCE-MRI Derived Model and CFD Analysis," J. Biomech., 59, pp. 80–89.

[23] Bird R, Stewart W, Lightfoot E. (2007). Transport Phenomena (Revised Second ed.). John Wiley & Sons. ISBN 978-0-470-11539-8

[24] Blackburn, S. C., & Stanton, M. P. (2014). Anatomy and physiology of the peritoneum. Semin Pediatr Surg, 23(6), 326-330.

[25] Blanco, A., Giger-Pabst, U., Solass, W., Zieren, J., & Reymond, M. A. (2013). Renal and hepatic toxicities after pressurized intraperitoneal aerosol chemotherapy (PIPAC). Ann Surg Oncol, 20(7), 2311-2316. doi:10.1245/s10434-012-2840-2

[26] Bonnot, P. E., Piessen, G., Pocard, M., Meunier, B., Bereder, J. M., Abboud, K., . . . Glehen, O. (2018). CYTO-CHIP: Cytoreductive surgery versus cytoreductive surgery and hyperthermic intraperitoneal chemotherapy for gastric cancer with peritoneal metastasis: A propensity-score analysis from BIG RENAPE and FREGAT working groups. Journal of Clinical Oncology, 36(4 suppl), 8-8. doi: 10.1200/JCO.2018.36.4 suppl.8

[27] Bouassida, M., Mighri, M. M., Becha, D., Hamzaoui, L., Sassi, S., Azzouz, M. M., . . . Sassi, S. (2012). Huge abdominal tumor: peritoneal solitary fibrous tumor. Gastrointest Cancer Res, 5(5), 179-180.

[28] Boucher, Y., Jain, R.K. Microvascular pressure is the principal driving force for interstitial hypertension in solid tumours: implications for vascular collapse. Cancer Research. 1992; 52(18):5110–5114.

[29] Boussios, S., Moschetta, M., Karathanasi, A., Tsiouris, A. K., Kanellos, F. S., Tatsi, K., ... Christodoulou, D. K. (2018). Malignant peritoneal mesothelioma: clinical aspects, and therapeutic perspectives. Ann Gastroenterol, 31(6), 659-669.

[30] Broeckx, G., & Pauwels, P. (2018). Malignant peritoneal mesothelioma: a review. Transl Lung Cancer Res, 7(5), 537-542.

[31] Bryan, M. L., Fitzgerald, N. C., Levine, E. A., Shen, P., Stewart, J. H., & Votanopoulos, K. I. (2014). Cytoreductive surgery with hyperthermic intraperitoneal chemotherapy in sarcomatosis from gastrointestinal stromal tumor. Am Surg, 80(9), 890-895.

[32] Burges A, Schmalfeldt B. Ovarian Cancer: Diagnosis and Treatment. Deutsches Ärzteblatt International. 2011;108(38):635-641. doi:10.3238/arztebl.2011.0635.

[33] Byrnes, K. G., Walsh, D., Dockery, P., McDermott, K., & Coffey, J. C. (2018). Anatomy of the mesentery: Current understanding and mechanisms of attachment. Semin Cell Dev Biol.

[34] Capobianco, A., Cottone, L., Monno, A., Manfredi, A. A., & Rovere-Querini, P. (2017). The peritoneum: healing, immunity, and diseases. J Pathol, 243(2), 137-147.

[35] Caponi, S., Vasile, E., Funel, N., De Lio, N., Campani, D., Ginocchi, L., ... Boggi, U. (2013). Adjuvant chemotherapy seems beneficial for invasive intraductal papillary mucinous neoplasms. Eur J Surg Oncol, 39(4), 396-403.

[36] Carlier, C., Mathys, A., De Jaeghere, E., Steuperaert, M., De Wever, O., & Ceelen, W. (2017). Tumour tissue transport after intraperitoneal anticancer drug delivery. International Journal of Hyperthermia, 33(5), 534-542.

[37] Carvalho, F. M., Carvalho, J. P., Pereira, R. M., Ceccato, B. P., Jr., Lacordia, R., & Baracat, E. C. (2012). Leiomyomatosis peritonealis disseminata associated with endometriosis and multiple uterus-like mass: report of two cases. Clin Med Insights Case Rep, 5, 63-68.

[38] Ceelen W, Flessner M. Intraperitoneal therapy for peritoneal tumors: biophysics and clinical evidence. Nat rev clin oncol. 2010; 7:108-15.

[39] Chato J. Thermal properties of tissues. In Skalak R, and Chien S (Eds.), Handbook of Bioengineering. McGraw-Hill, New York, pp. 9.1 – 9.13.(1987)

[40] Chaudhary, P. (2015). Acinar Cell Carcinoma of the Pancreas: A Literature Review and Update. Indian J Surg, 77(3), 226-231.

[41] Chauhan V, Lanning R, Diop-Frimpong B, Mok W, Brown E, Padera T et al. Multiscale Measurements Distinguish Cellular and Interstitial Hindrances to Diffusion In Vivo. Biophys J. 2009; 97:330-6.

[42] Cheong, Y. C., Laird, S. M., Li, T. C., Shelton, J. B., Ledger, W. L., & Cooke, I. D. (2001). Peritoneal healing and adhesion formation/reformation. Human Reproduction Update, 7(6), 556-566.

[43] Chiang, W., & Tynski, Z. (2018). Primary Peritoneal Angiosarcoma Metastatic to Liver and Bone without History of Radiation Therapy. Case Rep Pathol, 2018, 1257284.

[44] Cho, H., Ackerstaff, E., Carlin, S., Lupu, M. E., Wang, Y., Rizwan, A., O'Donoghue, J., Ling, C. C., Humm, J. L., Zanzonico, P. B., . . . Koutcher, J. A. (2009). Noninvasive multimodality imaging of the tumor microenvironment: registered dynamic magnetic resonance imaging and positron emission tomography studies of a preclinical tumor model of tumor hypoxia. Neoplasia (New York, N.Y.), 11(3), 247-59, 2p following 259

[45] Cho, K. R., & Shih Ie, M. (2009). Ovarian cancer. Annu Rev Pathol, 4, 287-313. doi:10.1146/annurev.pathol.4.110807.092246

[46] Cickovski T, Aras K, Alber M, Izaguirre J, Swat M, Glazier J, et al. From genes to organisms via the cell: a problem-solving environment for multicellular development. Comp in Science and Eng. 2007; 9:50–60.

[47] Coffey, J. C., & O'Leary, D. P. (2016). The mesentery: structure, function, and role in disease. Lancet Gastroenterol Hepatol, 1(3), 238-247.

[48] Colin P, De Smet L, Vervaet C, Remon JP, Ceelen W, Van Bocxlaer J, et al. A model based analysis of IPEC dosing of paclitaxel in rats. Pharmaceut Res. 2014; 31:2876–86.

[49] Colombo, N., Speyer, J. L., Green, M., Canetta, R., Beller, U., Wernz, J. C., . . . et al. (1989). Phase II study of carboplatin in recurrent ovarian cancer: severe hematologic toxicity in previously treated patients. Cancer Chemother Pharmacol, 23(5), 323-328.

[50] Cortez, A. J., Tudrej, P., Kujawa, K. A., & Lisowska, K. M. (2018). Advances in ovarian cancer therapy. Cancer Chemother Pharmacol, 81(1), 17-38.

[51] Cowan, R. A., O'Cearbhaill, R. E., Zivanovic, O., & Chi, D. S. (2017). Current status and future prospects of hyperthermic intraoperative intraperitoneal chemotherapy (HIPEC) clinical trials in ovarian cancer. Int J Hyperthermia, 33(5), 548-553.

[52] Crippa, S., Salvia, R., Warshaw, A. L., Dominguez, I., Bassi, C., Falconi, M., . . . Castillo, C. F. (2008). Mucinous cystic neoplasm of the pancreas is not an aggressive entity: lessons from 163 resected patients. Ann Surg, 247(4), 571-579.

[53] da Silva, R. G., & Sugarbaker, P. H. (2006). Analysis of prognostic factors in seventy patients having a complete cytoreduction plus perioperative intraperitoneal chemotherapy for carcinomatosis from colorectal cancer. J Am Coll Surg, 203(6), 878-886.

[54] Davies Cde, L., Lundstrom, L. M., Frengen, J., Eikenes, L., Bruland, S. O., Kaalhus, O., . . . Brekken, C. (2004). Radiation improves the distribution and uptake of liposomal doxorubicin (caelyx) in human osteosarcoma xenografts. Cancer Res, 64(2), 547-553.

[55] de Bree, E., & Helm, C. W. (2012). Hyperthermic intraperitoneal chemotherapy in ovarian cancer: rationale and clinical data. Expert Rev Anticancer Ther, 12(7), 895-911.

[56] de Bree, E., Michelakis, D., Stamatiou, D., Romanos, J., & Zoras, O. (2017). Pharmacological principles of intraperitoneal and bidirectional chemotherapy. Pleura Peritoneum, 2(2), 47-62.

[57] de Lima Vazquez, V., Stuart, O. A., Mohamed, F., & Sugarbaker, P. H. (2003). Extent of parietal peritonectomy does not change intraperitoneal chemotherapy pharmacokinetics. Cancer Chemother Pharmacol, 52(2), 108-112.

[58] de Mestier, L., Volet, J., Scaglia, E., Msika, S., Kianmanesh, R., & Bouche, O. (2012). Is palliative laparoscopic hyperthermic intraperitoneal chemotherapy effective in patients with malignant hemorrhagic ascites? Case Rep Gastroenterol, 6(1), 166-170.

[59] De Smet, L., Ceelen, W., Remon, J. P., & Vervaet, C. (2013). Optimization of drug delivery systems for intraperitoneal therapy to extend the residence time of the chemotherapeutic agent. ScientificWorldJournal, 2013, 720858.

[60] De Vlieghere E, Carlier C, Ceelen W, Bracke M, De Wever O. Data on in vivo selection of SK-OV-3 Luc ovarian cancer cells and intraperitoneal tumor formation with low inoculation numbers. Data Brief. 2016; 6:542-9. doi: 10.1016/j.dib.2015.12.037.

[61] De Vlieghere E. "Dissemination and adhesion of peritoneal cancer cells to the peritoneal wal". Intraperitoneal Cancer Therapy: Principles and Practice 1st edition Ceelen W, Levine E. CRC press

[62] Dedrick, R. L. (1985). Theoretical and Experimental Bases of Intraperitoneal Chemotherapy. Seminars in Oncology, 12(3), 1-6.

[63] Dedrick, R. L., & Flessner, M. F. (1997). Pharmacokinetic problems in peritoneal drug administration: tissue penetration and surface exposure. J Natl Cancer Inst, 89(7), 480-487.

[64] Dedrick, R. L., Myers, C. E., Bungay, P. M., & DeVita, V. T., Jr. (1978). Pharmacokinetic rationale for peritoneal drug administration in the treatment of ovarian cancer. Cancer Treat Rep, 62(1), 1-11.

[65] Deisboeck T, Wang Z, Macklin P, Cristini V. Multiscale Cancer Modeling. Annu Rev Biomed Eng.. 2011; 13:10.1146/annurev-bioeng-071910-124729. doi:10.1146/annurev-bioeng-071910-124729.

[66] Detroz, B., Laurent, S., Honore, P., Blaffart, F., Limet, R., & Meurisse, M. (2004). Rationale for hyperthermic intraperitoneal chemotherapy (HIPEC) in the treatment or prevention of peritoneal carcinomatosis. Acta Chir Belg, 104(4), 377-383.

[67] Dicken, B. J., Bigam, D. L., Cass, C., Mackey, J. R., Joy, A. A., & Hamilton, S. M. (2005). Gastric adenocarcinoma: review and considerations for future directions. Ann Surg, 241(1), 27-39.

[68] Dogan, A., Solass, W., & Tempfer, C. B. (2016). Cytoreductive surgery followed by hyperthermic intraperitoneal chemotherapy for recurrent adult granulosa cell tumor: A case report. Gynecol Oncol Rep, 16, 21-23.

[69] Doubeni, C. A., Doubeni, A. R., & Myers, A. E. (2016). Diagnosis and Management of Ovarian Cancer. Am Fam Physician, 93(11), 937-944.

[70] Dudar, T. E., & Jain, R. K. (1984). Differential response of normal and tumor microcirculation to hyperthermia. Cancer Res, 44(2), 605-612.

[71] Ehehalt F, Saeger H, Schmidt C, Grützmann R. Neuroendocrine tumors of the pancreas. Oncologist. 2009 May;14(5):456-67. doi: 10.1634/theoncologist.2008-0259. Epub 2009 May 1.

[72] Eichholtz-Wirth H, Hietel B . Heat sensitization to cisplatin in two cell lines with different drug sensitivities. Int J Hyperthem 1990,47–55.

[73] Einstein, A. "Über die von der molekularkinetischen Theorie der Wärme geforderte Bewegung von in ruhenden Flüssigkeiten suspendierten Teilchen". Annalen der Physik. 1905; 322:549–60.

[74] Elias, D., Gilly, F., Boutitie, F., Quenet, F., Bereder, J. M., Mansvelt, B., ... Glehen, O. (2010). Peritoneal colorectal carcinomatosis treated with surgery and perioperative intraperitoneal chemotherapy: retrospective analysis of 523 patients from a multicentric French study. J Clin Oncol, 28(1), 63-68.

[75] El-Kareh A, Secomb T. A Theoretical Model for Intraperitoneal Delivery of Cisplatin and the Effect of Hyperthermia on Drug Penetration Distance. Neoplasia. 2004; 6(2):117-127. doi:-

[76] El-Kareh, A.W., Secomb, T.W. A Mathematical Model for Cisplatin Cellular Pharmacodynamics. Neoplasia. 2003; 5:161-9.

[77] Elsayes, K. M., Staveteig, P. T., Narra, V. R., Leyendecker, J. R., Lewis, J. S., & Brown, J. J. (2006). MRI of the Peritoneum: Spectrum of Abnormalities. American Journal of Roentgenology, 186(5), 1368-1379. doi: 10.2214/AJR.04.1522

[78] Erlichman C, Vidgen D, Wu A. Antineoplastic drug cytotoxicity in a human bladder cancer cell line: implications for intravesical chemotherapy. Urol Res. 1987; 15:13–6

[79] Esquis, P., Consolo, D., Magnin, G., Pointaire, P., Moretto, P., Ynsa, M. D., ... Chauffert, B. (2006). High intra-abdominal pressure enhances the penetration and antitumor effect of intraperitoneal cisplatin on experimental peritoneal carcinomatosis. Ann Surg, 244(1), 106-112. doi:10.1097/01.sla.0000218089.61635.5f

[80] Facchiano, E., Risio, D., Kianmanesh, R., & Msika, S. (2012). Laparoscopic Hyperthermic Intraperitoneal Chemotherapy: Indications, Aims, and Results: A Systematic Review of the Literature. Annals of Surgical Oncology, 19(9), 2946-2950.

[81] Facy, O., Al Samman, S., Magnin, G., Ghiringhelli, F., Ladoire, S., Chauffert, B., ... Ortega-Deballon, P. (2012). High pressure enhances the effect of hyperthermia in intraperitoneal chemotherapy with oxaliplatin: an experimental study. Ann Surg, 256(6), 1084-1088.

[82] Facy, O., Radais, F., Ladoire, S., Delroeux, D., Tixier, H., Ghiringhelli, F., . . . Ortega-Deballon, P. (2011). Comparison of hyperthermia and adrenaline to enhance the intratumoral accumulation of cisplatin in a murine model of peritoneal carcinomatosis. J Exp Clin Cancer Res, 30, 4. doi:10.1186/1756-9966-30-4

[83] Fagotti, A., Gallotta, V., Romano, F., Fanfani, F., Rossitto, C., Naldini, A., . . . Scambia, G. (2010). Peritoneal carcinosis of ovarian origin. World J Gastrointest Oncol, 2(2), 102-108

[84] Favoriti P, Carbone G, Greco M, Pirozzi F, Pirozzi RE, Corcione F. Worldwide burden of colorectal cancer: a review. Updates Surg. 2016; 68(1):7-11. doi: 10.1007/s13304-016-0359-y.

[85] Feldman, A. L., Libutti, S. K., Pingpank, J. F., Bartlett, D. L., Beresnev, T. H., Mavroukakis, S. M., . . . Alexander, H. R. (2003). Analysis of factors associated with outcome in patients with malignant peritoneal mesothelioma undergoing surgical debulking and intraperitoneal chemotherapy. J Clin Oncol, 21(24), 4560-4567.

[86] Ferretti S, Allegrini P, Becquet M, McSheehy P. Tumour Interstitial Fluid Pressure as an Early-Response Marker for Anticancer Therapeutics. Neoplasia. 2009; 11(9): 874–881. doi:

[87] Flessner M, Dedrick R, Schultz J. A distributed model of peritoneal-plasma transport: analysis of experimental data in the rat. Am J Physiol. 1985; 248:413–24

[88] Flessner, M. F. (2005). The transport barrier in intraperitoneal therapy. Am J Physiol Renal Physiol, 288(3), F433-442.

[89] Flessner, M. F. (2016). Pharmacokinetic problems in peritoneal drug administration: an update after 20 years. Pleura and Peritoneum, 1(4), 183-191.

[90] Flessner, M. F., Dedrick, R. L., & Schultz, J. S. (1984). A Distributed Model of Peritoneal-Plasma Transport - Theoretical Considerations. American Journal of Physiology, 246(4), R597-R607.

[91] Flessner, M., Henegar, J., Bigler, S., & Genous, L. (2003). Is the peritoneum a significant transport barrier in peritoneal dialysis? Perit Dial Int, 23(6), 542-549.

[92] Foster, J. M., Sleightholm, R., Patel, A., Shostrom, V., Hall, B., Neilsen, B., . . . Smith, L. (2019). Morbidity and Mortality Rates Following Cytoreductive Surgery Combined With Hyperthermic Intraperitoneal Chemotherapy Compared With Other High-Risk Surgical Oncology Procedures. JAMA Netw Open, 2(1), e186847.

[93] Fujii, S., Matsusue, E., Kanasaki, Y. et al. Detection of peritoneal dissemination in gynecological malignancy: evaluation by diffusion-weighted MR imaging. Eur Radiol (2008) 18: 18. https://doi.org/10.1007/s00330-007-0732-9

[94] Fujimoto, S., Shrestha, R. D., Kokubun, M., Ohta, M., Takahashi, M., Kobayashi, K., . . . et al. (1988). Intraperitoneal hyperthermic perfusion combined with surgery effective for gastric cancer patients with peritoneal seeding. Ann Surg, 208(1), 36-41.

[95] Fukumura D, Jain. RK. Tumour microvasculature and microenvironment: Targets for anti-angiogenesis and normalization. Microvascular research. 2007; 74(2-3):72-84. doi:10.1016/j.mvr.2007.05.003.

[96] Gardner S. A mechanistic, predictive model of dose-response curves for cell cycle phase-specific and-nonspecific drugs. Cancer Res. 2000; 60:1417–25

[97] Geretti, E., Leonard, S. C., Dumont, N., Lee, H., Zheng, J., De Souza, R., ... Hendriks, B. S. (2015). Cyclophosphamide-Mediated Tumor Priming for Enhanced Delivery and Antitumor Activity of HER2-Targeted Liposomal Doxorubicin (MM-302). Mol Cancer Ther, 14(9), 2060-2071. doi:10.1158/1535-7163.MCT-15-031

[98] Gilks, C. B., & Prat, J. (2009). Ovarian carcinoma pathology and genetics: recent advances. Hum Pathol, 40(9), 1213-1223.

[99] Gilly, F. N., Cotte, E., Brigand, C., Monneuse, O., Beaujard, A. C., Freyer, G., & Glehen, O. (2006). Quantitative prognostic indices in peritoneal carcinomatosis. Eur J Surg Oncol, 32(6), 597-601.

[100] Glehen, O., Kwiatkowski, F., Sugarbaker, P. H., Elias, D., Levine, E. A., De Simone, M., . . . Rat, P. (2004). Cytoreductive surgery combined with perioperative intraperitoneal chemotherapy for the management of peritoneal carcinomatosis from colorectal cancer: a multi-institutional study. J Clin Oncol, 22(16), 3284-3292.

[101] Go, H. S., Hong, H. S., Kim, J. W., & Woo, J. Y. (2012). CT appearance of primary peritoneal serous borderline tumour: a rare epithelial tumour of the peritoneum. Br J Radiol, 85(1009), e22-25.

[102] Goere, D., Souadka, A., Faron, M., Cloutier, A. S., Viana, B., Honore, C., . . . Elias, D. (2015). Extent of colorectal peritoneal carcinomatosis: attempt to define a threshold above which HIPEC does not offer survival benefit: a comparative study. Ann Surg Oncol, 22(9), 2958-2964.

[103] Goetze, O. T., Al-Batran, S. E., Chevallay, M., & Monig, S. P. (2018). Multimodal treatment in locally advanced gastric cancer. Updates Surg, 70(2), 173-179.

[104] Goh Y;Kong H, Wang CH. Simulation of the delivery of doxorubicin to hepatoma. Pharm Res. 2001; 18(6):761-770. Doi.-

[105] Gonzalez-Bayon, L., Gonzalez-Moreno, S., & Ortega-Perez, G. (2006). Safety considerations for operating room personnel during hyperthermic intraoperative intraperitoneal chemotherapy perfusion. Eur J Surg Oncol, 32(6), 619-624. doi:10.1016/j.ejso.2006.03.019

[106] Gonzalez-Moreno, S., Gonzalez-Bayon, L. A., & Ortega-Perez, G. (2010). Hyperthermic intraperitoneal chemotherapy: Rationale and technique. World J Gastrointest Oncol, 2(2), 68-75.

[107] González-Moreno, S., González-Bayón, L., Ortega-Pérez, G., & González-Hernando, C. (2009). Imaging of Peritoneal Carcinomatosis. The Cancer Journal, 15(3), 184-189. doi: 10.1097/PPO.0b013e3181a58ec3

[108] Gonzalez-Moreno, S., Ortega-Perez, G., Alonso-Casado, O., Galipienzo-Garcia, J., Linero-Noguera, M. J., & Salvatierra-Diaz, D. (2018). Techniques and Safety Issues for Intraperitoneal Chemotherapy. Surg Oncol Clin N Am, 27(3), 495-506. doi:10.1016/j.soc.2018.02.005

[109] Goodman, M. D., McPartland, S., Detelich, D., & Saif, M. W. (2016). Chemotherapy for intraperitoneal use: a review of hyperthermic intraperitoneal chemotherapy and early post-operative intraperitoneal chemotherapy. Journal of gastrointestinal oncology, 7(1), 45-57.

[110] Gore, R. M., Berlin, J. W., Mehta, U. K., Newmark, G. M., & Yaghmai, V. (2005). GI carcinoid tumours: appearance of the primary and detecting metastases. Best Pract Res Clin Endocrinol Metab, 19(2), 245-263.

[111] Gremonprez F, Descamps B, Izmer A, Vanhove C, Vanhaecke F, De Wever O, Ceelen W. Pretreatment with VEGF(R)-inhibitors reduces interstitial fluid pressure, increases intraperitoneal chemotherapy drug penetration, and impedes tumor growth in a mouse colorectal carcinomatosis model. Oncotarget. 2015; 6(30):29889-900. doi: 10.18632/oncotarget.5092

[112] Griniatsos J, Michail O. Appendiceal neuroendocrine tumors: Recent insights and clinical implications. World J Gastrointest Oncol. 2010;2(4):192–196. doi:10.4251/wjgo.v2.i4.192

[113] Hanbidge, A. E., Lynch, D., & Wilson, S. R. (2003). US of the Peritoneum. RadioGraphics, 23(3), 663-685. doi:10.1148/rg.233025712

[114] Haroon, S., Zia, A., Idrees, R., Memon, A., Fatima, S., & Kayani, N. (2013). Clinicopathological spectrum of ovarian sex cord-stromal tumors; 20 years' retrospective study in a developing country. J Ovarian Res, 6(1), 87.

[115] Hasovits C, Clarke S. Pharmacokinetics and pharmacodynamics of intraperitoneal cancer chemotherapeutics. Clin pharmacokinet. 2012; 51:203-24.

[116] Hauck, M. L., Coffin, D. O., Dodge, R. K., Dewhirst, M. W., Mitchell, J. B., & Zalutsky, M. R. (1997). A local hyperthermia treatment which enhances antibody uptake in a glioma xenograft model does not affect tumour interstitial fluid pressure. Int J Hyperthermia, 13(3), 307-316.

[117] Hayes, S. J., Clark, P., Mathias, R., Formela, L., Vickers, J., & Armstrong, G. R. (2007). Multiple adenomatoid tumours in the liver and peritoneum. J Clin Pathol, 60(6), 722-724.

[118] Hayes-Jordan, A., Green, H. L., Lin, H., Owusu-Agyemang, P., Fitzgerald, N., Arunkumar, R., ... Anderson, P. (2014). Complete cytoreduction and HIPEC improves survival in desmoplastic small round cell tumor. Ann Surg Oncol, 21(1), 220-224.

[119] Healy JC. Detection of peritoneal metastases. Cancer Imaging. 2015;1(2):4–12. Published 2015 May 5. doi:10.1102/1470-7330.2001.002

[120] Healy, J. & Reznek, R. The peritoneum, mesenteries and omenta: normal anatomy and pathological processes. Eur Radiol (1998) 8: 886. https://doi.org/10.1007/s003300050485

[121] Heldin C, Rubin K, Pietras K, Ostman A. High interstitial fluid pressure - an obstacle in cancer therapy. Nat Rev Cancer. 2004; 4(10):806-13. doi:10.1038/nrc1456

[122] Helm, J. H., Miura, J. T., Glenn, J. A., Marcus, R. K., Larrieux, G., Jayakrishnan, T. T., . . . Johnston, F. M. (2015). Cytoreductive surgery and hyperthermic intraperitoneal chemotherapy for malignant peritoneal mesothelioma: a systematic review and meta-analysis. Ann Surg Oncol, 22(5), 1686-1693.

[123] Helmlinger, G., Netti, P.A., Lichtenbeld, H.C., Melder, R.J., Jain, R.K. Solid stress inhibits the growth of multicellular tumour spheroids. Nature Biotechnology. 1997; 15(8):778–783. 9.

[124] Hettinga J, Konings A, and Kampinga H. Reduction of cellular cisplatin resistance by hyperthermia—a review. Int J Hypertherm. 1997; 13:439–57.

[125] Hewitt, M. , Anderson, K. , Hall, G. , Weston, M. , Hutson, R. , Wilkinson, N. , Perren, T. , Lane, G. and Spencer, J. (2007), Women with peritoneal carcinomatosis of unknown origin: efficacy of image-guided biopsy to determine site-specific diagnosis. BJOG: An International Journal of Obstetrics & Gynaecology, 114: 46-50. doi:10.1111/j.1471-0528.2006.01176.x

[126] Hildebrandt, B., Wust, P., Ahlers, O., Dieing, A., Sreenivasa, G., Kerner, T., . . . Riess, H. (2002). The cellular and molecular basis of hyperthermia. Crit Rev Oncol Hematol, 43(1), 33-56..

[127] Hoekstra, A. V., Riben, M. W., Frumovitz, M., Liu, J., & Ramirez, P. T. (2005). Well-differentiated papillary mesothelioma of the peritoneum: a pathological analysis and review of the literature. Gynecol Oncol, 98(1), 161-167.

[128] Honore, C., Atallah, V., Mir, O., Orbach, D., Ferron, G., LePechoux, C., . . . Network, F. S. C. (2017). Abdominal desmoplastic small round cell tumor without extraperitoneal metastases: Is there a benefit for HIPEC after macroscopically complete cytoreductive surgery? PLoS One, 12(2).

[129] Honore, C., Gelli, M., Francoual, J., Benhaim, L., Elias, D., & Goere, D. (2017). Ninety percent of the adverse outcomes occur in 10% of patients: can we identify the populations at high risk of developing peritoneal metastases after curative surgery for colorectal cancer? Int J Hyperthermia, 33(5), 505-510.

[130] Horta, M., & Cunha, T. M. (2015). Sex cord-stromal tumors of the ovary: a comprehensive review and update for radiologists. Diagn Interv Radiol, 21(4), 277-286.

[131] Howell, S. B., Zimm, S., Markman, M., Abramson, I. S., Cleary, S., Lucas, W. E., & Weiss, R. J. (1987). Long-term survival of advanced refractory ovarian carcinoma patients with small-volume disease treated with intraperitoneal chemotherapy. J Clin Oncol, 5(10), 1607-1612.

[132] http://www.ajnr.org/content/ajnr/suppl/2014/05/22/ajnr.A3917.DC1/3917 tables.pdf (accessed on 28/11/2018)

[133] Huh, J., Byun, J. H., Hong, S. M., Kim, K. W., Kim, J. H., Lee, S. S., . . . Lee, M. G. (2016). Malignant pancreatic serous cystic neoplasms: systematic review with a new case. BMC Gastroenterol, 16(1), 97.

[134] Hutton, R. L., & Dalton, S. R. (2007). Primary peritoneal serous borderline tumors. Arch Pathol Lab Med, 131(1), 138-144.

[135] Hylander, B. L., Sen, A., Beachy, S. H., Pitoniak, R., Ullas, S., Gibbs, J. F., . . . Repasky, E. A. (2015). Tumor priming by Apo2L/TRAIL reduces interstitial fluid pressure and enhances efficacy of liposomal gemcitabine in a patient derived xenograft tumor model. J Control Release, 217, 160-169. doi:10.1016/j.jconrel.2015.08.047

[136] Isaza-Restrepo, A., Martin-Saavedra, J. S., Velez-Leal, J. L., Vargas-Barato, F., & Riveros-Duenas, R. (2018). The Peritoneum: Beyond the Tissue - A Review. Frontiers in Physiology, 9.

[137] Jacquet, P., Stuart, O. A., Chang, D., & Sugarbaker, P. H. (1996). Effects of intra-abdominal pressure on pharmacokinetics and tissue distribution of doxorubicin after intraperitoneal administration. Anticancer Drugs, 7(5), 596-603.

[138] Jain R, Cook A , Steele E. Haemodynamic and transport barriers to the treatment of solid tumors. Int J Radiat Biol. 1991; 60(1-2):85-100. Doi:10.1080/09553009114551621

[139] Jain RK (2005) Normalization of tumor vasculature: an emerging concept in antiangiogenic therapy. Science 307: 58–62.

[140] Jang S, Wientjes M, Au J. S.Enhancement of paclitaxel delivery to solid tumors by apoptosis-inducing pretreatment: Effect of treatment schedule. J Pharmacol Exp Ther. 2001; 296:1035–42.

[141] Jerzak, K. J., & MacKay, H. J. (2016). Ovarian Sex Cord-Stromal Tumors: The Challenge of Rare Gynecologic Malignancies. J Oncol Pract, 12(10), 947-948.

[142] Ji, Z. H., Peng, K. W., & Li, Y. (2016). Intraperitoneal free cancer cells in gastric cancer: pathology of peritoneal carcinomatosis and rationale for intraperitoneal chemotherapy/hyperthermic intraperitoneal chemotherapy in gastric cancer. Transl Gastroenterol Hepatol, 1, 69.

[143] Ji, Z. H., Peng, K. W., Yu, Y., Li, X. B., Yonemura, Y., Liu, Y., ... Li, Y. (2017). Current status and future prospects of clinical trials on CRS + HIPEC for gastric cancer peritoneal metastases. Int J Hyperthermia, 33(5), 562-570.

[144] Juarez-Salcedo, L. M., Sokol, L., Chavez, J. C., & Dalia, S. (2018). Primary Gastric Lymphoma, Epidemiology, Clinical Diagnosis, and Treatment. Cancer Control, 25(1), 1073274818778256.

[145] Kalyanasundaram S, Calhoun V, Leong K. A finite element model for predicting the distribution of drugs delivered intracranially to the brain. Am J Physiol. 1997; 273(5 Pt 2):R1810-1821. doi –

[146] Kampan N, Madondo M, McNally O, Quinn M, Plebanski M. Paclitaxel and Its Evolving Role in the Management of Ovarian Cancer. BioMed Research. 2015; Article ID 413076, http://dx.doi.org/10.1155/2015/413076

[147] Kastelein, A. W., Vos, L. M. C., de Jong, K. H., van Baal, J., Nieuwland, R., van Noorden, C. J. F., ... Lok, C. A. R. (2018). Embryology, anatomy, physiology and pathophysiology of the peritoneum and the peritoneal vasculature. Semin Cell Dev Biol.

[148] Katz, M. H., & Barone, R. M. (2003). The rationale of perioperative intraperitoneal chemotherapy in the treatment of peritoneal surface malignancies. Surg Oncol Clin N Am, 12(3), 673-688.

[149] Kelly, K. J. (2015). Management of Appendix Cancer. Clin Colon Rectal Surg, 28(4), 247-255.

[150] Khosrawipour, V., Bellendorf, A., Khosrawipour, C., Hedayat-Pour, Y., Diaz-Carballo, D., Forster, E., ... Fakhrian, K. (2016). Irradiation Does Not Increase the Penetration Depth of Doxorubicin in Normal Tissue After Pressurized Intra-peritoneal Aerosol Chemotherapy (PIPAC) in an Ex Vivo Model. In Vivo, 30(5), 593-597.

[151] Khurram, M. S., Shaikh, H., Khan, U., Edens, J., Ibrar, W., Hamza, A., ... Hadid, T. (2017). Benign Multicystic Peritoneal Mesothelioma: A Rare Condition in an Uncommon Gender. Case Rep Pathol, 2017, 9752908.

[152] Kim E, Stamatelos S, Cebulla J, Bhujwalla Z, Popel A, Pathak A. Multiscale imaging and computational modeling of blood flow in the tumor vasculature. Ann Biomed Eng. 2012; 40:2425–41

[153] Kim M, Gillies R, Rejniak K. Current Advances in Mathematical Modelling of Anti-Cancer Drug Penetration into Tumour Tissues. Frontiers in Oncology. 2013;3:278. doi:10.3389/fonc.2013.00278.

[154] Kishi, K., Homma, S., Tanimura, S., Matsushita, H., & Nakata, K. (2001). Hypoglycemia induced by secretion of high molecular weight insulin-like growth factor-II from a malignant solitary fibrous tumor of the pleura. Intern Med, 40(4), 341-344.

[155] Klosowska-Wardega A, Hasumi Y, Burmakin M, Ahgren A, Stuhr L, et al. (2009) Combined anti-angiogenic therapy targeting PDGF and VEGF receptors lowers the interstitial fluid pressure in a murine experimental carcinoma. PLoS One 4: e8149.

[156] Kondo A, Maeta M, Oka A, Tsujitani S, Ikeguchi M, Kaibara N. Hypotonic intraperitoneal

[157] Kondo, A., Maeta, M., Oka, A., Tsujitani, S., Ikeguchi, M., & Kaibara, N. (1996). Hypotonic intraperitoneal cisplatin chemotherapy for peritoneal carcinomatosis in mice. British Journal of Cancer, 73(10), 1166-1170. doi:DOI 10.1038/bjc.1996.225

[158] Krishnamurthy S, Balasubramaniam R. Role of Imaging in Peritoneal Surface Malignancies. Indian J Surg Oncol. 2016;7(4):441–452. doi:10.1007/s13193-016-0539-8

[159] Kruger-Thiemer E, Eriksen S. Mathematical Model of Sustained-Release Preparations and Its Analysis. J Pharm Sci. 1966; 55:1249–53

[160] Kuipers, E. J., Grady, W. M., Lieberman, D., Seufferlein, T., Sung, J. J., Boelens, P. G., ... Watanabe, T. (2015). Colorectal cancer. Nat Rev Dis Primers, 1, 15065.

[161] Kurihara N, Kubota T, Hoshiya Y, Otani Y, Kumai K, Kitajima M. Antitumor activity of cis-diaminedichloroplatinum (II) depends on its time x concentration product against human gastric cancer cell lines in vitro. J Surg Oncol. 1995; 60:238–41

[162] Kusamura, S., Dominique, E., Baratti, D., Younan, R., & Deraco, M. (2008). Drugs, carrier solutions and temperature in hyperthermic intraperitoneal chemotherapy. J Surg Oncol, 98(4), 247-252. doi:10.1002/jso.21051

[163] Kusumoto T, Maehara Y, Baba H, Takahashi I, Kusumoto H, Ohno S,Sugimachi K. Sequence dependence of the hyperthermic potentiation of carboplatin-induced cytotoxicity and intracellular platinum accumulation in HeLa cells. Br J Cancer 1993; 68, 259–63

[164] Kwakman, R., Schrama, A. M., van Olmen, J. P., Otten, R. H., de Lange-de Klerk, E. S., de Cuba, E. M., Te Velde, E. A. (2016). Clinicopathological Parameters in Patient Selection for Cytoreductive Surgery and Hyperthermic Intraperitoneal Chemotherapy for Colorectal Cancer Metastases: A Meta-analysis. Ann Surg, 263(6), 1102-1111.

[165] Kyriazi, S., Kaye, S. B., & deSouza, N. M. (2010). Imaging ovarian cancer and peritoneal metastases—current and emerging techniques. Nature Reviews Clinical Oncology, 7, 381. doi: 10.1038/nrclinonc.2010.47

[166] Lagast, N., Carlier, C., & Ceelen, W. P. (2018). Pharmacokinetics and Tissue Transport of Intraperitoneal Chemotherapy. Surg Oncol Clin N Am, 27(3), 477-494.

[167] Lambert, L. A., & Harris, A. (2016). Palliative cytoreductive surgery and hyperthermic intraperitoneal chemoperfusion: current clinical practice or misnomer? J Gastrointest Oncol, 7(1), 112-121.

[168] Lee, J., Curtin, J. P., Muggia, F. M., Pothuri, B., Boyd, L. R., & Blank, S. V. (2018). Timing is everything: intraperitoneal chemotherapy after primary or interval debulking surgery for advanced ovarian cancer. Cancer Chemother Pharmacol, 82(1), 55-63.

[169] Lee, Y. K., Jun, H. J., Nahm, J. H., Lim, T. S., Park, J. S., Ahn, J. B., ... Kim, H. S. (2013). Therapeutic strategies for well-differentiated papillary mesothelioma of the peritoneum. Jpn J Clin Oncol, 43(10), 996-1003.

[170] Leunig, M., Goetz, A. E., Gamarra, F., Zetterer, G., Messmer, K., & Jain, R. K. (1994). Photodynamic therapy-induced alterations in interstitial fluid pressure, volume and water content of an amelanotic melanoma in the hamster. Br J Cancer, 69(1), 101-103.

[171] Levasseur L, Slocum H, Rustum Y, Greco W. Modeling of the time-dependency of in vitro drug cytotoxicity and resistance. Cancer Res. 1998; 58:5749–61

[172] Li, T., Wang, Y. N., Khokhlova, T. D., D'Andrea, S., Starr, F., Chen, H., . . . Hwang, J. H. (2015). Pulsed High-Intensity Focused Ultrasound Enhances Delivery of Doxorubicin in a Preclinical Model of Pancreatic Cancer. Cancer Res, 75(18), 3738-3746. doi:10.1158/0008-5472.CAN-15-0296

[173] Lin, H. H., Lin, J. K., Jiang, J. K., Lin, C. C., Lan, Y. T., Yang, S. H., . . . Chang, S. C. (2014). Clinicopathological analysis of colorectal carcinoid tumors and patient outcomes. World J Surg Oncol, 12, 366.

[174] Linninger A, Somayaji M, Mekarski M, Zhang L Prediction of convection-enhanced drug delivery to the human brain. J Theor Biol 2008; 250(1):125-38. doi:10.1016/j.jtbi.2007.09.009

[175] Lins, C. M., Elias, J., Jr., Cunha, A. F., Muglia, V. F., Monteiro, C. R., Valeri, F. V., & Feres, O. (2009). MR imaging features of peritoneal adenomatoid mesothelioma: a case report. Clinics (Sao Paulo), 64(3), 264-269.

[176] Litvan, J., Aghazarian, M., Wiley, E., Guleria, S., & Dudek, A. Z. (2014). Primary peritoneal angiosarcoma: a case report. Anticancer Res, 34(9), 5001-5006.

[177] Lochhead P, El-Omar E, Gastric Tumors: an overview, Atlas Genet Cytogenet Oncol Haematol. 2009;13(10):761-767.

[178] Los G, Mutsaers P, Lenglet WJ, Baldew G, McVie J. Platinum distribution in intraperitoneal tumors after intraperitoneal cisplatin treatment. Cancer Chemother Pharmacol. 1990; 25(6):389-94. 10.1007/BF00686048

[179] Los, G., Sminia, P., Wondergem, J., Mutsaers, P. H., Havemen, J., ten Bokkel Huinink, D., ... McVie, J. G. (1991). Optimisation of intraperitoneal cisplatin therapy with regional hyperthermia in rats. Eur J Cancer, 27(4), 472-477.

[180] Los, G., Verdegaal, E. M., Mutsaers, P. H., & McVie, J. G. (1991). Penetration of carboplatin and cisplatin into rat peritoneal tumor nodules after intraperitoneal chemotherapy. Cancer Chemother Pharmacol, 28(3), 159-165.

[181] Lu Z, Tsai M, Lu D, Wang J, Wientjes M, Au J. Tumor-penetrating microparticles for intraperitoneal therapy of ovarian cancer. J Pharmacol Exp Ther. 2008; 327:673-82

[182] Ma J, Verweij J, Kolker HJ, van Ingen HE, Stoter G, Schellens JH. Pharmacokinetic-dynamic relationship of cisplatin in vitro: simulation of an i.v. bolus and 3 h and 20 h infusion. Br J Cancer. 1994; 69:858–62

[183] Machado, N. O., Al Qadhi, H., & Al Wahibi, K. (2015). Intraductal Papillary Mucinous Neoplasm of Pancreas. N Am J Med Sci, 7(5), 160-175.

[184] Maciver, A. H., Lee, N., Skitzki, J. J., Boland, P. M., & Francescutti, V. (2017). Cytoreduction and hyperthermic intraperitoneal chemotherapy (CS/HIPEC) in colorectal cancer: Evidence-based review of patient selection and treatment algorithms. Eur J Surg Oncol, 43(6), 1028-1039.

[185] Magdoom, K. , Pishko, G., Kim, J. , and Sarntinoranont, M. , 2012, "Evaluation of a Voxelized Model Based on DCE-MRI for Tracer Transport in Tumor," ASME J. Biomech. Eng., 134(9), p. 091004.

[186] Makhija, S., Leitao, M., Sabbatini, P., Bellin, N., Almadrones, L., Leon, L., . . . Barakat, R. (2001). Complications associated with intraperitoneal chemotherapy catheters. Gynecol Oncol, 81(1), 77-81.

[187] Markman, M. (2003). Intraperitoneal antineoplastic drug delivery: rationale and results. Lancet Oncol, 4(5), 277-283.

[188] McConnell Y, Mack L, Gui X, et al. Cytoreductive Surgery with Hyperthermic Intraperitoneal Chemotherapy: An Emerging Treatment Option for Advanced Goblet Cell Tumors of the Appendix. Ann Surg Oncol (2014) 21: 1975. https://doi.org/10.1245/s10434-013-3469-5

[189] McDermott, F. D., Heeney, A., Courtney, D., Mohan, H., & Winter, D. (2014). Rectal carcinoids: a systematic review. Surg Endosc, 28(7), 2020-2026.

[190] McLaughlin P, Filippone A and Maher M. Neoplastic Diseases of the Peritoneum and Mesentery. American Journal of Roentgenology. 2013;200: W420-W430. 10.2214/AJR.12.8494

[191] McMullen JRW, Selleck M, Wall NR, Senthil M. Peritoneal carcinomatosis: limits of diagnosis and the case for liquid biopsy. Oncotarget. ;8(26):43481–43490. doi:10.18632/oncotarget.16480

[192] Minchinton A, Tannock I. Drug penetration in solid tumors. Nat Rev Cancer. 2006; 6:583–92

[193] Mittal, R., Chandramohan, A., & Moran, B. (2017). Pseudomyxoma peritonei: natural history and treatment. Int J Hyperthermia, 33(5), 511-519.

[194] Miyagi Y, Fujiwara K, Kigawa J, Itamochi H, Nagao S, Aotani E, et al. Intraperitoneal carboplatin infusion may be a pharmacologically more reasonable route than intravenous administration as a systemic chemotherapy. A comparative pharmacokinetic analysis of platinum using a new mathematical model after intraperitoneal vs. intravenous infusion of carboplatin–a Sankai Gynecology Study Group (SGSG) study. Gynecol Oncol. 2005; 99(3):591-6. 10.doi:10.1016/j.ygyno.2005.06.055

[195] Moen, I., Tronstad, K. J., Kolmannskog, O., Salvesen, G. S., Reed, R. K., & Stuhr, L. E. (2009). Hyperoxia increases the uptake of 5-fluorouracil in mammary tumors independently of changes in interstitial fluid pressure and tumor stroma. BMC Cancer, 9, 446. doi:10.1186/1471-2407-9-446

[196] Mohamed, F., & Sugarbaker, P. H. (2003). Carrier solutions for intraperitoneal chemotherapy. Surg Oncol Clin N Am, 12(3), 813-824.

[197] Moschetta, M., Pretto, F., Berndt, A., Galler, K., Richter, P., Bassi, A., . . . Giavazzi, R. (2012). Paclitaxel enhances therapeutic efficacy of the F8-IL2 immunocytokine to EDA-fibronectin-positive metastatic human melanoma xenografts. Cancer Res, 72(7), 1814-1824. doi:10.1158/0008-5472.CAN-11-1919

[198] Munkholm-Larsen, S., Cao, C. Q., & Yan, T. D. (2009). Malignant peritoneal mesothelioma. World J Gastrointest Surg, 1(1), 38-48.

[199] Mutsaers, S. E. (2004). The mesothelial cell. Int J Biochem Cell Biol, 36(1), 9-16.

[200] Mutsaers, S. E., & Wilkosz, S. (2007). Structure and function of mesothelial cells. Cancer Treat Res, 134, 1-19.

[201] Naveed, S., Qari, H., Banday, T., Altaf, A., & Para, M. (2014). Mucinous Cystic Neoplasms of Pancreas. Gastroenterology Res, 7(2), 44-50.

[202] Nederman T, Carlsson J. Penetration and binding of vinblastine and 5-fluorouracil in cellular spheroids. Cancer Chemother Pharmacol. 1984; 13:131–35.

[203] Nia, H. T., Liu, H., Seano, G., Datta, M., Jones, D., Rahbari, N., Incio, J., Chauhan, V. P., Jung, K., Martin, J. D., Askoxylakis, V., Padera, T. P., Fukumura, D., Boucher, Y., Hornicek, F. J., Grodzinsky, A. J., Baish, J. W., Munn, L. L., . . . Jain, R. K. (2016). Solid stress and elastic energy as measures of tumour mechanopathology. Nature biomedical engineering, 1, 0004.

[204] Nogales, F. F., Dulcey, I., & Preda, O. (2014). Germ cell tumors of the ovary: an update. Arch Pathol Lab Med, 138(3), 351-362.

[205] Nolph KD, Twardowski ZJ, Khanna R, Prowant BF, Ponferrada LP, Schmidt LM, Moore HL. Tidal peritoneal dialysis with racemic or L-lactate solutions. Perit Dial Int 1990;10(2):161-164.

[206] Northrop, J. A., & Lee, J. H. (2007). Large bowel carcinoid tumors. Curr Opin Gastroenterol, 23(1), 74-78.

[207] Occhionorelli, S., Tartarini, D., Pascale, G., Maccatrozzo, S., Stano, R., & Vasquez, G. (2016). Benign multicystic mesothelioma of peritoneum complicating acute appendicitis in a man: a case report. J Med Case Rep, 10, 44.

[208] Omiyale AO. Clinicopathological review of pancreatoblastoma in adults. Gland Surg. 2015;4(4):322–328. doi:10.3978/j.issn.2227-684X.2015.04.05

[209] Onyekachi Henry Ogbonna, Marie Carmel Garcon, Kostas N. Syrigos, and Muhammad Wasif Saif, "Mixed Acinar-Neuroendocrine Carcinoma of the Pancreas with Neuroendocrine Predominance," Case Reports in Medicine, vol. 2013, Article ID 705092, 3 pages, 2013. https://doi.org/10.1155/2013/705092.

[210] Osborne, E. M., Briere, T. M., Hayes-Jordan, A., Levy, L. B., Huh, W. W., Mahajan, A., ... McAleer, M. F. (2016). Survival and toxicity following sequential multimodality treatment including whole abdominopelvic radiotherapy for patients with desmoplastic small round cell tumor. Radiother Oncol, 119(1), 40-44. doi:10.1016/j.radonc.2015.10.016

[211] Otsuka, T., Morizane, C., Nara, S., Ueno, H., Kondo, S., Shimada, K., ... Okusaka, T. (2013). Gemcitabine in patients with intraductal papillary mucinous neoplasm with an associated invasive carcinoma of the pancreas. Pancreas, 42(5), 889-892.

[212] Ozawa S, Sugiyama Y, Mitsuhashi Y, Kobayashi T, Inaba M. Cell killing action of cell cycle phase-non-specific antitumor agents is dependent on concentration-time product. Cancer Chemother Pharmacol. 1988; 21:185–90

[213] Ozols, R. F., Locker, G. Y., Doroshow, J. H., Grotzinger, K. R., Myers, C. E., & Young, R. C. (1979). Pharmacokinetics of adriamycin and tissue penetration in murine ovarian cancer. Cancer Res, 39(8), 3209-3214.

[214] Ozturk D, Yonucu S, Yilmaz D, Unlu M. Influence of vascular normalization on interstitial flow and delivery of liposomes in tumors. Phys Med Biol 2015; 60(4):1477-1496. doi: 10.1088/0031-9155/60/4/1477

[215] Papavramidis, T., & Papavramidis, S. (2005). Solid Pseudopapillary Tumors of the Pancreas: Review of 718 Patients Reported in English Literature. Journal of the American College of Surgeons, 200(6), 965-972. doi: 10.1016/j.jamcollsurg.2005.02.011

[216] Papavramidis, T., & Papavramidis, S. (2005). Solid Pseudopapillary Tumors of the Pancreas: Review of 718 Patients Reported in English Literature. Journal of the American College of Surgeons, 200(6), 965-972. doi: 10.1016/j.jamcollsurg.2005.02.011

[217] Patel CM, Sahdev A, Reznek RH. CT, MRI and PET imaging in peritoneal malignancy. Cancer Imaging. 2011;11(1):123–139. Published 2011 Aug 24. doi:10.1102/1470-7330.2011.0016

[218] Patel, R. R., & Planche, K. (2013). Applied peritoneal anatomy. Clin Radiol, 68(5), 509-520.

[219] Paul, B. K., Ihemelandu, C., & Sugarbaker, P. H. (2018). Prior Surgical Score: An Analysis of the Prognostic Significance of an Initial Nondefinitive Surgical Intervention in Patients With Peritoneal Carcinomatosis of a Colorectal Origin Undergoing Cytoreductive Surgery and Perioperative Intraperitoneal Chemotherapy. Dis Colon Rectum, 61(3), 347-354.

[220] Perentes, J. Y., Wang, Y., Wang, X., Abdelnour, E., Gonzalez, M., Decosterd, L., . . . Krueger, T. (2014). Low-Dose Vascular Photodynamic Therapy Decreases Tumor Interstitial Fluid Pressure, which Promotes Liposomal Doxorubicin Distribution in a Murine Sarcoma Metastasis Model. Transl Oncol. doi:10.1016/j.tranon.2014.04.010

[221] Pestieau, S. R., Schnake, K. J., Stuart, O. A., & Sugarbaker, P. H. (2001). Impact of carrier solutions on pharmacokinetics of intraperitoneal chemotherapy. Cancer Chemother Pharmacol, 47(3), 269-276.

[222] Pfannenberg, C., Schwenzer, N.F., & Bruecher, B.L. (2012). State-of-the-art imaging of peritoneal carcinomatosis. RoeFo - Fortschritte auf dem Gebiete der Roentgenstrahlen und der bildgebenden Verfahren, 184(3), 205-213.

[223] Pilati, P., Rossi, C. R., Mocellin, S., Foletto, M., Scagnet, B., Pasetto, L., & Lise, M. (2001). Multimodal treatment of peritoneal carcinomatosis and sarcomatosis. Eur J Surg Oncol, 27(2), 125-134. doi:10.1053/ejso.2000.1021

[224] Pishko, G., Astary, G., Mareci, T., Sarntinoranont, M. (2011). Sensitivity analysis of an image-based solid tumor computational model with heterogeneous vasculature and porosity. Annals of biomedical engineering, 39(9), 2360-73.

[225] Prat, J. (2012). Ovarian carcinomas: five distinct diseases with different origins, genetic alterations, and clinicopathological features. Virchows Arch, 460(3), 237-249.

[226] Provenzano P, Eliceiri K, Campbell J, Inman D, White J, Keely P. Collagen reorganization at the tumor-stromal interface facilitates local invasion BMC Med. 2006; 4:38.

[227] Psathas, G., Zarokosta, M., Zoulamoglou, M., Chrysikos, D., Thivaios, I., Kaklamanos, I., . . . Mariolis-Sapsakos, T. (2017). Leiomyomatosis peritonealis disseminata: A case report and meticulous review of the literature. Int J Surg Case Rep, 40, 105-108.

[228] Raptopoulos, V. & Gourtsoyiannis Peritoneal Carcinomatosis N. Eur Radiol (2001) 11: 2195. https://doi.org/10.1007/s003300100998

[229] Raspagliesi, F., Quattrone, P., Grosso, G., Cobellis, L., & Di Re, E. (1996). Malignant degeneration in leiomyomatosis peritonealis disseminata. Gynecol Oncol, 61(2), 272-274.

[230] Reid, B. M., Permuth, J. B., & Sellers, T. A. (2017). Epidemiology of ovarian cancer: a review. Cancer Biol Med, 14(1), 9-32.

[231] Reinhold, H. S., & Endrich, B. (1986). Tumour microcirculation as a target for hyperthermia. Int J Hyperthermia, 2(2), 111-137.

[232] Ro C, Chai W, Yu VE, Yu R. Pancreatic neuroendocrine tumors: biology, diagnosis,and treatment. Chin J Cancer. 2013;32(6):312–324. doi:10.5732/cjc.012.10295

[233] Robella, M., Vaira, M., Borsano, A., & M, D. E. S. (2018). Analysis of patient selection policy and pattern of recurrence after cytoreductive surgery and hyperthermic intraperitoneal chemotherapy for colorectal carcinomatosis. Minerva Chir, 73(2), 133-141.

[234] Robinson J, Eriksen S. Theoretical formulation of sustained-release dosage forms. J Pharm Sci. 1966; 55:1254-63.

[235] Rose, P. G. (2016). First-Line Chemotherapy for Ovarian Cancer: Inferences From Recent Studies. Oncologist, 21(11), 1286-1290.

[236] Rossi, C. R., Deraco, M., De Simone, M., Mocellin, S., Pilati, P., Foletto, M., ... Lise, M. (2004). Hyperthermic intraperitoneal intraoperative chemotherapy after cytoreductive surgery for the treatment of abdominal sarcomatosis: clinical outcome and prognostic factors in 60 consecutive patients. Cancer, 100(9), 1943-1950. doi:10.1002/cncr.20192

[237] Roy P, Chetty R. Goblet cell carcinoid tumors of the appendix: An overview. World J Gastrointest Oncol. 2010;2(6):251–258. doi:10.4251/wjgo.v2.i6.251

[238] Royer B, Kalbacher E, Onteniente S, Jullien V, Montange D, Piedoux S, et al. Intraperitoneal clearance as a potential biomarker of cisplatin after intraperitoneal perioperative chemotherapy: a population pharmacokinetic study. British Journal of Cancer. 2012;106(3):460-467. doi:10.1038/bjc.2011.557.

[239] Sadowitz P, Hubbard B, Dabrowiak J, Goodisman J, Tacka K, Aktas M, et al. Kinetics of cisplatin binding to cellular DNA and modulations by thiol-blocking agents and thiol drugs. Drug Metab Dispos. 2002; 30:183–90

[240] Salman, B., Brat, G., Yoon, YS. et al. The Diagnosis and Surgical Treatment of Pancreatoblastoma in Adults: A Case Series and Review of the Literature J Gastrointest Surg (2013) 17: 2153. https://doi.org/10.1007/s11605-013-2294-2

[241] Satoh, Y., Ichikawa, T., Motosugi, U., Kimura, K., Sou, H., Sano, K., & Araki, T. (2011). Diagnosis of Peritoneal Dissemination: Comparison of 18F-FDG PET/CT, Diffusion-Weighted MRI, and Contrast-Enhanced MDCT. American Journal of Roentgenology, 196(2), 447-453. doi: 10.2214/AJR.10.4687

[242] Schmidt, S., Meuli, R. A., Achtari, C., & Prior, J. O. (2015). Peritoneal Carcinomatosis in Primary Ovarian Cancer Staging: Comparison Between MDCT, MRI, and 18F-FDG PET/CT. Clinical Nuclear Medicine, 40(5), 371-377. doi: 10.1097/rlu.0000000000000768

[243] Schneider, G., Siveke, J. T., Eckel, F., & Schmid, R. M. (2005). Pancreatic cancer: basic and clinical aspects. Gastroenterology, 128(6), 1606-1625.

[244] Schultz, K. A., Harris, A. K., Schneider, D. T., Young, R. H., Brown, J., Gershenson, D. M., . . . Frazier, A. L. (2016). Ovarian Sex Cord-Stromal Tumors. J Oncol Pract, 12(10), 940-946.

[245] Sen, A., Capitano, M. L., Spernyak, J. A., Schueckler, J. T., Thomas, S., Singh, A. K., . . . Repasky, E. A. (2011). Mild elevation of body temperature reduces tumor interstitial fluid pressure and hypoxia and enhances efficacy of radiotherapy in murine tumor models. Cancer Res, 71(11), 3872-3880. doi:10.1158/0008-5472.CAN-10-4482

[246] Seshadri RA, Hemanth Raj E. Diagnostic Laparoscopy in the Preoperative Assessment of Patients Undergoing Cytoreductive Surgery and HIPEC for Peritoneal Surface Malignancies. Indian J Surg Oncol. 2016;7(2):230–235. doi:10.1007/s13193-015-0486-9

[247] Shah D, Shin B, Veith J, Tóth K, Bernacki R, Balthasar J. Use of an Anti-Vascular Endothelial Growth Factor Antibody in a Pharmacokinetic Strategy to Increase the Efficacy of Intraperitoneal Chemotherapy. J Pharmacol Exp Ther. 2009; 329(2):580-591. doi: 10.1124/jpet.108.149443

[248] Shim, S. H., Kim, D. Y., Lee, S. W., Park, J. Y., Kim, J. H., Kim, Y. M., . . . Nam, J. H. (2013). Laparoscopic management of early-stage malignant nonepithelial ovarian tumors: surgical and survival outcomes. Int J Gynecol Cancer, 23(2), 249-255.

[249] Shimada, K., Iwase, K., Aono, T., Takeda, S., Yoshida, H., Koma, M., . . . Tanaka, Y. (2009). A case of advanced mucinous cystadenocarcinoma of the pancreas with peritoneal dissemination responding to gemcitabine. Gan To Kagaku Ryoho, 36(6), 995-998.

[250] Simkens, G. A., Rovers, K. P., Nienhuijs, S. W., & de Hingh, I. H. (2017). Patient selection for cytoreductive surgery and HIPEC for the treatment of peritoneal metastases from colorectal cancer. Cancer Manag Res, 9, 259-266.

[251] Simone, C. G., Markham, M. J., & Dizon, D. S. (2016). Chemotherapy in ovarian germ cell tumors: A systematic review. Gynecol Oncol, 141(3), 602-607.

[252] Simsek, C., Esin, E., & Yalcin, S. (2019). Metronomic Chemotherapy: A Systematic Review of the Literature and Clinical Experience. J Oncol, 2019, 5483791. doi:10.1155/2019/5483791

[253] Sitarz, R., Skierucha, M., Mielko, J., Offerhaus, G. J. A., Maciejewski, R., & Polkowski, W. P. (2018). Gastric cancer: epidemiology, prevention, classification, and treatment. Cancer Manag Res, 10, 239-248.

[254] Skipper H. The effects of chemotherapy on the kinetics of leukemic cell behavior. Cancer Res. 1965; 25:1544–50

[255] Smith J, Ngo H, Martin M, Wolf J. An evaluation of cytotoxicity of the taxane and platinum agents combination treatment in a panel of human ovarian carcinoma cell lines. J Ggynecol Oncol. 2005; 98(1):141-145.

[256] Solass, W., Giger-Pabst, U., Zieren, J., & Reymond, M. A. (2013). Pressurized intraperitoneal aerosol chemotherapy (PIPAC): occupational health and safety aspects. Ann Surg Oncol, 20(11), 3504-3511.

[257] Solass, W., Kerb, R., Murdter, T., Giger-Pabst, U., Strumberg, D., Tempfer, C., . . . Reymond, M. A. (2014). Intraperitoneal chemotherapy of peritoneal carcinomatosis using pressurized aerosol as an alternative to liquid solution: first evidence for efficacy. Ann Surg Oncol, 21(2), 553-559.

[258] Solass, W., Struller, F., Horvath, P., Konigsrainer, A., Sipos, B., & Weinreich, F. J. (2016). Morphology of the peritoneal cavity and pathophysiological consequences. Pleura and Peritoneum, 1(4), 193-201.

[259] Soltani M, Chen P. Effect of tumor shape and size on drug delivery to solid tumors. J Biol Eng. 2012; 6(1):4. doi: 10.1186/1754-1611-6-4

[260] Soltani M, Chen P. Numerical Modelling of Fluid Flow in Solid Tumours. PLoS ONE. 2011; 6(6):e20344. doi:10.1371/journal.pone.0020344.

[261] Sommariva, A., Zagonel, V., & Rossi, C. R. (2012). The role of laparoscopy in peritoneal surface malignancies selected for hyperthermic intraperitoneal chemotherapy (HIPEC). Ann Surg Oncol, 19(12), 3737-3744.

[262] Spratt, J. S., Adcock, R. A., Muskovin, M., Sherrill, W., & McKeown, J. (1980). Clinical delivery system for intraperitoneal hyperthermic chemotherapy. Cancer Res, 40(2), 256-260.

[263] Stachowska-Pietka J,Waniewski J, Flessner M, Lindholm B. Distributed model of peritoneal fluid absorption. J Physiol Heart Circ Physiol. 2006; 291(4):H1862–H1874. doi:10.1152/ajpheart.01320.2005

[264] Stachowska-Pietka, J., Waniewsk,i J., Flessner, M., Lindholm, B. Computer simulations of osmotic ultrafiltration and small-solute transport in peritoneal dialysis: a spatially distributed approach. Am J Physiol Ren Physiol. 2012; 302:1331–41.

[265] Steinkamp M, Winner K, Davies S, Muller C, Zhang Y, Hoffman R, et al. Ovarian Tumor Attachment, Invasion, and Vascularization Reflect Unique Microenvironments in the Peritoneum: Insights from Xenograft and Mathematical Models. Front Oncol. 2013; 3:97.

[266] Stelin, G., & Rippe, B. (1990). A phenomenological interpretation of the variation in dialysate volume with dwell time in CAPD. Kidney Int, 38(3), 465-472.

[267] Steuperaert M, Debbaut C, Carlier C, et al. A 3D CFD model of the interstitial fluid pressure and drug distribution in heterogeneous tumor nodules during intraperitoneal chemotherapy. Drug Deliv. ;26(1):404–415. doi:10.1080/10717544.2019.1588423

[268] Steuperaert M, Falvo D'Urso Labate G, Debbaut C, De Wever O, Vanhove C, Ceelen W, Segers P. Mathematical Modeling of Intraperitoneal Drug Delivery: Simulation of Drug Distribution in a Single Tumor Nodule. Drug Deliv. 2017; 24:491-501

[269] Steuperaert, M., Debbaut, C., Segers, P., & Ceelen, W. (2017). Modelling drug transport during intraperitoneal chemotherapy. Pleura Peritoneum, 2(2), 73-83.

[270] Struller, F., Weinreich, F. J., Horvath, P., Kokkalis, M. K., Beckert, S., Konigsrainer, A., & Reymond, M. A. (2017). Peritoneal innervation: embryology and functional anatomy. Pleura Peritoneum, 2(4), 153-161.

[271] Struller, F., Weinreich, F. J., Horvath, P., Kokkalis, M. K., Beckert, S., Konigsrainer, A., & Reymond, M. A. (2017). Peritoneal innervation: embryology and functional anatomy. Pleura Peritoneum, 2(4), 153-161.

[272] Strum, W. B. (2016). Colorectal Adenomas. New England Journal of Medicine, 374(11), 1065-1075.

[273] Stylianopoulos, T. (2017). The Solid Mechanics of Cancer and Strategies for Improved Therapy. Journal of biomechanical engineering, 139(2), 10.1115/1.4034991.

[274] Stylianopoulos, T., Martin, J.D., Chauhan, V.P., Jain, S.R., Diop-Frimpong, B., et al. Causes, consequences, and remedies for growth-induced solid stress in murine and human tumours. Proceedings of the National Academy of Sciences. 2012; 109(38):15101–15108.

[275] Sugarbaker, P. H. (1996). Treatment of peritoneal carcinomatosis from colon or appendiceal cancer with induction intraperitoneal chemotherapy. Cancer Treat Res, 82, 317-325.

[276] Sugarbaker, P. H. (2019). Prevention and Treatment of Peritoneal Metastases: a Comprehensive Review. Indian J Surg Oncol, 10(1), 3-23.

[277] Sugarbaker, P. H., & Van der Speeten, K. (2016). Surgical technology and pharmacology of hyperthermic perioperative chemotherapy. J Gastrointest Oncol, 7(1), 29-44.doi:10.3978/j.issn.2078-6891.2015.105

[278] Sugarbaker, P. H., Averbach, A. M., Jacquet, P., Stephens, A. D., & Stuart, O. A. (1996). A simplified approach to hyperthermic intraoperative intraperitoneal chemotherapy (HIIC) using a self retaining retractor. Cancer Treat Res, 82, 415-421.

[279] Sugarbaker, P. H., Gianola, F. J., Speyer, J. C., Wesley, R., Barofsky, I., & Meyers, C. E. (1985). Prospective, randomized trial of intravenous versus intraperitoneal 5-fluorouracil in patients with advanced primary colon or rectal cancer. Surgery, 98(3), 414-422.

[280] Sugarbaker, P. H., Graves, T., DeBruijn, E. A., Cunliffe, W. J., Mullins, R. E., Hull, W. E., . . . Schlag, P. (1990). Early postoperative intraperitoneal chemotherapy as an adjuvant therapy to surgery for peritoneal carcinomatosis from gastrointestinal cancer: pharmacological studies. Cancer Res, 50(18), 5790-5794.

[281] Sugarbaker, P. H., Mora, J. T., Carmignani, P., Stuart, O. A., & Yoo, D. (2005). Update on chemotherapeutic agents utilized for perioperative intraperitoneal chemotherapy. Oncologist, 10(2), 112-122.

[282] Swat M, Hester S, Balter A, Heiland R, Zaitlen B, Glazier J. Multicell simulations of development and disease using the CompuCell3D simulation environment. Methods Mol. Biol. 2009; 500:361–428

[283] Taghian, A. G., Abi-Raad, R., Assaad, S. I., Casty, A., Ancukiewicz, M., Yeh, E., . . . Powell, S. N. (2005). Paclitaxel decreases the interstitial fluid pressure and improves oxygenation in breast cancers in patients treated with neoadjuvant chemotherapy: clinical implications. J Clin Oncol, 23(9), 1951-1961. doi:10.1200/JCO.2005.08.119

[284] Tailor TD, Hanna G, Yarmolenko PS, Dreher MR, Betof AS, et al. (2010) Effect of pazopanib on tumor microenvironment and liposome delivery. Mol Cancer Ther 9: 1798–1808.

[285] Tan W, Wang F, Lee T, Wang CH. Computer simulation of the delivery of etanidazole to brain tumor from PLGA wafers: Comparison between linear and double burst release systems Biotechnol Bioeng 2003; 82:278–288. DOI: 10.1002/bit.10571

[286] Tempany C, Zou K, Silverman S, Brown D, Kurtz A, McNeil B. . Staging of Advanced Ovarian Cancer: Comparison of Imaging Modalities—Report from the Radiological Diagnostic Oncology Group. Radiology. 2000 Jun;215(3):761-7.

[287] Tempfer, C. B., Celik, I., Solass, W., Buerkle, B., Pabst, U. G., Zieren, J., . . . Reymond, M. A. (2014). Activity of Pressurized Intraperitoneal Aerosol Chemotherapy (PIPAC) with cisplatin and doxorubicin in women with recurrent, platinum-resistant ovarian cancer: preliminary clinical experience. Gynecol Oncol, 132(2), 307-311.

[288] Tentes, A. A., Kyziridis, D., Kakolyris, S., Pallas, N., Zorbas, G., Korakianitis, O., . . . Prasopoulos, P. (2012). Preliminary results of hyperthermic intraperitoneal intraoperative chemotherapy as an adjuvant in resectable pancreatic cancer. Gastroenterol Res Pract, 2012, 506571.

[289] Tentes, A. A., Pallas, N., Karamveri, C., Kyziridis, D., & Hristakis, C. (2018). Cytoreduction and HIPEC for peritoneal carcinomatosis of pancreatic cancer. J BUON, 23(2), 482-487.

[290] Teo C,Tan W, Lee T,Wang CH. Transient interstitial fluid flowin brain tumors: Effect on drug delivery. Chem Eng Sci. 2005; 60(17):4803 – 4821

[291] Thurber G, Yang K, Reiner T, Kohler R, Sorger P, Mitchison T, et al. Single-cell and subcellular pharmacokinetic imaging allows insight into drug action in vivo. Nat Commun. 2013; 4:1504

[292] Tofts, P., & Parker, G. (2013). DCE-MRI: Acquisition and analysis techniques. In P. Barker, X. Golay, & G. Zaharchuk (Eds.), Clinical Perfusion MRI: Techniques and Applications (pp. 58-74). Cambridge: Cambridge University Press. doi:10.1017/CBO9781139004053.006

[293] Troger V, Fischel J, Formento P, Gioanni J, Milano G. Effects of prolonged exposure to cisplatin on cytotoxicity and intracellular drug concentration. Eur J Cancer. 1992; 28:82–6

[294] Tsai M, Lu Z, Wang J, Yeh T, Wientjes M, Au J Effects of carrier on disposition and antitumor activity of intraperitoneal Paclitaxel. Pharm Res. 2007; 24:1691-701

[295] van Baal, J. O., Van de Vijver, K. K., Nieuwland, R., van Noorden, C. J., van Driel, W. J., Sturk, A., . . . Lok, C. A. (2017). The histophysiology and pathophysiology of the peritoneum. Tissue Cell, 49(1), 95-105.

[296] van de Vaart, P. J., van der Vange, N., Zoetmulder, F. A., van Goethem, A. R., van Tellingen, O., ten Bokkel Huinink, W. W., . . . Begg, A. C. (1998). Intraperitoneal cisplatin with regional hyperthermia in advanced ovarian cancer: pharmacokinetics and cisplatin-DNA adduct formation in patients and ovarian cancer cell lines. Eur J Cancer, 34(1), 148-154.

[297] Van der Speeten, K., Govaerts, K., Stuart, O. A., & Sugarbaker, P. H. (2012). Pharmacokinetics of the perioperative use of cancer chemotherapy in peritoneal surface malignancy patients. Gastroenterol Res Pract, 2012, 378064.

[298] Van der Speeten, K., Stuart, O. A., Chang, D., Mahteme, H., & Sugarbaker, P. H. (2011). Changes induced by surgical and clinical factors in the pharmacology of intraperitoneal mitomycin C in 145 patients with peritoneal carcinomatosis. Cancer Chemotherapy and Pharmacology, 68(1), 147-156.

[299] Van Dyke, T. J., Johlin, F. C., Bellizzi, A. M., & Howe, J. R. (2016). Serous Cystadenocarcinoma of the Pancreas: Clinical Features and Management of a Rare Tumor. Dig Surg, 33(3), 240-248.

[300] Vasseur, B., Cadiot, G., Zins, M., Flejou, J. F., Belghiti, J., Marmuse, J. P., . . . Ruszniewski, P. (1996). Peritoneal carcinomatosis in patients with digestive endocrine tumors. Cancer, 78(8), 1686-1692.

[301] Vazquez V, Stuart O, Mohamed F, Sugarbaker P. Extent of parietal peritonectomy does not change intraperitoneal chemotherapy pharmacokinetics. Cancer Chemother Pharmacol. 2003; 52:108-12

[302] Venkatasubramanian R, Arenas R, Henson M, Forbes N. Mechanistic modelling of dynamic MRI data predicts that tumour heterogeneity decreases therapeutic response. Brit J Cancer 2010; 103:486–97

[303] Verwaal, V. J., van Ruth, S., de Bree, E., van Slooten, G. W., van Tinteren, H., Boot, H., & Zoetmulder, F. A. N. (2003). Randomized trial of cytoreduction and hyperthermic intraperitoneal chemotherapy versus systemic chemotherapy and palliative surgery in patients with peritoneal carcinomatosis of colorectal cancer. Journal of Clinical Oncology, 21(20), 3737-3743.

[304] Wang CH, Li J, Teo CS, Lee T. The delivery of BCNU to brain tumors. J Control Release. 1999; 61(1-2):21-41.

[305] Wang CH, Li J. Three-dimensional simulation of IgG delivery to tumors Chem Eng Sci, 1998; 53(20):3579-3600. doi:10.1016/S0009-2509(98)00173-0

[306] Wang, S., Shin, I. S., Hancock, H., Jang, B. S., Kim, H. S., Lee, S. M., . . . Dreher, M. R. (2012). Pulsed high intensity focused ultrasound increases penetration and therapeutic efficacy of monoclonal antibodies in murine xenograft tumors. J Control Release, 162(1), 218-224. doi:10.1016/j.jconrel.2012.06.025

[307] Wardlaw, R., & Smith, J. W. (2008). Gastric carcinoid tumors. Ochsner J, 8(4), 191-196.

[308] Warrick C. An improvement on the practice of tapping; whereby that operation, instead of a relief for symptoms, becomes an absolute cure for an ascites, exemplified in the case of Jane Roman; and recommended to the consideration of the Royal Society, by Christopher Warrick, of Truro, Surgeon. Phil Trans 1744;43(473):12-19.

[309] Warshaw, A. L., & Fernandez-del Castillo, C. (1992). Pancreatic carcinoma. N Engl J Med, 326(7), 455-465.

[310] Werb, Z., & Lu, P. (2015). The Role of Stroma in Tumor Development. Cancer J, 21(4), 250-253. doi:10.1097/PPO.0000000000000127

[311] White, S. K., Stephens, A. D., & Sugarbaker, P. H. (1996). Hyperthermic intraoperative intraperitoneal chemotherapy safety considerations. AORN J, 63(4), 716-724.

[312] Willett CG, Boucher Y, di Tomaso E, Duda DG, Munn LL, et al. (2004) Direct evidence that the VEGF-specific antibody bevacizumab has antivascular effects in human rectal cancer. Nat Med 10: 145–147.

[313] Winer, L., Macedo, F. I., Alfawaz, A., Sommariva, A., Cecchetto, G., Podda, A., . . . Moller, M. G. (2018). Novel Therapy for Pediatric Angiosarcoma With Cytoreductive Surgery and Hyperthermic Intraperitoneal Chemotherapy. J Pediatr Hematol Oncol, 40(8), e505-e510.

[314] Winner K, Steinkamp M, Lee R, Swat M, Muller C, Moses M et al. Spatial Modelling of Drug Delivery Routes for Treatment of Disseminated Ovarian Cancer. Cancer Res 2016; 76(6):1320-1334. doi: 10.1158/0008-5472.CAN-15-162

[315] Wolfgang, C. L., Herman, J. M., Laheru, D. A., Klein, A. P., Erdek, M. A., Fishman, E. K., & Hruban, R. H. (2013). Recent progress in pancreatic cancer. CA Cancer J Clin, 63(5), 318-348.

[316] Wu M, Frieboes H, McDougall S, Chaplain M, Cristini V, Lowengrub J. The effect of interstitial pressure on tumor growth: coupling with the blood and lymphatic vascular systems. Journal of theor biol. 2013; 320:131-51.

[317] Xu W, Mezencev R, Kim B, Wang L, McDonald J, Sulchek T. Cell Stiffness Is a Biomarker of the Metastatic Potential of Ovarian Cancer Cells. Batra SK, ed. PLoS ONE. 2012 ;7:e46609. doi:10.1371/journal.pone.0046609.

[318] Yalçın, B. , Yağcı-Küpeli, B. , Ekinci, S. , Orhan, D. , Oğuz, B. , Varan, A. , Kutluk, T. and Akyüz, C. (2019), Solid pseudopapillary neoplasm of the pancreas in children: Hacettepe experience. ANZ Journal of Surgery, 89: E236-E240. doi:10.1111/ans.15111

[319] Yangong, H., Shi, C., Shahbaz, M., Zhengchuan, N., Wang, J., Liang, B., . . . Niu, J. (2014). Diagnosis and treatment experience of rectal carcinoid (a report of 312 cases). Int J Surg, 12(5), 408-411.

[320] Ye H, Tanenbaum L, Na Y, Mantzavinou A, Fulci G, del Carmen M, et al. Sustained, low-dose intraperitoneal cisplatin improves treatment outcome in ovarian cancer mouse models. J Control Release. 2015; 220:358-67.

[321] Yoo C, Kim BJ, Kim KP, et al. Efficacy of Chemotherapy in Patients with Unresectable or Metastatic Pancreatic Acinar Cell Carcinoma: Potentially Improved Efficacy with Oxaliplatin-Containing Regimen. Cancer Res Treat. 2017;49(3):759–765. doi:10.4143/crt.2016.371

[322] Yu, H. H., Yonemura, Y., Hsieh, M. C., Lu, C. Y., Wu, S. Y., & Shan, Y. S. (2019). Experience of applying cytoreductive surgery and hyperthermic intraperitoneal chemotherapy for ovarian teratoma with malignant transformation and peritoneal dissemination. Ther Clin Risk Manag, 15, 129-136.

[323] Yun, W. S., & Bae, J. M. (2016). Primary peritoneal serous carcinoma, an extremely rare malignancy: A case report and review of the literature. Oncol Lett, 11(6), 4063-4065.

[324] Zeamari, S., Floot, B., van der Vange, N., & Stewart, F. A. (2003). Pharmacokinetics and pharmacodynamics of cisplatin after intraoperative hyperthermic intraperitoneal chemoperfusion (HIPEC). Anticancer Res, 23(2B), 1643-1648.

[325] Zeitlinger M, Derendorf H, Mouton J, Cars O, Craig W, Andes D et al. Protein binding: do we ever learn? Antimicrob Agents Chemother. 2011; 55(7): 3067–3074. doi: 10.1128/AAC.01433-10

[326] Zhan W, Xu X. A Mathematical Model for Thermosensitive Liposomal Delivery of Doxorubicin to Solid Tumour. J drug del. 2013; 2013(3):172529. DOI: 10.1155/2013/172529

[327] Zhan, W, Gedroyc, W, Xu, X, 2014a. Effect of heterogeneous microvasculature distribution on drug delivery to solid tumour. J. Phys. D Appl. Phys. 47 (47), 475401.

[328] Zhang, G., Liu, G., Zhao, D., Cui, X., & Li, G. (2014). Desmoplastic small round cell tumor of the abdomen and pelvis: clinicopathological characters of 12 cases. ScientificWorldJournal, 2014, 549612.

[329] Zhao, J, Salmon, H., Sarntinoranont, M. (2007) Effect of heterogeneous vasculature on interstitial transport within a solid tumor. Microvasc Res. May;73(3):224-36.

[330] Zhu, X.P., Li, K.L., Kamaly-Asl, I.D., et al. Quantification of endothelial permeability, leakage space, and blood volume in brain tumors using combined T1 and T2* contrast-enhanced dynamic MR imaging. J Magn Reson Imaging 2000;11:575–585

[331] Zimm, S., Cleary, S. M., Lucas, W. E., Weiss, R. J., Markman, M., Andrews, P. A., . . . Howell, S. B. (1987). Phase I/pharmacokinetic study of intraperitoneal cisplatin and etoposide. Cancer Res, 47(6), 1712-1716.

[332] Znati, C. A., Rosenstein, M., Boucher, Y., Epperly, M. W., Bloomer, W. D., & Jain, R. K. (1996). Effect of radiation on interstitial fluid pressure and oxygenation in a human tumor xenograft. Cancer Res, 56(5), 964-968.

[333] Zouros E, Manatakis DK, Delis SG, Agalianos C, Triantopoulou C, Dervenis C. Adult pancreatoblastoma: A case report and review of the literature. Oncol Lett. 2015;9(5):2293–2298. doi:10.3892/ol.2015.3001